Investigation of different photocatalytically activated polymeric membranes for micropollutant removal from water

Zur Erlangung des akademischen Grades einer

DOKTORIN DER INGENIEURWISSENSCHAFTEN

von der KIT-Fakultät für Chemieingenieurwesen und Verfahrenstechnik des

Karlsruher Instituts für Technologie (KIT)

genehmigte

DISSERTATION

von

M.Sc. Shabnam Lotfi
aus dem Iran

Tag der mündlichen Prüfung: 23.07.2024

Erstgutachterin: Prof. Dr. Sabine Enders

Zweitgutachter: Prof. Dr. Matthias Kraume

"And one has to understand that braveness is not the absence of fear but rather the strength to keep on going forward despite the fear."

Paulo Coelho

To all the brave women of my country, Iran, whose courage is undeniable!

Table of Contents

Acknowledgements

Abstract

The presence of trace contaminants in water can pose significant risks to both human health and the environment. These pollutants are often found in water at concentrations ranging from a few ng/L to mg/L. Conventional water and wastewater treatment plants are not capable of removing such low concentrations of these compounds, and therefore, the effective elimination of micropollutants is currently an important research topic. Photocatalysis has shown promising results in removing micropollutants. The suitability of these processes depends on the complex interactions of various factors, and so far, the influence of all factors is not well understood. This lack of understanding leads to lower space-time yields and thus higher costs of the removal process. However, operational shortcomings (e.g., the separation of photocatalyst particles in a slurry reactor or the lower space-time yield in batch operation) still need to be addressed for successful practical applications. Membrane technology shows great potential to alleviate such flaws. The successful application of photocatalysis using membrane technology depends on several factors, in particular the characteristics of the membrane, the process design, and the operational conditions. Experiments were performed using two different membrane materials (PES: polyethersulfone; PVDF: polyvinyl fluoride), different pollutants (steroid hormones [estradiol, estrone, progesterone, testosterone] and methylene blue) and TiO_2 as photocatalyst.

Various factors were investigated experimentally as part of the dissertation. The necessary photocatalytic activity can be achieved by using TiO_2 as a catalyst. Results indicate that the local distribution of TiO_2 has an important influence on the extent of degradation and depends on the surface properties of the polymer used. A major factor influencing the removal process is the configuration of the photocatalytic membrane reactor, with the flow-through mode (continuous flow passing through the membrane pores) offering superior performance. The flow-through mode leads to an increase in the reaction volume in a shorter residence time, since here the reaction takes place not only on the membrane surface but also in the pores. This results in an improvement of the space-time yield.

Assessing the impact of different factors on the photocatalytic degradation of steroid hormones indicated that photocatalytic degradation can be achieved in a relatively short residence time, in a few seconds, getting close to the concentrations demanded by the World Health Organization. Variations in the light intensity illustrated that it could only boost the degradation of micropollutants to a certain point and after that removal efficiency is independent of the higher intensities. Zeta potential measurements showed a negative surface charge of the membrane in a wide range of pH. Accordingly, pH is an important parameter since the studied estradiol has a pKa value of 10.3. At pH values less than 10.3, this hormone

exists in the molecular form. At pH values greater than 10.3, this hormone exists in the anionic form and hormone degradation decreases significantly due to electrostatic repulsion. The experiments showed that the temperature influence is complex, but the hormone degradation decreases with increase in the temperature.

Long-term stability plays an important role in the practical use of membrane processes. Investigations into the long-term stability using an accelerated aging methodology were carried out using methylene blue as a model pollutant for cost reasons. The PES membrane with a TiO_2 coating showed a slight yellow color after irradiation. Furthermore, it was observed that the performance of this membrane decreased with the irradiation time. In contrast, no color change was observed in the PVDF membrane coated with TiO_2 and the performance of this membrane remained high despite irradiation. SEM images indicated that the PES-TiO_2 membrane was more affected by irradiation than the PVDF-TiO_2 membrane. The TOC (Total Organic Carbon) amount released from the membranes after irradiation was low for both membranes, with TiO_2 coating exerting a different influence on PES and PVDF. In the case of the PVDF membrane, the presence of TiO_2 leads to a significantly higher TOC value and in the case of the PES membrane, the presence of TiO_2 leads to a lower TOC value. The loss of the TiO_2 photocatalyst was investigated by ICP-OES (Inductively Coupled Plasma Optical Emission spectroscopy). Using the PES-TiO_2 membrane, only a very small loss of TiO_2 was observed after 250 h of irradiation. In contrast, the TiO_2 loss for the PVDF membrane was about 20% after 250 h of irradiation. Despite this loss, the performance of this membrane in photocatalytic degradation of methylene blue was maintained.

Based on these studies, PVDF can be recommended as a membrane material for the removal of a low hormone concentration for further reduction below 5 ng/L. The evaluation of the experiments showed possibilities for a significant reduction of the irradiation time. Furthermore, a very low final concentration lower than 5 ng/L could be achieved. This extremely low value has already been achieved in the literature, but this was done using a batch process or a catalyst that is not stable over time. For practical implementation, however, the mutual influence of the individually evaluated variables must still be understood in the future so that an optimal process can become a reality.

Zusammenfassung

Die Anwesenheit von Schadstoffspuren im Wasser kann sowohl für die menschliche Gesundheit als auch für die Umwelt erhebliche Risiken mit sich bringen. Diese Schadstoffe finden sich im Wasser häufig in Konzentrationen von einigen ng/L bis mg/L. Konventionelle Wasser- und Abwasseraufbereitungsanlagen sind nicht in der Lage, solch niedrige Konzentrationen Verbindungen zu beseitigen, und daher ist die effiziente Eliminierung von Schadstoffspuren ein wichtiger aktueller Forschungsgegenstand. Aktuelle Forschungen zeigten, dass photokatalytische Membranverfahren geeignete Verfahren zur Beseitigung der Schadstoffspuren sein könnten. Die Eignung dieser Verfahren hängt in einer komplexen Weise von verschiedenen Faktoren ab, wobei bisher der Einfluss aller Faktoren noch nicht ausreichend verstanden ist. Dieses mangelnde Verständnis führt zu einer geringen Raum-Zeit Ausbeute und somit zu hohen Kosten.

Für die erfolgreiche praktische Anwendung sind jedoch noch Mängel (z.B. die Abtrennung von Photokatalysatorpartikel in einem Slurry-Reaktor oder die geringere Raum-Zeit-Ausbeute im Batch-Betrieb) zu beheben. Der im Rahmen der Forschungsaktivitäten verfolgte Ansatz ist die Membrantechnologie. Der erfolgreiche Einsatz der Photokatalyse mittels Membrantechnolgie hängt von verschiedenen Faktoren, insbesondere von den Eigenschaften der Membran selbst, der Verfahrensauslegung und den operativen Bedingungen, ab. Die Experimente wurden unter Verwendung von zwei verschiedenen Membranmaterialien (PES: Polyethersulfon; PVDF: Polyvinylflorid), verschiedenen Schadstoffen (Hormone [Estradiol, Estron, Progesteron, Testosteron] und Methylenblau) und TiO_2 als Photokatalysator durchgeführt.

Im Rahmen der Dissertation wurden verschiedene Faktoren experimentell untersucht. Die notwendige photokatalytische Aktivität kann durch die Verwendung von TiO_2 erreicht werden, wobei die lokale Verteilung von TiO_2 einen wichtigen Einfluss hat und von der Art des verwendeten Polymers abhängt. Eine wesentliche Einflussgröße auf das Verfahren ist die Konfiguration des photokatalytischen Membranreaktors, wobei die Durchflussfahrweise eine bessere Leistung bietet. Die Durchflussfahrweise führt zu einer kürzeren Verweilzeit und zu einer Vergrößerung des Reaktionsvolumens, da hier die Reaktion nicht nur an der Oberfläche, sondern auch in den Poren stattfindet. Daraus folgt, eine Verbesserung der Raum-Zeit Ausbeute.

Die Prüfung der Auswirkungen verschiedener Faktoren auf den photokatalytischen Abbau von Steroidhormonen zeigte, dass der photokatalytische Abbau in einer kurzen Verweildauer von wenigen Sekunden erreicht werden kann und damit nahe an den von der Weltgesundheitsorganisation geforderten

Wert von 1 ng/L herankommt. Die Variation der Lichtintensität verdeutlichte, dass sie den Abbau von Schadstoffspuren nur bis zu einem bestimmten Punkt verstärken kann und danach die bereitgestellte zusätzliche Energie verschwendet wird. Zeta-Potentialmessungen zeigten eine negative Oberflächenladung der Membran in einem breiten pH-Bereich. Demzufolge ist der pH-Wert der ein wichtiger Parameter ist, da das untersuchte Estradiol einen pK_A-Wert von 10,3 hat. Bei pH-Werten kleiner als 10,3 liegt dieses Hormon im molekularen Zustand vor und der pH-Wert hat kaum einen Einfluss. Bei pH-Werten größer als 10,3 liegt dieses Hormon in der anionischen Form vor und der Hormonabbau nimmt aufgrund der elektrostatischen Abstoßung drastisch ab. Die Experimente zeigten, dass der Temperatureinfluss komplex ist, jedoch nimmt der Hormonabbau mit höherer Temperatur ab.

Für den praktischen Einsatz von Membranverfahren spielt die Langzeitstabilität eine wichtige Rolle. Untersuchungen bzgl. der Langzeitstabilität wurden aus Kostengründen unter Verwendung von Methylenblau durchgeführt. Die PES-Membran mit einer TiO_2-Beschichtung zeigte nach der Bestrahlung eine leichte Gelbfärbung. Weiterhin wurde beobachtet, dass die Leistungsfähigkeit mit der Bestrahlungsdauer abnimmt. Im Gegensatz dazu, konnte keine farbliche Veränderung der mit TiO_2 beschichteten PVDF-Membran festgestellt werden. Die Leistungsfähigkeit dieser Membran blieb trotz Bestrahlung unverändert hoch. SEM-Aufnahmen zeigten, dass die PES-TiO_2 Membran deutlich mehr durch die Bestrahlung beeinflusst, wird als die PVDF-TiO_2 Membran. Der TOC-(Total Organic Carbon) Wert, der nach der Bestrahlung aus den Membranen ausgeschieden wird, ist für beide Membrane gering, wobei TiO_2 einen unterschiedlichen Einfluss ausübt. Im Falle der PVDF-Membran führt die Anwesenheit von TiO_2 zu einem deutlich höheren TOC-Wert und im Falle der PES-Membran führt die Anwesenheit von TiO_2 zu einem geringeren TOC-Wert. Der Verlust des Photokatalysators TiO_2 wurde mit der ICP-OES (Inductively Coupled Plasma Optical Emission spectroscopy) untersucht. Bei Verwendung der PES-TiO_2 Membran konnte nach 250 h Bestrahlung nur ein sehr geringer Verlust an TiO_2 beobachtet werden. Im Gegenatz dazu, betrug der TiO_2-Verlust bei der PVDF-Membran nach 250 h Bestrahlung etwa 20%. Trotz dieses Verlustes blieb die Leistungsfähigkeit dieser Membran beim photokatalytischen Abbau von Methylenblau erhalten.

Anhand dieser Untersuchungen kann PVDF als Membranmaterial für die Entfernung einen niedrigen Hormonkonzentration zur weiteren Reduktion unter 5ng/L empfohlen werden. Die Auswertung der Experimente zeigte Möglichkeiten auf, die eine signifikante Reduktion der Bestrahlungsdauer erlaubt. Weiterhin konnte eine sehr niedrige Endkonzentration kleiner als 5ng/L erreicht werden. Dieser extrem niedrige Wert wurde in der Literatur schon erreicht, jedoch wurde dazu ein Batch-Verfahren verwendet oder ein Katalysator, der nicht langzeitstabil ist. Für die praktische Umsetzung müssen jedoch in Zukunft

noch die gegenseitige Beeinflussung der einzelnen Stellgrößen verstanden werden, so dass ein optimales Verfahren Realität werden kann.

Scientific papers and contributions of authors

During this PhD, 4 scientific papers were produced as stated below:

1. Title: Comparison of Photocatalytic Membrane Reactor Types for the Degradation of an Organic Molecule by TiO_2-Coated PES Membrane,

Journal: Catalysts 10 (7), 725

Authors: Chhabilal Regmi, Shabnam Lotfi, Jonathan Cawettiere Espíndola, Kristina Fischer, Agnes Schulze, Andrea Iris Schäfer.

Contribution of authors:

Chhabilal Regmi: writing the main manuscript, literature review, experiments design and data interpretation.

Shabnam Lotfi: performing experiments using flow-along and flow-through photocatalytic membrane reactors, data interpretation and presentation, and contribution to writing and revising the manuscript.

Jonathan Cawettiere Espíndola: idea of using specific parameters (space-time yield (STY) and photocatalytic space-time yield (PSTY)) for comparison of different reactor configurations, calculation of these parameters using the experimental data, contribution in writing and revising the manuscript.

Kristina Fischer: preparing and supervising the TiO_2 nanoparticle synthesis, membrane coating, and experiments of batch photocatalytic membrane reactor, revision of the manuscript.

Agnes Schulze: supervision of the TiO_2 nanoparticle synthesis, membrane coating, and experiments of batch photocatalytic membrane reactor, revision of the manuscript, membrane preparation, characterization, and batch experiments funding acquisition.

Andrea Iris Schäfer: supervision of experiments using flow-along and flow-through photocatalytic membrane reactors, supervision and advice on photocatalytic membrane reactors comparisons, supervision on manuscripts writing and revisions, flow-along and flow-through experiments funding acquisition.

2. Title: Photocatalytic degradation of steroid hormone micropollutants by TiO_2-coated polyethersulfone membranes in a continuous flow-through process

Authors: Shabnam Lotfi, Kristina Fischer, Agnes Schulze, Andrea Iris Schäfer.

Journal: Nature Nanotechnology 17 (4), 417-423

Contribution of authors:

Shabnam Lotfi: writing the original manuscript, performing the photocatalytic experiments and analysing the data, presenting the data, experimental design and method development.

Kristina Fischer: developing and synthesizing the TiO_2 nanoparticle photocatalysts, supervision of nanoparticle and membrane characterisation, manuscript revision, providing funding and resources for nanoparticle synthesis and membrane coating.

Agnes Schulze: supervision on developing and synthesizing the TiO_2 nanoparticle photocatalysts, manuscript revision, supervision of nanoparticle and membrane characterisation, providing funding and resources for nanoparticle synthesis and membrane coating.

Andrea Iris Schäfer: developing the concept of project and experiments, method development, manuscript revision, supervision on performing experiments, data interpretation, providing funding and resources for photocatalytic membrane filtration and sample analysis.

3. Title: Poly(vinylidene fluoride) membrane with immobilized TiO_2 for degradation of steroid hormone micropollutants in a photocatalytic membrane reactor

Authors: Siqi Liu, Eleonore Veron, Shabnam Lotfi, Kristina Fischer, Agnes Schulze, Andrea Iris Schäfer.

Journal: Journal of Hazardous Materials 447, 130832

Contribution of authors:

Siqi Liu: writing the original manuscript, data interpretation, and conducting experiments including membrane characterization experiments.

Eleonore Veron: writing and revising the manuscript, performing the photocatalytic experiments and analysis, membrane characterization experiments, data analysis and interpretation.

Shabnam Lotfi: supervision of photocatalytic experiments, concept development, experimental design and method development, data analysis and interpretation, manuscript revision.

Kristina Fischer: developing and synthesizing the TiO_2 nanoparticle photocatalysts, supervision of nanoparticle and membrane characterization, manuscript revision, providing funding and resources for nanoparticle synthesis and membrane coating.

Agnes Schulze: supervision on developing and synthesizing the TiO_2 nanoparticle photocatalysts, manuscript revision, supervision of nanoparticle and membrane characterization, providing funding and resources for nanoparticle synthesis and membrane coating.

Andrea Iris Schäfer: developing the concept of project and experiments, method development, manuscript revision, supervision on data interpretation, providing funding and resources for photocatalytic membrane filtration and sample analysis.

4. Accelerated ageing method for the determination of photostability of polymer-based photocatalytic membranes

Authors: Camila S. Raota, Shabnam Lotfi, Roman Lyubimenko, Bryce S. Richards, Andrea I. Schäfer

Journal: Journal of Membrane Science, 121944

Contribution of authors:

Camila S. Raota: writing and revising the original manuscript, data interpretation.

Shabnam Lotfi: writing and revising the manuscript, concept development, experimental design and method development, experiments on TiO_2 coated membranes, data analysis and interpretation, presenting the data.

Roman Lyubimenko: writing and revising the manuscript, concept development, experimental design and method development, experiments on palladium porphyrin coated membranes, data analysis and interpretation, presenting the data.

Bryce S. Richards: concept development, method development, manuscript revision, supervision of data interpretation, providing funding and resources.

Andrea I. Schäfer: concept development and project idea, method development, manuscript revision, supervision of data interpretation, providing funding and resources.

List of Acronyms

Abbreviation	Description
Al	Aluminum
AO7	Acid Orange 7
AOPs	Advanced Oxidation Technologies
ATR-FTIR	Attenuated Total Reflection-FTIR Spectrometer
BET	Brunauer-Emmett-Teller
DEA	Diethanolamine
DFT	Density Functional Theory
DO	Dissolved Oxygen
DRS	Diffuse Reflectance Spectra
E1	Estrone
E2	17β-Estradiol
EDCs	Endocrine Disruptive Compounds
EDX	Energy-Dispersive X-Ray Spectroscopy
EE2	Ethinylestradiol
EQSs	Environmental Quality Standards
EtOH	Ethanol
FET	Frontier Electron Theory
FSA	Flow Scintillation Analysis
GC TOF MS	Gas Chromatography–Time-Of-Flight Mass Spectrometry
GC-MS	Gas Chromatography–Mass Spectrometry
h^+	Photogenerated Hole
HCl	Hydrochloric Acid
HPLC	High-Performance Liquid Chromatography
ICP-OES	Inductively Coupled Plasma Optical Emission Spectroscopy
IEP	Isoelectric Point
KCl	Potassium Chloride
LC-MS/MS	Liquid Chromatography with Tandem Mass Spectrometry
LED	Light-Emitting Diode
LOD	Limit Of Detection
LOQ	Limit Of Quantification
MB	Methylene Blue
MeOH	Methanol
MP	Micropollutants
NaCl	Sodium Chloride
$NaHCO_3$	Sodium Hydrogencarbonate
NaOH	Sodium Hydroxide
NF	Nanofiltration
NMR	Nuclear Magnetic Resonance
NP	Nanoparticle
P	Progesterone

PAA	Polyacrylic Acid
PAN	Polyacrylonitrile
PAN	Polyacrylonitrile
PE	Polyethylene
PEEK	Polyetheretherketone
PES	Polyethersulfone
PM	Photocatalytic Membrane
PP	Polypropylene
PS	Polysulfone
PTFE	Polytetrafluoroethylene
PVA	Polyvinyl Alcohol
PVDF	Polyvinylidene Fluoride
ROSs	Reactive Oxygen Species
SCHER	Scientific Committee on Health and Environmental Risks
SEM	Scanning Electron Microscopy
SPE+LC	Solid Phase Extraction-Liquid Chromatography
SS 316	Stainless Steel 316
SSA	Specific Surface Area
T	Testosterone
TGA	Thermogravimetry Analysis
TiO$_2$	Titanium Dioxide
TOC	Total Organic Carbon
ToF-SIMS	Time-Of-Flight Secondary Ion Mass Spectrometry
TTIP	Titanium (IV) Isopropoxide
UF	Ultrafiltration
UHPLC	Ultra-High-Performance Liquid Chromatography
UV	Ultraviolet
UV-Vis-NIR	Ultraviolet-Visible-Near-Infrared
WFD	Water Framework Directive
WHO	World Health Organization
WO$_3$	Tungsten Trioxide
WWTPs	Wastewater Treatment Plants
XPS	X-Ray Photoelectron Spectroscopy
XRD	X-Ray Diffraction Analysis
ZnO	Zinc Oxide

List of Symbols

Symbol	Description	Unit
r	Diffusion path	m
D_m	Diffusion coefficient	m^2/s
$t_{D,rad}$	Diffusion time in the radial direction	s
u_r	Velocity of feed in radial direction	m/s
u_Z	Velocity of feed in axial direction	m/s
$h_{D,r}$	Distance in radial direction	m
$\bar{t}$	Mean residence time	s
TMP	Transmembrane pressure	bar
λ	Wavelength	nm
E_g	Band gap Energy	eV
E	Photon energy	*kJ/mol*
h	Planck's constant	Js
ν	Frequency of the radiation	Hz
c	Velocity of light	m/s
Ref	Reflectance data	a.u.
ζ	Zeta potential	mV
η	Electrolyte viscosity	Pa·s
κ_B	Electrolyte conductivity	mS/cm
ε	Dielectric coefficient of electrolyte	-
ε_0	Permittivity	F/m
U	Streaming potential	mV/Pa
A	Absorbance data	a.u.
T	Transmittance	%
I_0	Intensity of absorbed light of a reference	a.u.
I	Intensity of absorbed light of a sample	a.u.
Q	Volumetric flow rate	cm^3/s
w	Width	cm
l	Length	cm
h	Height	cm
th	Thickness	cm
$\mathcal{E}$	Porosity	%
$V_{channel}$	Channel volume	cm^3
$V_{membrane}$	Membrane volume	cm^3
Vr	Reactor volume	cm^3
c_0	Initial concentration	g/cm^3 or mg/L
$c_{\bar{t}}$	Concentration at the time $\bar{t}$	g/cm^3 or mg/L
k	Apparent rate constant	/s
M_{MB}	Molar mass of MB	g/mol

$A_{membrane}$	Active membrane area	cm²
NPL	Normalized light power	W/cm^3
m_{TiO2}	Catalyst weight	g
P	Electric power	W
PI	Light power intensity	W/cm^2
m_{ads}	Mass adsorbed	ng/cm^2
c_p	Permeate concentration	mg/L or ng/L
c_F	Feed concentration	mg/L or ng/L
V_p	Volume of permeate sample	L
V_F	Volume of feed	L
EC_p	Permeate electrical conductivity	mS/cm
EC_f	Feed electrical conductivity	mS/cm
SEC	Specific energy consumption	kWh/m^3
STY_1	Space-time yield considering reactor volume	mol/(cm^3 s)
STY_2	Space-time yield considering membrane surface area	mol/(cm^2 s)
STY_3	Space-time yield considering mass of photocatalyst	mol/(g s)
$PSTY_{1 \text{ and } 2}$	Photocatalytic space-time yield	mol/(W s)
R	Removal	%
r″	Rate of disappearance	mol/m^{2}s
J_m	Water flux	L/m^{2}h
L	Permeability	L/m^{2}hbar
ΔX_{abs}	Absolute error of a property	%
ΔX_{rel}	Relative error	%
$\bar{X}$	Average value of a property	%
X_{max} and X_{min}	Maximum and minimum values	%
ΔE	Experimental error	%
ΔDet	Uncertainty of radio detector	%
ΔS	Uncertainty of system	%
ΔP	Uncertainty of pressure sensor	%
ΔT	Uncertainty of temperature sensor	%
ΔEC	Uncertainty of conductivity sensor	%
$\Delta light$	Uncertainty of light source	%
ΔQ	Uncertainty of membrane permeability	%
$\Delta Prep$	Uncertainty of solution prepration	%
$\Delta UHPLC$	Uncertainty of UHPLC	%
ΔNC	Uncertainty of net counts from the FSA detector	%
Δf_{tot}	Uncertainty of the sum of flow rates of LS and UHPLC pumps	%
σ_{NC}	Standard deviation of net counts	Counts/min

σ_S	Standard deviation of the sample counting	Counts/min
σ_{BG}	Standard deviation of the background counting	Counts/min
ΔR	Uncertainty of hormone removal	%

Chapter One

1 Introduction

1.1 Micropollutants in the Environment

In 2019, the world health organization (WHO) reported that 785 million people worldwide (1 in 10 people) suffer from a lack of basic clean water service including the 144 million who drink untreated surface water **(World Health Organization 2019**) and in 2022, it was reported that at least 2 billion consume a water source contaminated with faeces **(World Health Organization 2022)**. The presence of micropollutants (MP) in the environment has caused critical issues over the past decade. They are called MPs since they can severely impact the environment at very low concentrations. MPs can act as endocrine disruptive compounds (EDCs) and interfere with the normal endocrine system in the body. Removing MPs has attracted enormous attention, especially the ones which pass the conventional wastewater treatment plants (WWTPs) and enter the outlet stream. These include estrogenic hormones, pesticides, various industrial chemicals, and personal care products **(Schwarzenbach *et al.* 2006, Adeel *et al.* 2017)**. Among different MPs, estrogenic hormones like 17β-Estradiol (E2) and Ethinylestradiol (EE2) are serious concerns since they can cause considerable biological responses in the body even at very low concentrations (ng/L-µg/L) **(Sumpter and Johnson 2005)**. Unfortunately, hormones are fed to the animals in husbandry to increase animal production. But these compounds are not completely consumed by them and therefore a fraction of them enter the sewage system **(Cheng *et al.* 2020)**. This amount was reported to be 83,000 kg/yr only in the United States and European Union while the annual release of natural estrogenic hormones by the human population in the world is estimated to be 30,000 kg/yr **(Adeel *et al.* 2017)**. By using animal manure in farming as a nutrient source, exposure of estrogenic hormones to the ground and surface water intensified **(Biswas *et al.* 2017)**. **Figure 1-1** demonstrates the distribution of MPs around the world.
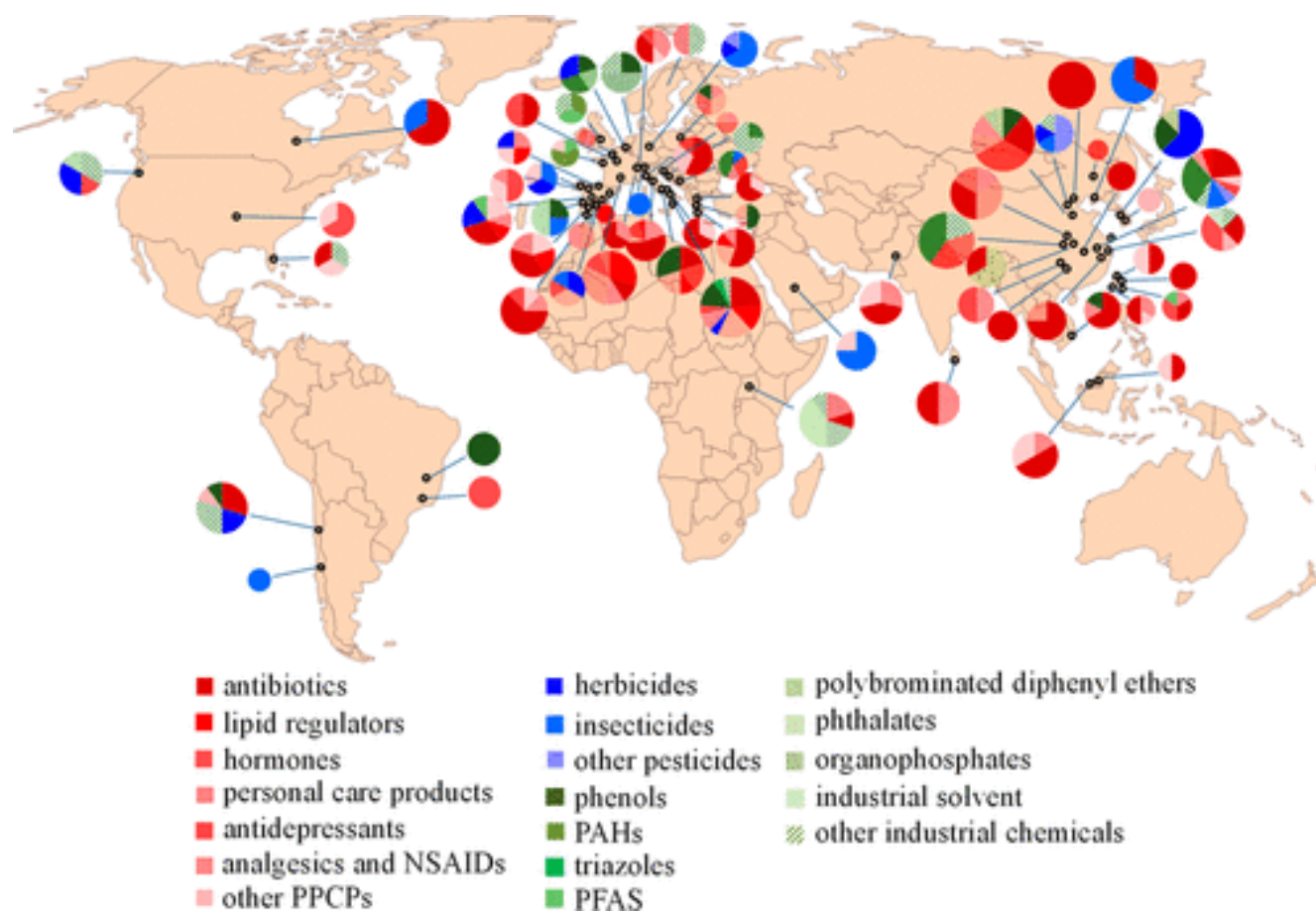
Figure 1-1 MPs and their subgroup are categorized into 3 main groups: pharmaceuticals and personal care products, pesticides, and industrial chemicals distinguished by red, blue and green respectively. The MP type is selected if the measured environmental value is higher than the predicted no-effect concentration or the drinking water equivalent level. Reprinted (adapted) with permission from **(Yang *et al.* 2022)**. Copyright 2022 American Chemical Society.

1.2 Objectives of this study

This study was conducted to explore the potential of photocatalysis as a promising technology for MP removal and investigated the knowledge gaps that might hinder its applicability. Using photocatalysts for the degradation of steroid hormones has been reported to be successful. To name a few, **Menon *et al.* 2021** used TiO$_2$–ZnO nanocomposite and UV-visible light for the degradation of estrogenic compounds in the concentration range of 0.05-10 mg/L. They achieved 100% degradation for concentrations below 1 mg/L and above 25% for concentrations less than 10 mg/L. **Menon *et al.*** reported very promising results by showing the complete removal of estrogenicity of the solution and not only the degradation of molecular structure. However, the concentration of hormones examined in this work was significantly higher than what is reported from different water sources around the world (mostly reported in the ng/L range **(Du *et al.* 2020, Yarahmadi *et al.* 2018)**). Other researchers like **(Han *et al.* 2012)**, **(Padovan *et al.* 2021)** and **(Orozco-Hernández *et al.* 2019)** lowered the concentration of steroid hormones in their

research to µg/L using TiO₂ as a photocatalyst and obtained good results in the elimination of these micropollutants. However, these researchers utilized different variations of a batch process which has issues including but not limited to i) further photocatalysts separation requirement, ii) difficulties of non-continuous operation, and iii) maximum photocatalyst loss.

To overcome the issues raised by previous studies (as mentioned above), a hybrid system composed of membrane technology coupled with an advanced oxidation process was utilized. Both membrane technology and photocatalysis proved to be capable of removing contaminants in water treatment processes. Photocatalytic membrane reactors offer promising solutions to overcome the main issues of common slurry photocatalytic reactors (photocatalysts suspended in the solution) stated above.

This study used a custom-built photocatalytic membrane reactor with polymeric membranes coated with a well-established TiO₂ photocatalyst and the system was examined under different conditions. This system was first examined by **(Lyubimenko *et al.* 2019)** with an organic photosensitizer and **(Berger *et al.* 2020)** with TiO₂ as photocatalyst for photocatalytic degradation of MB as a model pollutant with easy concentration detection at high concentrations. The results obtained by these studies were very promising with efficient removal of MB in a few seconds in a continuous operation. These two studies also chose different membranes/photocatalysts to focus on in their research. **Berger *et al.* 2020** focused on ceramic membranes coated with TiO₂ by atomic layer deposition methodology to overcome the shortage of polymeric membranes which is the degradation of the polymer structure under UV light irradiation. This group successfully degrades MB with maximum degradation of 80-90% at the highest residence time (~3 s) and highest light intensity (25 mW/cm²). However, they also faced issues like the brittle nature of ceramic membranes which made handling it difficult, on top of ceramic membranes being significantly more expensive than polymeric ones. **Lyubimenko *et al.* 2019** chose another direction by changing the photocatalyst type to organic photosensitizers to be able to utilize a wider range of wavelengths and sun irradiance for the degradation of contaminants. After working on MB as a model compound, **Lyubimenko *et al.*** continued their research further on by degrading estrogenic hormones as real micropollutants (**Lyubimenko *et al.* 2021**) parallel to this thesis working on polymeric TiO₂ membranes. Using organic photosensitizer coated on the polymeric membrane, estrogenic hormones were successfully degraded, in particular, E2 concentration was reduced close to 1 ng/L from a 100 ng/L solution. However, organic photosensitizers had an issue of degradation under light exposure **(Raota *et al.* 2023)**.

With all these being said and considering other research which has been done or was in progress in parallel, this thesis aimed to address the following questions:

i.   What is the performance of the proposed flow-through PMR in comparison with the flow-along and batch reactor with the submerged photocatalytic membrane in the solution (Chapter 5)?

ii. What are the limiting factors of operation in a PMR while degrading the steroid hormones in a low concentration as low as in the environment (Chapter 6)?

iii. What is the degree of the photostability of the photocatalytic membranes tested under accelerated ageing and analyzed with different techniques (Chapter 7)?

iv. How improving the membrane structure and TiO_2 coating can enhance steroid hormone degradation (Chapter 8)?

1.3   References

Adeel, M., X. Song, Y. Wang, D. Francis and Y. Yang (2017). "Environmental impact of estrogens on human, animal and plant life: A critical review." Environment International **99**: 107-119.

Berger, T. E., C. Regmi, A. I. Schäfer and B. S. Richards (2020). "Photocatalytic degradation of organic dye *via* atomic layer deposited TiO_2 on ceramic membranes in single-pass flow-through operation." Journal of Membrane Science **604**: 118015.

Biswas, S., W. L. Kranz, C. A. Shapiro, D. D. Snow, S. L. Bartelt-Hunt, M. Mamo, D. D. Tarkalson, T. C. Zhang, D. P. Shelton, S. J. Van Donk and T. L. Mader (2017). "Effect of rainfall timing and tillage on the transport of steroid hormones in runoff from manure amended row crop fields." Journal of Hazardous Materials **324**: 436-447.

Cheng, D., H. H. Ngo, W. Guo, S. W. Chang, D. D. Nguyen, Y. Liu, Q. Wei and D. Wei (2020). "A critical review on antibiotics and hormones in swine wastewater: Water pollution problems and control approaches." Journal of Hazardous Materials **387**: 121682.

Du, B., G. Fan, W. Yu, S. Yang, J. Zhou and J. Luo (2020). "Occurrence and risk assessment of steroid estrogens in environmental water samples: A five-year worldwide perspective." Environmental Pollution **267**: 115405.

Han, J., Y. Liu, N. Singhal, L. Wang and W. Gao (2012). "Comparative photocatalytic degradation of estrone in water by ZnO and TiO_2 under artificial UVA and solar irradiation." Chemical Engineering Journal **213**: 150-162.

Lyubimenko, R., D. Busko, B. S. Richards, A. I. Schäfer and A. Turshatov (2019). "Efficient Photocatalytic Removal of Methylene Blue Using a Metalloporphyrin–Poly(vinylidene fluoride) Hybrid Membrane in a Flow-Through Reactor." ACS Applied Materials & Interfaces **11**: 31763-31776.

Lyubimenko, R., O. I. Gutierrez Cardenas, A. Turshatov, B. S. Richards and A. I. Schäfer (2021). "Photodegradation of steroid-hormone micropollutants in a flow-through membrane reactor coated with Pd(II)-porphyrin." Applied Catalysis B: Environmental **291**: 120097.

Menon, N. G., L. George, S. S. V. Tatiparti and S. Mukherji (2021). "Efficacy and reusability of mixed-phase TiO_2–ZnO nanocomposites for the removal of estrogenic effects of 17β-Estradiol and 17α-Ethinylestradiol from water." Journal of Environmental Management **288**: 112340.

Orozco-Hernández, L., L. M. Gómez-Oliván, A. Elizalde-Velázquez, R. Natividad, L. Fabian-Castoño and N. SanJuan-Reyes (2019). "17-β-Estradiol: Significant reduction of its toxicity in water treated by photocatalysis." Science of the Total Environment **669**: 955-963.

Padovan, R. N., L. S. de Carvalho, P. L. de Souza Bergo, C. Xavier, A. Leitão, Á. J. dos Santos Neto, F. M. Lanças and E. B. Azevedo (2021). "Degradation of hormones in tap water by heterogeneous solar TiO_2-photocatalysis: Optimization, degradation products identification, and estrogenic activity removal." Journal of Environmental Chemical Engineering **9**: 106442.

Raota, C. S., S. Lotfi, R. Lyubimenko, B. S. Richards and A. I. Schäfer (2023). "Accelerated ageing method for the determination of photostability of polymer-based photocatalytic membranes." Journal of Membrane Science: 121944.

Schwarzenbach, R. P., B. I. Escher, K. Fenner, T. B. Hofstetter, C. A. Johnson, U. Von Gunten and B. Wehrli (2006). "The Challenge of Micropollutants in Aquatic Systems." Science **313**: 1072-1077.

Sumpter, J. P. and A. C. Johnson (2005). "Lessons from Endocrine Disruption and Their Application to Other Issues Concerning Trace Organics in the Aquatic Environment." Environmental Science & Technology **39**: 4321.

World Health Organisation. (2019, 18.06.2019). " 1 in 3 people globally do not have access to safe drinking water – UNICEF, WHO", from https://www.who.int/news/item/18-06-2019-1-in-3-people-globally-do-not-have-access-to-safe-drinking-water-unicef-who.

World Health Organisation. (2022, 21.03.2022). "Drinking-water", from https://www.who.int/news-room/fact-sheets/detail/drinking-water.

Yang, Y., X. Zhang, J. Jiang, J. Han, W. Li, X. Li, K. M. Yee Leung, S. A. Snyder and P. J. J. Alvarez (2022). "Which Micropollutants in Water Environments Deserve More Attention Globally?" Environmental Science & Technology **56**: 13-29.

Yarahmadi, H., S. V. Duy, M. Hachad, S. Dorner, S. Sauvé and M. Prévost (2018). "Seasonal variations of steroid hormones released by wastewater treatment plants to river water and sediments: Distribution between particulate and dissolved phases." Science of the Total Environment **635**: 144-155.

Chapter Two

2 Literature review

2.1.1 Steroid hormones

Steroid hormones are a group of steroid compounds derived from cholesterol. Steroid hormones are vital in regulating the neurons and cells related to the neuroendocrine and endocrine systems of the body. These molecules enter the cell through the plasma membrane directly and are responsible for making new proteins or turning genes on/off. In **Figure 2-1**, the structure of three types of steroid hormones can be seen. The structure is particularly important since it affects photocatalytic degradation as will be discussed later in section **2.7.6**.
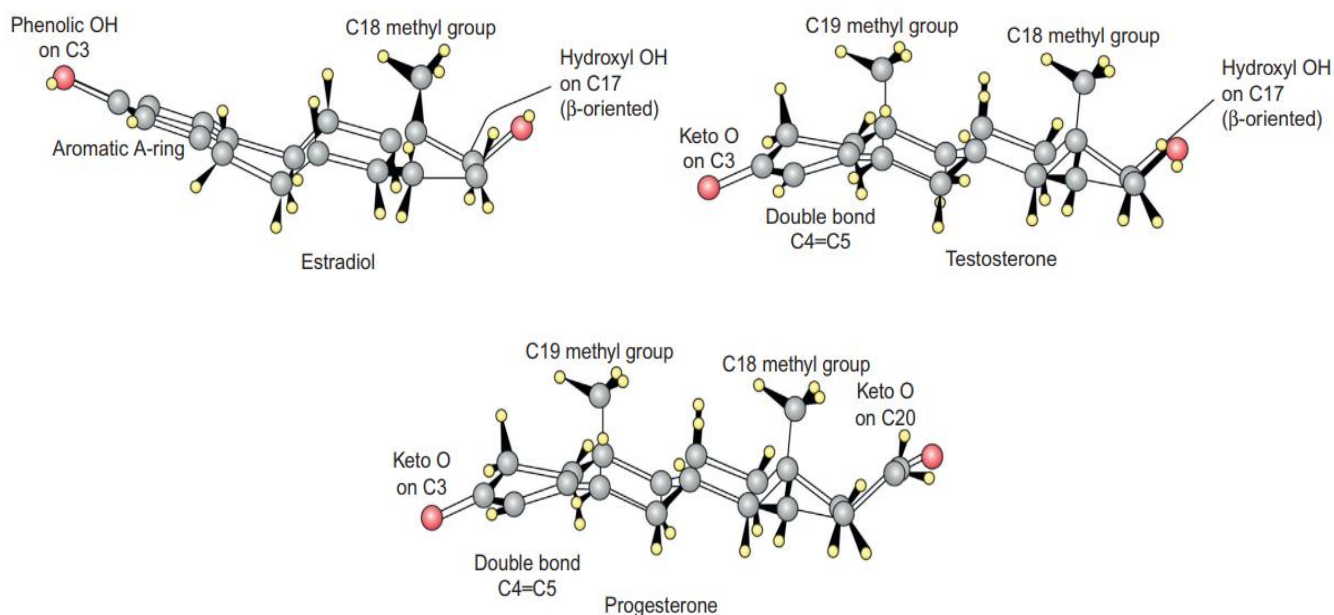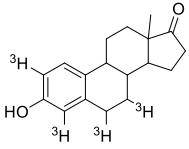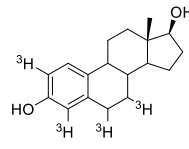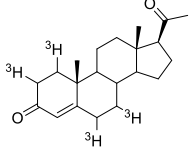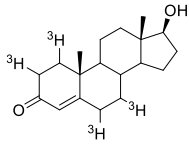
Figure 2-1 Steroid hormone structure obtained *via* X-ray crystallography, reprinted (adapted) from **(Litwack 2022)**. Copyright 2023 with permission from Elsevier

Some characteristics of these hormones, including molecular weight, hydrogen bond donner and accepter, pKa, the solubility limits in water, ethanol and methanol, stokes diameter and estrogenic activity of these four steroid hormones based on E2 as the reference compound are presented in **Table 2-2**.

Table 2-1 Chemical structure and properties of steroid hormones E1, E2, P, T, reprinted (adapted) from (**Lotfi et.al 2022**).

	Estrone (E1)	**Estradiol (E2)**	**Progesterone (P)**	**Testosterone (T)**
Chemical structure (including ^{3}H attached)				
Formula	$C_{18}H_{22}O_2$	$C_{18}H_{24}O_2$	$C_{19}H_{28}O_2$	$C_{21}H_{30}O_2$
OH hydrogen bond donors	1	2	0	1
OH hydrogen bond acceptors	2	2	2	2
Molecular weight (g/mol)	270.4	272.4	314.5	288.4
pKa	10.3-10.8 (**Lewis and Archer 1979, Perrin *et al.* 1981, Bhandari *et al.* 2009**)	10.2-10.7 (**Lewis and Archer 1979, Perrin *et al.* 1981, Bhandari *et al.* 2009**)	N.D.**	N.D.
Log K_{OW}	3.13 (**Hansch *et al.* 1995, Bhandari *et al.* 2009**)	4.01 (**Hansch *et al.* 1995, Bhandari *et al.* 2009**)	3.9 (**Hansch *et al.* 1995**)	3.3 (**Hansch *et al.* 1995**)
Solubility in water (mg/L)	0.8-1.5 (22-25°C) (**Hurwitz and Liu 1977, Liu *et al.* 1977, Yamamoto and Liljestrand 2004, Shareef *et al.* 2006**)	1.7-3.9 (20-22°C) (**Lundberg 1979, Yamamoto and Liljestrand 2004**)	6.9-10.1 (20°C) (**Barry and Eini 1976, Lundberg 1979**)	22.8-70.1 (20°C) (**Lata and Dac 1965, Gale and Saunders 1971, Barry and Eini 1976, Fedorova *et al.* 1976, Lundberg 1979, Lundberg *et al.* 1979**)
Solubility in methanol (g/L)	5.2 (25°C) (**Ruchelman 1967**)	25.5 (25°C) (**Ruchelman and Haines 1967, Salole 1986**)	--	224 (30°C) (**Ruchelman 1971**)
Solubility in ethanol (g/L)	6.8 (25°C) (**Ruchelman 1967**)	2.9 g/L (25°C) (**Ruchelman and Haines 1967, Salole 1986**)	54.4 (21°C) (**Sieminska *et al.* 1997**)	--
Stokes diameter (nm)	0.82*	0.80*	0.86*	0.82*

Estimated from the molar mass

**N.D.: not defined, there is no ionized form for P and T*

Considering the estrogenic activity of E2 as 1, others are evaluated in comparison with E2, and the estrogenic activity of other natural steroid hormones would be 0.36-0.47, NA-0.006, and 0.005 for estrone (E1), progesterone (P) and testosterone (T) respectively **(Brion *et al.* 2012, Yost *et al.* 2013)**. Steroid hormones can act as endocrine disruptive compounds and cause higher activity than normal by binding with the receptor and activating the receptor to produce a biological response (agonist effect). Or else, they can block the receptor and prevent the natural substances from interacting with the receptor (antagonist effect) as demonstrated in **Figure 2-2**.
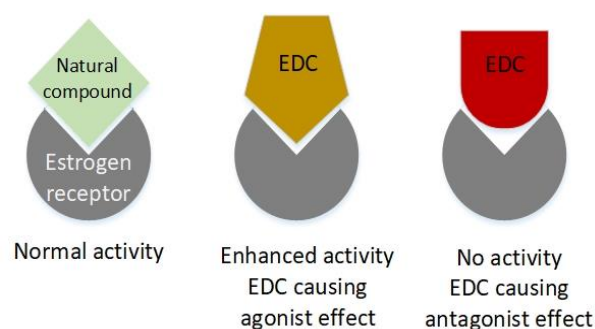
Figure 2-2 Interaction of compounds with estrogenic receptor.

Therefore, the accumulation of these compounds in the surface water causes an unwanted concentration of them for the consumers of the water like fishes, marine life, or humans through drinking water. Unfortunately, the presence of steroid hormones as MPs in different sources of water, namely groundwater, surface water, and effluent of WWTPs has been reported by many researchers around the world (**Table 2-2**). This means that WWTPs fail to remove them and prevent the exposure of living beings significantly.

Table 2-2 Concentration of steroid hormones in Effluent of WWTPs in different locations around the world.

Location	Estrogenic hormone type	Concentration (ng/L)	Ref.
Effluent from wastewater and surface water from Seville (South of Spain)	E2	72-7760	**(Camacho-Muñoz *et al.* 2009)**
	E3	9-8400	
	E1	539-8240	
	17α-Ethinylestradiol	33-8240	
Effluent from Jiangxinzhou Domestic WWTP (Nanjing, China)	E1	28	**(Zhang *et al.* 2012)**
	E2	15	
	E3	13	
Effluent from Rio de Janeiro wastewater treatment plant (Brazil)	E2	24	**(Silva *et al.* 2017)**
	EE2	34	
	E3	827	
Effluents from 18 selected municipal treatment plants across Canada	E1	1-96	**(Servos *et al.* 2005)**
	E2	0.2-15	

	E1	3-78	
	E2	4-107	
Effluent from Darvill, Pietermaritzburg sewage treatment plant, (South Africa)	E3	<1	**(Manickum and John 2014)**
	EE2	1-8	
	P	0-25	
	T	0-26	
	E2	18 (±0.71)	
Colorado River from Lake Mead, (USA)	E1	26 (±2.1)	**(Benotti *et al.* 2009)**
	P	56 (±2.1)	
	T	280 (±14)	

Various sources of steroid hormones in the water systems are shown in **Figure 2-3**. Accumulation of these hormones in water sources like surface water causes prolonged exposure of aquatic life to them which leads to many diseases related to the endocrine system such as de-masculinization of male fish or reducing testis size **(Adeel *et al.* 2017)**. These diseases reduce the population of male fish and create an unbalanced situation in the environment. Failure of WWTPs to eliminate steroid hormones from their inlet leads to contamination of the food chain and drinking water, which ended up in higher chances of cancer or chronic illnesses among humans **(Aris *et al.* 2014, Adeel *et al.* 2017)**.
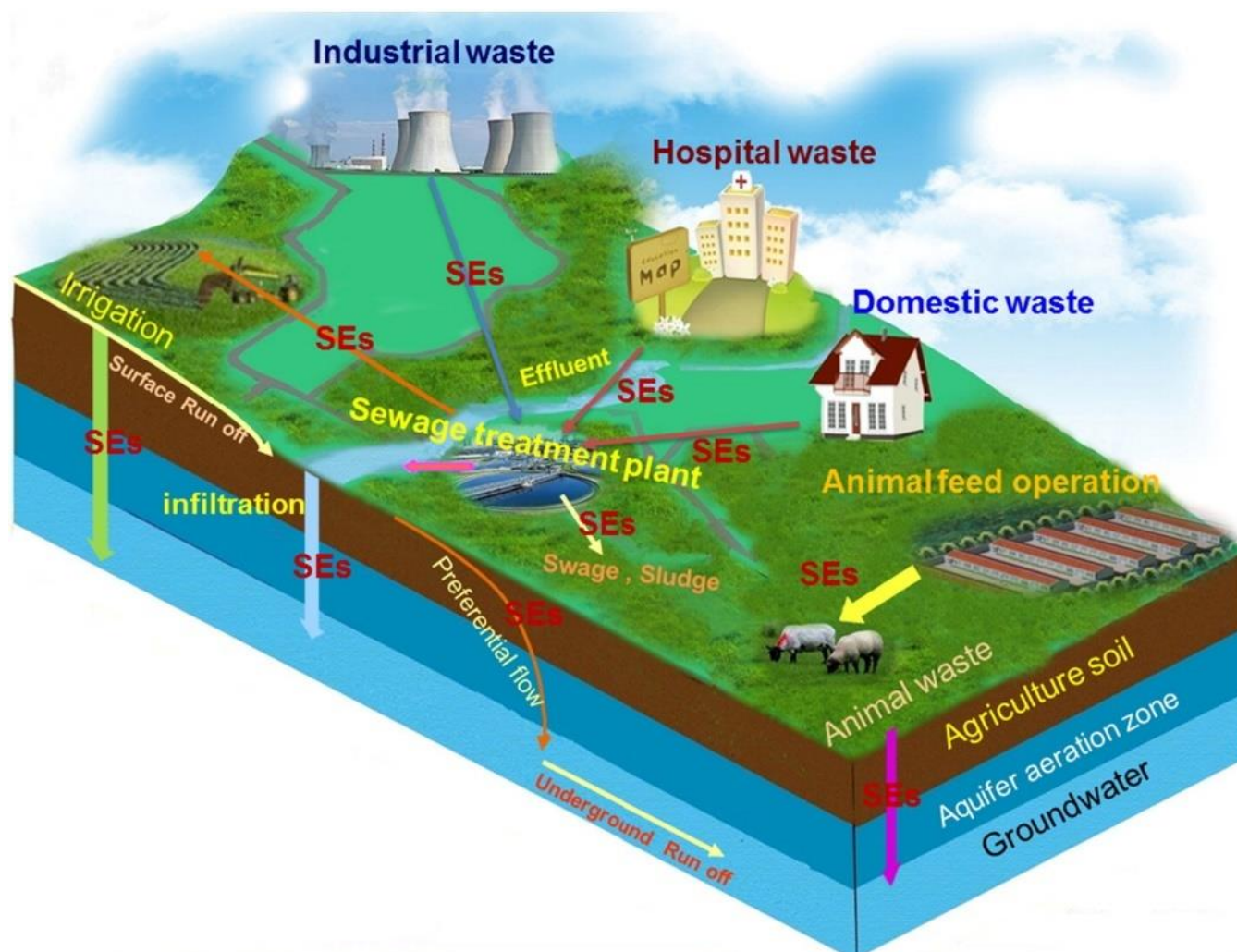
Figure 2-3 Sources of steroid hormones (SE) and their flow to the environment, reprinted from (**Adeel** *et al.* **2017**), Copyright 2023 with permission from Elsevier.

2.1.2   Measures by European Commission and World Health Organization

In 2000, European Commission was requested to identify a list of priority substances which make a significant risk to the aquatic environment and human health following strategies in Article 16 of the Water Framework Directive **(WFD, 2000/60/EC)**[1]. Also, the Commission was supposed to set environmental quality standards (EQSs) and review the list at least every four years. According to the water framework, all member states are responsible to take measures to reduce the exposure of these priority substances, specifically phasing out emissions from the source. In 2001 **(Decision 2455/2001)**[2],

---

[1] Water Framework Directive (WFD) 2000/60/EC: Directive 2000/60/EC of the European Parliament and of the Council of 23 October 2000 establishing a framework for Community action in the field of water policy. Update to be posted: https://environment.ec.europa.eu/topics/water/water-framework-directive_en

[2] 2455/2001/EC. Decision No 2455/2001/EC of the European Parliament and of the Council of 20 November 2001 establishing the list of priority substances in the field of water policy and amending Directive 2000/60/EC [cf. Annex 10 of Water Framework Directive].

the first list of priority substances was established including 33 items. In 2008 **(2008/105/EC or EQS Directive, EQSD)** environmental quality standards were set for the 33 priority substances. In 2011, the proposal for Directive of the European Parliament and of the **Council (COM (2011) 876 final — 2011/0429 (COD))**[3], mentioned E2 in the priority list with annual average EQS in inland surface water 0.4 ng/L and outer surface water as 0.8 ng/L. But no maximum allowable concentration was set for this compound. In 2013 **(Directive 2013/39/EU)**[4], 12 chemicals were added to the list of priority substances which made a total number of 45 items. The directive mentioned that diclofenac, E2 and 17-alpha-ethinylestradiol shall be added to the watch list of substances for Union-wide monitoring to gather data about the impact of their risk.

In 2017, the European Commission stated the WHO suggestion for 3 substances as a precautionary benchmark as no harm to aquatic life, E2, bisphenol and nonylphenol with the concentration of 1 ng/L, 0.1 μg/L and 0.3 μg/L respectively. WHO specified that aquatic life is more sensitive to endocrine-disruptive compounds than humans. Scientific Committee on Health and Environmental Risks **(SCHER)**[5] agreed with the environmental quality standard of 0.4 ng/L for E2 which is close to the value of 1 ng/L set for drinking water. In 2020, article 13 of **DIRECTIVE (EU) 2020/2184**[6] reported the requirement of the first watch list for human water consumption and that E2 and nonylphenol should be considered regarding their endocrine-disrupting properties for human health. The first watch list of compounds of concern in water for human consumption was provided in January 2022 by the European Commission which includes E2 and nonylphenol. In Germany, the main source of MP entrance to the water sources is wastewater treated in municipal wastewater treatment plants. In 2018, some WWTPs in Baden-Württemberg and North Rhine-Westphalia already had a fourth treatment stage and could remove a wide variety of MP by 80% **(Ahting *et al.* 2018)**. While other states like Hesse, Bavaria and Berlin have plans to upgrade the WWTPs. The most common methods used by these advanced WWTPs are ozonation or adsorption by activated carbon or a combination of them. Knowing the critical state of MP in the water bodies in the environment, removal of them should be considered priorities. Therefore, in the next sections, MP removal is discussed.

---

[3] Proposal for a DIRECTIVE OF THE EUROPEAN PARLIAMENT AND OF THE COUNCIL amending Directives 2000/60/EC and 2008/105/EC as regards priority substances in the field of water policy.
[4] DIRECTIVE 2013/39/EU OF THE EUROPEAN PARLIAMENT AND OF THE COUNCIL of 12 August 2013 amending Directives 2000/60/EC and 2008/105/EC as regards priority substances in the field of water policy.
[5] Chemicals and the water framework directive: draft environmental quality standards" 17β-estradiol (E2). SCHER adapted this opinion at its 12th plenary on 30 March 2011.
[6] Directive (EU) 2020/2184 of the European Parliament and of the Council of 16 December 2020 on the quality of water intended for human consumption.

2.2   Micropollutant removal

The presence of MPs reported in the environment proves that conventional WWTPs fail to eliminate these compounds. Therefore, other advanced technologies are needed like Advanced Oxidation Technologies (AOPs). AOPs normally consist of two main steps i) generation of oxidizing agents, and ii) attack on organic or inorganic contaminants. Hydroxyl radicals $^{\bullet}OH$ has the second-highest oxidation potential (2.7 eV) after fluorine among different oxidizing agents such as fluorine (F_2), superoxide (O_2^{-}), and chlorine (Cl_2) (**Loddo *et al.* 2018**). Some AOPs are Fenton and photo-Fenton processes (**Pérez *et al.* 2002, Zhao *et al.* 2010**) which use either ferrous ion and hydrogen peroxide or Fe^{+2}/Fe^{+3} and UV light to generate reactive oxygen species (ROSs), ozone-based reactions including O_3, O_3/H_2O_2, and O_3/catalysts, non-thermal plasma (**Hama Aziz *et al.* 2017**), photocatalysis which uses different photocatalysts like semiconductors or photosensitizers to produce $^{\bullet}OH$ and other ROSs (**Turchi and Ollis 1990**), cavitation and electron beam irradiation (**Loddo *et al.* 2018**).

2.3   Photocatalysis

Photocatalysis benefits from the high oxidation power of radicals such as $^{\bullet}OH$ and has proved to be a promising approach for removing recalcitrant MPs from water and wastewater (**Ahmad *et al.* 2016**). In a photocatalytic process, a photocatalyst will be excited by the energy of photons (ultraviolet (UV) or visible light) and generates highly reactive radicals (**Andreozzi *et al.* 1999**). Compared to other AOP types, photocatalysis does not require any additional chemicals like H_2O_2 for ROS production and can be performed at ambient temperature and pressure which is highly favorable (**Iglesias *et al.* 2016**). However, having a noticeably low quantum yield for $^{\bullet}OH$ production is considered one of the greatest drawbacks of photocatalysis (**Loeb *et al.* 2019**). The cost of the light source is considered the main obstacle as it is economically nonviable for WWTPs (**Malato *et al.* 2009**). Some cost-cutting strategies are using renewable energies or implementing an optimized coupling plan with other steps in a WWTP (**Malato *et al.* 2009**).

(A)

(B)

| Oxygen (O_2) | Superoxide anion ($O_2^{\cdot -}$) | Peroxide ($O_2^{\cdot -2}$) |
| Hydrogen peroxide (H_2O_2) | Hydroxyl ion (OH^-) | Hydroxyl radical ($^\cdot OH$) |

(C)

$^\cdot OH/H_2O$	**2.73 eV**
$Cl^\cdot/Cl^-$	2.43 eV
O_3/O_2	2.07 eV
H_2O_2/H_2O	1.78 eV
O_2/H_2O	1.23 eV
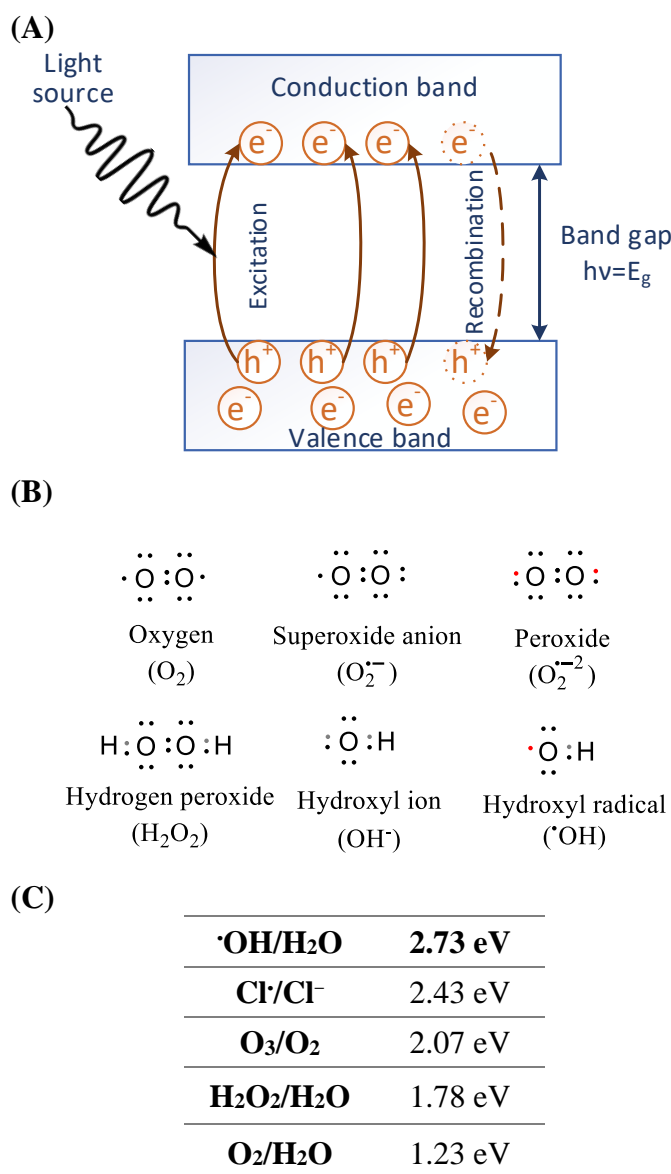
Figure 2-4 (A) Excitation of electron in a semiconductor, (B) molecular structure of ROSs, (C) redox couples with standard reduction potentials given relative to the normal hydrogen electrode (**Hodges** *et al.* **2018**).

The mechanism of photocatalytic degradation includes different steps (**Table 2-3**), starting from illuminating the photocatalyst (e.g., a semiconductor) surface with the light source. In a semiconductor, the electron in the highest position in the valence band can be excited with the energy of a photon and jump to the lowest position in the conduction band. The energy level between the highest level of the valence band and the lowest level of the conduction band is called the energy band gap (**Onishi 2012**). For the electron to be excited, the photon should have enough energy equal to or higher than the band gap of the photocatalyst. The excitation of an electron to a higher level generates electron-hole pairs ($h_{VB}^+ + e_{CB}^-$) which are highly reactive (**Figure 2-4A**). In the next step, the generated electron hole reacts with other molecules and produces reactive oxygen species (ROSs). Then the produced ROSs and the hole can react with the pollutant molecules in their vicinity and degrade them into smaller molecules. The molecular structure of some ROS molecules and a comparison between different reduction potentials of them are presented in **Figure 2-4B** and **Figure 2-4C**.

Each of these reactions involves the photocatalytic degradation of organic compounds that takes place in fractions of a second. To name a few, the generation of electron and hole happens in femtosecond, the formation of $^\cdot OH$ happens in the range of 100 ps to 250 ns, oxidation of an organic compound by $^\cdot OH$ needs 100 ns and the direct reaction between the photogenerated hole and the electron donor (organic compound) happens in ps-ns (**Friedmann** *et al.* **2010**).

Table 2-3 Mechanism of photocatalytic degradation of MP, **(Turchi and Ollis 1990, Litter 1999, Akpan and Hameed 2009, Pan _et al._ 2014)**.

Process	Reaction
Photocatalyst excitation by UV photon:	$TiO_2 + h\nu(UV) \rightarrow h_{VB}^+ + e_{CB}^-$
Electron and hole trapping:	$h_{VB}^+ + H_2O_{ads} \rightarrow {}^{\bullet}OH + H^+$
	$h_{VB}^+ + OH_{ads}^- \rightarrow {}^{\bullet}OH$
	$2h_{VB}^+ + 2H_2O \rightarrow 2H_2O_2 + 2H^+$
	$e_{CB}^- + O_2 \rightarrow O_2^{\bullet-}$
	$O_2^{\bullet-} + H^+ \rightarrow HO_2^{\bullet}$
	$O_2^{\bullet-} + H_2O \rightarrow OH^- + HO_2^{\bullet}$
	$O_2^{\bullet-} + HO_2^{\bullet} + H^+ \rightarrow H_2O_2 + O_2$
	$HO_2^{\bullet} + e_{CB}^- + H^+ \rightarrow H_2O$
	$HO_2^{\bullet} \rightarrow H_2O_2 + O_2$
	$H_2O_2 + O_2^{\bullet-} \rightarrow {}^{\bullet}OH + O_2 + OH^-$
	$H_2O_2 + h\nu(UV) \rightarrow 2{}^{\bullet}OH$
	$H_2O_2 + h\nu(UV) \rightarrow {}^{\bullet}OH + OH^-$
	$H_2O_2 + e_{CB}^- \rightarrow OH^- + {}^{\bullet}OH$
Photocatalytic degradation:	$h_{VB}^+ + MP \rightarrow$ oxidation products
	${}^{\bullet}OH + MP \rightarrow$ degradation products
	$O_2^{\bullet-} + MP \rightarrow$ degradation products
	$HO_2^{\bullet} + MP \rightarrow$ degradation products
Electron–hole pairs recombination:	$h_{VB}^+ + e_{CB}^- \rightarrow$ energy

The attack of ROS ($^{\bullet}OH$) on the MP can happen in four scenarios, i) both $^{\bullet}OH$ and MP are adsorbed to the surface, ii) MP is adsorbed but $^{\bullet}OH$ is free in the solution, iii) $^{\bullet}OH$ is adsorbed and the MP is free in the solution, iv) both $^{\bullet}OH$ and MPs are in the solution **(Turchi and Ollis 1990)**. Considering the super short lifetime of ROSs and consequently the small length of the path on which they can move, the reaction must happen in the close vicinity of the photocatalyst surface. Carretero-Genevrier _et al_. **(Carretero-Genevrier _et al._ 2012)** reported the diffusion length of $^{\bullet}OH$ from the TiO_2 surface to be less than 10 nm.

Several semiconductor-based photocatalysts have been evaluated by researchers for photocatalytic degradation of organic compounds, such as titanium dioxide (TiO_2), tungsten trioxide (WO_3), zinc oxide (ZnO) and many other composite materials **(Riaz and Park 2020)**. However, among these TiO_2 is the most commonly used compound which is the target of this research and is discussed in detail in the next section.

2.3.1   TiO₂ as a photocatalyst

TiO₂ is one of the favorite choices among photocatalysts for the photodegradation of MPs as it is readily available, non-toxic, inexpensive, and chemically stable that is photoactive in its crystal form **(Fischer et al. 2014)**. However, TiO₂ has a relatively high energy band gap, around 3.2 eV for the anatase phase and needs UV light for excitation (<387 nm). This means it can use only a small fraction of the solar spectrum (<5%) which is considered a disadvantage **(ASTM-International 2012)**. The first report of organic compound decomposition by TiO₂ was stated in 1921 by Renz at the University of Lugano (Switzerland) **(Renz 1921)**. The photocatalytic activity of TiO₂ depends on a few parameters such as crystal structure, particle size, surface morphology, and the porosity of the structure among which the crystal structure is the most important one **(Cao et al. 2016)**.
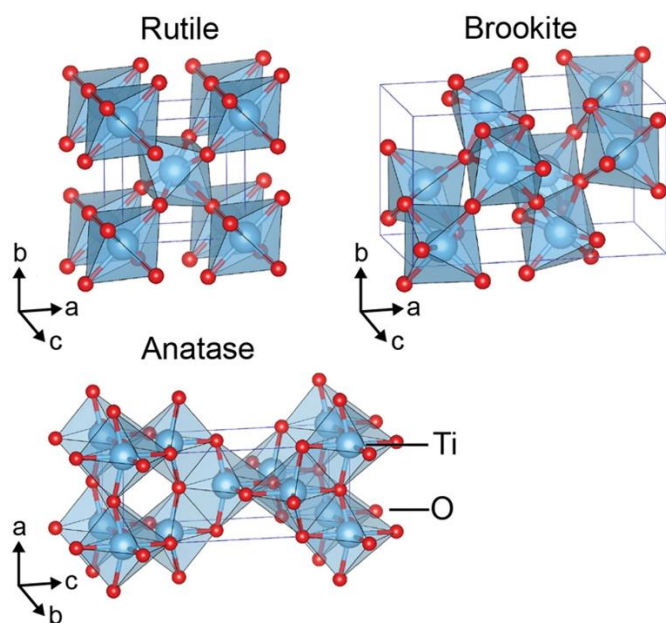
Figure 2-5 Crystal structures of TiO₂ rutile, brookite and anatase polymorphs, reprinted (adapted) from **(Haggerty et al. 2017)**.

TiO₂ forms three main crystal phases, anatase, rutile and brookite demonstrated in **Figure 2-5**. In all TiO₂ crystal phases, titanium (Ti^{+4}) is connected to 6 oxygen atoms (O^{-2}) which form TiO_6 octahedra. The most photocatalytic active phase is anatase **(Fujishima et al. 2008)**. Luttrell et al. **(Luttrell et al. 2014)** investigated the reason behind the difference between the photocatalytic activity of rutile and anatase and reported a few potential explanations. They concluded that other than surface orientation, exciton (electron-hole pair) diffusion efficiency is significantly important. Their measurement showed that the electron-hole pair from deeper layers (higher thickness) contributes to the surface reactions in anatase compared to rutile, thus making anatase a more efficient photocatalyst **(Luttrell et al. 2014)**. Kakuma et al. **(Kakuma et al. 2015)** examined the differences between the photocatalytic activity of anatase and the rutile phase based on the generation of ˙OH and other surface species. They reported that the generation of ˙OH on the rutile phase was extremely lower, while on the other hand, the generation of H_2O_2 and ˙O_2^- was higher on the rutile surface. The plausible reaction mechanism for organic compound decomposition by anatase and rutile offered by Kakuma et al. **(Kakuma et al. 2015)** is demonstrated in **Figure 2-6**.
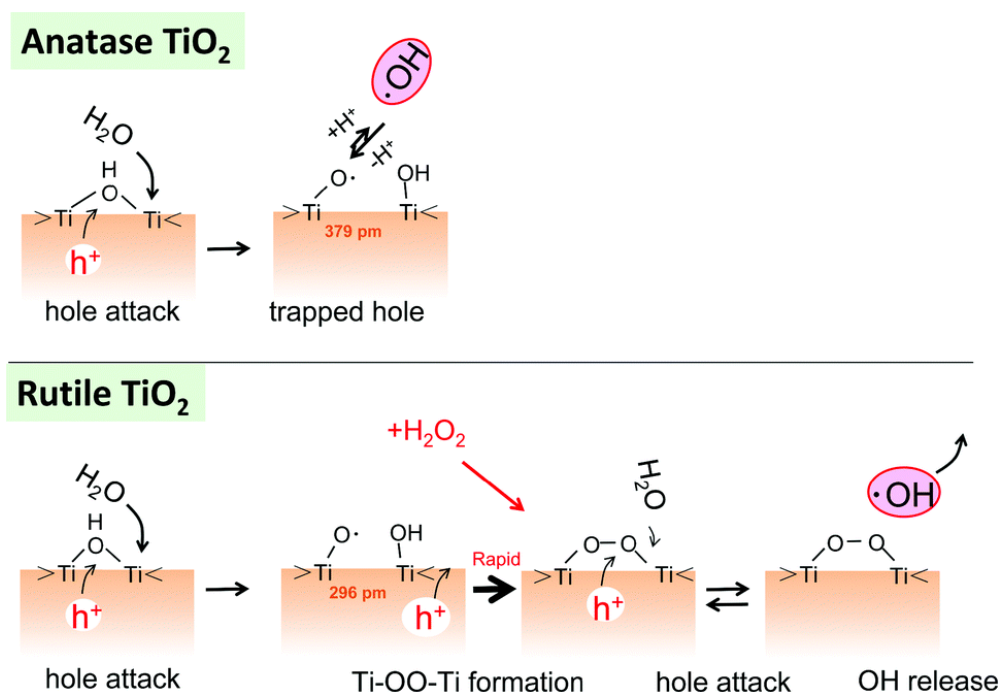
Figure 2-6 Proposed mechanism of ˙OH generation on TiO₂ (anatase and rutile) surface, Reprinted from (**Kakuma et al. 2015**), Copyright 2023 with permission from the Royal Society of Chemistry.

Furthermore, the anatase crystal phase of TiO_2 has an indirect band gap while rutile and brookite have a direct band gap (**Landmann et al. 2012**). This means that in anatase crystal, the electron in the conduction band and the hole in the valence band have a crystal momentum difference and the electron cannot directly jump from the bottom of the conduction band to the top of the valence band. In this case, when the electron and hole recombine, a phonon is released (as heat) instead of light (**Xu et al. 2011, Kakuma et al. 2015**). This allows the electron-hole recombination in anatase to be much slower compared to the other two phases which results in the longer lifetime of the electron-hole pair and consequently, increases the chance of surface reaction. The lifetime of photo-excited charge carriers is estimated to be longer than 10 ns for a single anatase crystal with high quality, excluding the contribution of impurities, defects, particle size and hole traps (**Xu et al. 2011**). Similarly, Yamada et al. (**Yamada and Kanemitsu 2012**) found out that the photoexcited electrons have a longer lifetime (>1 µs) compared to rutile (24 ns), while the population of photogenerated holes decline rapidly in a few nanoseconds in both crystal phases. They attributed these long-lasting electrons to the higher photoactivity of the anatase phase.

Considering all differences in these three crystal phases, both theoretical and experimental studies reported that a mixture of TiO_2 crystal phases is superior to the pure phase in the decomposition of compounds, even though the pure phase of anatase has higher photocatalytic activity than other pure phases (**Hurum et al. 2003, Li et al. 2008**).

2.4   Micropollutant removal *via* photocatalysis

Photocatalytic degradation of MPs is performed in two basic modes, photocatalyst nanoparticles dispersed in the slurry reactor and photocatalyst immobilized on a support. A slurry reactor has the advantage of the high surface area of photocatalyst and, with a good mixing, potential low mass transfer limitation. However, the separation of photocatalysts from the reactor media is a great challenge in this reactor type. Also, increasing the concentration of the photocatalyst is limited by the opacity of the solution which prevents the light penetrating deep into the reactor. To solve these issues, photocatalysts can be immobilized on different types of supports like glass, or metals **(Marinangeli and Ollis 1977, Hofstadler *et al.* 1994, Molinari *et al.* 2000)**. This approach eliminates the concern of photocatalyst loss and release of nanoparticles to the outlet stream. But immobilizing photocatalysts will lead to a limitation in the mass transfer of pollutants to the surface of the photocatalyst and therefore drop in the efficiency of the process. However, getting benefits from porous materials like porous polymeric membranes has been suggested to remove the mass transfer limitation barriers **(Alvarez *et al.* 2018)**. When the reaction takes place in a nano-confined area, such as nanometer pores, the probability of molecules reaching the photocatalyst surface and reacting with ROS improves **(Coleman *et al.* 2004)**. Considering the short lifetime of highly oxidative radicals, which are being produced on the photocatalyst surface during photocatalysis, the exposure of pollutants from the bulk to these substances is very challenging. Therefore, when the flow is forced to pass through a confined system like membrane pores, there is a significant improvement in the probability of the radicals reacting with the pollutants **(Zou *et al.* 2021)**.

2.5   TiO$_2$ Photocatalysis for steroid hormone elimination

Photocatalytic degradation of steroid hormones using TiO$_2$ as the photocatalyst has been reported to eliminate different types of hormones effectively **(Zhang *et al.* 2007, Li Puma *et al.* 2010, Mboula *et al.* 2015, Liz *et al.* 2017, Fischer *et al.* 2018, Orozco-Hernández *et al.* 2019)**. Orozco-Hernández *et al.* **(Orozco-Hernández *et al.* 2019)** showed that TiO$_2$ photocatalysis could decrease the E2 concentration by almost 85% and reduce its estrogenic activity by 85-95% in almost 60 minutes under UVA light (315-400 nm) in a 14 L pilot batch reactor. The concentration of E2 used in their experiments was 1 ng/L and 1 µg/L measured with HPLC following prior extraction and the correspondence estrogenic activity was measured by *Cyprinus carpio* as a bioindicator organism and oxidative stress biomarkers. A comparison between photocatalysis and photolysis by Coleman *et al.* **(Coleman *et al.* 2004)** indicated a significantly faster reduction of estrogenic activity by TiO$_2$ photocatalysis compared to direct photolysis using a High-Pressure Mercury lamp. In the study by Coleman *et al.* **(Coleman *et al.* 2004)**, using TiO$_2$ immobilized on titanium alloy and UV light, complete removal of estrogenic activity of E1, E2, and EE2 below the

detection limit was observed from 10 µg/L initial concentration (detection limit 53 ng/L for E2 and EE2, and 100 ng/L for E1). From different studies using TiO_2 at both lab and pilot scales, TiO_2 proved to be a suitable choice as a photocatalyst. **Table 2-4** presents a comparison of a few pieces of research that studied the photocatalytic degradation of steroid hormones using TiO_2 as the photocatalyst.

Table 2-4 Different studies reporting photocatalytic degradation of steroid hormones using TiO_2.

PMR	MP	Photocatalyst	Light source	Initial concentration	Removal	Detection analysis	Ref.
Flat-plate photochemical reactor (recycle mode)	E1 E2	TiO_2 Degussa P25	Solar	250 µg/L	85%	SPE+LC-UV	(Padovan *et al.* 2021)
Batch photoreactor (0.5 L), stirred and aerated	E2 EE2	TiO_2-ZnO nanocomposite 10 mg/L	UV light Visible	0.05-10 mg/L	(UV)100-60%* (Vis) 100-40%	GC×GC TOF MS	(Menon *et al.* 2021)
Bubble column (Pilot, 14 L)	E2	TiO_2 Degussa P25 (100 mg/L)	UV 254 nm	1 ng/L & 1 µg/L	85% (<detection limit)	HPLC+ toxicity test	(Orozco-Hernández *et al.* 2019)
Batch photoreactor (1 L) with magnetic stirrer	E2 (in a mixture of 5 compounds)	TiO_2 Degussa P25 (1.5 g/L)	mercury-vapor lamp (40-48% UV)	2 mg/L**	Complete (<detection limit of 52 µg/L)	GC-MS	(Alvarez-Corena *et al.* 2016)
Cross-flow (recirculation)	E1 E2	PVDF-PVP-TiO_2	365 nm (2.5 mW/cm^2)	200 µg/L 200 µg/L	93% 73%	LC-MS/MS	(Wang *et al.* 2016)
Batch reactor with circulation	E2	TiO_2-modified PTFE mesh sheets	black fluorescent lamps (0.24 mW/cm^2)	90 µg/L	90% (20 min)	HPLC	(Nakashima *et al.* 2003)

* E2 transformation, complete mineralization was found to be lower

** 2 mg/L concentration of a mixture of all 5 compounds

Most researchers **(Padovan *et al.* 2021, Menon *et al.* 2021, Orozco-Hernández *et al.* 2019, Alvarez-Corena *et al.* 2016, Wang *et al.* 2016, Nakashima *et al.* 2003)** who worked on the removal of steroid hormones selected a high initial concentration which eases the detection of the compounds. However, these concentrations are way above what can be found in the environment. Therefore, more research on the removal of steroid hormones is needed with the concentration relevant to the environmental concentration.

2.5.1   Photocatalytic degradation pathway of steroid hormone

One of the critical issues in using AOPs for the degradation of MPs is the generation of intermediate products during the process. These unwanted products in some cases can have higher potencies than the parent compound and cause serious health issues. Souissi *et al.* **(Souissi *et al.* 2014)** reported higher

estrogenic activity of irradiated solution containing E1 and the intermediate products after photolysis (initial concentration of E1 0.01 mg/L, high-pressure mercury lamp as a light source). They reported nine intermediate products which all contained the phenolic group with the addition of the hydroxyl group to different rings and therefore expressed higher estrogenic activity than the non-irradiated solution. Phenolic moiety is indicated to be responsible for the estrogenic activity of the endocrine disruptive compounds and compounds like testosterone which have a cyclohexenone moiety instead of a phenolic group have considerably weaker estrogenic activity. Other than phenolic moiety, hydroxyl groups are important in the interaction of compounds with estrogenic receptors *via* hydrogen bonds **(Mombelli 2012)**. Therefore, in the case of E1 where there is a carbonyl group instead of the hydroxyl group of E2 at position C17 **(Figure 2-7)**, estrogenic activity is significantly lower **(Arnold *et al.* 1997)**. In general, there are two main oxidation pathways for photocatalytic degradation of estrogens, i) abstraction of hydrogen by the photogenerated hole (h^+) **(Figure 2-7A)**, ii) direct attack of produced ˙OH **(Figure 2-7B)** **(Ohko *et al.* 2002, Mai *et al.* 2008)**. Therefore, phenolic moiety in E2 is the starting point in photocatalytic degradation.
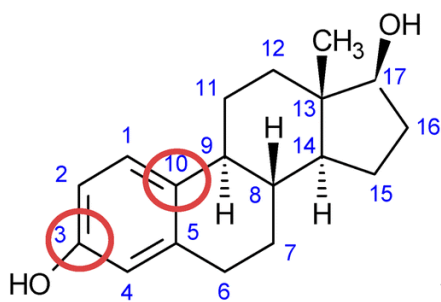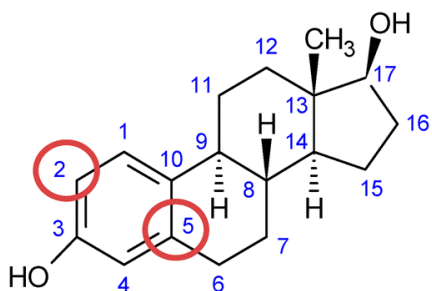
Figure 2-7 Molecular structure of E2 and proposed reaction sites, (A) direct attack by hole generated in the valence band of TiO₂ (electron extraction), (B) attack by ˙OH generated in photocatalysis, Reprinted from **(Ramírez-Sánchez *et al.* 2017)** Copyright 2023 with permission from the Royal Society of Chemistry.

Ohko *et al.* and Mai *et al.* **(Ohko *et al.* 2002, Mai *et al.* 2008)** performed frontier electron density theoretical calculations for E2 and both reported that the carbon at positions 3 and 10 **(Figure 2-7)** has the highest electron density. Therefore, it is more likely that the reaction is starting from these sites by electron extraction. In the study of Ohko *et al.* and Mai *et al.*, the positions of carbon atoms which are susceptible to electron subtraction are (in decreasing order) C10 > C3 > C2 > C4 > C5 > C1 and the sites which ˙OH most probably attack are (in decreasing order) C2 > C5 > C4> C1 > C10 > C3. Ohko *et al.* **(Ohko *et al.* 2002)** used fluorescence analysis in their experiments to detect E2 and the intermediate products after photocatalytic degradation of E2 with TiO₂ suspension. No intermediate products were detected by fluorescence analysis, and it was attributed to the fact that most probably none of the

intermediate products has phenolic moiety in their structure. Considering the high benefits of employing membranes as support for photocatalysts and integration of a separation unit with degradation, the next photocatalytic membrane reactors are described in more detail.

2.6   Photocatalytic membrane reactor

Integration of photocatalysis in membrane processes is called photocatalytic membrane reactors **(Mozia 2010, Argurio *et al.* 2018).** The combination of a photoreactor with membrane filtration can be designed in two main process configurations; i) photocatalysts suspended in the solution and an external membrane filtration unit (**Figure 2-8A** and **B**), and ii) photocatalysts immobilized on the membrane (both in pores and on the outer surface) (**Figure 2-8B** and **C**) **(Ollis 2003, Argurio *et al.* 2018)**. In the second case, when photocatalysts are incorporated in the membrane structure, system configurations can be designed in 3 main ways, i) a photocatalytic membrane (PM) submerged in the solution containing the pollutant, ii) filtration and photocatalytic degradation happening simultaneously and the flow of pollutant pass along by the surface of the membrane and hence reaction is happening on the surface of photocatalytic membrane , iii) similar to the second mode but the pollutant solution forced to flow through the membrane pores and therefore the reaction is happening in both surface and the membrane surface.
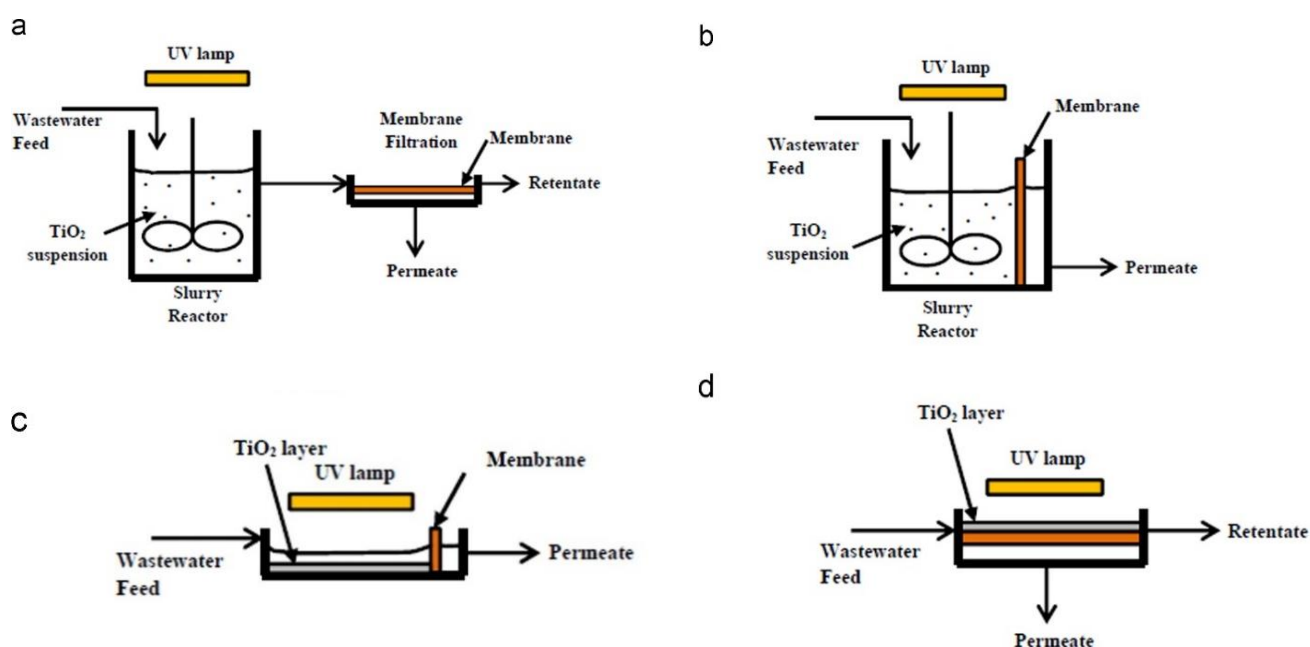
Figure 2-8 Configurations of PMRs (A) slurry reactor and a membrane filtration unit; (B) photocatalytic membrane submerged in a slurry reactor; (C) photocatalytic membrane in a photocatalyst coated reactor; and (D) photocatalytic membrane for simultaneous degradation and separation, Reprinted (adapted) from (**Leong *et al.* 2014**), Copyright 2023 with permission from Elsevier.

Immobilization of photocatalysts on the surface and inside the structure of membranes has shown great advantages including photocatalyst recovery and reuse in multiple runs continuously (**Mozia 2010**). In

this case, the membrane can act as both a support for the photocatalyst and a barrier for large molecules. Horovitz *et al.* (**Horovitz *et al.* 2016**) investigated N-doped TiO_2-coated ceramic membranes to degrade carbamazepine (1 mg/L) in two main configurations of flow passing along the surface and through the pores of membranes (**Figure 2-8 C&D**). The photocatalytic activity inside the pores of the membrane (200 and 800 nm) accounted for about 90% of the total photocatalytic degradation. This means that the photocatalytic degradation process was limited by the diffusion of pollutants to the photocatalyst inside the pores (**Horovitz *et al.* 2016**). Furthermore, a hybrid photocatalytic membrane (PM) has the benefit of reducing the fouling potential when filtering organic compounds which have been attributed to the degradation of pollutants into smaller molecules (**Mozia 2010, Song *et al.* 2012**). Mendret *et al.* (**Mendret *et al.* 2013**) figured out that flow-through mode PMR improved the reduction of membrane fouling, although high photocatalytic degradation of acid orange 7 (AO7) was not achieved. The low removal of AO7 by photocatalysis was attributed to the short contact time of the pollutant with the photocatalyst surface. In the flow-through process, the solution is forced to pass through the membrane pores, therefore, it is in contact with the photocatalyst deposited in both surface and the pores and it enhances the degradation significantly. Researchers such as (**Zhang *et al.* 2021, Zou *et al.* 2021**) had noticed a considerable enhancement in this mode and attributed it to the higher collision probability when the solution is passing the confined areas of pores (diameter of a few nanometers). Even though the residence time in the membrane pores in this mode is short (a few seconds), the throughput of the whole process and the degradation efficiency are sufficiently high considering the continuous flow of the PMR (**Lyubimenko *et al.* 2021**).

While the benefits of operating a PMR have been recognized, an important PMR design parameter is the selection of the membrane material on which the photocatalyst will be immobilized. This material selection determines the accessibility and functionality of the photocatalyst and hence directly impacts photocatalytic degradation.

2.6.1 Membrane material

Different substrate materials including polymeric, ceramic, and glass substrates can be used as photocatalyst substrates. A suitable substrate for the photocatalytic membrane process should have good chemical and mechanical stability under UV light illumination, and resistance to the attack of ROSs to withstand long-term photocatalytic operation (**Ahmad *et al.* 2016**). While choosing the suitable substrate for immobilization of photocatalyst, critical characteristics are i) high specific surface area for good photocatalytic reaction performance, ii) strong adhesion between photocatalyst and membrane to avoid photocatalyst loss during filtration, and iii) high hydrophilicity which results in good permeability

(Leong *et al.* 2014, Fischer *et al.* 2015). In principle, polymeric membranes are good substrate choices due to their facile fabrication and great availability. Yet, many polymeric materials might not be sufficiently stable to endure the harsh conditions of photocatalysis, and hence stability testing is required **(Molinari *et al.* 2000)**. Alternatively, ceramic membranes are an interesting option due to their higher stability towards light exposure and ROSs. However, ceramic membranes are expensive, brittle by nature, and have a lower adsorption capacity of MPs which is believed to be an important factor in photocatalytic processes **(Abdullah *et al.* 2018, Loddo *et al.* 2018)**. The importance of adsorption in photocatalytic degradation is related to material choice and will be discussed in the subsequent sections.

Last but not least important point in membrane selection is the membrane morphology such as pore size, pore shape, tortuosity, thickness, and porosity. Depending on the photocatalyst particle size and the membrane pore size, the catalyst immobilization may result in a permeability decline. **Horovitz *et al.* (Horovitz *et al.* 2016)** noticed a 50% permeability decline after coating 200 nm α-Al$_2$O$_3$ membrane with TiO$_2$ and only a 12% permeability decline for 800 nm. While membrane characteristics must be chosen carefully to achieve the desired permeability which determines the required transmembrane pressure and hence the energy consumption, good contact between ROS and MPs in pores and retention of contaminants such as bacteria and viruses are further important considerations in water treatment. Having a membrane acts as a physical barrier to bacteria and viruses typically requires an ultrafiltration (UF) membrane **(Van der Bruggen *et al.* 2003)**. However, PMR applications are particularly attractive due to the lower energy consumption compared to nanofiltration (NF), which is typically required to remove MPs. NF operates at pressures of about 3-20 bar **(Van der Bruggen *et al.* 2003)** and generates a concentrate to be disposed of, where the potential in situ degradation offered by PMR is a definite advantage. It may assist the PMR operation if the membrane substrate can retain MPs, which is why NF can be an interesting substrate for investigation, although the thin active layers of polymeric thin-film composite membranes are unlikely to withstand ROS and ceramic membranes with adequate MP retention are to date not available. Once the substrate is chosen, an adequate method for photocatalyst immobilization must be identified.

2.6.2 Immobilizing methods

Immobilization of photocatalyst in/onto the membrane is normally done either by embedding the nanoparticles into the membrane structure during the membrane preparation method or by coating the membrane surface with the nanoparticles (**Figure 2-9**). In the former approach, photocatalyst nanoparticles are embedded into the structure of the membrane, and the exposed light will first hit the membrane instead of the photocatalyst **(Zakria *et al.* 2021)**. If light penetrates enough into the membrane

and reaches the photocatalyst, then the generated ROS needs to diffuse to the surface for reaction with pollutants which reduces the efficiency of this method. However, this way has the advantage that the photocatalyst loss is minimal. Moreover, it has been shown that the addition of TiO_2 nanoparticle to the polymeric membrane enhances its performance such as antifouling properties and better flux **(Vatanpour *et al.* 2012)**. Paredes *et al.* **(Paredes *et al.* 2019)** used a dual-layer hollow fiber membrane with TiO_2 embedded in the structure of the fiber's outer layer aiming to have higher membrane performance (flux and hydrophilicity) and photocatalytic degradation of pollutants. They found out that compared to the TiO_2-P25 nanoparticles, the elimination of pollutants with photocatalytic membrane was superior depending on the structure of the solution to be treated.
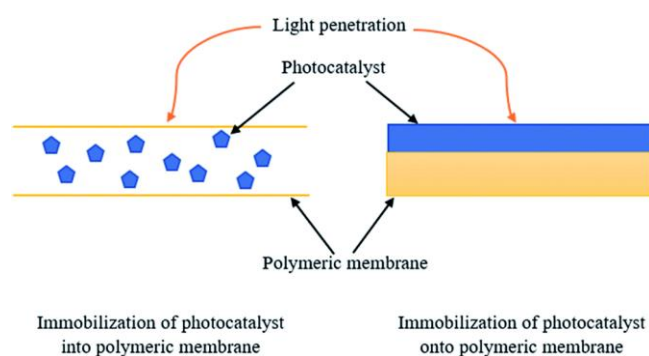
Figure 2-9 Photocatalyst embedded inside the membrane, and photocatalyst deposited on the surface of the membrane. Reprinted from (**Zakria *et al.* 2021**), Copyright 2023 with permission from the Royal Society of Chemistry.

In the second approach, photocatalysts are coated on the surface of the membrane. Two approaches for photocatalyst coating on the membranes are common, i) physical coatings such as dip-coating **(Fischer *et al.* 2018)**, filtration, and physical vapor deposition to name a few, and ii) chemical coating methods such as sol-gel **(Thompson *et al.* 2018)**, chemical vapor deposition **(Romanos *et al.* 2012)**, atomic layer deposition **(Berger *et al.* 2020)**, plasma spray coating **(Lin *et al.* 2012)**, magnetron sputtering **(Takeda *et al.* 2001)**, and in-situ growth process (e.g. hydrothermal growth) **(Yang *et al.* 2015)**.

Some of these methods, in particular chemical vapor deposition or atomic layer deposition, offer ideal control through conformal and uniform coatings but can be complex and relatively costly. On the contrary, dip-coating has been widely used for catalyst coating on different types of substrates and is both simple and viable. In this way, coating thickness can be adjusted by a few parameters such as the mass of the catalyst in solution, immersion duration, withdrawal speed and dipping cycles **(Qing *et al.* 2020)**. In this way, depending on the pore size and porosity of the membrane, photocatalysts diffuse to the pores. Naturally, the uniformity of photocatalyst distribution over the thickness of the membrane and the coating thickness throughout the membrane is more difficult to control in dip coating as evidenced by energy-dispersive x-ray spectroscopy with scanning electron microscopy (EDX-SEM) images **(Qing *et al.* 2020)**. To increase the uptake of photocatalyst by membrane material during coating, membrane materials can be modified prior to the coating which is discussed in the next section.

2.6.3   Enhanced coating

The attachment of photocatalysts to the membrane surface can be a physical attachment or of a chemical nature. As simple as the dip-coating method is, one drawback is the weak physical attachment of nanoparticles and the probability of photocatalysts loss during the filtration process. Therefore, aiming to increase the loading plus strength of attachment between the membrane surface and photocatalysts molecules, modifications on the membrane surface are suggested. The addition of carboxylic groups to the membrane surface enables the TiO_2 nanoparticles to bond covalently with the membrane surface (**Fischer *et al.* 2018**). Moreover, polymeric membranes have a hydrophobic nature, and the attachment of carboxylic groups increases the hydrophilicity of the membrane which helps both the filtration and the deposition of TiO_2 (**Leong *et al.* 2014**).

The chemical grafting method is one of the common ways to modify the membrane surface by adding chemicals like polyacrylic acid (PAA). Other methods like plasma treatment of membranes or electron beam modification for attachment of carboxylic group to the membrane are promising and improve the loading of TiO_2 with great adhesion (**You *et al.* 2012, Fischer *et al.* 2018**). **Figure 2-10** demonstrates an example of plasma treatment of PVDF membrane together with graft polymerization and TiO_2 coating.
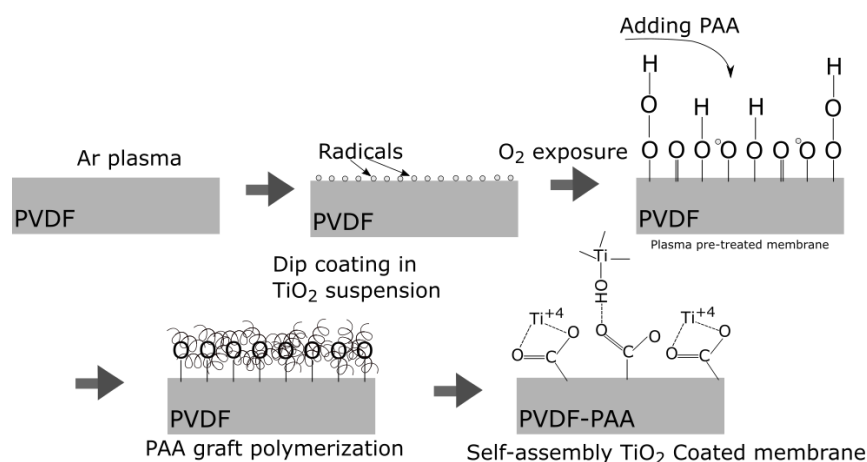
Figure 2-10 Plasma-induced graft polymerization of PAA on PVDF membrane, and self-assembly of TiO_2 nanoparticles on the modified membrane with COOH group, adapted from (**You *et al.* 2012**), Copyright 2023 with permission from Elsevier.

After modification of the PVDF membrane (**Figure 2-10** last step), TiO_2 nanoparticles can attach to the membrane surface either by connecting Ti^{+4} to the oxygen atoms of carboxylate groups or by forming hydrogen bonds between the carbonyl group and the surface hydroxyl group of TiO_2 (**You *et al.* 2012, Leong *et al.* 2014**). Another example of membrane surface modification before coating with TiO_2 was done by Mansourpanah *et al.* (**Mansourpanah *et al.* 2009**). In this study, the prepared PES/polyimide membrane was immersed into a diethanolamine (DEA) solution (1 and 5 wt%) to add hydroxyl groups

to the surface of the membrane. Then this membrane was then dip-coated into TiO$_2$ nanoparticle solution (0.01 and 0.03 wt%) and compared with the membrane without DEA. **Figure 2-11** shows the attached TiO$_2$ on the surface of the membrane and the difference in the attachment sites.
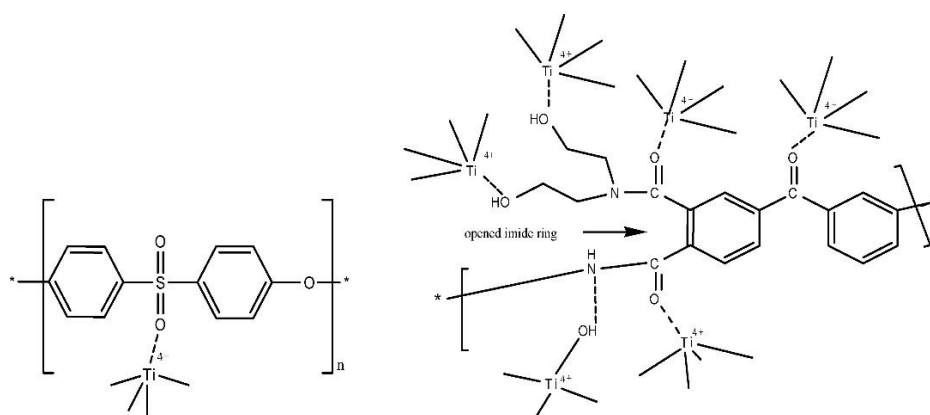
Figure 2-11 Attachment of TiO$_2$ (Ti^{+4}) to the (A) PES surface and (B) DEA-modified PI surface, reprinted (adapted) from (**Mansourpanah *et al.* 2009**). Copyright 2023 with permission from Elsevier.

Other than the membrane material and coating procedure, there are some factors which limit the photocatalytic degradation of MPs. These parameters are discussed in the next sections.

2.7 Limiting factors of operation in a photocatalytic membrane reactor

When operating in a PMR, there are different factors which are critical in the performance of photocatalytic degradation. These can be categorized into two main parts of i) operation parameters in a PMR system including the light source and intensity, water flux, reaction temperature, and photocatalyst concentration, and ii) water solution chemistry namely MP concentration, MP type (molecular structure), pH and surface charge, and presence of other components in the solution. Moreover, the photostability of the photocatalytic membrane is a critical point which can limit the degradation efficiency. Each of these parameters is discussed in the following sections.

2.7.1 Light source and intensity

In terms of operational parameters, the light source (wavelength) is selected based on the bandgap of the photocatalyst. The band gap of the crystal phase of TiO$_2$ (anatase form) is 3.2 eV which means that this semiconductor requires UV light (<387 nm) to be excited (**Ahmad *et al.* 2016**). The intensity of the UV region of sunlight suitable for activation of TiO$_2$ anatase form (300 to 387 nm) is about 3.65 mW/cm^2 which is less than 5% of total sunlight irradiance (**ASTM-International 2012**). Therefore, the operation of a PMR with TiO$_2$ as the photocatalyst is limited to the use of UV light sources.

Light intensity determines the number of photons that are available to irradiate the surface, which then excites electrons and generates ROS **(Ollis *et al.* 1991)** through the chain of reactions mentioned in **Table 2-3**. Therefore, the system yield is highly dependent on the light intensity. For each system, light intensity must be adjusted such that sufficient photons are available while excess will result in energy wastage. In general, three phases are proposed for the dependency of photocatalysis on light intensity. In the first region, below 25 mW/cm^2, the degradation rate rises directly with the increase in light intensity (rate of reaction $\propto$ light intensity). Above a certain value (mostly reported 20-25 mW/cm^2, the rate of electron-hole recombination increases and therefore with a decline in the efficiency of the system, the degree of dependency lowers (rate of reaction $\propto$ (light intensity)$^{1/2}$). After this region, the rate of degradation gets independent of light intensity and the extra energy added to the system is wasted as heat **(Herrmann 2010)**.

2.7.2   Water flux

Water flux is operationally fixed by transmembrane pressure or permeate flow rate as well as intrinsic membrane permeability and determines i) the residence time of a pollutant inside the PMR, and ii) the mass transfer of molecules to the surface of the membrane. In a flow-through PMR, MPs are brought in contact with the photocatalyst inside pores that resemble microchannels **(Renken and Kiwi-Minsker 2010)** and this enhances the mass transfer of MPs to the surface compared to batch or flow-along configurations where transport across boundary layers on surfaces limits photocatalytic reactions **(Gao *et al.* 2020)**. Further, when water flux is increased, this results in increased solute flux, which means that a higher number of MPs is brought to the confined pore for a shorter time. Therefore, the reaction rate could be increased if the amount of solute is limiting the reaction. This phenomenon was shown by Berger *et al.* **(Berger *et al.* 2020)** where the rate of reaction was similar in increasing feed concentration and increasing the water flux. Considering the short length of ROS diffusion, the presence of molecules at the closest vicinity of the surface is important and could limit the reaction efficiency.

2.7.3   Temperature

The temperature of the reaction environment can be adjusted in the process. While the photocatalytic reaction has the benefit of working at room temperature because the energy required for the reaction is provided by the photons **(Malato *et al.* 2009)**. However, adsorption is an important initial step in heterogeneous catalysis (similar to photocatalysis), as explained by Hermann **(Herrmann 2005)**. Adsorption is an exothermic reaction, and based on Van't Hoff's law, a decrease in temperature increases the adsorption constant and hence increases the adsorption rate of MP to the photocatalyst surface

(Herrmann 2005). However, TiO$_2$-mediated photocatalytic reactions between $^•$OH and organic pollutants may occur both in the adsorbed phase and in solution in the close vicinity of the surface **(Ollis et al. 1991, Carretero-Genevrier et al. 2012)**. Temperature further affects the dissolved oxygen (DO) content **(Malato et al. 2009)**. DO declines with temperature from almost 11 to 5 mg/L from 10 to 60 ℃. Oxygen reacts with electrons to generate reactive species **(Malato et al. 2009)**, and if the process is limited by DO availability, then a lower temperature may enhance the process due to the increased oxygen solubility. In addition, DO at the surface can decrease electron-hole recombination through the reaction with electrons and the production of ROS, which will enhance the photocatalytic degradation reaction.

2.7.4   Photocatalyst concentration

One of the main parameters in determining the efficiency of photocatalytic degradation in a PMR is the concentration of the photocatalyst. At low photocatalyst concentrations, the rate of degradation will increase proportionally with the rise in photocatalyst concentration. When the loading of photocatalysts increases, after a certain limit, the rate of degradation would be independent of photocatalyst concentration and adding more photocatalysts will not improve the performance of PMR **(Molinari et al. 2020)**.

2.7.5   Micropollutant concentration

The concentration of MP in the solution to be treated is one of the important parameters that affect the efficiency of the process. MPs are by definition in low concentrations in the solution which can limit the reaction kinetics. At this low concentration level (ng/L range), the reaction typically follows first-order (or apparent first-order) kinetics which means that reaction sites are readily available. At higher feed concentrations, the surface of the membrane may saturate, the reaction gets independent of feed concentration and the reaction rate follows a zero-order reaction rate **(Malato et al. 2009, Herrmann 2010)**. This surface saturation means fewer available free spots for the reaction and therefore decrease in the final removal of the MP.

2.7.6   Micropollutant type

MP structure (chemical characteristics) affects both adsorption and degradation. The structure of the molecule to be degraded, such as the electron density of aromatic rings, and the number of double/triple or saturated bonds can alter the degradation rate **(Coleman et al. 2005, Wang et al. 2009, Ramírez-Sánchez et al. 2017)**. Paredes et al. compared the photodegradation of eight different pharmaceuticals and reported the importance of the molecule's chemical structure **(Paredes et al. 2019)**. In the mechanism

of the photocatalytic reaction, if the reaction happens between $^{\bullet}OH$ generated on the surface of TiO_2 and the pollutant, the structure can have a minimal effect as the $^{\bullet}OH$ is highly reactive and non-selective. However, when the reaction is happening between the generated hole in the valence band and the adsorbed pollutant, the molecule structure (functional group, charge, and size) is significantly vital due to the importance of structure in the adsorption of molecules to the TiO_2 surface which is needed for reaction with the hole (**Friedmann** *et al.* **2010**).

2.7.7   pH and surface charge

The pH value of water has multiple effects on photocatalysis. Firstly, the MP speciation is affected by functional groups dissociating at different pH values. Secondly, the surface charge of the photocatalytic membrane is typically pH dependent. The surface of TiO_2 is covered with hydroxyl groups associated with either OH^- or H_2O, with a surface coverage of 5 to 10 OH^-/nm^2 (**Turchi and Ollis 1990**). Therefore, its surface charge can be described as follows (equations **2-1** and **2-2**) based on the isoelectric point (IEP) (**Ahmed** *et al.* **2011**). The IEP for TiO_2 nanoparticles was reported between pH 3.8 to 6 when the particle size decreases from 104 nm to 6 nm (**Suttiponparnit** *et al.* **2011**).

$$pH < pH_{IEP} \qquad TiOH + H^+ \rightarrow TiOH_2^+ \tag{2-1}$$

$$pH > pH_{IEP} \qquad TiOH + OH^- \rightarrow TiO^- + H_2O \tag{2-2}$$

Further, pH plays an important role in the adsorption of pollutants. Above pKa (if applicable), steroid hormones are in their deprotonated form and may be repelled by negatively charged surfaces (**Schäfer** *et al.* **2011**). This slower adsorption is expected to lower the efficiency of photocatalysis. In addition to membrane and steroid hormones characteristics, pH naturally affects the amount of $^{\bullet}OH$ generation, as a result of different amounts of OH^- in the reaction environment at acidic and alkaline pH (**Zhang** *et al.* **2007**).

2.7.8   Presence of other compounds in the solution

The presence of other species in the background solution that occur in natural waters can also influence photocatalytic degradation. These species can be categorized into organic substances such as humic acid, ions, and metals such as calcium, magnesium, or iron (**Molinari** *et al.* **2017**). Organic substances can hinder the degradation of MPs by occupying the adsorption sites and reducing the efficiency of MP degradation (**Chen** *et al.* **2013**). In the case of ions and metals, their presence can be both positive and negative. On the one hand, these substances can scavenge the generated electron and reduce electron-hole recombination which is a positive point (**Molinari** *et al.* **2017**). On the other hand, by scavenging

the generated ˙OH, the efficiency of MP degradation can drop **(Choo *et al.* 2008)**. The adverse effect of nitrate in the groundwater was observed by Paredes *et al.* **(Paredes *et al.* 2019)** in the comparison between groundwater and secondary effluent of WWTP. In the direct photolysis, Paredes *et al.* noticed a faster kinetic in the secondary effluent of a WWTP and attributed this observation to the presence of some compounds like nitrate or organic matter which can favor the generation of ˙OH radical. However, in the TiO_2-coated membrane, degradation was high regardless of the water matrix **(Paredes *et al.* 2019)**.

Moreover, in case the presence of other compounds leads to higher turbidity of the solution, it can block the light penetration and reduce the process efficiency. Inorganic ions can react with the photogenerated electron and holes or the hydroxyl radical and produce other types of radicals which are all less reactive compared to the ˙OH or the hole. Some examples are present in equations **2-3**, **2-4**, **2-5**, **2-6**, and **2-7**. Therefore, the overall photocatalytic reaction will decrease **(Konstantinou and Albanis 2004)**.

$$HCO_3^- + {}^{\bullet}OH \rightarrow CO_3^{\bullet-} + H_2O \qquad \textbf{2-3}$$

$$CO_3^{2-} + {}^{\bullet}OH \rightarrow CO_3^{\bullet-} + OH^- \qquad \textbf{2-4}$$

$$CO_3^{\bullet-} + e^- \rightarrow CO_3^{2-} \qquad \textbf{2-5}$$

$$Cl^- + {}^{\bullet}OH \rightarrow Cl^{\bullet} + OH^- \qquad \textbf{2-6}$$

$$Cl^{\bullet} + e^- \rightarrow Cl^- \qquad \textbf{2-7}$$
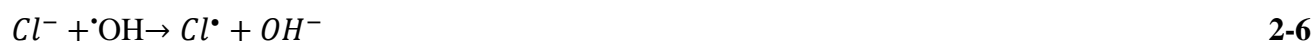
Therefore, investigating the presence of other natural substances depends on the concentration of compounds and the studied system. The next parameter that can limit the photocatalytic degradation of MP is the photostability of the photocatalytic membrane which defines the duration of an efficient application. The photostability of photocatalytic membranes is explained in detail in the next section.

2.7.9   Photostability of photocatalytic membranes

As stated in the previous sections, photocatalytic membranes are capable of degrading hazardous MPs with high efficiency. Polymeric membranes are yet one of the most feasible choices due to their low cost, easy large-scale production, high mechanical stability, and great flexibility **(Mozia *et al.* 2015)**. However, polymeric materials have the main disadvantage, being susceptible to degradation when exposed to long-term UV light and generating ROS **(Leong *et al.* 2014, Molinari *et al.* 2020)**. Therefore, the photostability of photocatalytic membranes, which is the ability to withstand the harsh condition of UV light exposure and attack of in-situ generated ROS is of high importance for the long-term functionality of the system. Different parameters contribute to the photostability of a photocatalytic membrane and decline in its efficiency, namely: i) membrane material (polymeric *vs* ceramic), ii)
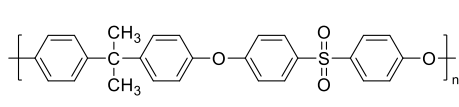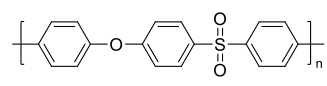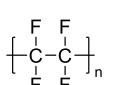
photocatalyst material (organic *vs* inorganic), iii) bond between photocatalyst and membrane (physical *vs* chemical), iv) oxidizing potential of ROS, v) light source (wavelength, intensity, and duration).
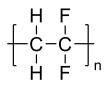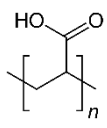
The first parameter to evaluate is membrane material. The functional group forming the molecular structure of the material and the energy required for bond dissociation defines the stability of the material in harsh conditions. Some well-known materials in membrane manufacturing include polysulfone (PS) and polyethersulfone (PES), Polytetrafluoroethylene (PTFE), Polyvinylidene fluoride (PVDF), polyacrylonitrile (PAN), polyvinyl alcohol (PVA) and polyethylene (PE) **(Zakria *et al.* 2021)**. The energy required to break functional groups in some common polymers is presented in **Table 2-5**. Considering the energy of a photon required for bond scission, the corresponding wavelength can be calculated *via* Planck's equation **(Schwalm 2007)**.

$$E = \frac{hc}{\lambda}$$

2-8

where E is the energy of the photon (kJ/mol), *h* is 6.626×10^{-34} Js, *c* is the velocity of light 3×10^8 m/s and λ is the light wavelength (m).

Table 2-5 Functional groups of common polymers in membrane manufacturing, related bond dissociation energy and the corresponding wavelength providing the same energy level **(Giannetti 2005, Luo 2007)**.

Polymer	Chemical bonding	Bond dissociation energy, kJ/mol	Wavelength for bond scission, nm
PS PES 	O_2S-C_{ph} (in $H_3CSO_2-C_6H_5$)	344 ± 8	348 ± 8
	$C-CH_3$ (in $CH_3-tert-C_4H$)	364 ± 3	329 ± 3
	$C-C_{ph}$ (in $CH_3-C_6H_5$)	427 ± 4	280 ± 3
	$C_{ph}-O-C_{ph}$ (in $C_6H_5-OC_6H_5$)	327 ± 4	366 ± 3
	$C_{ph}-H$ (orto)	321–334	358–372
	$C_{ph}-H$ (*meta*)	399 ± 13	300 ± 9
	$C_{ph}=C_{ph}$	518	231
PTFE 	F–C (in HCF_2-CF_2H)	518 ± 18	231 ± 8
	C–C (in HCF_2-CF_2H)	400 ± 15	299 ± 11

PVDF	F–C (in HCF$_2$–CH$_2$F)	482 ± 14	248 ± 8
	C–C (in HCF$_2$–CH$_2$F)	410 ± 16	292 ± 11
	H–C (in HCF$_2$–CH$_2$F)	430 ± 16	278 ± 10
Polyacrylic acid (PAA)	C–C homolytic dissociation	367.8	325
	C–C (radical-induced) retro-polymerization	77.4	UV-Vis-NIR

It can be concluded that a simple material like polypropylene which only consists of the methyl group (-CH-) is more prone to degradation as the energy associated with the UVA range of the solar spectrum (315-400 nm) is sufficient for methyl group bond cleavage. This was observed by **(Allen and Edge 1992, Chin *et al.* 2006)** that polypropylene was degraded faster than other studied polymers under only UV light.

Among others, the sulfur group is highly susceptible to breaking under UV light **(Allen and Edge 1992, Chin *et al.* 2006)**. Comparing functional groups in **Table 2-5**, it can be understood that the highest energy is required for breakage of the F–C bond in PTFE and then PVDF which can be proof for observation by researchers that these membranes are more resistant than others **(Chin *et al.* 2006)**. If membranes are functionalized with additives, such as PAA, to increase the hydrophilicity or attachment of photocatalyst (Section Enhanced coating 2.6.3), it can be expected that the carboxylic groups added to the membrane surface are even more likely to undergo chain scission **(Lalia *et al.* 2013)**.

The next parameter affecting the photostability of photocatalytic membranes is the photocatalyst material, which can be an organic compound or a semiconductor, for example. The semiconductor materials like TiO$_2$ or ZnO are strong toward light exposure, although they must be excited with UV light which can degrade the polymeric membrane. On the other hand, organic photocatalysts like porphyrin (a photosensitizer) can be activated by visible light which is less damaging to the polymeric membrane. However, the photosensitizer itself is highly prone to degradation (photobleaching) under light exposure, even visible light **(Lacombe and Pigot 2016)**.

The photocatalyst material also determines which one of the ROSs is mainly produced in the process. As presented in **Figure 2-4**, the oxidation potential of the oxidative potential of $^{\bullet}$OH is the highest among the other common ROSs in photocatalysis. Researchers **(Yang *et al.* 2009, Lima *et al.* 2019)** stated that in TiO$_2$ photocatalysis, the dominant generated ROS responsible for the degradation of their target pollutant is $^{\bullet}$OH. This species is unselective and highly reactive with a short lifetime. Therefore, $^{\bullet}$OH can

attack any compound in its vicinity and degrade it. Whereas the selectivity and lifetime of $^1O_2$ (produced by photosensitizers as an example) differ in different polymer materials, with higher selectivity toward unsaturated electron-rich bonds. Therefore, depending on the interaction between $^1O_2$ and the polymer, the stability of the photocatalytic membranes varies **(Rabek and Rånby 1978, Ogilby *et al.* 1996)**.

The photocatalyst deposition method is another important parameter affecting the final photostability and efficiency of the photocatalytic membrane. Considering the physical or chemical bonds between the photocatalyst and membrane, the strength of the attachment is determined. The physical bonds like Van der Waals or H-bonding are significantly weaker than the chemical ones such as covalent or ionic bonds and therefore more likely to break under photocatalysis conditions. Another point to consider is that the layer of photocatalyst on the membrane surface can absorb the UV light which consequently prevents the membrane from deterioration by direct photolysis **(Molinari *et al.* 2000, Chin *et al.* 2006, Petrochenko *et al.* 2013)**.

The last yet important parameter is the light properties, wavelength, intensity, and duration of exposure. By reducing the wavelength of light, the energy of each photon rises. UV light has the highest energy even though it comprises less than 5% of the total solar light intensity **(ASTM-International)**. The intensity of light defines the number of photons emitted per unit of time and area. Both an increase in light intensity and extending the duration of exposure expose the photocatalytic membrane to a more detrimental condition.

All in all, choosing the proper material for photocatalysis purposes requires extensive laboratory research which takes months if the aim is to compare with the industrial-scale application of the photocatalytic membrane. A review by Mills *et al.* in 2012 **(Mills *et al.* 2012)**, presented standards in the field of photocatalysis, including standards for photocatalytic activity determination of surfaces, water and air purification, antibacterial activity (sterilization) and self-cleaning performance of semiconductor photocatalytic materials. There are more recent guidelines for the assessment of photocatalysis application and performance like EN 17120:2019 which is developed by a technical committee working for the European Committee of Standardization (EN/TC 386 2019 **(The European Committee for Standardization 2019)**). However, this guideline is only focused on the method development for pollutant removal (phenol as the standard) by photocatalyst in powder form and not on the lifetime of either the photocatalyst or the support material **(The European Committee for Standardization 2019)**. Unfortunately, no standards have been developed so far for evaluating the photostability of photocatalytic membranes.

Most studies reported short time light exposure for material selection from a few hours to a few days which is not comparable to the real application **(Molinari *et al.* 2000, Chin *et al.* 2006, Mozia *et al.* 2015)**. However, long-duration experiments (months) for material selections are not feasible either. To address this issue, accelerated ageing experiments are presented to shorten the time required for approval of material before industrial-scale application **(Martin *et al.* 2003)**. In this method, the light intensity is increased, and the exposure time is reduced to keep a constant light dose (intensity × duration). The negative aspect of this method is that the high energy of UV light can be detrimental to polymers in extreme light intensities and makes the comparison with real applications difficult **(Pospíšil *et al.* 2006)**.

2.7.10 Evaluation of photostability

Various techniques have been utilized for evaluating the photostability of photocatalytic membranes. These techniques can be categorized into a few sections: i) visual observation, ii) microscopic methods (Scanning electron microscopy, Atomic force microscopy, etc.), iii) spectroscopic methods (light absorption *via* UV-vis spectroscopy, Fourier Transform Infrared (FTIR) spectroscopy, Nuclear magnetic resonance (NMR) spectroscopy, X-ray photoelectron spectroscopy (XPS), EDX spectroscopy, and vi) mass spectroscopy (Time-of-Flight Secondary Ion Mass spectrometry (ToF-SIMS), Inductively coupled plasma optical emission spectroscopy (ICP-OES) mass spectrometry, Total organic carbon (TOC).

Molinari *et al.* **(Molinari *et al.* 2000)** examined 11 polymeric membranes by irradiating them in water for 24 hr under a 500 W medium-pressure mercury lamp with a max wavelength of 365 nm and intensity of 6.4 mW/cm^2. They measured the TOC level of water samples and water flux before and after irradiation and reported that polyacrylonitrile (PAN), fluoride+polypropylene (PP) and PS+PP are more stable than others. Chin *et al.* **(Chin *et al.* 2006)** reported PVDF and PTFE membranes to be suitable choices for photocatalytic experiments by exposing different polymeric membranes to oxidative conditions (200 mM H_2O_2) and UV light (2.1 mW/cm^2, light source 365 nm) for 10 days. They evaluated the stability of membranes based on pure water flux, the release of TOC, scanning electron microscopic images and FTIR spectrum before and after ageing experiments.

2.8   References

Abdullah, N., M. A. Rahman, M. H. Dzarfan Othman, J. Jaafar and A. F. Ismail (2018). Chapter 2 - Membranes and Membrane Processes: Fundamentals. Current Trends and Future Developments on (Bio-) Membranes. A. Basile, S. Mozia and R. Molinari, Elsevier: 45-70.

Adeel, M., X. Song, Y. Wang, D. Francis and Y. Yang (2017). "Environmental impact of estrogens on human, animal and plant life: A critical review." Environment International **99**: 107-119.

Ahmad, R., Z. Ahmad, A. U. Khan, N. R. Mastoi, M. Aslam and J. Kim (2016). "Photocatalytic systems as an advanced environmental remediation: Recent developments, limitations and new avenues for applications." Journal of Environmental Chemical Engineering **4**: 4143-4164.

Ahmed, S., M. G. Rasul, R. Brown and M. A. Hashib (2011). "Influence of parameters on the heterogeneous photocatalytic degradation of pesticides and phenolic contaminants in wastewater: a short review." Journal of Environmental Management **92**: 311-330.

Ahting, M., F. Brauer, A. Duffek, I. Ebert, A. Eckhardt, E. Hassold, M. Helmecke, I. Kirst, B. Krause and P. Lepom (2018). Recommendations for reducing micropollutants in waters, German Environment Agency.

Akpan, U. G. and B. H. Hameed (2009). "Parameters affecting the photocatalytic degradation of dyes using TiO2-based photocatalysts: a review." Journal of Hazardous Materials **170**: 520-529.

Allen, N. S. and M. Edge (1992). Fundamentals of polymer degradation and stabilization, Springer Science & Business Media.

Alvarez, P. J. J., C. K. Chan, M. Elimelech, N. J. Halas and D. Villagrán (2018). "Emerging opportunities for nanotechnology to enhance water security." Nature Nanotechnology **13**: 634-641.

Alvarez-Corena, J. R., J. A. Bergendahl and F. L. Hart (2016). "Advanced oxidation of five contaminants in water by UV/TiO$_2$: Reaction kinetics and byproducts identification." Journal of Environmental Management **181**: 544-551.

Andreozzi, R., V. Caprio, A. Insola and R. Marotta (1999). "Advanced oxidation processes (AOP) for water purification and recovery." Catalysis today **53**: 51-59.

Argurio, P., E. Fontananova, R. Molinari and E. Drioli (2018). "Photocatalytic Membranes in Photocatalytic Membrane Reactors." Processes **6**: 162.

Aris, A. Z., A. S. Shamsuddin and S. M. Praveena (2014). "Occurrence of 17α-ethynylestradiol (EE2) in the environment and effect on exposed biota: a review." Environment International **69**: 104-119.

Arnold, S. F., Judith M. Bergeron, Dat Q. Tran, Bridgette M. Collins, Peter M. Vonier, David Crews, William A. Toscano Jr and J. A. McLachlan. (1997). "Synergistic Responses of Steroidal Estrogens in Vitro (Yeast) and in Vivo (Turtles)." Biochemical and Biophysical Research Communications **235**: 336-342.

ASTM-International "G173-03 (2012) Standard tables for reference solar spectral irradiances: Direct normal and hemispherical on 37° tilted surface." West Conshohocken, PA; ASTM International.

Barry, B. and D. E. Eini (1976). "Solubilization of hydrocortisone, dexamethasone, testosterone and progesterone by long-chain polyoxyethylene surfactants." Journal of Pharmacy and Pharmacology 28: 210-218.

Benotti, M. J., B. D. Stanford, E. C. Wert and S. A. Snyder (2009). "Evaluation of a photocatalytic reactor membrane pilot system for the removal of pharmaceuticals and endocrine disrupting compounds from water." Water Research **43**: 1513-1522.

Berger, T. E., C. Regmi, A. I. Schäfer and B. S. Richards (2020). "Photocatalytic degradation of organic dye *via* atomic layer deposited TiO$_2$ on ceramic membranes in single-pass flow-through operation." Journal of Membrane Science **604**: 118015.

Bhandari, A., R. Y. Surampalli, C. D. Adams, P. Champagne, S. K. Ong, R. D. Tyagi and T. C. Zhang (2009). Contaminants of emerging environmental concern. Reston, Virginia, USA, American Society of Civil Engineers.

Brion, F., Y. Le Page, B. Piccini, O. Cardoso, S. K. Tong, B. C. Chung and O. Kah (2012). "Screening Estrogenic Activities of Chemicals or Mixtures In Vivo Using Transgenic (cyp19a1b-GFP) Zebrafish Embryos." PLoS ONE **7**: e36069.

Camacho-Muñoz, D., J. Martin, J. L. Santos, I. Aparicio and E. Alonso (2009). "An affordable method for the simultaneous determination of the most studied pharmaceutical compounds as wastewater and surface water pollutants." Journal of separation science **32**: 3064-3073.

Cao, Y., X. Li, Z. Bian, A. Fuhr, D. Zhang and J. Zhu (2016). "Highly photocatalytic activity of brookite/rutile TiO_2 nanocrystals with semi-embedded structure." Applied Catalysis B: Environmental **180**: 551-558.

Carretero-Genevrier, A., C. Boissiere, L. Nicole and D. Grosso (2012). "Distance dependence of the photocatalytic efficiency of TiO_2 revealed by in situ ellipsometry." Journal of the American Chemical Society **134**: 10761-10764.

Chen, Y., K. Zhang and Y. Zuo (2013). "Direct and indirect photodegradation of estriol in the presence of humic acid, nitrate and iron complexes in water solutions." Science of the Total Environment **463-464**: 802-809.

Chin, S. S., K. Chiang and A. G. Fane (2006). "The stability of polymeric membranes in a TiO_2 photocatalysis process." Journal of Membrane Science **275**: 202-211.

Choo, K. H., D. I. Chang, K. W. Park and M. H. Kim (2008). "Use of an integrated photocatalysis/hollow fiber microfiltration system for the removal of trichloroethylene in water." Journal of Hazardous Materials **152**: 183-190.

Coleman, H. M., E. J. Routledge, J. P. Sumpter, B. R. Eggins and J. A. Byrne (2004). "Rapid loss of estrogenicity of steroid estrogens by UVA photolysis and photocatalysis over an immobilised titanium dioxide catalyst." Water Research **38**: 3233-3240.

Coleman, H. M., M. I. Abdullah, B. R. Eggins and F. L. Palmer (2005). "Photocatalytic degradation of 17β-oestradiol, oestriol and 17α-ethynyloestradiol in water monitored using fluorescence spectroscopy." Applied Catalysis B: Environmental **55**: 23-30.

Fedorova, E., L. Shashkina and V. Fedorov (1976). "Towards a method of determining the solubility of testosterone derivatives." Pharmaceutical Chemistry Journal 10: 412-415.

Fischer, K., M. Grimm, J. Meyers, C. Dietrich, R. Gläser and A. Schulze (2015). "Photoactive microfiltration membranes *via* directed synthesis of TiO2 nanoparticles on the polymer surface for removal of drugs from water." Journal of Membrane Science **478**: 49-57.

Fischer, K., P. Schulz, I. Atanasov, A. Abdul Latif, I. Thomas, M. Kühnert, A. Prager, J. Griebel and A. Schulze (2018). "Synthesis of High Crystalline TiO_2 Nanoparticles on a Polymer Membrane to Degrade Pollutants from Water." Catalysts **8**: 376.

Fischer, K., R. Gläser and A. Schulze (2014). "Nanoneedle and nanotubular titanium dioxide – PES mixed matrix membrane for photocatalysis." Applied Catalysis B: Environmental **160-161**: 456-464.

Friedmann, D., C. Mendive and D. Bahnemann (2010). "TiO_2 for water treatment: Parameters affecting the kinetics and mechanisms of photocatalysis." Applied Catalysis B: Environmental **99**: 398-406.

Fujishima, A., X. Zhang and D. Tryk (2008). "TiO_2 photocatalysis and related surface phenomena." Surface Science Reports **63**: 515-582.

Gale, M. M. and L. Saunders (1971). "The solubilisation of steroids by lysophosphatidylcholine. Testosterone, estradiol and their 17α-ethinyl derivations." Biochimica et Biophysica Acta (BBA)-Lipids and Lipid Metabolism 248: 466-470.

Gao, Y., N. Yan, C. Jiang, C. Xu, S. Yu, P. Liang, X. Zhang, S. Liang and X. Huang (2020). "Filtration-enhanced highly efficient photocatalytic degradation with a novel electrospun rGO@TiO$_2$ nanofibrous membrane: Implication for improving photocatalytic efficiency." Applied Catalysis B: Environmental **268**: 118737.

Giannetti, E. (2005). "Thermal stability and bond dissociation energy of fluorinated polymers: A critical evaluation." Journal of Fluorine Chemistry **126**: 623-630.

Haggerty, J. E. S., L. T. Schelhas, D. A. Kitchaev, J. S. Mangum, L. M. Garten, W. Sun, K. H. Stone, J. D. Perkins, M. F. Toney, G. Ceder, D. S. Ginley, B. P. Gorman and J. Tate (2017). "High-fraction brookite films from amorphous precursors." Scientific Reports **7**: 15232.

Hama Aziz, K. H., H. Miessner, S. Mueller, D. Kalass, D. Moeller, I. Khorshid and M. A. M. Rashid (2017). "Degradation of pharmaceutical diclofenac and ibuprofen in aqueous solution, a direct comparison of ozonation, photocatalysis, and non-thermal plasma." Chemical Engineering Journal **313**: 1033-1041.

Hansch, C., A. Leo and D. H. Hoekman (1995). Exploring QSAR: Hydrophobic, electronic, and steric constants. Washington DC, American Chemical Society.

Herrmann, J. M. (2005). "Heterogeneous photocatalysis: state of the art and present applications." Topics in Catalysis **34**: 49-65.

Herrmann, J. M. (2010). "Photocatalysis fundamentals revisited to avoid several misconceptions." Applied Catalysis B: Environmental **99**: 461-468.

Hodges, B. C., E. L. Cates and J. H. Kim (2018). "Challenges and prospects of advanced oxidation water treatment processes using catalytic nanomaterials." Nature Nanotechnology **13**: 642-650.

Hofstadler, K., R. Bauer, S. Novalic and G. Heisler (1994). "New Reactor Design for Photocatalytic Wastewater Treatment with TiO2 Immobilized on Fused-Silica Glass Fibers: Photomineralization of 4-Chlorophenol." Environmental Science & Technology **28**: 670-674.

Horovitz, I., D. Avisar, M. A. Baker, R. Grilli, L. Lozzi, D. Di Camillo and H. Mamane (2016). "Carbamazepine degradation using a N-doped TiO$_2$ coated photocatalytic membrane reactor: Influence of physical parameters." Journal of Hazardous Materials **310**: 98-107.

Hurum, D. C., A. G. Agrios, K. A. Gray, T. Rajh and M. C. Thurnauer (2003). "Explaining the enhanced photocatalytic activity of Degussa P25 mixed-phase TiO$_2$ using EPR." The Journal of Physical Chemistry B **107**: 4545-4549.

Hurwitz, A. R. and S. T. Liu (1977). "Determination of Aqueous Solubility and pKa Values of Estrogen." Journal of Pharmaceutical Sciences 66: 624-627.

Iglesias, O., M. J. Rivero, A. M. Urtiaga and I. Ortiz (2016). "Membrane-based photocatalytic systems for process intensification." Chemical Engineering Journal **305**: 136-148.

Kakuma, Y., A. Y. Nosaka and Y. Nosaka (2015). "Difference in TiO$_2$ photocatalytic mechanism between rutile and anatase studied by the detection of active oxygen and surface species in water." Physical Chemistry Chemical Physics **17**: 18691-18698.

Konstantinou, I. K. and T. A. Albanis (2004). "TiO$_2$-assisted photocatalytic degradation of azo dyes in aqueous solution: kinetic and mechanistic investigations." Applied Catalysis B: Environmental **49**: 1-14.

Lacombe, S. and T. Pigot (2016). "Materials for selective photo-oxygenation vs. photocatalysis: preparation, properties and applications in environmental and health fields." Catalysis Science & Technology **6**: 1571-1592.

Lalia, B. S., V. Kochkodan, R. Hashaikeh and N. Hilal (2013). "A review on membrane fabrication: Structure, properties and performance relationship." Desalination **326**: 77-95.

Landmann, M., E. Rauls and W. G. Schmidt (2012). "The electronic structure and optical response of rutile, anatase and brookite TiO$_2$." Journal of Physics: Condensed Matter **24**: 195503.

Lata, G. F. and L. K. Dac (1965). "Steroid solubility studies with aqueous solutions of urea and ureides." Archives of Biochemistry and Biophysics 109: 434-441.

Leong, S., A. Razmjou, K. Wang, K. Hapgood, X. Zhang and H. Wang (2014). "TiO$_2$ based photocatalytic membranes: A review." Journal of Membrane Science **472**: 167-184.

Lewis, K. M. and R. D. Archer (1979). "pKa values of estrone, 17β-estradiol and 2-methoxyestrone." Steroids 34: 485-499.

Li Puma, G., V. Puddu, H. K. Tsang, A. Gora and B. Toepfer (2010). "Photocatalytic oxidation of multicomponent mixtures of estrogens (estrone (E1), 17β-estradiol (E2), 17α-ethynylestradiol (EE2) and estriol (E3)) under UVA and UVC radiation: Photon absorption, quantum yields and rate constants independent of photon absorption." Applied Catalysis B: Environmental **99**: 388-397.

Li, G., S. Ciston, Z. Saponjic, L. Chen, N. Dimitrijevic, T. Rajh and K. Gray (2008). "Synthesizing mixed-phase TiO$_2$ nanocomposites using a hydrothermal method for photo-oxidation and photoreduction applications." Journal of Catalysis **253**: 105-110.

Lima, K. V. L., E. S. Emídio, R. F. Pupo Nogueira, N. d. S. L. S. Vasconcelos and A. B. Araújo (2019). "Application of a stable Ag/TiO$_2$ film in the simultaneous photodegradation of hormones." Journal of Chemical Technology & Biotechnology **95**: 2656-2663.

Lin, Y. F., K. L. Tung, Y.-S. Tzeng, J. H. Chen and K. S. Chang (2012). "Rapid atmospheric plasma spray coating preparation and photocatalytic activity of macroporous titania nanocrystalline membranes." Journal of Membrane Science **389**: 83-90.

Litter, M. I. (1999). "Heterogeneous photocatalysis: transition metal ions in photocatalytic systems." Applied Catalysis B: Environmental **23**: 89-114.

Litwack, G. (2022). Chapter 16 - Steroid Hormones. Human Biochemistry (Second Edition). G. Litwack. Boston, Academic Press**:** 517-558.

Liu, S., C. Carney and A. Hurwitz (1977). "Adsorption as a possible limitation in solubility determination." Journal of Pharmacy and Pharmacology 29: 319-321.

Liz, M. V. d., R. M. d. Lima, B. d. Amaral, B. Marinho, J. Schneider, N. Nagata and P. Peralta-Zamora (2017). "Suspended and Immobilized TiO$_2$ Photocatalytic Degradation of Estrogens: Potential for Application in Wastewater Treatment Processes." Journal of the Brazilian Chemical Society **29**: 380-389.

Loddo, V., M. Bellardita, G. Camera-Roda, F. Parrino and L. Palmisano (2018). Heterogeneous Photocatalysis: A Promising Advanced Oxidation Process. Current Trends and Future Developments on (Bio-) Membranes, Elsevier**:** 1-43.

Loeb, S. K., P. J. J. Alvarez, J. A. Brame, E. L. Cates, W. Choi, J. Crittenden, D. D. Dionysiou, Q. Li, G. Li-Puma, X. Quan, D. L. Sedlak, T. David Waite, P. Westerhoff and J. H. Kim (2019). "The Technology Horizon for Photocatalytic Water Treatment: Sunrise or Sunset?" Environmental Science & Technology **53**: 2937-2947.

Lotfi, S., K. Fischer, A. Schulze and A. I. Schäfer (2022). "Photocatalytic degradation of steroid hormone micropollutants by TiO_2 coated polyethersulfone membranes in a continuous flow-through process." Nature Nanotechnology **17**: 417–423.

Lundberg, B. (1979). "Temperature effect on the water solubility and water-octanol partition of some steroids." Acta Pharm Suec 16: 151-159.

Lundberg, B., T. Lövgren and B. Heikius (1979). "Simultaneous Solubilization of Steroid Hormones II: Androgens and Estrogens." Journal of Pharmaceutical Sciences 68: 542-545.

Luo, Y. R. (2007). Comprehensive handbook of chemical bond energies, CRC press.

Luttrell, T., S. Halpegamage, J. Tao, A. Kramer, E. Sutter and M. Batzill (2014). "Why is anatase a better photocatalyst than rutile? - Model studies on epitaxial TiO_2 films." Scientific Reports **4**: 1-8.

Lyubimenko, R., O. I. Gutierrez Cardenas, A. Turshatov, B. S. Richards and A. I. Schäfer (2021). "Photodegradation of steroid-hormone micropollutants in a flow-through membrane reactor coated with Pd(II)-porphyrin." Applied Catalysis B: Environmental **291**: 120097.

Mai, J., W. Sun, L. Xiong, Y. Liu and J. Ni (2008). "Titanium dioxide mediated photocatalytic degradation of 17beta-estradiol in aqueous solution." Chemosphere **73**: 600-606.

Malato, S., P. Fernández-Ibáñez, M. I. Maldonado, J. Blanco and W. Gernjak (2009). "Decontamination and disinfection of water by solar photocatalysis: Recent overview and trends." Catalysis Today **147**: 1-59.

Manickum, T. and W. John (2014). "Occurrence, fate and environmental risk assessment of endocrine disrupting compounds at the wastewater treatment works in Pietermaritzburg (South Africa)." Sci Total Environ **468-469**: 584-597.

Mansourpanah, Y., S. S. Madaeni, A. Rahimpour, A. Farhadian and A. H. Taheri (2009). "Formation of appropriate sites on nanofiltration membrane surface for binding TiO_2 photo-catalyst: Performance, characterization and fouling-resistant capability." Journal of Membrane Science **330**: 297-306.

Marinangeli, R. E. and D. F. Ollis (1977). "Photoassisted heterogeneous catalysis with optical fibers: I. Isolated single fiber." AIChE Journal **23**: 415-426.

Martin, J. W., J. W. Chin and T. Nguyen (2003). "Reciprocity law experiments in polymeric photodegradation: a critical review." Progress in Organic Coatings **47**: 292-311.

Mboula, V. M., V. Héquet, Y. Andrès, Y. Gru, R. Colin, J. M. Doña-Rodríguez, L. M. Pastrana-Martínez, A. M. T. Silva, M. Leleu, A. J. Tindall, S. Mateos and P. Falaras (2015). "Photocatalytic degradation of estradiol under simulated solar light and assessment of estrogenic activity." Applied Catalysis B: Environmental **162**: 437-444.

Mendret, J., M. Hatat-Fraile, M. Rivallin and S. Brosillon (2013). "Hydrophilic composite membranes for simultaneous separation and photocatalytic degradation of organic pollutants." Separation and Purification Technology **111**: 9-19.

Menon, N. G., L. George, S. S. V. Tatiparti and S. Mukherji (2021). "Efficacy and reusability of mixed-phase TiO_2–ZnO nanocomposites for the removal of estrogenic effects of 17β-Estradiol and 17α-Ethinylestradiol from water." Journal of Environmental Management **288**: 112340.

Mills, A., C. Hill and P. K. J. Robertson (2012). "Overview of the current ISO tests for photocatalytic materials." Journal of Photochemistry and Photobiology A: Chemistry **237**: 7-23.

Molinari, R., M. Mungari, E. Drioli, A. Di Paola, V. Loddo, L. Palmisano and M. Schiavello (2000). "Study on a photocatalytic membrane reactor for water purification." Catalysis Today **55**: 71-78.

Molinari, R., P. Argurio, K. Szymański, D. Darowna and S. Mozia (2020). "Photocatalytic membrane reactors for wastewater treatment." Current Trends and Future Developments on (Bio-) Membranes: 83-116.

Molinari, R., P. Argurio, M. Bellardita and L. Palmisano (2017). 3.5 Photocatalytic Processes in Membrane Reactors. Comprehensive Membrane Science and Engineering. E. Drioli, L. Giorno and E. Fontananova, Elsevier. **3**: 101-138.

Mombelli, E. (2012). "Evaluation of the OECD (Q)SAR Application Toolbox for the profiling of estrogen receptor binding affinities." SAR and QSAR in Environmental Research **23**: 37-57.

Mozia, S. (2010). "Photocatalytic membrane reactors (PMRs) in water and wastewater treatment. A review." Separation and Purification Technology **73**: 71-91.

Mozia, S., D. Darowna, R. Wróbel and A. W. Morawski (2015). "A study on the stability of polyethersulfone ultrafiltration membranes in a photocatalytic membrane reactor." Journal of Membrane Science **495**: 176-186.

Nakashima, T., Y. Ohko, Y. Kubota and A. Fujishima (2003). "Photocatalytic decomposition of estrogens in aquatic environment by reciprocating immersion of TiO_2-modified polytetrafluoroethylene mesh sheets." Journal of Photochemistry and Photobiology A: Chemistry **160**: 115-120.

Ogilby, P. R., M. Kristiansen, D. O. Mártire, R. D. Scurlock, V. L. Taylor and R. L. Clough (1996). Formation and Removal of Singlet ($a^1\Delta_g$) Oxygen in Bulk Polymers: Events That May Influence Photodegradation. Polymer Durability: 113-126.

Ohko, Y., K. I. Iuchi, C. Niwa, T. Tatsuma, T. Nakashima, T. Iguchi, Y. Kubota and A. Fujishima (2002). "17β-Estradiol Degradation by TiO_2 Photocatalysis as a Means of Reducing Estrogenic Activity." Environmental Science & Technology **36**: 4175-4181.

Ollis, D. F. (2003). "Integrating photocatalysis and membrane technologies for water treatment." Annals of the New York Academy of Sciences **984**: 65-84.

Ollis, D. F., E. Pelizzetti and N. Serpone (1991). "Photocatalyzed destruction of water contaminants." Environmental Science & Technology **25**: 1522-1529.

Onishi, T. (2012). Chapter 2 - Quantum Chemistry in Functional Inorganic Materials. Advances in Quantum Chemistry. J. R. Sabin and E. J. Brändas, Academic Press. **64:** 31-81.

Orozco-Hernández, L., L. M. Gómez-Oliván, A. Elizalde-Velázquez, R. Natividad, L. Fabian-Castoño and N. SanJuan-Reyes (2019). "17-β-Estradiol: Significant reduction of its toxicity in water treated by photocatalysis." Science of the Total Environment **669**: 955-963.

Padovan, R. N., L. S. de Carvalho, P. L. de Souza Bergo, C. Xavier, A. Leitão, Á. J. dos Santos Neto, F. M. Lanças and E. B. Azevedo (2021). "Degradation of hormones in tap water by heterogeneous solar TiO_2-photocatalysis: Optimization, degradation products identification, and estrogenic activity removal." Journal of Environmental Chemical Engineering **9**: 106442.

Pan, Z., E. A. Stemmler, H. J. Cho, W. Fan, L. A. LeBlanc, H. H. Patterson and A. Amirbahman (2014). "Photocatalytic degradation of 17alpha-ethinylestradiol (EE2) in the presence of TiO_2-doped zeolite." Journal of Hazardous Materials **279**: 17-25.

Paredes, L., S. Murgolo, H. Dzinun, M. H. Dzarfan Othman, A. F. Ismail, M. Carballa and G. Mascolo (2019). "Application of immobilized TiO_2 on PVDF dual layer hollow fibre membrane to improve the photocatalytic removal of pharmaceuticals in different water matrices." Applied Catalysis B: Environmental **240**: 9-18.

Pérez, M., F. Torrades, X. Domenech and J. Peral (2002). "Fenton and photo-Fenton oxidation of textile effluents." Water Research **36**: 2703-2710.

Perrin, D. D., B. Dempsey and E. P. Serjeant (1981). pKa prediction for organic acids and bases. London; New York, Chapman and Hall.

Petrochenko, P. E., G. Scarel, G. K. Hyde, G. N. Parsons, S. A. Skoog, Q. Zhang, P. L. Goering and R. J. Narayan (2013). "Prevention of Ultraviolet (UV)-Induced Surface Damage and Cytotoxicity of Polyethersulfone Using Atomic Layer Deposition (ALD) Titanium Dioxide." JOM **65**: 550-556.

Pospíšil, J., J. Pilař, N. C. Billingham, A. Marek, Z. Horák and S. Nešpůrek (2006). "Factors affecting accelerated testing of polymer photostability." Polymer Degradation and Stability **91**: 417-422.

Qing, W., F. Liu, H. Yao, S. Sun, C. Chen and W. Zhang (2020). "Functional catalytic membrane development: A review of catalyst coating techniques." Advances in Colloid and Interface Science **282**: 102207.

Rabek, J. F. and B. Rånby (1978). "The role of singlet oxygen in the photooxidation of polymers." Photochemistry and Photobiology **28**: 557-569.

Ramírez-Sánchez, I. M., M. Á. Méndez-Rojas and E. R. Bandala (2017). CHAPTER 25 Photocatalytic Degradation of Natural and Synthetic Estrogens with Semiconducting Nanoparticles. Advanced Environmental Analysis: Applications of Nanomaterials **2:** 153-177.

Renken, A. and L. Kiwi-Minsker (2010). Microstructured Catalytic Reactors. Advances in Catalysis, Elsevier. **53:** 47-122.

Renz, C. (1921). "Lichtreaktionen der oxyde des titans, cers und der erdsäuren." Helvetica Chimica Acta **4**: 961-968.

Riaz, S. and S.-J. Park (2020). "An overview of TiO_2-based photocatalytic membrane reactors for water and wastewater treatments." Journal of Industrial and Engineering Chemistry **84**: 23-41.

Romanos, G. E., C. P. Athanasekou, F. K. Katsaros, N. K. Kanellopoulos, D. D. Dionysiou, V. Likodimos and P. Falaras (2012). "Double-side active TiO_2-modified nanofiltration membranes in continuous flow photocatalytic reactors for effective water purification." Journal of Hazardous Materials **211-212**: 304-316.

Ruchelman, M. W. (1967). "Solubility studies of estrone in organic solvents using gas-liquid chromatography." Analytical Biochemistry 19: 98-108.

Ruchelman, M. W. (1971). "Solubility Studies of Testosterone in Organic Solvents Using Gas Chromatography." Journal of Chromatographic Science 9: 235-240.

Ruchelman, M. W. and P. Haines (1967). "Solubility Studies of Estradiol in Organic Solvents Using Gas-Liquid Chromatography." Journal of Chromatographic Science 5: 290-296.

Salole, E. G. (1986). Estradiol. Analytical profiles of drug substances, Elsevier. 15: 283-318.

Schäfer, A. I., I. Akanyeti and A. J. Semiao (2011). "Micropollutant sorption to membrane polymers: a review of mechanisms for estrogens." Advances in Colloid and Interface Science **164**: 100-117.

Schwalm, R. (2007). CHAPTER 2 - The UV Curing Process. UV Coatings. R. Schwalm. Amsterdam, Elsevier**:** 19-61.

Servos, M. R., D. T. Bennie, B. K. Burnison, A. Jurkovic, R. McInnis, T. Neheli, A. Schnell, P. Seto, S. A. Smyth and T. A. Ternes (2005). "Distribution of estrogens, 17beta-estradiol and estrone, in Canadian municipal wastewater treatment plants." Science of the Total Environment **336**: 155-170.

Shareef, A., M. J. Angove, J. D. Wells and B. B. Johnson (2006). "Aqueous solubilities of Estrone, 17β-Estradiol, 17α-Ethynylestradiol, and Bisphenol A." Journal of Chemical & Engineering Data 51: 879-881.

Sieminska, L., M. Ferguson, T. W. Zerda and E. Couch (1997). "Diffusion of steroids in porous sol-gel glass: application in slow drug delivery." Journal of Sol-Gel Science and Technology 8: 1105-1109.

Silva, L. L. S., J. C. S. Sales, J. C. Campos, D. M. Bila and F. V. Fonseca (2017). "Advanced oxidative processes and membrane separation for micropollutant removal from biotreated domestic wastewater." Environmental Science and Pollution Research **24**: 6329-6338.

Song, H., J. Shao, Y. He, B. Liu and X. Zhong (2012). "Natural organic matter removal and flux decline with PEG–TiO_2-doped PVDF membranes by integration of ultrafiltration with photocatalysis." Journal of Membrane Science **405-406**: 48-56.

Souissi, Y., S. Kinani, S. Bouchonnet, S. Bourcier, C. Malosse, M. Sablier, N. Creusot, E. Mombelli and S. Ait-Aissa (2014). "Photolysis of estrone generates estrogenic photoproducts with higher activity than the parent compound." Environmental Science and Pollution Research **21**: 7818-7827.

Suttiponparnit, K., J. Jiang, M. Sahu, S. Suvachittanont, T. Charinpanitkul and P. Biswas (2011). "Role of Surface Area, Primary Particle Size, and Crystal Phase on Titanium Dioxide Nanoparticle Dispersion Properties." Nanoscale Research Letters **6**: 27.

Takeda, S., S. Suzuki, H. Odaka and H. Hosono (2001). "Photocatalytic TiO_2 thin film deposited onto glass by DC magnetron sputtering." Thin solid films **392**: 338-344.

The European Committee for Standardization (2019). Photocatalysis- Water purification-Performance of photocatalytic materials by measurement of phenol degradation.

Thompson, W. A., C. Perier and M. M. Maroto-Valer (2018). "Systematic study of sol-gel parameters on TiO_2 coating for CO_2 photoreduction." Applied Catalysis B: Environmental **238**: 136-146.

Turchi, C. S. and D. F. Ollis (1990). "Photocatalytic degradation of organic water contaminants: mechanisms involving hydroxyl radical attack." Journal of Catalysis **122**: 178-192.

Van der Bruggen, B., C. Vandecasteele, T. Van Gestel, W. Doyen and R. Leysen (2003). "A review of pressure-driven membrane processes in wastewater treatment and drinking water production." Environmental Progress **22**: 46-56.

Vatanpour, V., S. S. Madaeni, A. R. Khataee, E. Salehi, S. Zinadini and H. A. Monfared (2012). "TiO_2 embedded mixed matrix PES nanocomposite membranes: Influence of different sizes and types of nanoparticles on antifouling and performance." Desalination **292**: 19-29.

Wang, M., F. Qu, R. Jia, S. Sun, G. Li and H. Liang (2016). "Preliminary Study on the Removal of Steroidal Estrogens Using TiO_2-Doped PVDF Ultrafiltration Membranes." Water **8**: 134.

Wang, N., L. Zhu, Y. Huang, Y. She, Y. Yu and H. Tang (2009). "Drastically enhanced visible-light photocatalytic degradation of colorless aromatic pollutants over TiO₂ *via* a charge-transfer-complex path: A correlation between chemical structure and degradation rate of the pollutants." <u>Journal of Catalysis</u> **266**: 199-206.

Worch, E. (1993). "Eine neue Gleichung zur Berechnung von Diffusionskoeffizienten geloster Stoffe." Vom Wasser 81: 289-297.

Xu, M., Y. Gao, E. M. Moreno, M. Kunst, M. Muhler, Y. Wang, H. Idriss and C. Woll (2011). "Photocatalytic activity of bulk TiO₂ anatase and rutile single crystals using infrared absorption spectroscopy." <u>Physical Review Letters</u> **106**: 138302.

Yamada, Y. and Y. Kanemitsu (2012). "Determination of electron and hole lifetimes of rutile and anatase TiO₂ single crystals." <u>Applied Physics Letters</u> **101:** 133907.

Yamamoto, H. and H. M. Liljestrand (2004). "Partitioning of selected estrogenic compounds between synthetic membrane vesicles and water: effects of lipid components." Environmental Science & Technology 38: 1139-1147.

Yang, L., L. E. Yu and M. B. Ray (2009). "Photocatalytic Oxidation of Paracetamol: Dominant Reactants, Intermediates, and Reaction Mechanisms." <u>Environmental Science & Technology</u> **43**: 460-465.

Yang, Y., L. Luo, M. Xiao, H. Li, X. Pan and F. Jiang (2015). "One-step hydrothermal synthesis of surface fluorinated TiO2/reduced graphene oxide nanocomposites for photocatalytic degradation of estrogens." <u>Materials Science in Semiconductor Processing</u> **40**: 183-193.

Yost, E. E., M. T. Meyer, J. E. Dietze, B. M. Meissner, L. Worley-Davis, C. M. Williams, B. Lee and S. W. Kullman (2013). "Comprehensive Assessment of Hormones, Phytoestrogens, and Estrogenic Activity in an Anaerobic Swine Waste Lagoon." <u>Environmental Science & Technology</u> **47**: 13781-13790.

You, S. J., G. U. Semblante, S. C. Lu, R. A. Damodar and T. C. Wei (2012). "Evaluation of the antifouling and photocatalytic properties of poly(vinylidene fluoride) plasma-grafted poly(acrylic acid) membrane with self-assembled TiO₂." <u>Journal of Hazardous Materials</u> **237-238**: 10-19.

Zakria, H. S., M. H. D. Othman, R. Kamaludin, S. H. Sheikh Abdul Kadir, T. A. Kurniawan and A. Jilani (2021). "Immobilization techniques of a photocatalyst into and onto a polymer membrane for photocatalytic activity." <u>RSC Advances</u> **11**: 6985-7014.

Zhang, S., T. Hedtke, X. Zhou, M. Elimelech and J.-H. Kim (2021). "Environmental Applications of Engineered Materials with Nanoconfinement." <u>ACS ES&T Engineering</u> **1**: 706-724.

Zhang, W., Y. Li, Q. Wu and H. Hu (2012). "Removal of Endocrine-Disrupting Compounds, Estrogenic Activity, and Escherichia coliform from Secondary Effluents in a TiO2-Coated Photocatalytic Reactor." <u>Environmental Engineering Science</u> **29**: 195-201.

Zhang, Y., J. L. Zhou and B. Ning (2007). "Photodegradation of estrone and 17beta-estradiol in water." <u>Water Research</u> **41**: 19-26.

Zhao, Y., M. Huang, M. Ge, X. Tang and L. Liu (2010). "Influence factor of 17beta-estradiol photodegradation by heterogeneous Fenton reaction." <u>Journal of Environmental Monitoring</u> **12**: 271-279.

Zou, Y., K. Xiao, Q. Qin, J.-W. Shi, T. Heil, Y. Markushyna, L. Jiang, M. Antonietti and A. Savateev (2021). "Enhanced Organic Photocatalysis in Confined Flow through a Carbon Nitride Nanotube Membrane with Conversions in the Millisecond Regime." <u>ACS Nano</u> **15**: 6551-6561.

Chapter Three

3   Materials and Methods

3.1   Overview

In this chapter, the photocatalytic membrane system and the modifications specified for a set of experiments are described. The setup for testing the photostability of the photocatalytic membrane and the protocol of experiments are presented. All the materials used during experiments including the photocatalytic membranes and chemicals are addressed in detail. Further, the analytical tools for the evaluation of photocatalytic membranes plus the detection of micropollutants (MPs) are explained extensively.

3.2   Chemicals

Methylene blue (MB) was supplied in powder from Sigma-Aldrich, dye content of 99.0% and used as a model pollutant in the comparison of photocatalytic membrane reactors (PMR) configuration (flow-through and flow-along). A stock solution of 1 g/L was prepared prior to experiments by dissolving the powder in MilliQ water (MilliQ A+ system, pH 5.6–6.0, type 1, Merck Millipore; >18.2 MΩ/cm at 25 °C, Germany). From this stock solution, fresh feed solution (1 mg/L) was prepared daily in the background solution of 1 mM $NaHCO_3$ and 10 mM NaCl. Background solution was also prepared as a stock solution by dissolving powders of NaCl (VWR Chemicals, Germany, 99.9% purity) and $NaHCO_3$ (Bernd Kraft, Germany, 99.7% purity) to get 1 M and 0.1 M respectively. In some experiments, due to the hydrolysis of $NaHCO_3^-$ to OH^- (equations **3-1** and **3-2**) by exposure to air, the pH of $NaHCO_3$ stock solution was increased from an initial value of 8.3±0.1. Therefore, wherever is needed, the pH value is reported as a higher range of 8.6±0.4.

$$NaHCO_3 + H_2O \leftrightarrow NaOH + H_2CO_3 \qquad \textbf{3-1}$$

$$H_2CO_3 \leftrightarrow H_2O + CO_2(g) \qquad \textbf{3-2}$$

Two types of steroid hormones were used as MP in photocatalytic filtration experiments evaluating the limiting factor of the PMR system and different polymeric membranes. For feed concentrations below 100 ng/L, radiolabeled hormones were considered. For higher feed concentrations, a mixture of radiolabeled and non-radiolabeled was added to reach the desired concentration.

Radiolabeled steroid hormones, estrone (E1), 17-β-estradiol (E2), progesterone (P), and testosterone (T) were provided by Perkin Elmer (USA) in ethanol (EtOH) solution. The native solutions were kept in the

freezer at -70 ℃ before usage. A stock solution of 10 µg/L in MilliQ water was prepared frequently and kept at 4 ℃ before the experiment to prevent self-degradation of radiolabelled hormones. The final concentration of EtOH appeared in two different concentrations of 27.2 mg/L and 26.9 mg/L in the feed solution for a concentration of 100 ng/L feed concentration. The difference in concentrations was because of feed solution preparation from two native solution from two different delivered batches of hormones.

Non-radiolabeled steroid hormones were supplied in powder from Sigma-Aldrich with 98% purity. The stock solution was prepared in methanol (MeOH, VWR Chemicals, Germany, 98% purity, HPLC grade) due to the low solubility of steroid hormones in the water. Considering that MeOH and EtOH can both act as radical scavengers and alter the photocatalytic degradation experiments, it was necessary to keep their concentration constant in all experiments. Therefore, by adding MeOH to the feed solution depending on the final concentration of feed, MeOH was kept constant at 79.2 mg/L. One stock solution was prepared by adding 100 mg E2 to 10 mL MeOH and stirring thoroughly to ensure the complete mixing and achieving a 10 g/L concentration. A series of dilutions from this stock solution in MeOH was prepared such that in each experiment an almost amount of 80 µL was added to reach the desired final concentration. **Table 3-1** shows the concentrations and the withdrawn volumes from prepared stock solutions.

Table 3-1 Feed preparation with different concentrations, hormone concentration was adjusted such that 100 ng/L was radiolabeled hormone and the rest was non-radiolabeled hormone, feed volume 800 mL.

Target concentration (ng/L), (Including 100 ng/L radiolabeled)	Nonlabelled Stock solution (mg/L) *	Withdrawn volume from non-radiolabeled (µL) **	Stock solution radiolabeled hormone (µg/L)	Withdrawn volume from radiolabeled hormone stock solution (mL)
100	0	0	10	8
200	1	80	10	8
1,000	10	72	10	8
10,000	100	79	10	8
100,000	1,000	80	10	8
1,000,000	10,000	80	10	8

* All stock solutions were prepared by diluting from 10,000 mg/L stock solution prepared in methanol

** If added volume from the stock solution was less than 80.0 µL, the remaining volume was adjusted by adding methanol to reach 80 µL and fixing the methanol concentration to 79.2 mg/L

For the experiment with different pH, 1 M HCl and 1 M NaOH were utilized for pH adjustment. In the case of acidic pH, 1 M HCl was prepared from HCl 37% (VWR Chemicals, Germany, analytical grade) by adding 8.21 mL to 100 mL MilliQ water. For basic pH, 1 M NaOH was prepared fresh by dissolving 4.00 gr NaOH pellets (EMD Millipore, Germany, 99% purity) in 100 mL MilliQ water.

3.3   Polymeric membranes

Two main types of photocatalytic membranes were used in this study, polyethersulfone and polyvinylidene fluoride coated with titanium dioxide nanoparticles (PES-TiO$_2$ and PVDF-TiO$_2$). TiO$_2$ coating on membranes and modifications on the membrane before the coating were performed by collaborators at the Leibniz Institute of Surface Engineering (IOM), Leipzig, Germany. **Table 3-2** shows all the membranes used and their characteristics. Basic PES-TiO$_2$ and PVDF-TiO$_2$ were compared for i) evaluating limiting factors of operation in PMR, ii) assessing the photostability of membranes and iii) different configurations of PMRs. Then, different PVDF-TiO$_2$ with modifications on PVDF substrate, different suppliers and pore size of membranes were compared. Pristine membranes were supplied by IOM, PES and PVDF from Millipore Express® PLUS Membrane and GVS from GVS, Bologna, Italy. Two membranes from GVS Group and Novamem AG were kindly provided by IMT-KIT.

Table 3-2 Various (photocatalytic) membranes in this study.

	Supplier	Hydrophilicity	Pore (µm)	Thickness (µm)	Porosity	Modification on pristine membrane before TiO$_2$ coating
PES **PES-TiO$_2$-120C** **PES-TiO$_2$***	Millipore Express PLUS, GPWP02500	Hydrophile	0.22	160-185	60%	---
PVDF						---
PVDF-TiO$_2$						---
PVDF-PAA-TiO$_2$	Durapore® Membrane, GVWP04700	Hydrophile	0.22	125	60%	e-beam (150 kGy) in 0.01% PAA
PVDF-H$_2$O-TiO$_2$						e-beam (100 kGy) in H$_2$O
PVDF(GVS)-TiO$_2$	GVS	Hydrophile	0.45	150-200	59%	---
PVDF-PAA-TiO$_2$-0.1µm	Novamem AG	Hydrophobe	0.1	125	N.A.**	e-beam (150 kGy) in 0.01% PAA
PVDF-VVHP-PAA- TiO$_2$-0.1µm	Millipore	Hydrophobe	0.1	50	N.A.	e-beam (150 kGy) in 0.01% PAA

*Unless otherwise mentioned, TiO$_2$ refers to TiO$_2$-210C nanoparticles which the synthesis method is described afterwards.

** N.A. not available

Each membrane had one shiny side and one opaque side, and the shiny side indicated the surface with a smaller pore size. The difference between the upside and downside was noticed by scanning electron microscopic images (SEM). For a few membranes, to increase the loading of TiO$_2$ on membranes and to increase the attachment strength of nanoparticles to the membrane surface, some modifications have been

done on the pristine membrane by IOM before coating with TiO_2. This procedure is explained in detail by Schulze *et al.* **(Schulze *et al.* 2013)**. The reason for this modification was to add carboxyl groups to the membrane surface which enhances the attachment between TiO_2 nanoparticles and the membrane. In summary, membranes were dipped into either water or an aqueous solution of 0.01% polyacrylic acid (PAA). Then the solution was irradiated by the electron beam on a glass plate in a wet state at an irradiation dose of 100 or 150 kGy. Next membranes were washed with MilliQ water three times for 30 min each.

3.4 TiO_2 deposition on polymeric membranes

Coating of polymeric membranes by TiO_2 was performed by IOM by two main procedures and published elsewhere **(Fischer *et al.* 2017, Fischer *et al.* 2018)**. For the first TiO_2 synthesis method (membrane TiO_2-120C), two membrane coupons (3 × 9 cm) were placed in a Teflon beaker with the top side (smaller pore size) facing down. The beaker was filled with 8.1 mL titanium (IV) isopropoxide (TTIP, 97%, Sigma-Aldrich, Germany), hydrochloric acid (HCl, 37%, Sigma-Aldrich, Germany) with 0.1 M final concentration and MilliQ water to reach a total volume of 80 mL. The beaker (solution with the membrane inside) was closed and shaken for 4 hr at room temperature. After this step, the beaker was heated at 120 ℃ for 20 hr. After cooling the membranes were taken out and washed by shaking in MilliQ water three times for 30 min each. Lastly, membranes were dried in the air. Synthesised nanoparticle with this method was named TiO_2-120C following the synthesis temperature.

For the second synthesis method, the synthesis of TiO_2 nanoparticles was first completed and then the membrane was dip-coated in the solution. First, in a beaker, 4 mL TTIP and HCl 37% (0.1 M final concentration) were mixed and reached the volume of 80 mL with the addition of MilliQ water, without any membrane. The beaker was closed, and the solution was stirred for 15 min, then the beaker was heated up to 210 ℃ in an oven for 20 hr. This allowed the synthesis of TiO_2 nanoparticles. This one was named TiO_2-210C following the temperature of synthesis. Then for the homogeneous dispersion of nanoparticles and to prevent the agglomeration to form, the solution was sonicated with an ultrasonic probe for 90 seconds at 40 W (Sonoplus, HD2200 Generator, KE76 probe, BANDELIN electronic GmbH & Co., KG, Berlin, Germany). Then membrane coupons were placed inside the solution with the top side (smaller pore size) facing downward. After 5 min shaking the solution, the membrane was taken out and washed three times for 30 min with MilliQ water and then dried. **Table 3-3** shows the TiO_2 nanoparticles' characterization.

Table 3-3 Nanoparticles' characterization

Nanoparticles	Synthesis parameters		Crystal size (nm), 5-8% variation			Crystallite morphology			Ref.
	Temperature (°C)	HCl (M)	Anatase	Brookite	Rutile	Anatase	Brookite	Rutile	
TiO$_2$-120C	120	0.1	5	10	---	90%	10%	---	(Fischer *et al.* 2017)
TiO$_2$-210C	210	0.1	10	9	33	80%	15%	5%	(Fischer *et al.* 2018)

These two types of nanoparticles were compared at the beginning of the study based on scanning electron microscopic images (SEM), light absorption, surface charge, X-ray photoelectron spectroscopy (XPS) and X-ray diffraction analysis (XRD) data and at the end by photocatalytic degradation of MB. XPS and XRD are taken from the study by Fischer *et al.* **(Fischer *et al.* 2017, Fischer *et al.* 2018)**. The bandgap of synthesized TiO$_2$-210C nanoparticles was obtained by diffuse reflectance spectra (DRS) measurement and the Kubelka-Munk method. This part is explained in section **3.9**. Considering the overall results, membranes coated with the method of TiO$_2$-210C were chosen for further research. Therefore, unless otherwise mentioned, the TiO$_2$ label added to the name of the membrane means TiO$_2$-210C. All the nanoparticles coated on the membranes listed in **Table 3-2** are coated with TiO$_2$-210C except PES-TiO$_2$-120C.

To understand if the amount of available TiO$_2$ nanoparticles is limiting the photocatalytic reaction, different loading of TiO$_2$ on the membrane were prepared. For this purpose, the TiO$_2$ nanoparticles were synthesized following the standard procedure mentioned earlier. Then this solution was diluted a few times to give less TiO$_2$ available in the solution. Next, membranes were dipped into the solution with different concentrations which resulted in loadings from highest to lowest. Although XPS is only a surface characterization technique and shows the percentage of each compound maximum 1-10 nm depth from the surface **(Mudalige *et al.* 2019)**, these results were taken as a comparison.

3.5   Photocatalytic membrane reactor

Photocatalytic membrane degradation experiments have been performed in a modified version of the custom-built photocatalytic membrane reactor (PMR) previously described by Imbrogno *et al.* **(Imbrogno and Schäfer 2019)** (referred to as micro cross-flow system) and Lyubimenko *et al.* **(Lyubimenko *et al.* 2019)** as shown in **Figure 3-1**.

Feed was pumped to the membrane cell by a high-performance liquid chromatography (HPLC) double-piston pump (Blue Shadow 80P, Knauer, Germany) with the benefit of working at a constant and stable

flow rate. The pressure of the feed line was controlled by two pressure sensors, low-pressure WIKA S-20, 0-1 bar, and high-pressure WIKA A-10, 0-40 bar. The same as high-pressure feed, retentate pressure was controlled by a WIKA A-10, 0-40 bar. The low-pressure sensor was equipped with a safety valve which prevents the sensor to face more than 3 bars.
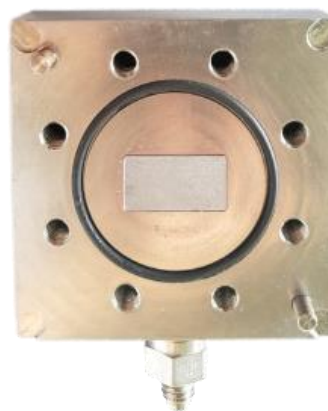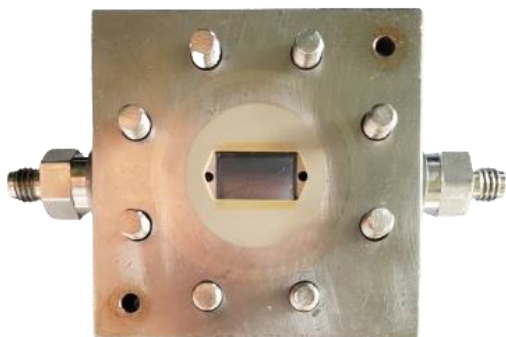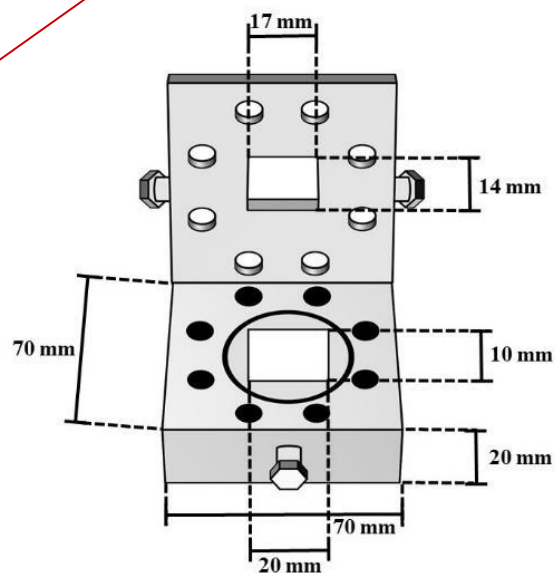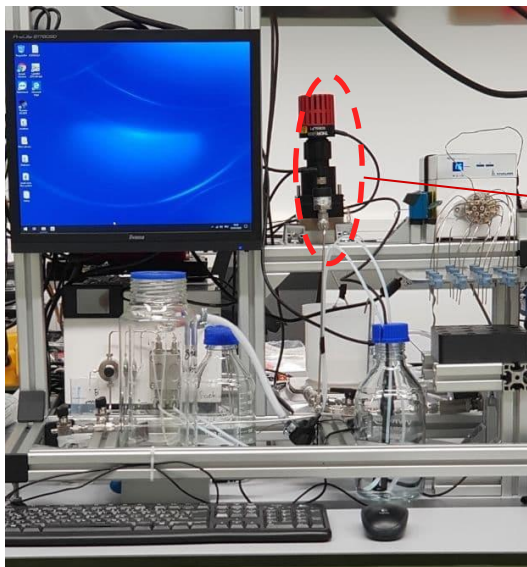
Figure 3-1 Photograph of PMR, the light source (LED) installed on top of the cell, the cell in the closed and open condition, schematic of the cell showing dimensions, only schematic was reprinted from **(Regmi *et al.* 2020).**

The membrane cell was designed and manufactured at the Institute for Micro Process Engineering (IMVT-KIT, Germany) (**Figure 3-1**). It was made of 316 stainless steel and included quartz glass (Zell Quarzglas, Germany) as a window for transmission of the UV light to the photoactive membrane surface with a 2 cm^2 active area. The membrane coupon was cut into a bigger size (4.9 cm^2) and a sealing made of PEEK was placed on top of it to avoid the flow leaking or passing outside of the filtration area. Therefore, from the 4.9 cm^2 area of the membrane coupon, only 2 cm^2 was exposed to the flow and considered as the filtration area and the rest was covered by PEEK sealing. However, the flow might also move toward the edges of the sealing through radial dispersion which is negligible and not considered in the filtration area (**Figure 3-2**). This problem is discussed first by Lyubimenco *et al.* (**Lyubimenko *et al.* 2021**) and proved to be insignificant.
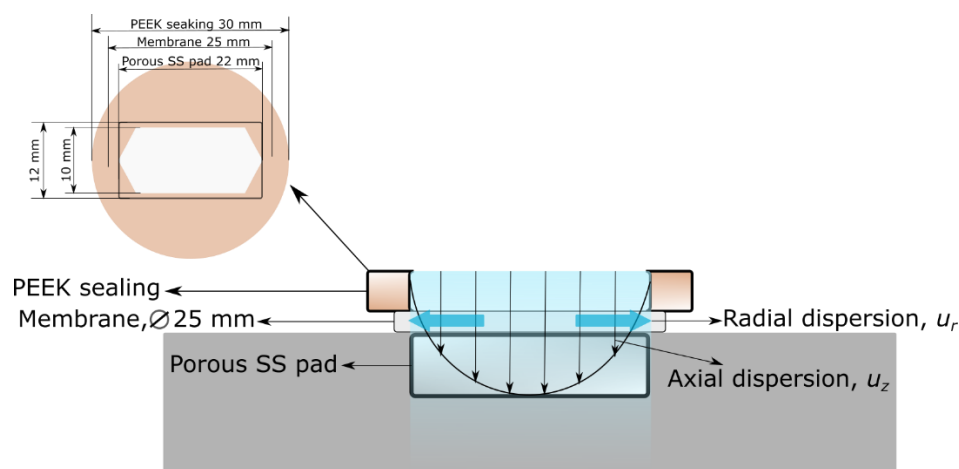
Figure 3-2 Flow and dispersion pattern through the membrane mounted on the stainless-steel porous support of cell and dimensions of PEEK sealing and the membrane.

To demonstrate the negligibility of the fluid transport in the radial direction, the following points were considered. It should be noted that the data required for below calculations (equations **3-3** and 3-4) are taken from the photocatalytic degradation of MB. The reason was that MB had a higher concentration in feed compared to hormones (1 mg/L versus max 200 ng/L) and also has had higher adsorption to the surface (meaning higher surface concentration). The considered data was MB volumetric flow of 0.2 cm³/min which resulted in 6.2 s residence time inside the membrane (the calculation of residence time is discussed later in the section **3.12**). At this flow rate, considering 2 cm² active membrane surface area, the velocity of MB solution passing through the membrane would be 0.001 m/s.

1) Radial diffusion to distances longer than 1 mm requires a residence time of more than 1000 s. Diffusion time in the radial direction ($t_{D,rad}$) can be calculated using equation **3-3**.

$$t_{D,rad} = \frac{r^2}{D_m}$$ **3-3**

where r is the diffusion path (m), and D_m is the diffusion coefficient of MB 7.7×10^{-10} m²/s **(Hori *et al.* 1987)**. Considering the residence time of the solution in the membrane which is almost 6 s at the lowest flow rate, then there is not enough time for the diffusion and therefore, radial diffusion is considered insignificant.

2) The dispersion of the solution in the radial direction is driven by convection due to the pressure gradient (assuming that diffusion is negligible). In this case, the velocity of the fluid in the radial direction is lower than the axial direction ($u_r \leq u_Z$), because the pressure gradient over the thickness of the membrane is considerably higher. The maximum distance that the solution can disperse in the radial direction ($h_{D,r}$) can be estimated by equation **3-4**.

$$h_{D,r} = u_r \bar{t}$$ **3-4**

where u_r is the flow velocity in the radial direction (m/s) and $\bar{t}$ is the mean residence time in the membrane. If $u_r \approx u_Z$, then the maximum distance would be almost 0.1 mm which is insignificant considering the filtration area (2 cm³) within the open area of PEEK sealing **Figure 3-2**.

This insignificant radial dispersion was also observed during the photocatalytic degradation of MB, in which 350 mL of MB was filtered at different flow rates.

(a)   (b)   (c)
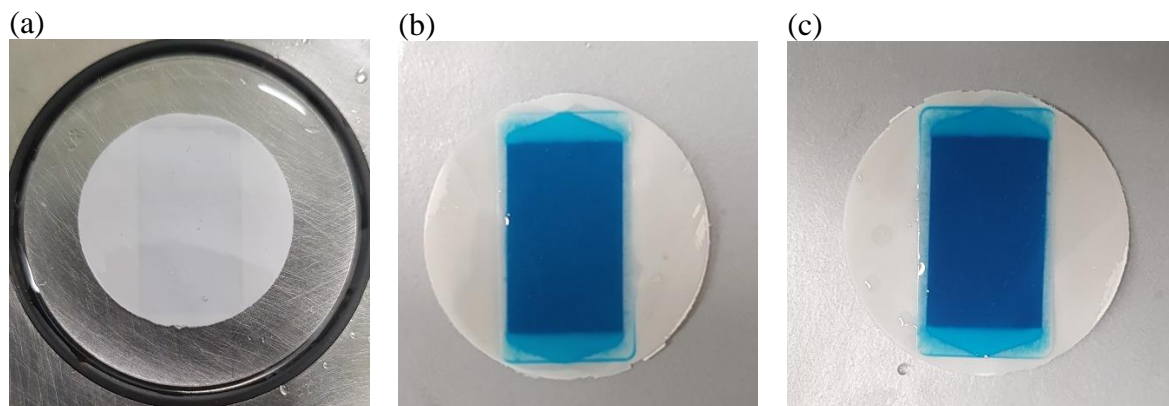
Figure 3-3 The photographs of (a) PVDF-TiO₂ membrane placed on the porous SS pad, (b) topside and (c) bottom side of the membrane after photocatalytic filtration. Experiment: photocatalytic degradation of MB 1 mg/L in background solution (10 mM NaCl and 1 MM NaHCO₃), 1 mL/min (300 L/m²h) flow rate corresponds to 1.2 s residence time inside the membrane, temperature 23±1 °C. The blue color displays the area restricted by the PEEK sealing, and the darker blue shows the area of quartz window and direct irradiation.

The hexagonal area demonstrated in **Figure 3-3** (b) and (c) accurately matches the hexagonal opening part of PEEK sealing which is 2 cm². A lighter shadow of blue can be seen which is darker on the bottom side and show the shape of a porous SS pad. In conclusion, the radial diffusion or convention to the area

underneath the seal was considered insignificant and, in all calculations, 2 cm^2 was considered the photocatalytic filtration area.

A UV light-emitting diode (UV-LED, M356LP1, THORLABS, USA) was used as the light source with a peak wavelength of 365 nm and was located on top of the quartz window of the membrane cell. It was powered by an LED driver (LEDD1, THORLABS, USA) with a max light intensity of 17 mW/cm^2 possible. In the case of higher light intensities required, high power LED driver (DC2200, THORLABS, USA) was connected and a light intensity of 44 mW/cm^2 was reached. The light intensity was measured using a thermal power meter (S175C sensor with PM100D meter, THORLABS, USA) with an active area of 18 cm×18 cm placed directly after the lamp. The light intensity after the quartz cell lost almost 35% of its power **(Berger *et al.* 2020)**. This was related to the distance between the light source and the membrane surface (inverse square law, power loss with distance) and the light absorption of the quartz window. However, due to the geometry of the cell, it was not possible to measure the intensity at the membrane surface consistently (with acceptable repetition), so all the light intensities reported in this dissertation were measured by placing the thermal sensor directly after the LED and above the quartz window causing a consistent overestimation of light intensity.

The feed solution was contained in a double-jacketed beaker connected to a cooling device (Minichiller 300, Peter Huber Kältemaschinenbau AG., Germany) to keep the temperature constant at room temperature (23 ±0.2 ℃). The feed container was covered by aluminum foil during the experiment to avoid the effect of other light sources in the lab. Feed temperature and conductivity were measured by a joint conductivity and temperature sensor (electrode B 202922.0, JUMO, Germany). The temperature sensor was measured with a thermocouple (NI USB TC01, National Instrument) connected directly to the permeate outlet of the cell. Considering the high thermal conductivity of the cell material (SS 316), it was assumed that the temperature measured by the thermocouple is the temperature of the liquid inside the piping.

The conductivity of the permeate feed was measured by an in-line conductivity sensor (ET131 headstage and ER825 multichannel detector by eDAQ Australia). A 1/16" plastic tube was inserted inside the C4D headstage and the conductivity of the flow was detected continuously. A calibration curve was needed to convert the response of the sensor in volts to mS/cm. Calibration was done by preparing solutions with different salt concentrations and measuring the conductivity by joint conductivity/temperature (the one used in the feed solution). Then by correlating the measured conductivity data with the corresponding voltage received by the in-line sensor, a calibration curve was plotted. The fitted equation was set in the

LabVIEW program to record the permeate conductivity data automatically. Calibration was done as often as needed by monitoring the data of different sensors.

All data were collected from different parts and transferred to a data acquisition card (USB-6000, National Instruments), and saved by LabView 2014. Also, the LabVIEW program was used to control the flow rate, light intensity, and different steps of the experiment.

3.6   Configuration comparison of photocatalytic membrane reactors

Three types of PMRs namely flow-along mode, flow-through mode and batch system were compared based on their efficiency (**Figure 3-4**). Flow-along and flow-through mode experiments were performed within this thesis, and the batch mode data were provided by collaborators (IOM) for the sake of comparison.
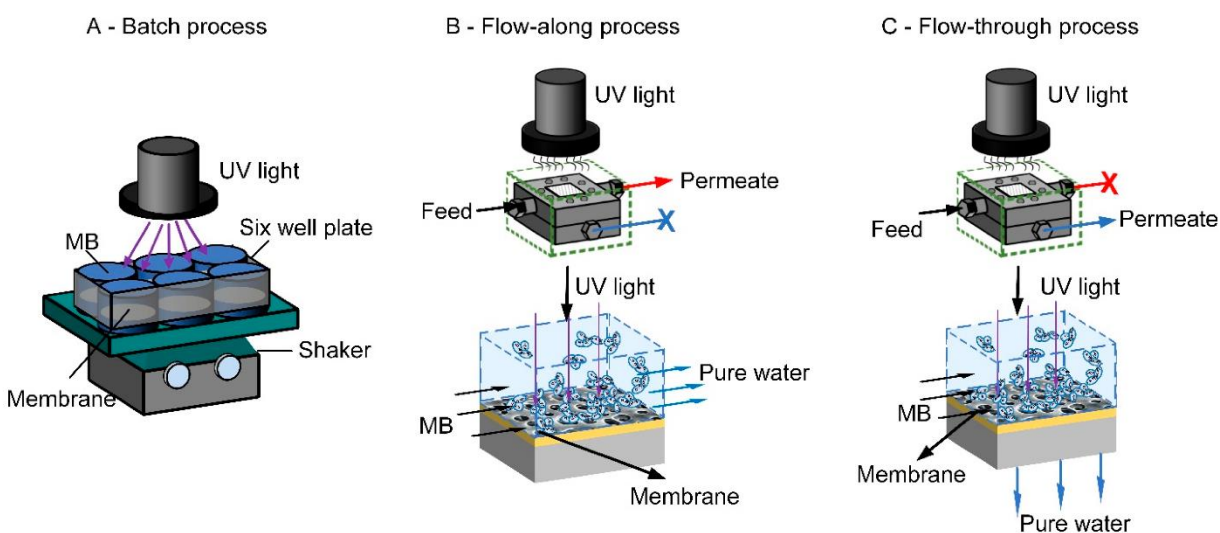
Figure 3-4 PMRs with different configurations, A) Batch process (IOM set-up), B) Flow-along, C) Flow-through, Reprinted from (**Regmi** *et al.* **2020**).

The criteria for this comparison were as follows:

- Efficiency in photocatalytic degradations of MB at different fluxes and light intensities
- Comparison of several figures of merit based on the throughput, energy efficiency and final MB removal, namely, adapted space-time yield (STY) and photocatalytic space-time yield (PSTY), specific energy consumption (SEC) and degradation rate constants.

The system configurations are described extensively in the next section and the figures of merit are explained in the kinetic section (3.12).

3.6.1 Photocatalytic degradation of dyes

For experiments with dye, the PMR was connected to an in-line UV/VIS Spectrophotometer (PerkinElmer Lambda 365) equipped with a flow-through cuvette (light path of 10 mm, Hellma Analytics) to analyze the permeate concentration of dyes continuously during the experiments. A cuvette filled with MilliQ water was used as a reference and the light absorption intensity of MB was measured continuously at the wavelength of 664 nm. Details of MB concentration measurements are explained later in section **3.11.1**. The schematic of the system configuration is illustrated in **Figure 3-5**. However, it should be noted that the decrease in absorption intensity of the MB does not always mean complete mineralization. Decrease in absorption intensity could be due to the breaking of the conjugate bonds of the MB molecules. Having this in mind, this parameter was used for comparison purposes between PMR configurations.
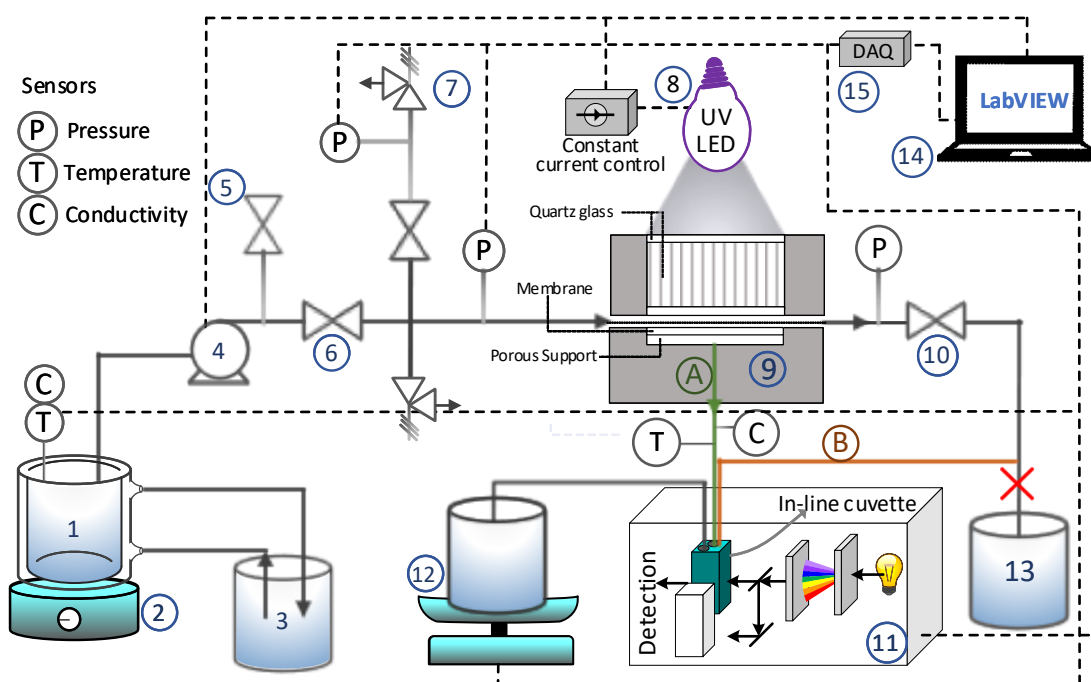
Figure 3-5 Schematic of the photocatalytic filtration system connected to UV-vis spectrophotometer, 1) feed tank (double jacketed beaker), 2) magnetic stirrer, 3) cooling device, 4) HPLC pump, 5) purge valve, 6) pump shut-off valve, 7) low-pressure sensor with shut-off-valve and low-pressure relief valve, 8) UV-LED (365 nm) and LED controller, 9) photocatalytic membrane cell, 10) retentate needle valve, 11) UV-vis spectrophotometer with an in-line cuvette, 12) permeate container on a balance, 13) retentate tank, 14) computer, 15) data acquisition card (DAQ). Mode A (green line) refers to the flow-through mode, and mode B (orange line refers) to the flow-along mode. In each mode, the other line was closed. Adapted from (**Lotfi** *et al.* **2022**).

The feed concentration was constant, meaning that there was no recycling of the feed. Permeate flow was collected on a balance (Ohaus AX622/E, USA) and the permeate flow rate was calculated by LabVIEW using the mass and density of water at room temperature. Experiments were performed in two different modes, flow-through and flow-along. In both modes, the permeability of membranes was first

measured with MilliQ water in flow-through mode at five different fluxes (30, 150, 300, 600, and 1500 L/m^{2}h). To perform the permeability test, MilliQ water with the temperature of the lab was needed, therefore, a bottle was filled with MilliQ water the evening before the experiment (~12 hr) to reach the lab temperature. The water flux of the PES-TiO$_2$ and PVDF-TiO$_2$ membranes at different transmembrane pressure (TMP) is presented in **Figure 3-6** which shows that the water flux did not change noticeably before and after the photocatalytic degradation experiments and therefore no damaged had occurred to the membrane.
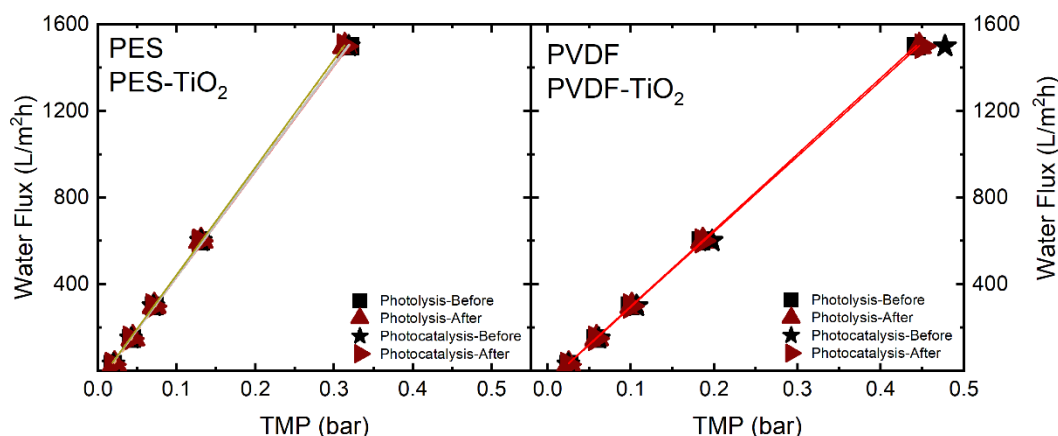
Figure 3-6 Water flux of PES, PES-TiO$_2$, PVDF, PVDF-TiO$_2$ before and after photolysis and photocatalysis (data shown are example of many experiments). Data of PES was reprinted from (**Regmi** *et al.* **2020**), and PES-TiO$_2$ was reprinted from (**Lotfi** *et al.* **2022**).

Prior to the experiment, a fresh feed solution was prepared from the stock solutions of MB and the background solution. 500 mL MilliQ water containing 0.5 mL of MB stock solution (1g/L), and 5 mL of NaCl and NaHCO$_3$ stock solution (1 M and 0.1 M respectively) were added to the feed container (500 mL double jacketed beaker). From this 500 mL, 50 mL was needed for flushing the pump, 100 mL for the dark phase (lamp off), 250 mL for the light phase (lamp on), and the rest to keep all piping and sensors fully immersed in the solution. The feed container was covered with aluminum foil to prevent the self-degradation of MB under the light sources in the lab. The solution was stirred continuously before the start of the experiment at high speed to ensure a homogenous solution. Before changing to the MB solution, the stirrer speed was set to a minimum to avoid the creation of bubbles in the line and the in-line cuvette. If a bubble reached the in-line cuvette of the UV-vis spectrophotometer, it altered the absorption data and, in most cases, the experiment had to be repeated.

In **flow-through mode** (mode **A** in **Figure 3-5**), the retentate valve was closed (valve number 10) and feed flow was forced to pass through the membrane pores. Permeate was sent to the UV-vis spectrophotometer for concentration measurement (the green line shows the permeate line of the cell). After the permeability test, the MilliQ water was replaced with an MB feed solution. Then, with valve

number 6 closed and 5 open (valve number 5 is the pump purge valve), the pump was purged at 100 mL/min to replace the water in the pump with MB solution and also to remove bubbles that could be created by exchanging the piping from MilliQ water to feed solution. Then at the same time, the flow was set to the specified flux of the experiment, valve number 6 was opened and 5 was closed. The first 100 mL of the MB solution was filtered under dark conditions, and the 250 mL under light exposure.

In **flow-along mode** (mode **B** in **Figure 3-5**), after the permeability test, the permeate side was closed (by a dead-end connection) and the feed flow passed along the surface of the membrane (top surface). The valve on the retentate side was open and the flow after the cell was sent to the UV-vis spectrophotometer for concentration analysis (the orange line shows the retentate line). Before exchanging the feed bottle with MilliQ solution, the system was running for a few minutes after closing the permeate side, to make sure no bubble was created in this step. Then the pump was stopped and the MilliQ bottle was replaced with MB feed solution. After this step, the same procedure was done as a flow-through. The filtration protocol for MB is described in detail in Supporting information of this chapter **Table 3-12**.

The experimental plan for the comparison of flow-along and flow-through is demonstrated in **Table 3-4**. The results of these experiments were compared with the data of the batch system which was provided by the IOM institute.

Table 3-4 Experimental plan performed to compare the performance of 3 configurations, flow-through, flow - along and batch (only batch experiments were performed by IOM).

Configuration*	MB (mg/L)	Light intensity (mW/cm²)	Flux (L/m²h)
Flow-through	1	2, 10, 17	300
Flow-along	1	10	60, 90, 150, 225, 300

* Experiments in the batch system were performed by the IOM institute, and the data were compared with the results of this research

The results of these two configurations were compared with the data given by the IOM institute operating in **batch mode**. The description of experiments provided by the IOM is as follows. For the determination of the photocatalytic activity, rings were cut out of the TiO_2-modified membrane. The ring diameter was 2.5 cm and the hole in the middle had a diameter of 1 cm. The final membrane area was 4.1 cm². Then, the ring was glued into the well of a six-well-plate. Now, the well was filled with 4 mL of a 13 mg/L or 1 mg/L aqueous solution of methylene blue. The six-well-plate was shaken at 200 rpm on a radial shaker without irradiation and dark adsorption of the membrane was determined after 20 min. When the methylene blue concentration decreased (dark adsorption), the solution was replaced with fresh

methylene blue solution until no further dark adsorption occurred. To measure the photocatalytic activity the samples were subsequently irradiated with a sunlamp (Heraus Original Hanau Suncare tanning tube 21/25 slim, 13 mW/cm^2) or a UV-Led (6 UV-LED arranged in a circle, 365 nm, 10 mW/cm^2, LZ1_00U600, LedEngin Inc.,) for different time scales. All measurements were carried out with a Tecan Infinite M200 multimode microplate reader at a wavelength of $\lambda = 660$ nm. The non-catalytical photolysis (without a membrane) of methylene blue was determined by three references. This value was then subtracted from the measured values to calculate the actual photocatalytic degradation.

3.7 Evaluation of limiting factors in a PMR efficiency

For evaluating the limiting factors of operation in a PMR system, E2 was chosen as the main micropollutant to assess its degradation efficiency. Almost all parameters were considered for comparison with both PES-TiO$_2$ and PVDF-TiO$_2$. First, the photocatalytic degradation of E2 was compared with the direct photolysis and adsorption in the dark phase. Parameters to evaluate were categorized into 3 main parts as shown in **Table 3-5**, i) operational parameters, ii) solution chemistry, and iii) photostability of photocatalytic membranes.

Table 3-5 Experimental plan for evaluating the limiting factors of operation in a PMR.

Category	Parameter	Range
Operational parameters	Photocatalytic degradation, Photolysis, Adsorption	Standard condition*: MP type: E2 Feed volume: 700 mL Light intensity: 10 mW/cm^2 Flux: 600 L/m^{2}h TiO$_2$ loading: 0.07±0.06 mg/cm^2 for PVDF-TiO$_2$ and 0.27 mg/cm^2 for PES-TiO$_2$ Temperature: 23±0.2 $^\circ$C MP concentration: 100 ng/L pH: 8.6±0.4 Membranes: PES and PVDF (for photolysis) PES-TiO$_2$ and PVDF-TiO$_2$ (for photocatalytic degradation and adsorption)
	Light intensity (mW/cm^2)	0.5, 2, 5, 10, 15, 20, 25, 44
	Flux (L/m^{2}h)	60, 150, 300, 600, 900, 1200, 1500, 3000
	Temperature (ºC)	10, 20, 30, 40, 50, 60
	TiO$_2$ loading (%) obtained by XPS data	Ti%: 6.4±0.6, 6, 5.5±0.3, 4.1±0.1, 3±0.3, 1.9±0.4
Solution chemistry	Concentration (Unit as indicated)	50 ng/L, 100 ng/L, 200 ng/L, 1 µg/L, 10 µg/L, 100 µg/L, 1 mg/L
	pH	2, 4, 6, 8, 9, 10, 11, 12

	Hormone Type	E2, E1, P, T, Mixture (200 ng/L, 25 mW/cm^2, 300 L/m^{2}h)
	Enhanced condition for higher removal	60 L/m^{2}h, 25/44 mW/cm^2
Photostability of photocatalytic membranes	Ageing duration	5, 25, 50, 75, 100, 125, 175, 250 h
	Conditions of MB photocatalytic degradation test	Pollutant: MB Feed Volume: 350 mL Light wavelength: 365 nm and 405 nm Light intensity: 98 mW/cm^2 for 365 nm and 124 mW/cm^2 for 405 nm Flux: 300 L/m^{2}h TiO$_2$ loading: 0.07±0.06 mg/cm^2 for PVDF-TiO$_2$ and 0.27 mg/cm^2 for PES-TiO$_2$ Temperature: 23±0.2 $^\circ$C MP concentration: 1 mg/L pH: 8.6±0.4 Membranes: PES and PVDF, PES-TiO$_2$ and PVDF-TiO$_2$
	Other methods for evaluation of membranes' photostability	Visual and SEM imaging, UV-vis light absorption, FTIR, Surface charge change (zeta potential), TOC release, loss of TiO$_2$ (ICP-OES)

* Unless otherwise mentioned, these values were used as the standard conditions.

The details of system configuration and experimental procedure are explained in the next sections and the analysis of the obtained data is discussed in the kinetic section **3.12**.

3.7.1   Photocatalytic degradation of hormones

For steroid hormone degradation, after the membrane cell, the UV-vis spectrophotometer was disconnected. The permeate line was connected to a 16-line switching valve (Azura V2.1S, Knauer, Germany). In this case, valve number 16 was always connected to waste, and 15 other lines were used to collect permeate samples in 2 mL vials for an Ultra-High-Performance Liquid Chromatography (UHPLC) analysis for concentration detection (**Figure 3-7**).
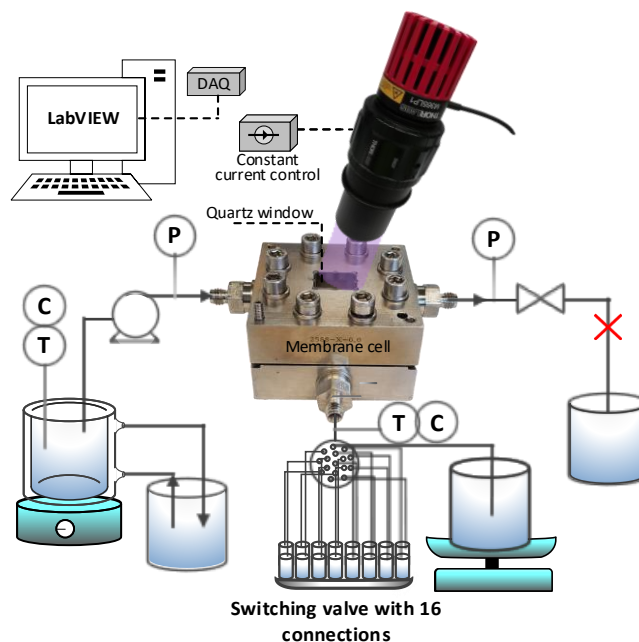
Figure 3-7 Photocatalytic membrane filtration set-up for hormone degradation, all components were similar to dye degradation (for details of the system refer to **Figure 3-5**). Adapted from (**Lotfi *et al.* 2022**).

For experiments with different temperatures in the reaction environment, the PMR system needed to be modified. For this purpose, one modification was done to decrease the temperature to 10-11 ℃ and another one to increase the temperature above the ambient. For these experiments, the feed temperature was kept constant at 23±0.2 ℃ and the temperature of the stainless-steel cell was altered directly. To cool down the system, the photocatalytic cell was placed in an ice bath fitted on stainless-steel cooling pipes connected to a cooling device (Minichiller 300, Peter Huber Kältemaschinenbau AG, Germany). The schematic of this configuration is illustrated in **Figure 3-8**. The temperature of the cooling device was set to 0 ℃, however, due to improper sealing, the lowest achieved temperature was 11±0.6 $^{\circ}$C. To heat the SS cell above room temperature, a heating plate (SU1300, Sunlab®) equipped with a temperature sensor was placed underneath the cell (**Figure 3-8**). The temperature sensor of the heating plate was fixed between the plate and the cell outlet to control the plate temperature. In both modifications, the temperature sensor of permeate side was fixed directly to the cell in the area between the feed inlet and permeate outlet to monitor the cell temperature. During the experiments, feed pressure was monitored continuously.
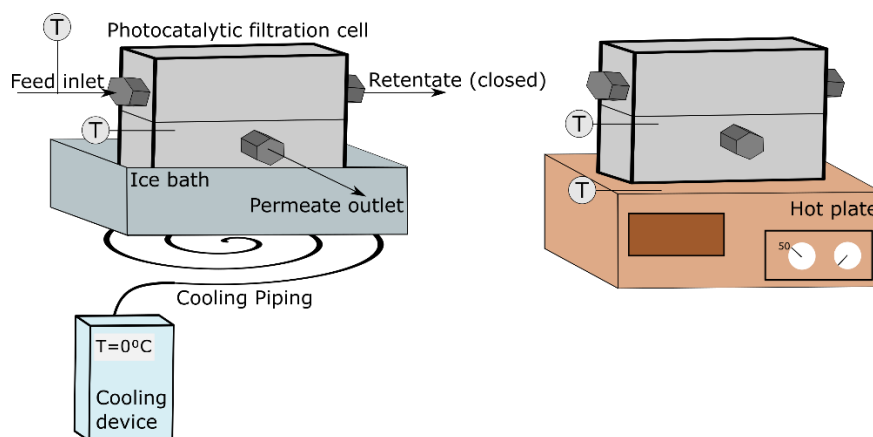
Figure 3-8 Modifications added to the system to decrease and increase the temperature of the reaction environment inside the cell.

The filtration protocol for hormones is described in detail in **Table 3-13**. The experimental plan was presented previously in **Table 3-5**. So, unless mentioned otherwise, 700 mL feed, 600 L/m^{2}h flux and 10 mW/cm^2 light intensity were chosen as standard conditions for all experiments. All parameters of pressure (±0.03 bar), conductivity (±0.1 mS/cm), pH (±0.2) and temperature (±0.1 $^{\circ}$C) were monitored during the experiments continuously.

3.8   Examination of the photocatalytic membrane photostability

Two basic photocatalytic membranes, PES-TiO$_2$ and PVDF-TiO$_2$, together with their pristine membranes, PES and PVDF, were selected for studying their photostability under light irradiation and exposure to reactive oxygen species (ROS). These membranes were the same ones used for the investigation of limiting factors in PMR operation with characteristics mentioned in **Table 3-2** and **Table 3-3**. The photostability testing was performed *via* an accelerated ageing technique, exposing membranes to high light irradiation for 250 hr.

3.8.1   Photodegradation chamber

The testing was done using a UV-violet-LED chamber (Compact UV-LED Chamber BSL-01 ECO+, Opsytec Dr. Gröbel GmbH) with two light light-emitting diodes. One LED array was 365 nm with 0-109 mW/cm^2 intensity and the other one was 405 nm with a light intensity of 0-135 mW/cm^2. These data were provided by the company assuming that the changes in between were considered linear. The chamber was equipped with a temperature sensor which provided the temperature of the air inside the chamber, stating the operation temperature would be 10-40 °C getting the benefit of an air inlet and outlet design. However, to keep the samples at room temperature (21 ± 1°C) during the ageing time, the bottom part of the chamber was modified with a water-cooled copper plate connected to a cooling device

(Minichiller 300, Peter Huber Kältemaschinenbau AG, Germany). The cooling device was set at 20 °C and worked constantly during the ageing test. This design ensured the minimal evaporation of water where samples were kept and hence keeping the membranes wet during the ageing process. The schematic of the chamber is demonstrated in **Figure 3-9**. Using the controller of the device, two parameters could be set, i) light intensity of each LED array by setting the LED power (0-100%), ii) duration of the light irradiance.
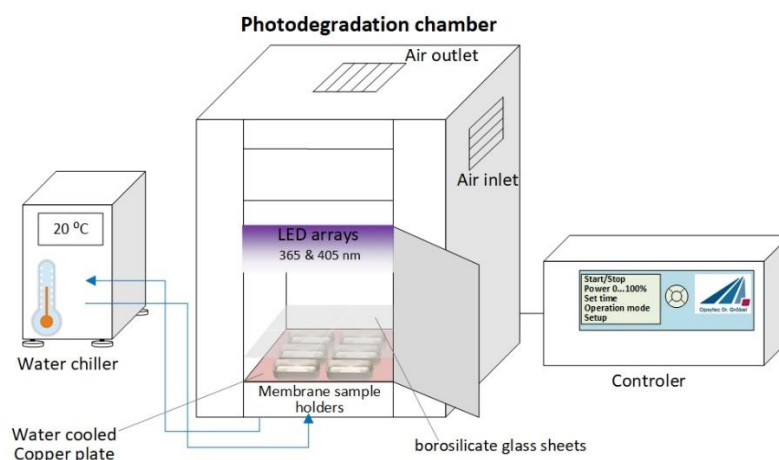
Figure 3-9 UV-violet-LED degradation chamber with a controller connected to the water chiller. Adapted from (**Raota** *et al.* **2023**).

Inside the UV-violet-LED chamber, membrane samples were put inside aluminum (Al) holders (Xceldent Official, 40 mm × 25 mm) containing 10 mL MilliQ water. Al was chosen as the holder material to provide good heat exchange and avoid temperature rise and ageing of membranes due to temperature. However, before performing some elemental characterizations, a set of membranes were aged in glass Petri dishes to avoid interference of Al. The complications arose by using Al holder is explained in chapter **4**. As illustrated in **Figure 3-9**, membrane holders were covered with borosilicate glass (Schott BF33, L100 × W100 × H3.3 mm) to reduce the evaporation of water. These sheets of glass caused losses in optical transmission of about 8% (405 nm region) and 10% (365 nm region) mostly because of reflection of light on the air-glass interface. **Figure 3-10A** shows the light intensity distribution inside the chamber provided by the supplier (**Opsytec Dr. Gröbel GmbH 2021**). It shows that the central area (12 cm × 12 cm) has the most homogenous light distribution above 85% relative light intensity. Considering this area, the arrangement of membranes inside the chamber was set. Membranes are shown as grey circles in this figure. The transmission spectra diagram of the borosilicate glass is shown in **Figure 3-10B** and taken by placing the glass in front of an integrating sphere of UV-vis spectrophotometer (Perkin Elmer Lambda 950, USA, ultraviolet-visible-near-infrared (UV-Vis-NIR) spectrophotometer).

A

B
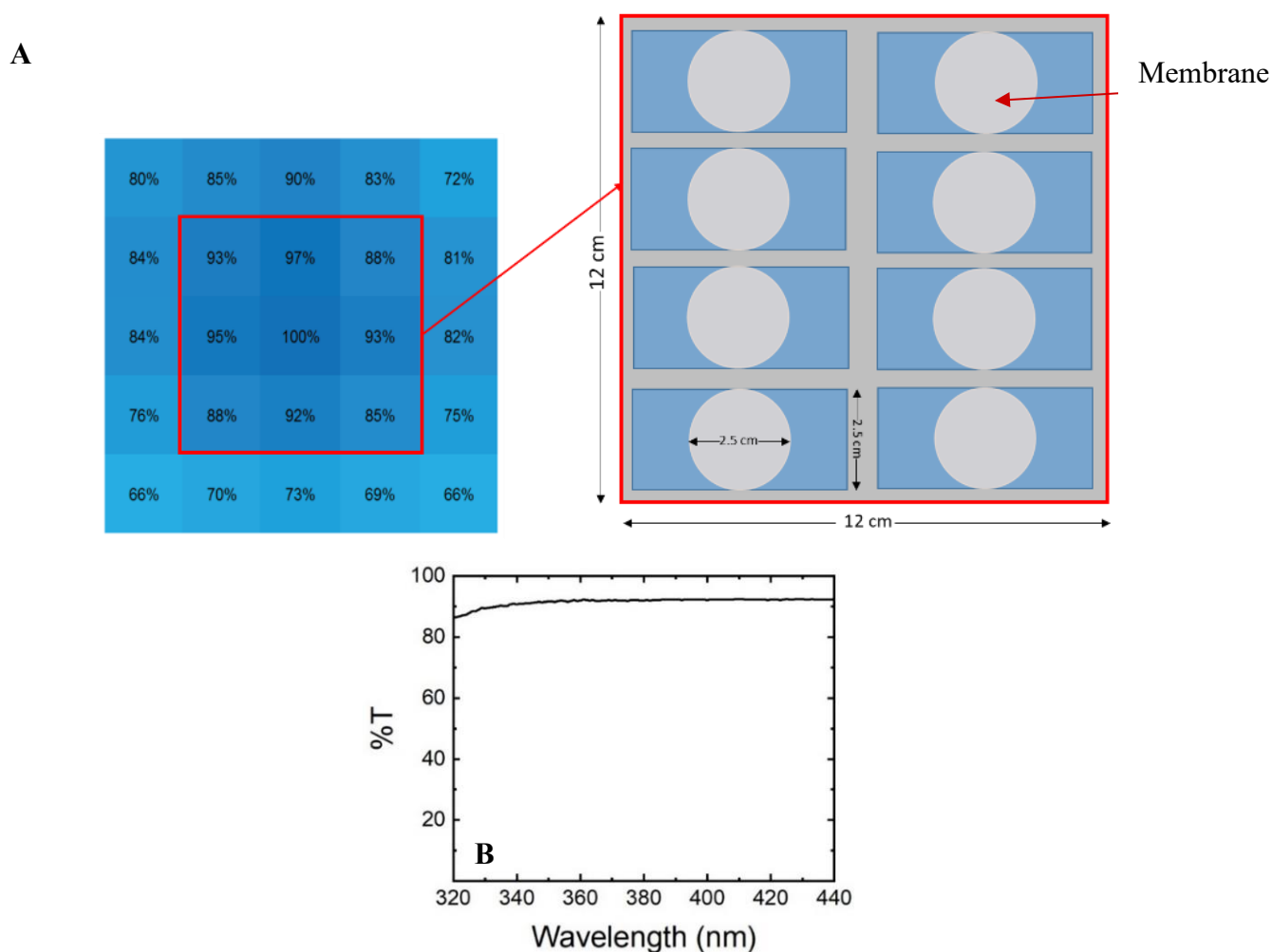
Figure 3-10 (A) light distribution pattern in UV-violet-LED chamber from device datasheet (**Opsytec Dr. Gröbel GmbH 2021**), (B) transmittance spectra of borosilicate sheet (**Raota *et al.* 2023**).

3.8.2 Accelerated ageing test

For evaluating the photostability of photocatalytic membranes *via* an accelerated ageing technique, membranes were exposed to light irradiance inside the UV-violet-LED chamber for maximum 10 days. A set of 8 membranes were placed inside the chamber all at once (with the arrangement shown in **Figure 3-10A**) and each membrane was taken out at different time intervals, in the order of 5, 25, 50, 75, 100, 125, 175, 250 hr. Before placing the membranes, each holder was rinsed carefully with MilliQ water, then they were placed in acid (12 mM HCl) and base (12 mM NaOH) solutions for almost 30 min and then rinsed again several times with tap water and MilliQ water. Then they were left to dry in the lab before usage. Then, 20 mL of water was added to the holder, and 10 mL of that was withdrawn in a clean glass bottle for further total organic carbon analysis to account for any residues from other sources.

Membranes were cut in coupons with 25 mm diameter and placed upward in the Al holder or glass petri dish with water such that the shiny side of the membrane with a smaller pore size was facing the light

exposure. Sample holders containing membrane and MilliQ water were placed inside the UV-violet-LED chamber and covered with borosilicate glasses as shown in **Figure 3-9** and **Figure 3-10**. Both LED arrays 365 nm and 405 nm were on at full power which was equal to 109 and 135 mW/cm^2 respectively. Considering the 8% loss due to the borosilicate glass sheets, the actual light intensity was 98 and 124 mW/cm^2 for 365 nm and 405 nm respectively. With the band gap of synthesized TiO_2 nanoparticles determined as 3.02 eV *via* light absorption and the Kubelka-Munk (explained in section 3.10), then both 365 and 405 nm could be beneficial for nanoparticle excitation and generation of ROS.

The water level of samples was regularly checked (at least every 25 hrs). At each time interval, one sample holder was taken out, it was covered with a glass sheet and transferred to another lab where the water sample could be weighed carefully with a precision balance (OHAUS, PA124C) and stored for further TOC analysis. In case the mass was less than 10 gr due to evaporation, then it was adjusted to 10 gr by adding MilliQ water. Aged membranes were stored in wet condition until further examinations including Visual photography, MB photocatalytic degradation efficiency, zeta potential measurement and light absorption. For SEM imaging, the aged membrane was left to dry in the air upward, so the top side is clear. For FTIR measurements, aged samples were dried in a rotary evaporator (Büchi Rotovapor R-210, Sigma Aldrich) at 30 mbar vacuum and 40 ºC for 1 hr.

3.8.3   Sample preparation for ICP-OES analysis for Ti detection

A set of membranes were aged in glass Petri dishes (diameter 10 cm) for Inductively coupled plasma atomic emission spectroscopy (ICP-OES) in the Institut für Angewandte Materialien - Angewandte Werkstoffphysik (IAM-AWP), Dr. Thomas Bergfeldt. Glass Petri dishes were cleaned carefully to remove any contaminants. For this purpose, Petri dishes were first placed in acid (12 mM HCl) for at least 5 hr. Then they were rinsed with MilliQ water and were left in the MilliQ water basin for a few hours. Next step Petri dishes were placed in the base (12 mM NaOH) solution for at least 5 hr. Later, they were rinsed with tap water and MilliQ water carefully. Finally, they were dried in the oven at 80 °C over the night (at least 12 h) so there is no residual water from cleaning.

For sample preparation, 20 mL of water was added to each glass petri dish. Then the membrane was placed in, and the petri dish was shaken a little bit, so any unattached TiO_2 could be released. Next, 10 mL of water was withdrawn from the petri dish and added to a clean vial for further analysis. The Petri dishes with membranes were placed in the UV-violet LED chamber and were covered with sheets of borosilicate glass to avoid evaporation during ageing. After the duration needed for ageing, samples were taken out of the UV-violet LED chamber. The remaining liquid in the Petri dish was collected and

transferred to a clean 20 mL glass vial. Then the Petri dish was rinsed with MilliQ water and this second liquid in the Petri dish was also added up to the glass vial. The total weight of the water was recorded. The liquid samples were then sent for ICP-OES analysis.

Samples were aged for 5, 125, and 250 hr in the light chamber for ICP-OES analysis. Also, two types of control samples were prepared. 1) without light exposure membrane (A-8 in **Table 3-6**): one control sample was prepared by ageing the membrane without any light exposure. Membranes were put in the glass petri dish and kept in dark for 250 hr to account for any release of TiO_2 without light exposure. 2) without membrane (A-7 in **Table 3-6**): second type of control sample was prepared by adding MilliQ water to the glass petri dish without a membrane and was placed in the UV-violet LED chamber with the light on for 250 hr to consider any release of elements from the glass petri dish itself. Blank samples were also analyzed with ICP-OES. **Table 3-6** mentions the samples and the final volume. To reduce the error and make sure no TiO_2 has been left in the petri dish, petri dishes were rinsed with a small amount of ultrapure water and this water was also added to the final volume for analysis. This resulted in a volume higher than 10 mL in some cases.

Table 3-6 Samples prepared for ICP-OES and their volume.

Sample	Description	Final volume (mL)
A-1	PES- TiO_2-5h-aged	10.42
A-2	PES- TiO_2-125h-aged	10.24
A-3	PES-TiO_2-250h-aged	11.14
A-4	TiO_2-PVDF-5h-aged	10.72
A-5	TiO_2-PVDF-125h-aged	12.57
A-6	TiO_2-PVDF-250h-aged	10.30
A-7	Control, petri dish with no membrane under light (250h)	10.00
A-8	Control, PES-TiO_2 in dark (250h)	8.85
A-9	Control, PVDF-TiO_2 in dark (250h)	8.49

3.9   Optimization of photocatalytic membrane

To enhance the photocatalytic degradation of MP, different approaches have been taken into account. First, the operation conditions were set to achieve the highest possible degradation by increasing the light intensity and decreasing the feed flux (meaning to increase the residence time). The next approach was to modify the surface of membranes to boost the loading of photocatalysts, by E-beam modification and

changing the physical properties of the membrane. The third approach was to decrease the pore size of the membranes to increase the possibility of collision between the MP and the photocatalyst deposited inside the pores. **Table 3-7** presents the experimental plan for this section. Membranes' characteristics and methods for surface modification were explained previously in **Table 3-2** and section **2.6.3** respectively.

Table 3-7 Experimental plan for optimizing the photocatalytic degradation of MP.

Category	Membrane	E2 removal experimental condition
Enhanced operational condition	PES-TiO$_2$ and PVDF-TiO$_2$	MP type: E2 Feed volume: 700 mL Light intensity: 44 mW/cm^2 for PES-TiO$_2$ and 25 mW/cm^2 Flux: 60 L/m^{2}h TiO$_2$ loading: 0.07 ± 0.06 mg/cm^2 for PVDF-TiO$_2$ and 0.27 mg/cm^2 for PES-TiO$_2$ Temperature: 23 ± 0.2 $^\circ$C MP concentration: 100 ng/L pH: 8.6 ± 0.4
Surface modification and different PVDF supplier	PVDF-PAA-TiO$_2$	
	PVDF-H$_2$O-TiO$_2$	
	PVDF(GVS)-TiO$_2$	The standard condition mentioned in **Table 3-5**
Smaller pore size membrane	PVDF100	
	VVHP	

3.10 Membrane and photocatalyst characterization

X-ray powder diffraction (XRD), X-ray photoelectron spectroscopy (XPS), contact angle measurement, and the experiment to investigate the stability of the nanoparticle attachment to the polymeric membrane surface have been performed by the IOM institute and for PES-TiO$_2$ and PES-TiO$_2$-120C was reported elsewhere **(Fischer *et al.* 2017, Fischer *et al.* 2018)**. Additionally, SEM imaging for membranes both in fresh condition and after accelerated ageing was performed by a Carl Zeiss Ltd. Ultra 55 SEM (Germany) by IOM institute. Before imaging, samples were sputtered by a 30 nm layer of chromium (Leybold Z400, Germany) and then images at an electron energy of 2 or 10 kV. For cross-section imaging, samples were torn apart to avoid squeezing or demolition of the surface. SEM images coupled with energy-dispersive X-ray spectroscopy (EDX) were also performed at the electron energy of 15 kV to determine the coating of TiO$_2$ over the thickness of membranes.

In the evaluation of the photostability of membranes, photographs of aged membranes were taken a week after the collection of all samples using a camera, SONY, SLT-A58, for visual observation of changes.

The ultraviolet-visible light absorption of membranes (both pristine and coated) was measured by a Perkin Elmer Lambda 950, USA, UV-Vis-NIR spectrophotometer. Samples were placed in a 4 cm × 4 cm silica fluorescence cuvette with a 10 mm light path (Starna Scientific, Spectrosil Quartz, United Kingdom) filled with MilliQ water. The cuvette was fixed in the center of an integrating sphere using a 3D printed holder. The exclusion port in the integrated sphere was kept open during the measurement to exclude the specular lights reflected from the cuvette surface. Using the integrating sphere had the benefit of accounting for all reflected lights.

For measuring the bandgap of synthesized nanoparticles coated on the polymeric membrane, diffuse reflectance spectra (DRS) measurement was performed using the same set-up (Perkin Elmer Lambda 950, USA, UV-Vis-NIR spectrophotometer with an integrated sphere), but this time the sample was adjusted at the rear side of the integrating sphere with 0% transmittance ordinate mode. In this mode also, the exclusion port was open during the measurement. The incident light was adjusted perpendicular to the sample and light striking the center of the sample after passing through the integrating sphere. For determining the bandgap of TiO_2 coated on the membrane, the diffuse reflectance value of the pristine membrane was measured and deducted from the coated membrane to get the data for the TiO_2 nanoparticles only. Then the Kubelka-Munk method was applied, and the bandgap was determined using the equations **3-5** and **3-6**:

$$F(Ref) = \frac{(1 - Ref)^2}{2Ref}$$

3-5

$$(hvF) \cong (hv - E_g)^2$$

3-6

where F is the Kubelka-Munk Function and Ref is the reflectance data obtained from DRS measurement, hv is the photon energy and E_g is the band gap of the photocatalyst. By plotting the $(hvF)^{\frac{1}{2}}$ versus the hv, the bandgap energy (E_g) was calculated.

An attenuated total reflection-FTIR spectrometer (ATR-FTIR, Spectrum Two, Perkin Elmer, resolution 4 cm^{-1}, 16 scans) was employed to evaluate the surface chemical compositions of fresh and aged membranes. The top surface of the membrane was also characterized before and after ageing by means of X-ray photoelectron spectroscopy, XPS, Kratos Analytical Ltd. Axis Ultra with a monochromatic Al Kalpha cathode (Manchester, UK). Thermogravimetry analysis (TGA, Perkin Elmer) was performed on fresh membranes to determine the loading of TiO_2 on the membranes. To do this, pristine and coated

membranes with a certain area were burnt under the air (oxidative condition) and the remaining mass was considered TiO_2 content. The temperature was gradually increased to 900 °C with a constant rate of 10 °C/min.

Brunauer-Emmett-Teller (BET) method was used to compare the specific surface area available of PES-TiO_2 and PVDF-TiO_2 membranes. Nitrogen was used as the gas for the adsorption data.

In photocatalytic membranes, the surface charge of the membrane can be determined by streaming potential measurements. Measurement of streaming potential is by flowing an electrolyte solution through a channel with charged walls by pressure which then the electric potential is measured (**Figure 3-11**). Having measured the streaming potential, zeta potential can be measured, and with that, the isoelectric point (IEP) of the surface is determined.
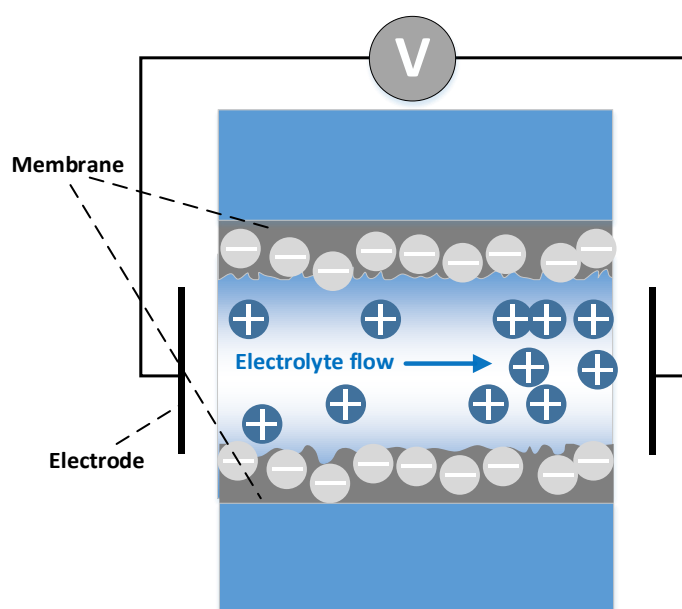
Figure 3-11 Schematics showing the streaming potential technique, electrolyte flow in a capillary channel and the charge separation along the channel.

The zeta potential is the electrical potential at the interface of flowing fluid and attached fluid to the surface **Figure 3-11**). It should be noted that zeta potential is an interfacial property, and it is present when a surface like a membrane is in contact with a liquid (electrolyte solution). The sign of the zeta potential (negative or positive) shows the dominant charge at the surface.

The surface charge of aged samples for assessing their changes during the ageing process was measured by Anton Paar Austria company. The measurement was done by an electrokinetic analyzer (SurPASS, Anton Paar, Austria) using streaming potential analysis. Other than this, the surface charge test of PES-TiO_2 and PVDF-TiO_2 were repeated with an electrokinetic analyzer by measuring the streaming potential

in IAMT-KIT. Samples were mounted in an adjustable gap cell with dimension 2 × 1 cm for rectangular samples shown in **Figure 3-12**. The gap height was adjusted to 100 µm. Measurement was performed with an electrolyte solution of 1 mM and 10 mM KCl and the pressure difference was set at 0.2 bar. All data were collected using Attract software (2.1.5, Anton Paar GmbH, Austria). Zeta potential data (ζ) was obtained by the software directly from streaming potential data using equation **3-7) (Szymczyk *et al.* 2013)**.

$$\zeta = \frac{dU_{str}}{d\Delta p} \times \frac{\eta}{\varepsilon \times \varepsilon_0} \times \kappa_B \qquad \textbf{3-7}$$

where *dU/dp* is the slope of the plot of streaming potential *vs.* differential pressure, *κB* is electrolyte conductivity, η is electrolyte viscosity, ε is the dielectric coefficient of electrolyte, and *ε0* is permittivity.
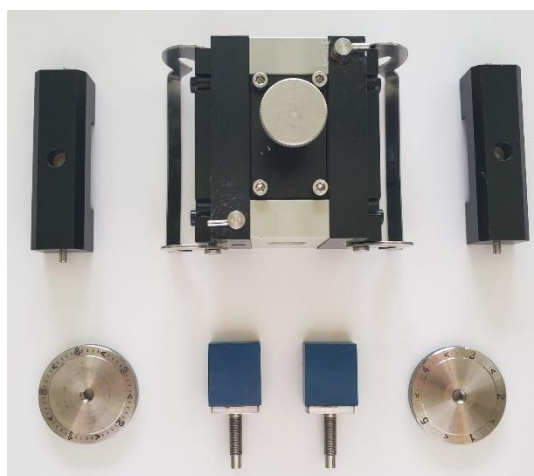
Figure 3-12 Adjustable gap cell for rectangular samples, the size of the rectangular sample was 2 cm × 1 cm.

3.11 Analytical Methods

This part includes a description of two analysis methodologies for MB and radiolabeled hormone concentration detection.

3.11.1 Concentration measurements of MB

The light absorption of the MB was measured using a UV/VIS Spectrophotometer (PerkinElmer Lambda 365, Double Beam UV-Visible Spectrophotometer). The UV-vis spectrophotometer measured the absorbance of the MB solution every 10 seconds online and reported the absorbance data (*A*). The extracted data was absorbance which is basically obtained by equations **3-8** and **3-9** in the Device software:

$$A = -log_{10}\frac{I}{I_0} \qquad \textbf{3-8}$$

$$T = \frac{I}{I_0}$$
<div align="right">**3-9**</div>

where A is absorbance (a.u.), T is transmittance (%), I_0 is the incident irradiation (energy from the light source) and I is the transmitted light (light which is not absorbed or reflected). Based on Beer-Lambert's law, the relation between absorbance and concentration is linear (equation **3-10**). Therefore, by plotting a calibration curve and the absorbance data, the concentration of MB was obtained. The calibration curve for MB is presented in **Figure 3-13**. The limit of detection of the UV-Vis spectrophotometer for detecting MB was 0.1 mg/L.

<div align="right">**3-10**</div>

$$A = l \times c_{MB} \times \varepsilon_{MB}$$
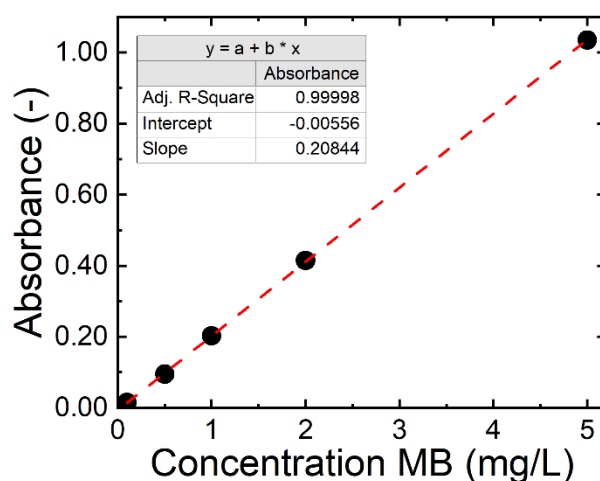
Figure 3-13 MB absorbance by UV-vis spectrophotometer at different concentration of MB (**Raota *et al.* 2023**).

3.11.2 Concentration measurements of radiolabeled hormones

The concentration of radiolabeled hormones in feed and permeates was determined using ultra-high-performance liquid chromatography (UHPLC, PerkinElmer) coupled with a flow scintillator analyzer (FSA, Radiomatic 625TR, Perkin Elmer). The methodology of UHPLC analysis with FSA was taken from the work of Lyubimenko *et al.* (**Lyubimenko *et al.* 2020**). Samples were kept in an autosampler (Flexar FX UHPLC, Perkin Elmer) at 4 °C. Then, 100 μL of the sample was injected into a UHPLC column (150 mm × 2.1 mm, Kinetex 1.7 μm C18, 100 Å) which was regulated at 50 °C in an LC column oven (Flexar LC, PerkinElmer). A guard column (C18, SecurityGuard Ultra, Phenomenex) was protecting the UHPLC column. The methanol-water elution of 40:60 was pumped using a UHPLC pump (FX-20 UHPLC binary solvent pump) with a flow rate of 0.25 mL/min. After the column, the eluent was mixed with a liquid scintillation cocktail (Ultima Flo M, PerkinElmer LAS GmbH, Germany) which was pumped at a flow rate of 4 mL/min by the internal volume scintillator pump of FSA to a static mixing tee. The activity of the mixed liquid was obtained by photon counting using two photomultiplier tubes

(PMT) and a coincidence counting circuit in the FSA detector. The schematic illustrating the analytical system is presented in **Figure 3-14**.
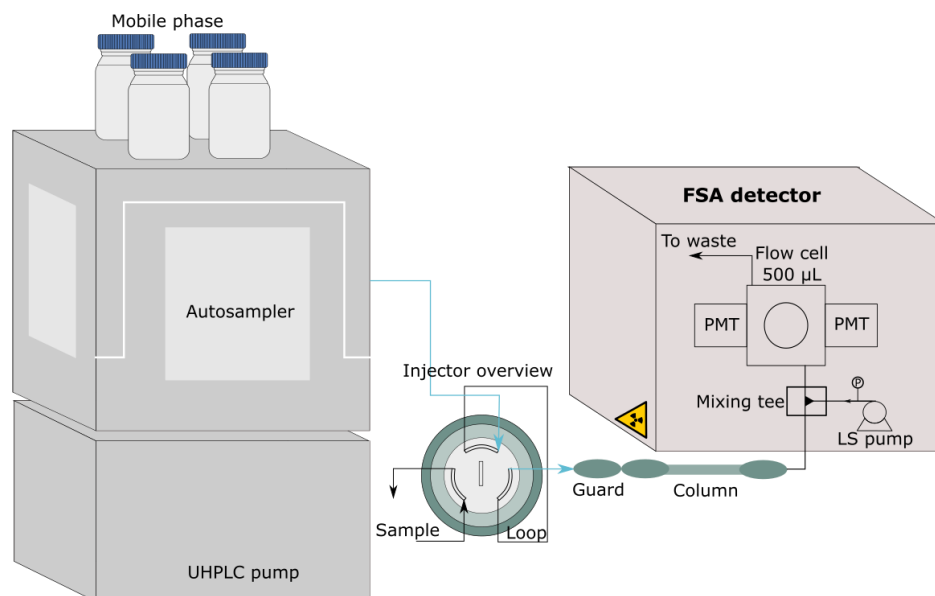
Figure 3-14 Simplified schematic of the UHPLC-FSA system with the details of the FSA detector.

Calibration curves were prepared each time by receiving a new stock solution. A calibration curve with data from different stock solutions for each steroid hormone and for the experiments with PES-TiO$_2$ and PVDF-TiO$_2$. The calibration equations can be found in **Table 3-8**. The limit of detection (LOD) with this method was 1.5-2.4 ng/L and the limit of the quantification was 3.4-4.3 ng/L **(Lyubimenko *et al.* 2020)**.

Table 3-8 Calibration equation of steroid hormones, E1, E2, P, and T in experiments of PES-TiO$_2$ and PVDF-TiO$_2$, Concentration (y)= constant (b)* HPLC peak area (x)

Hormone	b	Adj. R-Square
Progesterone (P)	27.58±0.81	0.994
Testosterone (T)	27.25±0.69	0.996
Estradiol (E2)	20.23±0.22	0.993
Estrone (E1)	22.22±0.18	0.999

A liquid scintillation counter (LSC, Tri-Carb 4910TR, Perkin Elmer) was used to determine the total concentration of radiolabeled steroid hormones. In this method, 1 mL of the sample was mixed with the scintillation liquid (Ultima-Gold LLT, Perkin Elmer) and the activity of the sample was analyzed. Although the sensitivity of this method was higher (LOD: 0.1–0.9 ng/L for E1 and E2 **(Schäfer *et al.* 2003)**), this method could not separate the hormones. Therefore, it was only used for concentration

determination of feed samples of a single hormone solution before and after the experiment and the samples in the dark phase of only 1 hormone in which no intermediate was expected to be present, hence the total activity was only related to the hormone itself.

Total organic carbon (TOC) was analyzed using two devices with different analysis methods. First, the samples were analyzed by a portable TOC analyzer (GE Sievers M9, USA). In this method, ammonium persulphate as oxidizer and phosphoric acid for acidification with a flow rate of 1 μL min^{-1} was used. In the second method, samples were analyzed in a TOC machine (TOC-L 03208, Shimadzu Corp.) with a 680 °C catalytic combustion methodology. This was done to compare oxidation with ammonium persulphate and catalytic combustion. The calibration curve of both devices is shown in **Figure 3-15**.
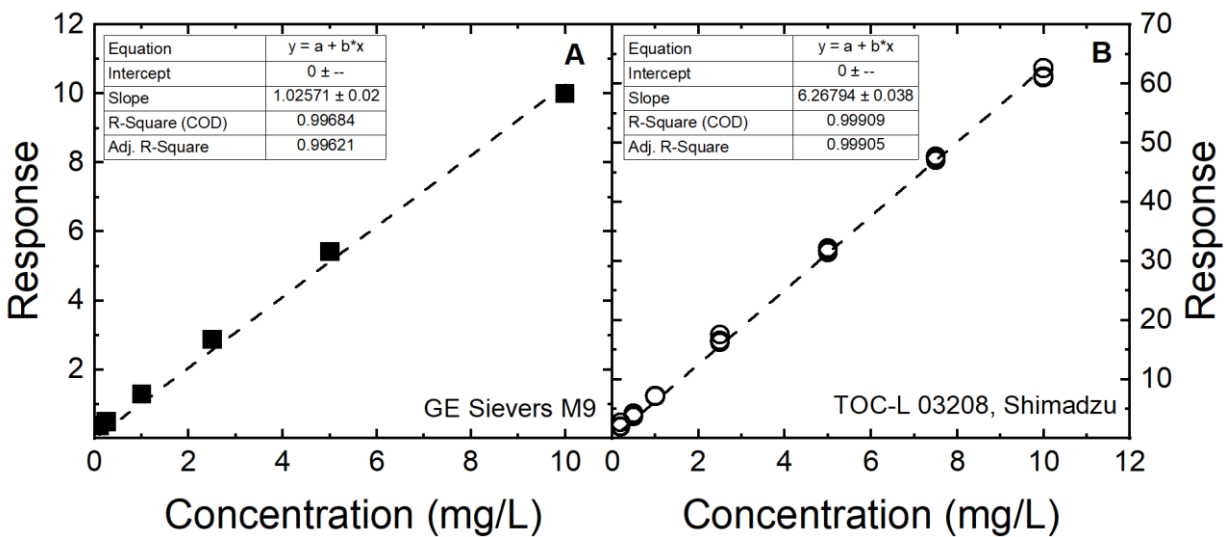
Figure 3-15 TOC calibration curve for two devices used in this work, (A) GE Sieveres M9, (B) TOC-L 03208 Shimadzu.

The content of Ti in the water samples released from aged membranes after light exposure was determined using inductively coupled plasma-optical emission spectrometry (ICP-OES). Before detection, a 5 mL sample was mixed with 1 ml HF and 0.5 ml HNO_3 and then digested at 80 °C overnight (about 14 h) in a graphite oven.

3.12 Kinetics

Several parameters have been used to compare membranes, and PMR configurations and to quantify photocatalytic degradation. **Table 3-9** presents the basic ones.

Table 3-9 Parameters for characterizations of photocatalytic membrane performance.

Water Flux (J_m, L/m²h)	$J_m = \dfrac{Q_p}{A}$	Q_p: Permeate flow rate (L/hr) A: active filtration area (m²)	3-11

Permeability (L, L/m²hbar)	$L = \dfrac{J_m}{\Delta P}$	ΔP: transmembrane pressure (bar)	3-12
Removal (R, %)	$R = \left(1 - \dfrac{c_P}{c_f}\right) \cdot 100$	c_f and c_P : feed and permeate concentration (ng/L) for hormone and (mg/L) for MB	3-13
rate of disappearance (r″, mol/m²s)	Flow-along and Flow-through PMRs: $-r''_A = -\dfrac{1}{A_{membrane}} \cdot \dfrac{dN_A}{dt}$ $= \dfrac{mole\ A\ reacted}{A_{membrane} \cdot t}$ $\rightarrow r'' = \dfrac{1}{A_{membrane}} \cdot Q_f \cdot (c_p - c_f) \cdot \dfrac{1}{M_{MB}}$ $\rightarrow r'' = \dfrac{1}{A_{membrane}} \cdot Q_f \cdot (c_f \cdot R) \cdot \dfrac{1}{M_{MB}}$ Batch PMR: $r''_{MB\ batch} = \dfrac{V_r}{\bar{t} \times A_{membrane}} \cdot (c_0 - c_{\bar{t}}) \cdot \dfrac{1}{M_{MB}}$	$A_{membrane}$: top surface of the membranes (m²) t: time of reaction (s) Q_f: feed flow rate (L/s) M: molecular weight to convert molar to mass concentration (mg/mole) V_r: reactor volume (m³) In batch c_f and c_P should be in mg/m³	3-14

The residence time was calculated in three parts of the PMR cell. In flow-along mode, the solution was only in the channel and the diffusion to the membrane was neglected. In the flow-through mode, the solution passed both the channel and the membrane. Equations **3-15**, **3-16** and **3-17** express residence time (s) calculations.

$$\bar{t}_{flow-along} = \frac{V_{channel}}{Q} = \frac{w_{channel} \times l_{channel} \times h_{channel}}{Q} \qquad \textbf{3-15}$$

$$\bar{t}_{membrane} = \frac{V_{membrane}}{Q} = \frac{w_{channel} \times l_{channel} \times th_{membrane} \times \varepsilon_{membrane}}{Q} \qquad \textbf{3-16}$$

$$\bar{t}_{flow-through} = \frac{V_{channel} + V_{membrane}}{Q} \qquad \textbf{3-17}$$

where Q is feed flow rate (cm³/s), w stands for the width (cm), l for length (cm), h for height (cm), th for thickness (cm) and ε for porosity. For these calculations, the following parameters were used (**Table 3-10**):

Table 3-10 Parameters for residence time determination, original source (**Regmi _et al._ 2020**).

Parameter	Unit	Value
Membrane width	cm	1
Membrane length	cm	2
Channel height	cm	0.07

Channel volume (flow-along reactor) *	cm^3	0.14
Membrane pore volume	cm^3	Depending on the membrane, refer to **Table 3-2**
Membrane porosity	%	
Membrane thickness	μm	
Filtration area	cm^2	2
Flow rate	mL/min	0.5-10

*Channel is considered as the space between the membrane surface and quartz window inside the cell

For comparing PMR configuration, batch, flow-along and flow-through, the figures of merit space-time yield (STY), photocatalytic space-time yield (PSTY) and specific energy consumption (SEC), adapted from Leblebici *et al.* and Claes *et al.* (**Leblebici *et al.* 2015, Claes *et al.* 2019**), were employed. STY is defined as the amount of pollutant degraded per reactor volume (or coated membrane surface area or catalyst weight) per time. Equations **3-18** and **3-19** were employed to calculate the STY for batch, flow-through and flow-along modes considering the reactor volume.

$$STY_{1,batch} = \frac{\text{Amount of pollutants degraded after } \bar{t}}{V_r \cdot \bar{t}} = \frac{V_r \cdot (c_0 - c_0 \cdot e^{-k\bar{t}})}{V_r \cdot \bar{t}} \cdot \frac{1}{M_{MB}}$$
$$= \frac{c_0 \cdot (1 - e^{-k\bar{t}})}{\bar{t} \cdot M_{MB}}$$

3-18

$$STY_{1,flow-along/through} = \frac{(c_0 - c_{\bar{t}}) \cdot Q}{V_r} \cdot \frac{1}{M_{MB}}$$

3-19

where $\bar{t}$ is the residence time (s), Vr is the reactor volume (cm^3), c_0 is the MB initial concentration (g/cm^3), $c_{\bar{t}}$ is the MB concentration at the time $\bar{t}$ (g/cm^3), k is the apparent rate constant (per s), Q is the volumetric flow rate in the flow-along/through process (cm^3/s) and M_{MB} is the molar mass of MB (g/mol). Unit conversion for MB initial concentration and flow rate was done. Considering the membrane surface area (TiO$_2$ coated) instead of reactor volume, STY$_2$ for the batch reactor can be calculated *via* equation **3-20** and for both the continuous flow processes equation **3-21** was utilized.

$$STY_{2,batch} = \frac{c_0 \cdot (1 - e^{-k\bar{t}}) \cdot V_r}{A_{membrane} \cdot \bar{t}} \cdot \frac{1}{M_{MB}}$$

3-20

$$STY_{2,flow-along/through} = \frac{(c_0 - c_{\bar{t}}) \cdot Q}{A_{membrane}} \cdot \frac{1}{M_{MB}}$$

3-21

where $A_{membrane}$ is the active membrane area (cm^2). This area was about double in the batch *vs.* the continuous-flow system. Considering the catalyst weight (instead of reactor volume or coated membrane

surface area), STY_3 for the batch reactor can be calculated *via* equation **3-22** and for both the flow-along/through processes equation **3-23** was used;

$$STY_{3,batch} = \frac{c_0 \cdot \left(1 - e^{-k\bar{t}}\right).V_r}{m_{TiO2} \cdot \bar{t}} \cdot \frac{1}{M_{MB}}$$ **3-22**

$$STY_{3,flow-along/through} = \frac{(c_0 - c_{\bar{t}}).Q}{m_{TiO2}} \cdot \frac{1}{M_{MB}}$$ **3-23**

where m_{TiO2} is the catalyst weight (g). PSTY was defined as the amount of pollutant degraded per time and power light consumption, $PSTY_1$, or power light intensity received by the system, $PSTY_2$. To evaluate the efficiency of the PMR considering the photonic energy consumption, $PSTY_1$ (mol/(Ws)) was calculated by dividing STY_1 by the normalized light power (NLP, W/cm³). NLP was defined as the normalized light power which can illuminate 1 cm³ of the reactor (equation **3-24**).

$$NLP = \frac{P}{V_r}$$ **3-24**

where P is the electric power of the light (W), and V_r is the reactor volume (cm³). Hence, $PSTY_1$ can be determined by equation **3-25**;

$$PSTY_1 = \frac{STY_1}{NLP}$$ **3-25**

To assess the efficiency of the reactor considering the light power intensity, $PSTY_2$ (mol/(W s)) was calculated by dividing STY_2 by the power intensity *via* equation **3-26**;

$$PSTY_2 = \frac{STY_2}{PI}$$ **3-26**

where PI is the light power intensity received by the system (W/cm²).

SEC (kWh/m³) was also used for reactor comparison and was adapted from Lawrence *et al*. **(Lawrence *et al*. 2019)**. SEC was defined as the electrical energy required to treat a volume of water. Hence, only energy efficiency and reactor productivity are considered. SEC is calculated *via* equation **3-27** for the batch reactor and equation **3-28** for both the flow-along/through configurations;

$$SEC_{batch} = \frac{P.\bar{t}}{V_r}$$ **3-27**

$$SEC_{flow-along/through} = \frac{P}{Q}$$ **3-28**

where P is the electric power of the light (W), $\bar{t}$ is the residence time (s), V_r is the reactor volume (cm^3), and Q is the volumetric flow rate in the flow-along/through (cm^3/s).

The mass adsorbed of MB and steroid hormone per unit area of the membrane (m_{ads}, ng/cm^2) was determined first by experimenting in the dark phase for the target pollutant and then performing a mass balance, presented in equation **3-29**;

$$m_{ads} = \frac{\left(c_f \cdot V_f - \sum_{i=1}^{n,sample} c_{p,i} \cdot V_{p,i}\right)}{A} \qquad \textbf{3-29}$$

where c_f and V_f are concentration and volume of feed, $c_{p,i}$ is the permeate concentration (mg/L for MB and ng/L for steroid hormones) and $V_{p,i}$ is the volume of permeate sample (L) collected in the dark phase and A is membrane surface area (m^2). Equally, by plotting the c_p/c_f versus cumulative permeate volume, the mass adsorbed (m_{ads}) could be determined *via* integration of the surface area above the plot and equation X can be re-written in equation **3-30**:

$$m_{ads} = \frac{1}{A} \cdot c_f \cdot \int_0^{V_p} (1 - \frac{c_p}{c_f}) dV \qquad \textbf{3-30}$$

However, considering the system volume (volume of the pipes and connections for sensors) and displacement of feed solution with MilliQ water, there was a delay between the start of the pump and sample collection for both pollutant and background salts. To compensate for this delay, data on permeate conductivity was collected (equal to tracer compound) and used as an indicator for the fastest response of the system assuming that there is no adsorption and no loss of NaCl and NaHCO$_3$ in the system. Consequently, equation **3-30** was re-written as equation **3-31**.

$$m_{ads} = \frac{1}{A} \cdot c_f \cdot \int_0^{V_f} (\frac{EC_p}{EC_f} - \frac{c_p}{c_f}) dV \qquad \textbf{3-31}$$

where EC_p and EC_f are the permeate and feed electrical conductivity (EC, mS/cm), respectively.

3.13 Removal values determination

In the case of PES-TiO$_2$, the permeate concentration was fluctuating considerably compared to the PVDF-TiO$_2$ degradation result. Therefore, for the results from this membrane, it was decided to use a fitting curve to compensate for the fluctuations. A curve fitting in software Origin 2018 to draw the concentration as a function of permeate volume in the light phase from 100 mL to 700 mL.

$$y = a \cdot x^b \qquad\qquad\qquad\qquad \textbf{3-32}$$

where y is the concentration ratio c_p/c_f (-), x is the cumulative permeate volume (V_p, mL), and a and b are determined from the curve fitting of experimental data. After obtaining the equation for every single experiment, the concentration ratio and removal were calculated at the cumulative permeate volume of 700 mL. An example is shown in **Figure 3-16** and **Table 3-11**.
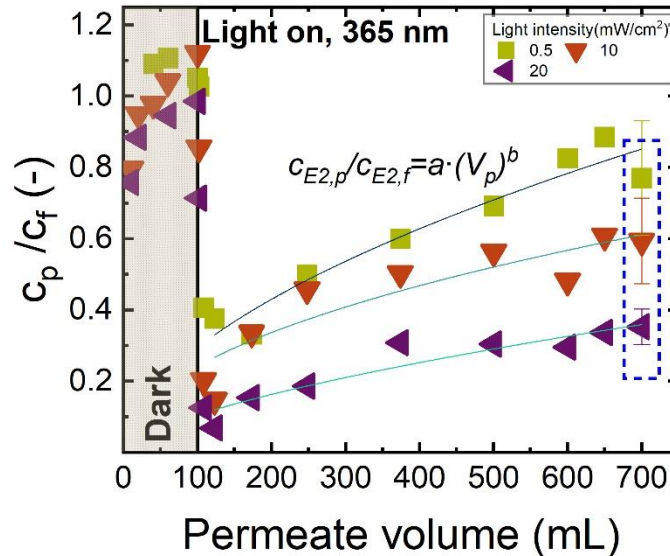
Figure 3-16 Example of curve-fitting to determine the removal at 700 mL permeate volume point for three example experiments PES-TiO$_2$, 0.5, 10 and 20 mW/cm^2, 600 L/m^{2}h, 23±0.2 °C, 8.6±0.4, 100 ng/L E2, 1 mM NaHCO$_3$, 10 mM NaCl, 27.2 mg/L EtOH and 79.2 mg/L MeOH. Original source (**Lotfi** *et al.* **2022).**

With the equation obtained from curve fitting, the concentration ratio at 700 mL was calculated and the removal was calculated from this data. The comparison of experimental values and curve fitting for these 3 experiments is shown in **Table 3-11**.

Table 3-11 Comparison of curve fitting and experimental data for three sample experiments with PES-TiO$_2$ at permeate volume of 700 mL. Original source (**Lotfi** *et al.* **2022).**

Experiment/Light intensity mW/cm²	a	b	Experimental c_p/c_f	Curve fitting c_p/c_f
0.5	0.02396 ± 0.01033	0.54508 ± 0.06939	0.77±0.16	0.85
10	0.02712 ± 0.01978	0.47547 ± 0.11791	0.59±0.12	0.61
20	0.00805 ± 0.01658	0.57935 ± 0.09639	0.35±0.05	0.36

The value calculated by curve-fitting was within the error range of the experimental value.

3.14 Error estimation

Few parameters were considered for determining the uncertainty of the obtained data, including 1) PMR setup and its components (ΔS) including pressure (ΔP), temperature (ΔT), and conductivity sensors (ΔEC) in the feed and permeate, and the light source ($\Delta light$), 2) variation in membrane permeability (ΔQ), 3) feed solution preparation considering the uncertainties of pipetting and volumetric flask ($\Delta Prep$), 4) uncertainties from analytical devices for concentration detection using UHPLC system and radio detector ΔUHPLC and ΔDet respectively. For MB concentration detection using a UV-vis spectrophotometer, uncertainty comprised the photometric reproducibility and photometric drift over the time of each experiment which was 1% from the device specification sheet. The uncertainty of each parameter obtained from data of different sensors in the system and was calculated using equations **3-33** and **3-34:**

$$\Delta X_{abs} = \frac{X_{max} - X_{min}}{2} \qquad\qquad \textbf{3-33}$$

$$\Delta X_{rel} = \frac{\Delta X_{abs}}{\bar{X}} \qquad\qquad \textbf{3-34}$$

In equation **3-33** the ΔX_{abs} is the absolute error of a property, X_{max} and X_{min} are the maximum and minimum values during the experiment. In equation **3-34**, ΔX_{rel} (%) is the relative error and $\bar{X}$ is the average value of a property during the experiment. The uncertainty of system components was then calculated *via* equation **3-35** after calculating the uncertainty of different properties:

$$\Delta S = \sqrt{\Delta T_{f,rel}^2 + \Delta T_{p,rel}^2 + \Delta p_{rel}^2 + \Delta EC_{f,rel}^2 + \Delta EC_{p,rel}^2 + \Delta light_{rel}^2} \qquad\qquad \textbf{3-35}$$

Data from the sensor were utilized to determine the ΔT_{rel}, Δp_{rel} ΔEC_{rel}, and $\Delta light_{rel}$ (%) for each experiment and the error was calculated. In total average ΔS from the average error of each property was almost 8%. Then the experimental error (ΔE) from all the considered properties was calculated using equation **3-36**. For the MB degradation experiment, ΔUHPLC and ΔDet were replaced by 2% for the uncertainty of UV-vis spectrophotometer for each permeate and feed detection. In other words, since analysis with UV-vis spectrometry is accurate (photometric reproducibility <0.001 absorbances at absorbance equal to 1), the uncertainty for feed and permeate concentration was considered the same and Δdet was multiplied by 2.

$$\Delta E = \sqrt{\Delta S^2 + \Delta Q^2 + \Delta Prep^2 + \Delta UHPLC_f^2 + \Delta UHPLC_p^2 + \Delta Det_f^2 + \Delta Det_p^2}$$ **3-36**

Where the subscripts f and p are symbols of feed and permeate.

The error propagation method for UHPLC analysis was taken from Lyubimenko *et al.* **(Lyubimenko *et al.* 2020)**. Uncertainties regarding the concentration analysis of radiolabeled hormones comprised of two parts i) UHPLC system which includes the marginal variation of mass of injected analyte (1%) and column temperature (0.4%) ii) flow scintillation analyzer which the major error comes from this part (ΔDet: 12-16%). Equation **3-37** was employed to calculate the uncertainty of FSA detection.

$$\Delta Det = \sqrt{\Delta NC^2 + \Delta f_{tot}^2}$$ **3-37**

where ΔNC is the uncertainty of net counts from the FSA detector and Δf_{tot} is the uncertainty of the sum of flow rates of LS and UHPLC pumps through the flow cell of the FSA-detector (0.6%). ΔNC is calculated as shown below (equations **3-38,3-39,3-40,3-41**, and **3-42**) :

$$NC = sample\ count - background\ count$$ **3-38**

$$\Delta Det = 2 \cdot \frac{\sigma_{NC}}{NC}$$ **3-39**

$$\sigma_{NC} = \sqrt{\sigma_{sample}^2 + \sigma_{BG}^2}$$ **3-40**

$$\sigma_{sample} = \sqrt{sample\ count}$$ **3-41**

$$\sigma_{BG=}\sqrt{background\ count}$$ **3-42**

where σ_{NC} is the standard deviation of net counts (2σ corresponds to 95.5% confidence limit), σ_S is the standard deviation of the sample counting and σ_{BG} is the standard deviation of the background counting (calculated to be 6 counts/min from blank injections) **(Lyubimenko *et al.* 2020)**.

Relative error of analysis with LSC was calculated using an empirical equation **3-43** and it was replaced by ΔUHPLC and ΔDet in equation **3-43**:

$$\Delta C_{LSC,rel} = 10.536 \cdot c_{c_{LSC\ measured}}^{-0.5441}$$ **3-43**

where $c_{c_{LSC\ measured}}$ is the concentration of permeate measured using LSC analysis.

Since removal is directly related to the error of concentration ratio **3-13**, the uncertainty of hormone removal could be calculated using equation **3-44**:

$$\Delta R = \Delta E \cdot \frac{c_P}{c_f}$$

3-44

where ΔE (equation **3-36**) includes the error coming from concentration measurement of both permeate and feed, system sensors and feed preparation.

3.15 Experimental protocol

Table 3-12 Filtration protocol, valve numbers are based on the schematic of the system **Figure 3-5**. Original source (**Regmi** *et. al* **2020**).

No.	Step	Conditions (duration, volume, pressure, flow…)	Justification
1	Mounting new membrane sample	Tighten 8 screws of the reactor using 2 Nm of torque	Keep the channel height constant in all experiments
2	Purging the pump / cleaning the pump	500 mL/min for 10 sec of MilliQ with valve ⑤ open and ⑥ closed	Preventing clogging of valves
3	Flushing out air bubbles	100 mL/min for 2 min of MilliQ with valve ⑤ closed and ⑥ & ⑩ open (cross-flow filtration condition)	Air bubbles interfere with sensors
4	Preconditioning membrane	10 mL/min for 10 min of MilliQ with valve ⑩ closed (flow-through mode)	Pre-compaction of the membrane
5	Pure water flux	Run different flow rates for 5 min in flow-through mode and collect the pressure data at 5, 2, 1, 0.5 & 0.1 mL/min (*via* LabView)	Permeability test with MilliQ water
6	Getting background of absorption for UV-vis spectrophotometer	Fill the reference cuvette with MilliQ water, and get the background at the planed flowrate of the experiment and 664 nm (pressing the autozero in UV-vis spectrophotometer software)	Considering the absorption coming from other components at 664 nm and the planned flow rate of the experiment. After this step, the spectrophotometer cover should not be open, otherwise, this step should be repeated.
7	Filling the pump with MB solution	Switch feed tank, run 100 mL/min for 30 sec with valve ⑤ open and ⑥ closed (in LabView)	- Changing from MilliQ to MB solution and filling the pump with MB - flushing out air bubbles resulting from changing the feed tank

No.	Step	Conditions (duration, volume, pressure, flow…)	Justification
8	Setting the pump to the flow rate of the experiment	(1 mL/min as a standard condition) with valve ⑤ and ⑩ closed and ⑥ open;	
9	Adsorption step in the dark	Run with LED off for 100 mL (100 min at 1 mL/min at the standard condition), Start the software to record the MB absorption continuously for 350 min at least	MB solution is filtered until permeate concentration is constant. During this time the "S"-shape of the concentration curve vs time (permeate volume) is observable
10	Degradation with light	Switch the LED on and run for 250 mL (250 min for 1 mL/min)	Degradation is ideally continued until a steady state of degradation is noticed
11	Repeat the flushing with MilliQ and pure water flux after the degradation	Repeat steps 2 & 5 with MilliQ	Pure water flux is repeated after the experiment to ascertain no significant membrane modification or fouling has occurred

Table 3-13 Filtration protocol, valve numbers are based on the schematic of the system **Figure 3-5**, the first 5 steps are similar for degradation of MB and steroid hormones. Original source (**Lotfi** *et. al* **2022**).

No.	Step	Conditions (duration, volume, pressure, flow…)	Justification
1	Mount new membrane sample	Tighten 8 screws of the reactor using 2 Nm of torque	Keep the channel height constant in all experiments
2	Purge the pump / cleaning the pump	500 mL/min for 10 sec of MilliQ with valve ⑤ open and ⑥ closed	Preventing clogging of valves
3	Flush out air bubbles	100 mL/min for 2 min of MilliQ with valve ⑤ closed and ⑥ & ⑩ open (cross-flow)	Air bubbles interfere with sensors
4	Preconditioning membrane	10 mL/min for 10 min of MilliQ with valve ⑩ closed (Flow through)	Pre-compaction of the membrane
5	Pure water flux	Run different flow rates for 5 min in flow-through mode and collect the pressure data (5, 2, 1, 0.5 & 0.1 mL/min) (in LabView)	Permeability test with MilliQ water
6	Fill the pump with hormone solution	Switch feed tank, run 100 mL/min for 30 sec with valve ⑤ open and ⑥ closed (in LabView)	- Change from MilliQ to hormone solution and fill the pump with hormone - flushing out air bubbles resulting from changing the feed tank

7	Set the pump to the flow rate of the experiment	(2 mL/min as a standard condition) with valve ⑤ and ⑩ closed and ⑥ open;	
8	Adsorption step in the dark	Run with LED off for 100 mL (50 min at 2 mL/min at the standard condition), taking 5 samples at points 10, 20, 40, and 60,100 mL. The sample volume is 2 mL.	SH solution is filtered until permeate concentration is constant. Sample points were chosen such that the "S"-shape is observable with at least 3 samples during adsorption (40, 60, 100mL)
9	Degradation with light	Switch the LED on and run for 600 mL (300 min for 2 mL/min), Samples are collected at points 102, 108, 123, 174, 248, 374, 500, 600, 650,700 mL (10 samples in total, 2 mL sample volume) (samples were collected automatically using LabView)	Sample positions are chosen such that at the beginning of degradation, the rapid change in permeate concentration is recorded while larger intervals are chosen during more stable conditions
10	Repeat the flushing with MilliQ and pure water flux after the degradation	Repeat steps 2 & 5 with MilliQ	Pure water flux after the experiment to ascertain no significant membrane modification or fouling has occurred
11	Flush the 15 sample-taking positions	Flush the 15 sample lines with MilliQ water for 1 min at 10 mL/min (programmed in LabView)	Removing the sample residues
12	Drying the system	Drying with air	Eliminate water remaining in tubes and prevent further dilution with water in subsequent experiments

3.16 References

Berger, T. E., C. Regmi, A. I. Schäfer and B. S. Richards (2020). "Photocatalytic degradation of organic dye *via* atomic layer deposited TiO_2 on ceramic membranes in single-pass flow-through operation." Journal of Membrane Science **604**: 118015.

Claes, T., A. Dilissen, M. E. Leblebici and T. Van Gerven (2019). "Translucent packed bed structures for high throughput photocatalytic reactors." Chemical Engineering Journal **361**: 725-735.

Fischer, K., A. Gawel, D. Rosen, M. Krause, A. Abdul Latif, J. Griebel, A. Prager and A. Schulze (2017). "Low-Temperature Synthesis of Anatase/Rutile/Brookite TiO_2 Nanoparticles on a Polymer Membrane for Photocatalysis." Catalysts **7**: 209.

Fischer, K., P. Schulz, I. Atanasov, A. Abdul Latif, I. Thomas, M. Kühnert, A. Prager, J. Griebel and A. Schulze (2018). "Synthesis of High Crystalline TiO_2 Nanoparticles on a Polymer Membrane to Degrade Pollutants from Water." Catalysts **8**: 376.

Hori, T., N. Kamon, H. Kojima, R. M. Rohner and H. Zollinger (1987). "Structure correlation between diffusion coefficients of simple organic compounds and of anionic and cationic dyes in water." Journal of the Society of Dyers and Colourists **103**: 265-270.

Imbrogno, A. and A. I. Schäfer (2019). "Comparative study of nanofiltration membrane characterization devices of different dimension and configuration (cross flow and dead end)." Journal of Membrane Science **585**: 67-80.

Lawrence, A., P. Thollander, M. Andrei and M. Karlsson (2019). "Specific energy consumption/use (SEC) in energy management forimproving energy efficiency in industry: Meaning, usage and differences." Energies **12**: 247.

Leblebici, M. E., G. D. Stefanidis and T. Van Gerven (2015). "Comparison of photocatalytic space-time yields of 12 reactor designs for wastewater treatment." Chemical Engineering and Processing: Process Intensification **97**: 106-111.

Lotfi, S., K. Fischer, A. Schulze and A. I. Schäfer (2022). "Photocatalytic degradation of steroid hormone micropollutants by TiO_2 coated polyethersulfone membranes in a continuous flow-through process." Nature Nanotechnology **17**: 417–423.

Lyubimenko, R., D. Busko, B. S. Richards, A. I. Schäfer and A. Turshatov (2019). "Efficient Photocatalytic Removal of Methylene Blue Using a Metalloporphyrin–Poly(vinylidene fluoride) Hybrid Membrane in a Flow-Through Reactor." ACS Applied Materials & Interfaces **11**: 31763-31776.

Lyubimenko, R., O. I. Gutierrez Cardenas, A. Turshatov, B. S. Richards and A. I. Schäfer (2021). "Photodegradation of steroid-hormone micropollutants in a flow-through membrane reactor coated with Pd(II)-porphyrin." Applied Catalysis B: Environmental **291**: 120097.

Lyubimenko, R., B. S. Richards, A. Turshatov and A. I. Schäfer (2020). "Separation and degradation detection of nanogram-per-litre concentrations of radiolabelled steroid hormones using combined liquid chromatography and flow scintillation analysis." Scientific Reports **10**: 7095.

Mudalige, T., H. Qu, D. Van Haute, S. M. Ansar, A. Paredes and T. Ingle (2019). Chapter 11 - Characterization of Nanomaterials: Tools and Challenges. Nanomaterials for Food Applications. A. López Rubio, M. J. Fabra Rovira, M. martínez Sanz and L. G. Gómez-Mascaraque, Elsevier**:** 313-353.

Opsytec Dr. Gröbel GmbH. (2021). "COMPACT UV-LED CHAMBER BSL-01."   Retrieved March, 2021, from https://www.opsytec.com/products/irradiation-chamber/bsl-01.

Raota, C. S., S. Lotfi, R. Lyubimenko, B. S. Richards and A. I. Schäfer (2023). "Accelerated ageing method for the determination of photostability of polymer-based photocatalytic membranes." Journal of Membrane Science: 121944.

Regmi, C., S. Lotfi, J. C. Espíndola, K. Fischer, A. Schulze and A. I. Schäfer (2020). "Comparison of Photocatalytic Membrane Reactor Types for the Degradation of an Organic Molecule by TiO_2-Coated PES Membrane." Catalysts **10**: 725.

Schäfer, A., L. Nghiem and T. Waite (2003). "Removal of the natural hormone estrone from aqueous solutions using nanofiltration and reverse osmosis." Environmental Science & Technology **37**: 182-188.

Schulze, A., M. F. Maitz, R. Zimmermann, B. Marquardt, M. Fischer, C. Werner, M. Went and I. Thomas (2013). "Permanent surface modification by electron-beam-induced grafting of hydrophilic polymers to PVDF membranes." RSC Advances **3**: 22518.

Szymczyk, A., Y. I. Dirir, M. Picot, I. Nicolas and F. Barrière (2013). "Advanced electrokinetic characterization of composite porous membranes." Journal of Membrane Science **429**: 44-51.

Results and discussions

Chapter Four

4   Characterization of photocatalytic membranes

The characteristic of the photocatalytic membranes is critical in the performance of the PMR and final elimination of micropollutants. This includes the coating of TiO_2 on the membrane and its uniformity surface (SEM and SEM-EDX), the surface composition of PMs analyzing by FTIR and XPS, TiO_2 content by TGA, TiO_2 crystallinity and its band gap, specific surface area obtained by the BET method.

4.1.1   Surface characterization

SEM images of pristine membranes before coating (**Figure 4-1A** and **B)** and after coating with TiO_2 (**Figure 4-1C and D)** were performed to show the morphology of the membranes and confirm the coating of the TiO_2 nanoparticles. Membrane pores can be seen in these images, and it is clear that the coating process did not block or damage the membrane structure. Both PES and PVDF membranes showed good coverage of TiO_2 on the surface of the membrane after coating.

To verify if the TiO_2 has penetrated through the membrane pores during the coating procedure, SEM-EDX measurement was also performed. **Figure 4-1E**, and **F** presents the cross-sectional image of TiO_2 coated membranes. The blue color is an indication of Ti and the lighter color in the middle of PVDF-TiO_2 is an indication that the TiO_2 content on both surfaces of the membrane was higher. However, in PES-TiO_2 image, the coverage of TiO_2 (blue color) is more homogenous throughout the membrane, even though for this membrane also the surface has higher intensity of TiO_2 nanoparticle. Therefore, the membrane's material (PES or PVDF) influenced the uptake of TiO_2.
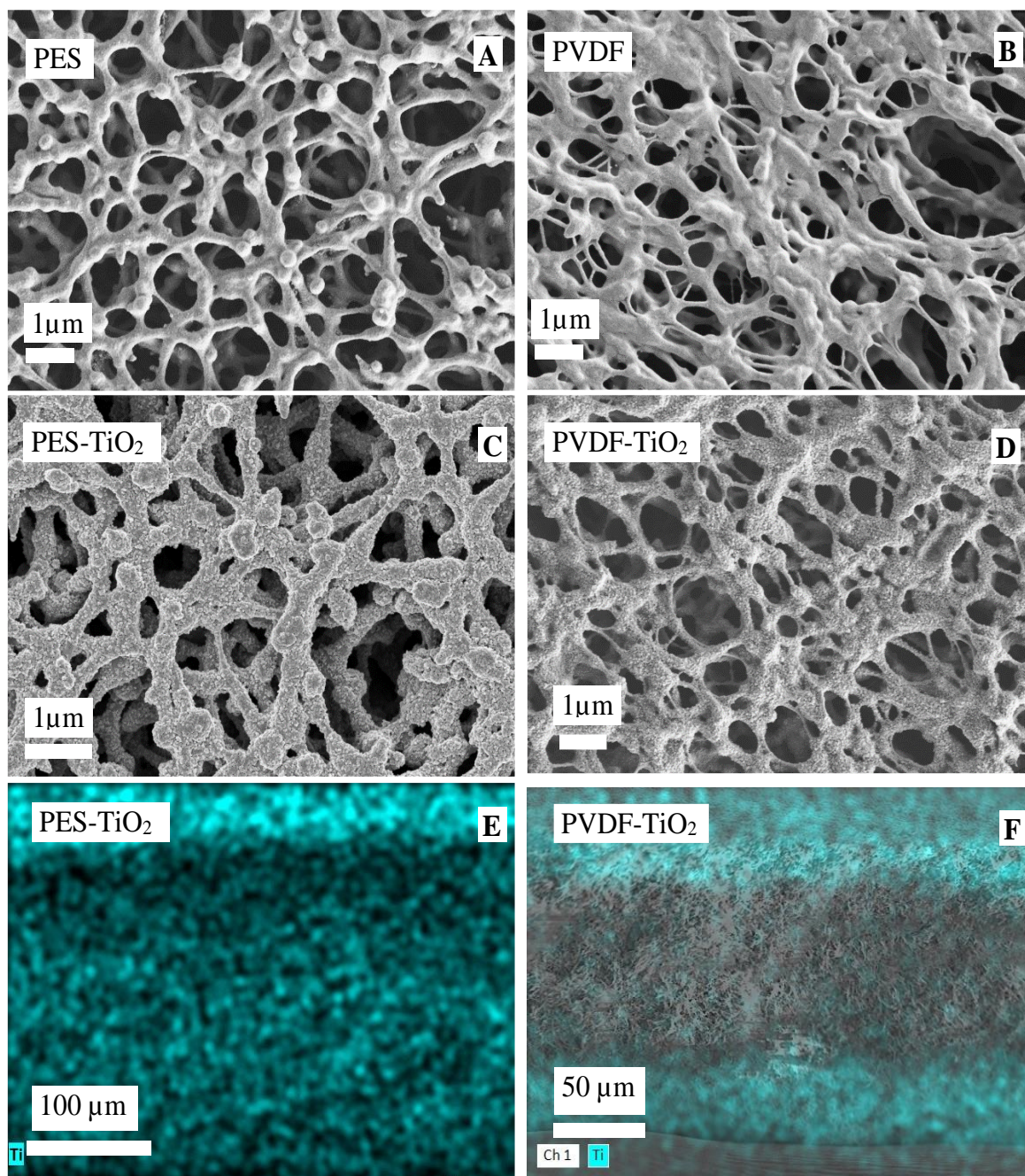
Figure 4-1 SEM images of (A) PES, (B) PVDF, (C) PES-TiO$_2$, and (D) PVDF-TiO$_2$, and SEM-EDX images of (E) PES-TiO$_2$ and (F) PVDF-TiO$_2$. SEM and SEM-EDX measurements were performed by IOM team[7]. Figure B Reprinted from **(Lui et al. 2023)**.

The size of nanoparticles is shown in **Table 3-3** (labelled as TiO$_2$-210C). PES-TiO$_2$ had an average particle size of 10 nm for anatase phase which is the most useful phase for photocatalytic purposes.

Next step, membranes were compared based on the absorption of light (**Figure 4-2**). In both cases, pristine membranes, PES and PVDF, had lower light absorption in comparison with the coated membranes. The addition of TiO_2 to the polymeric membrane increased the absorption of light by them with higher absorption for PES-TiO_2 at 365 nm. In **Figure 4-2**, sun irradiance (global 37 ° tilt: ASTM standard G-173) is demonstrated in the region of 300-700 nm. The integrated area underneath the sun irradiance between 300 and 387 is equal to 3.65 mW/cm^2. This range of wavelength is required for activation of the anatase phase of TiO_2 for ROS production. In the photocatalytic degradation experiments, a UV-LED was used as a light source with a peak wavelength of 365 nm. The integrated area of UV-LED shown in **Figure 4-2** is normalized to 10 mW/cm^2 as the standard light intensity used in most of the experiments.

C — ATOMIC PERCENTAGE (%)

	Ti	C	O	S	F
PES-TiO_2	6.6±1.2	54.3±2.4	36.1±0.5	3.6±0.5	---
PVDF-TiO_2	5.2±0.2	54.3±0.8	21.8±0.3	---	17.8±0.7
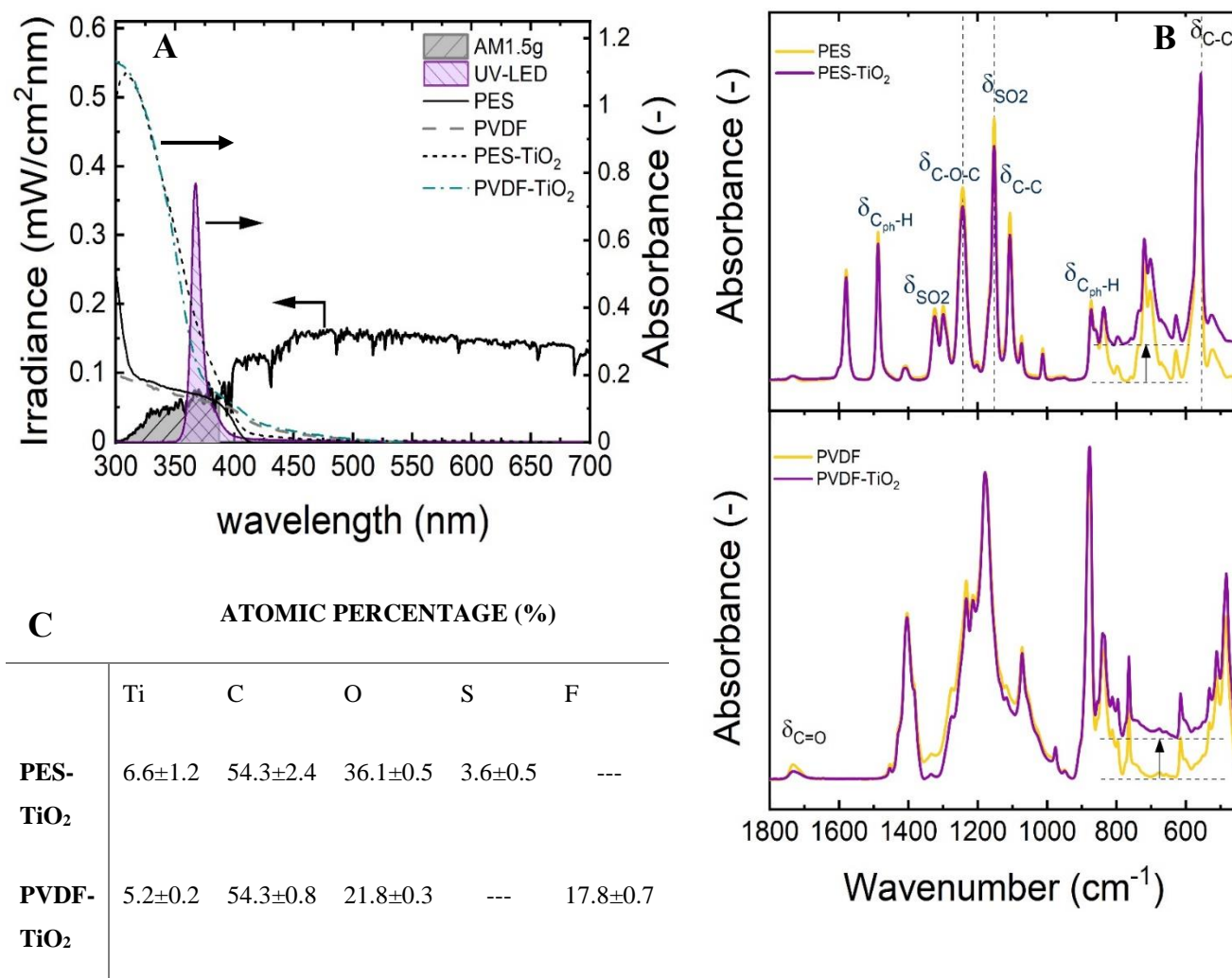
Figure 4-2 (A) Light absorption of PES and PVDF membrane and the TiO_2 coated membranes in the quartz cuvette filled with MilliQ water inside the integrating sphere, light absorbance related to the UV-LED, standard solar irradiance spectrum (global 37 ° tilt: ASTM standard G-173 (**ASTM-International**). (B) ATR-FTIR spectra of the pristine and coated membrane, PES, PES-TiO_2, PVDF, and PVDF-TiO_2 in the region of 1800-450 cm^{-1}. (C) The atomic percentage of elements on the surface of PMs obtained by XPS analysis, the data presented as the

average of five and three measurements for PES-TiO$_2$ and PVDF-TiO$_2$ respectively and the standard deviation of measurements. Original source of data is (**Lotfi** *et al.* **2022**) and (**Raota** *et al.* **2023**).

Membranes' surface was also characterized using attenuated total reflection Fourier Transform Infrared (ATR-FTIR) spectroscopy. Pristine and coated membranes were compared (**Figure 4-2**). In general, the binding between TiO$_2$ and membrane surface occurs through the connection of Ti^{+4} and oxygen atoms of the carboxyl group by three possible coordination modes monodentate, bridging bidentate, or chelating bidentate (**Figure 4-3**), or *via* the hydrogen binding between the carbonyl group and the hydroxyl group of titania (**Rotzinger** *et al.* **2004, Hojjati** *et al.* **2007**). Since the deposition of TiO$_2$ on the membrane surface was physical, no covalent bonds were formed, and no new peak was observed. Instead, in both polymeric membranes, coating with TiO$_2$ caused an increase in absorption in the spectra below 800 cm^{-1}.
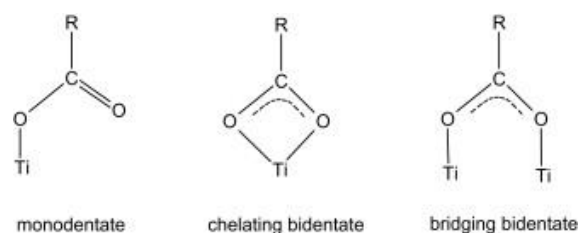
Figure 4-3 Coordination modes of carboxylate (from membrane surface) with Ti^{+4} cation, reprinted from (**Hojjati** *et al.* **2007**), Copyright 2023 with permission from Elsevier

This was also noticed by You *et al.* (**You** *et al.* **2012**) that observed a single broad absorption instead of peaks in the region below 800 cm^{-1} and was correlated to the vibrations of Ti-O and O-Ti-O bonds (**You** *et al.* **2012, Qian** *et al.* **2016**). Mansourpanah *et al.* (**Mansourpanah** *et al.* **2009**) also noted that by addition of TiO$_2$ to the polymeric membrane surface no significant changes appeared in the ATR-IR and concluded that probably non-covalence bonds were formed between Ti and polymer surface.

To have a better view of the amount of TiO$_2$ deposited on the membranes, thermogravimetry analysis (TGA) was performed (**Figure 4-4**). Membranes with the same diameter were burned under the air condition until 900 °C. The amount of TiO$_2$ on PES-TiO$_2$ was determined to be 0.39±0.04 mg/cm^2 and

0.09±0.05 mg/cm^2 on PVDF-TiO$_2$. The amount of mass is based on the top surface area of membranes and not the specific surface area.
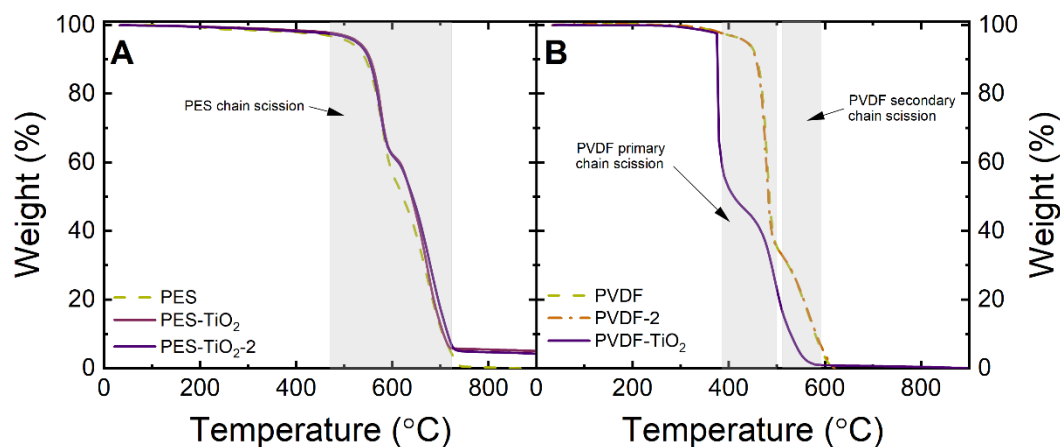
Figure 4-4 TiO$_2$ loading measurement on the membranes using TGA analysis, (A) PES and PES-TiO$_2$, (B) PVDF and PVDF-TiO$_2$, condition of measurement: 10 ºC/min heating rate, 20 mL/min airflow, reprinted (adapted) from **(Raota *et al.* 2023)**. The grey areas determine the polymer decomposition at different temperature range **(Wei *et al.* 2015, de Jesus Silva *et al.* 2020)**.

It can be seen that in the degradation of the PVDF membrane, there are two distinct sections from almost 400 to 500 ºC and from 500 to 600 ºC, appearing in the figure by a slight slope change in both PVDF and PVDF-TiO$_2$ membranes. Considering the difference between the bonding strength of C-H (321-399 kJ/mol) and C-C (364-427 kJ/mol) compared with C-F (518 kJ/mol) (refer to **Table 2-5**), it can be assumed that in the primary scission, C-C and C-H bonds will break following by scission of C-F in the secondary scission section **(de Jesus Silva *et al.* 2020)**. This distinction of degradation was less noticeable in the PES membrane.

The crystallinity of the synthesized TiO_2 nanoparticles was further approved by the appearance of the sharp peaks in X-Ray Diffraction spectra (XRD) (**Figure 4-5**). It shows that mixed phases of TiO_2 (anatase, rutile and brookite) were formed.
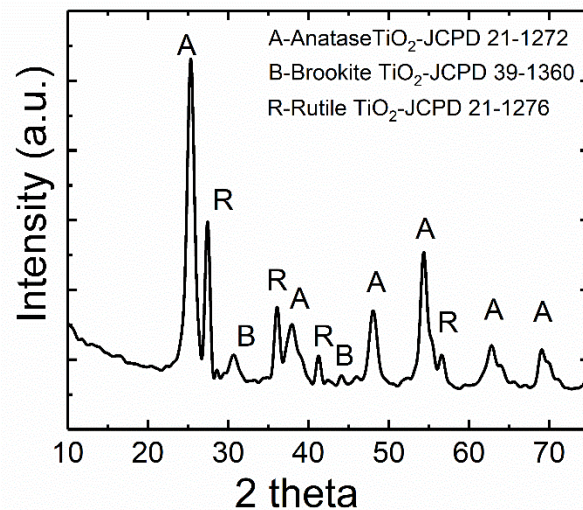
Figure 4-5 XRD spectra of the synthesized TiO_2 nanoparticles, reprinted from (**Regmi** *et al.* **2020**).

Using the Brunauer-Emmett-Teller method (BET) and density functional theory (DFT), the specific surface area (SSA) of membranes was obtained. PES-TiO_2 had higher SSA showing by both methods, 10.7 m^2/g and 8.5 m^2/g by BET and DFT respectively. Whereas, PVDF-TiO_2 had lower SSA, 4.0 m^2/g and 3.8 m^2/g by BET and DFT respectively.
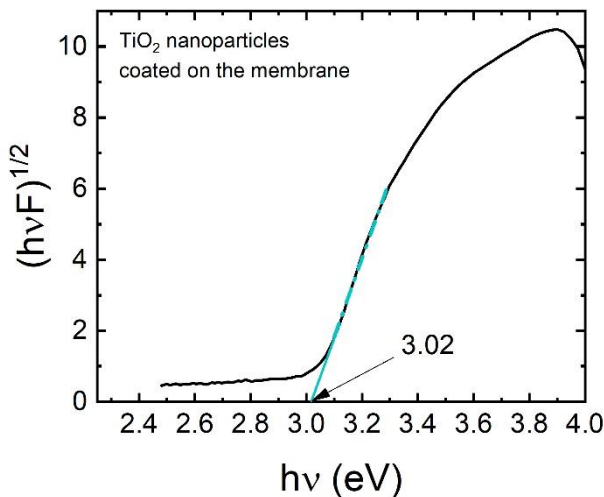
Figure 4-6 Bandgap calculation by Kubelka-Munk method and DRS spectra of TiO_2 coated on PES membrane, reprinted from (**Regmi** *et al.* **2020**).

The band gap of the synthesized TiO_2 nanoparticle was measured by the Kubelka-Munk method and using the diffuse reflectance spectra (DRS) measurement. Using equations **3-5** and **3-6**, **Figure 4-6** was plotted, and the band gap was obtained from it. Since the TiO_2 nanoparticle synthesis for both PES-TiO_2 and PVDF-TiO_2 membranes were the same and the deposition was performed after the synthesis of nanoparticle was performed, this band gap was considered for both. 3.02 eV equals 412 nm wavelength, and it shows that UV-LED 365 nm is sufficient for photocatalytic degradation experiments.

The zeta potential of membranes is shown in **Figure 4-7**.
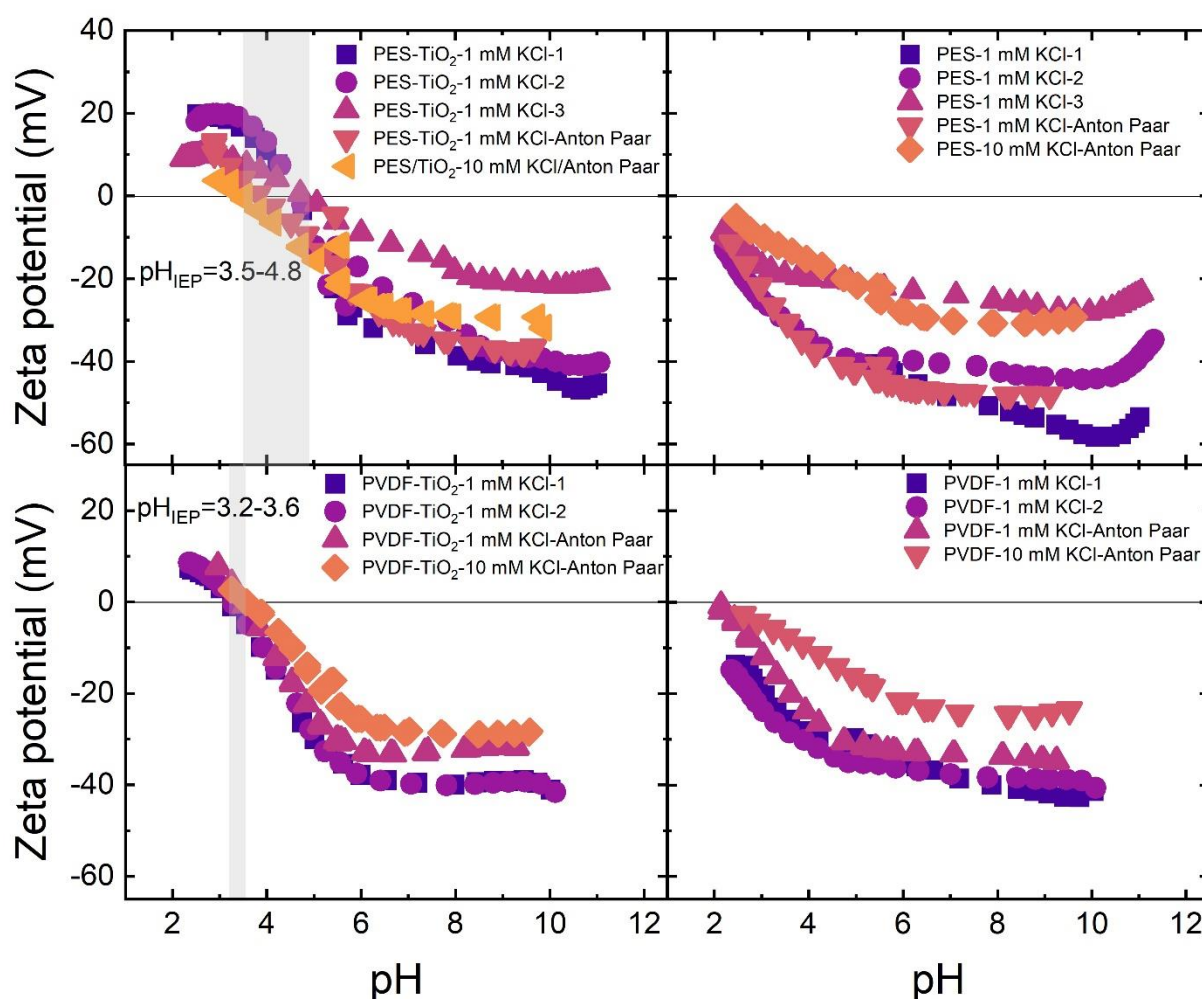
Figure 4-7 Reproducibility of zeta potential measurements, membranes PES, PES-TiO$_2$, PVDF, and PVDF-TiO$_2$. Measurements were repeated by the Anton Paar company, the same device. The electrolyte solution was 1 mM and 10 mM KCl. Reprinted (adapted) from (**Lotfi *et. al* 2022**).

In all experiments a large variation in the data was noticed, in particular for PES and PES-TiO$_2$. So, the measurements were repeated three times, and samples were sent to Anton-Paar to be tested as well. In the case of PES-TiO$_2$, IEP was between 3.9-4.6 testing with 1 mM KCl as the electrolyte solution and 3.5 when a higher concentration of 10 mM KCl was used as the electrolyte solution. PES did not reach the IEP in the range of tested pH. Extrapolation of data can give us a value below pH 1 for the IEP of PES. Zeta potential data for PVDF and PVDF-TiO$_2$ had better consistency and reproducibility. However, increasing the electrolyte concentration from 1 mM KCl to 10 mM, led to an increase in the value of zeta potential in the pH range of measurement, while the IEP was the same. The membrane pore size (in particular in microfiltration membranes with big pores like here >200 nm) and porosity of the membranes are considered the main contributors to the unsatisfactory reproducibility of zeta potentials at different pH values because the ionic conductance inside the pores affects the streaming potential measurements (**Yaroshchuk and Ribitsch 2002**). This lack of reproducibility in the data could be attributed to the

electrical conductivity of pores, because of the higher conductivity of the solution in pores compared to the bulk solution (**Fievet *et al.* 2001**). In an ion-penetrable membrane, if the distribution of acidic and basic groups is unbalanced, the surface potential is dependent on the electrolyte concentration when measuring the zeta potential. This dependency is due to the reason that the surface charge of the membrane could be different from the charge in pores and further in depth from the surface (**Shinagawa *et al.* 1992**). However, from the presented result in **Figure 4-7**, the main conclusion taken in this thesis was the range of IEP for each membrane. It was necessary to know the pH range which the membrane surface is negative or positive, so the affinity of the dyes or hormones to the membrane surface during photocatalytic degradation would be clear.

4.2   Photocatalytic degradation of MB

Photocatalytic degradation performance of membranes was evaluated by degradation of MB. MB was chosen as the standard compound for comparison due to its ease of concentration determination. In this step, PES-coated membranes, PES-TiO$_2$ and PES-TiO$_2$-120C, were compared based on their photocatalytic activity (**Figure 4-8**).
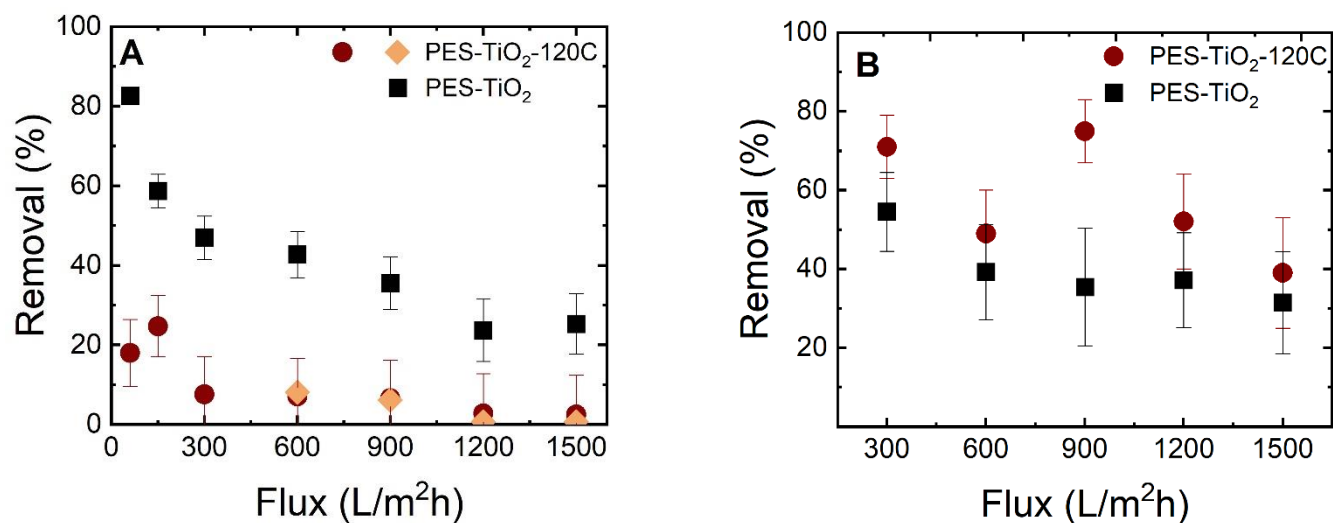
Figure 4-8 Photocatalytic removal of (A) MB and (B) E2 using two photocatalytic membranes at different fluxes, 10 mW/cm^2, 23±0.2 ^{o}C, pH 8.6±0.4, 1 mg/L MB, 1 mM NaHCO$_3$, 10 mM NaCl (MB data below 300 L/m^{2}h were reprinted from (**Regmi *et. al* 2020**) and the rest were reprinted from (**Lotfi *et. al* 2022**).

PES-TiO$_2$-120C had a significantly lower MB degradation while the rate of hormone removal for both membranes were quite similar. The main difference between these two series of experiments was the concentration of the pollutant to be degraded, with a significant difference of 1 mg/L MB and 100 ng/L E2. This could be one of the reasons for the low removal rate by one type of membrane. At this stage it was decided to exclude PES-TiO$_2$-120C from further examination.

PES-TiO$_2$ and PVDF-TiO$_2$ were also compared based on their MB degradation, illustrated in **Figure 4-9**.
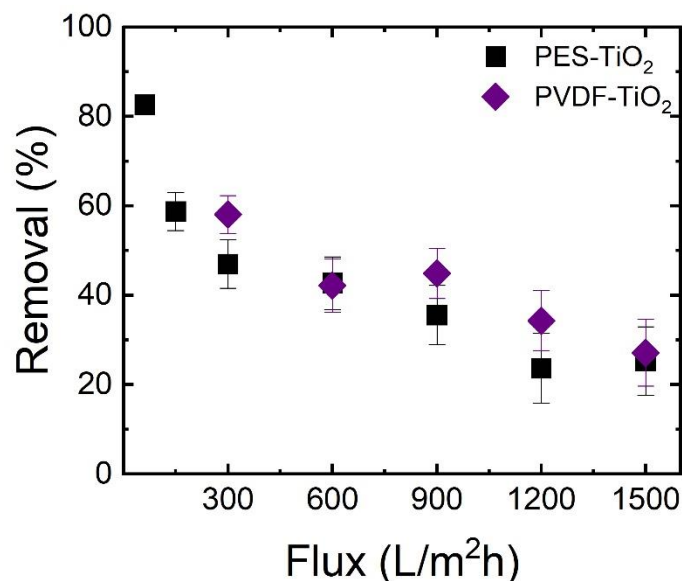
Figure 4-9 Comparison of MB photocatalytic degradation efficiency by PES-TiO$_2$ and PVDF-TiO$_2$, 10 mW/cm^2, 23±0.2 $^{\circ}$C, pH 8.6±0.4, 1 mg/L MB, 1 mM NaHCO$_3$, 10 mM NaCl, feed volume for PES-TiO$_2$ was 350 mL and for PVDF-TiO$_2$ 800 mL, this was due to the reason that removal did not reach a steady state phase in 350 mL filtration volume with PVDF-TiO$_2$. PES-TiO$_2$ data was reprinted (adapted) from (**Lotfi _et al._ 2022**) and PVDF-TiO$_2$ data was reprinted (adapted) from (**Liu _et al._ 2023**).

Even though the PES-TiO$_2$ membrane had higher TiO$_2$ loading shown by TGA and XPS analysis, PVDF-TiO$_2$ had higher MB removal compared to PES-TiO$_2$. However, the difference is small and is close to the error of experiments.

4.3   References

ASTM-International "G173-03(2012) Standard tables for reference solar spectral irradiances: Direct normal and hemispherical on 37° tilted surface." West Conshohocken, PA; ASTM International.

de Jesus Silva, A. J., M. M. Contreras, C. R. Nascimento and M. F. da Costa (2020). "Kinetics of thermal degradation and lifetime study of poly (vinylidene fluoride)(PVDF) subjected to bioethanol fuel accelerated aging." Heliyon **6**: e04573.

Fievet, P., A. Szymczyk, C. Labbez, B. Aoubiza, C. Simon, A. Foissy and J. Pagetti (2001). "Determining the zeta potential of porous membranes using electrolyte conductivity inside pores." Journal of Colloid and Interface Science **235**: 383-390.

Hojjati, B., R. Sui and P. A. Charpentier (2007). "Synthesis of TiO$_2$/PAA nanocomposite by RAFT polymerization." Polymer **48**: 5850-5858.

Lotfi, S., K. Fischer, A. Schulze and A. I. Schäfer (2022). "Photocatalytic degradation of steroid hormone micropollutants by TiO$_2$ coated polyethersulfone membranes in a continuous flow-through process." Nature Nanotechnology **17**: 417–423.

Mansourpanah, Y., S. S. Madaeni, A. Rahimpour, A. Farhadian and A. H. Taheri (2009). "Formation of appropriate sites on nanofiltration membrane surface for binding TiO$_2$ photo-catalyst: Performance, characterization and fouling-resistant capability." Journal of Membrane Science **330**: 297-306.

Qian, Y., L. Chi, W. Zhou, Z. Yu, Z. Zhang, Z. Zhang and Z. Jiang (2016). "Fabrication of TiO_2-modified polytetrafluoroethylene ultrafiltration membranes *via* plasma-enhanced surface graft pretreatment." Applied Surface Science **360**: 749-757.

Raota, C. S., S. Lotfi, R. Lyubimenko, B. S. Richards and A. I. Schäfer (2023). "Accelerated ageing method for the determination of photostability of polymer-based photocatalytic membranes." Journal of Membrane Science: 121944.

Regmi, C., S. Lotfi, J. C. Espíndola, K. Fischer, A. Schulze and A. I. Schäfer (2020). "Comparison of Photocatalytic Membrane Reactor Types for the Degradation of an Organic Molecule by TiO_2-Coated PES Membrane." Catalysts **10**: 725.

Rotzinger, F. P., J. M. Kesselman-Truttmann, S. J. Hug, V. Shklover and M. Grätzel (2004). "Structure and Vibrational Spectrum of Formate and Acetate Adsorbed from Aqueous Solution onto the TiO_2 Rutile (110) Surface." The Journal of Physical Chemistry B **108**: 5004-5017.

Shinagawa, T., H. Ohshima and T. Kondo (1992). "Isoelectric point of an ion-penetrable membrane." Biophysical Chemistry 43: 149-156.

Véron, E. (2021). PVDF membrane functionalized with TiO_2 for photocatalytic degradation of low concentrated steroid hormones in a flow-through filtration reactor. M.Sc. degree, Karlsruhe Institute of Technology (KIT).

Wei, Z., M. Peng, F. Qiu, X. Wang and J. Yang (2015). "Development of a novel preparation method for conductive PES ultrafine fibers with self-formed thin PES/CNTs composite layer by vapor treatment." RSC Advances **5**: 42305-42310.

Yaroshchuk, A. and V. Ribitsch (2002). "Role of Channel Wall Conductance in the Determination of ζ-Potential from Electrokinetic Measurements." Langmuir 18: 2036-2038.

You, S. J., G. U. Semblante, S. C. Lu, R. A. Damodar and T. C. Wei (2012). "Evaluation of the antifouling and photocatalytic properties of poly(vinylidene fluoride) plasma-grafted poly(acrylic acid) membrane with self-assembled TiO_2." Journal of Hazardous Materials **237-238**: 10-19.

Chapter Five

5   PMRs configuration comparison

PMRs can be operated in two distinct configurations, i) photocatalyst dispersed in a slurry reactor and using a membrane as a barrier to separate the photocatalyst and probably the photocatalytic degradation by-products, ii) photocatalyst deposited on/into membrane structure and the degradation and filtration happening simultaneously. As mentioned in the first chapter, operation in a slurry reactor has some advantages of higher specific surface area and/or less mass transfer limitation by good mixing **(McCullagh *et al.* 2010)**. However, this method has serious disadvantages such as photocatalyst recovery and its loss during operation, or solution turbidity as a result of high photocatalyst dosage **(Ling *et al.* 2004)**. On the other hand, operating in a flow PMR with photocatalyst deposited on/into membrane structure can have multiple advantages, i) no post-treatment step for photocatalyst separation from the clean water, ii) minimized photocatalyst loss, iii) photocatalytic membranes (PM) could be also a barrier for larger microorganisms and molecules such as bacteria or organic matter and decrease the membrane fouling potential **(Teixeira *et al.* 2016, Zheng *et al.* 2017)**. Immobilizing photocatalyst on a porous structure like porous polymeric membranes has the benefit of high specific surface area and short diffusion length in the membrane pores. Improving the probability of collision between the pollutant molecules and photocatalysts overcomes the issues of mass transfer limitation.

In this chapter, three PMR configurations with photocatalysts immobilized on/into membrane structure, batch mode, flow-along and flow-through were compared based on their performance in a PMR considering their throughput, energy efficiency, photocatalytic activity, and the final degradation performance. Throughput in a batch reactor is obtained by its volume and the residence time in the reactor. Whereas, in a continuous flow PMR, throughput is determined by the feed flow rate. Specific energy consumption (SEC) was used for comparison purposes as the power required to treat a specific volume of water. Photocatalytic activity and photocatalytic degradation rate are commonly used in literature to evaluate the efficiency of a reactor **(Horovitz *et al.* 2016, Liz *et al.* 2017, Janssens *et al.* 2017)**. However, for a meaningful comparison, neither of these parameters alone gives the correct answer. Therefore, parameters, space-time yield (STY) and photocatalytic space-time yield (PSTY), defined by Leblebici *et al.* **(Leblebici *et al.* 2015)** were used here to compare the performance of PMRs. These two parameters consider the throughput, energy consumption, and photocatalytic activity to evaluate the performance of PMRs. These data are published in Regmi *et al.* **(Regmi *et al.* 2020)** research.

5.1   Comparison of flow patterns in PMRs

When the photocatalytic reaction is happening inside photocatalytic membrane with nanometer pore size, they can be categorized as nanoreactors. Common features among these reactors are a parabolic velocity profile and quite homogeneous light distribution across the surface of the reactor **(Visan *et al.* 2019)**. Flow patterns in 3 modes of operations, photocatalytic membrane in batch, flow along the surface of photocatalytic membrane and flow through the pores of photocatalytic membrane, is illustrated in **Figure 5-1**. In each of these modes, only the pollutants in the closest vicinity of the photocatalysts can be degraded. In the batch process in which photocatalytic membrane is submerged in the solution and the flow pattern is determined by a magnetic stirrer **Figure 5-1A**, the collision between the pollutant molecule with the photocatalyst surface is slow and depends on the residence time that molecules are present in the solution. So, it can be concluded that although complete degradation of pollutants in this configuration could be possible with the required residence time, it takes a long time for all the pollutants to meet the photocatalysts surface while the solution is being mixed such as 30 min in the best case in the study of Fischer *et al.* **(Fischer *et al.* 2018)**.
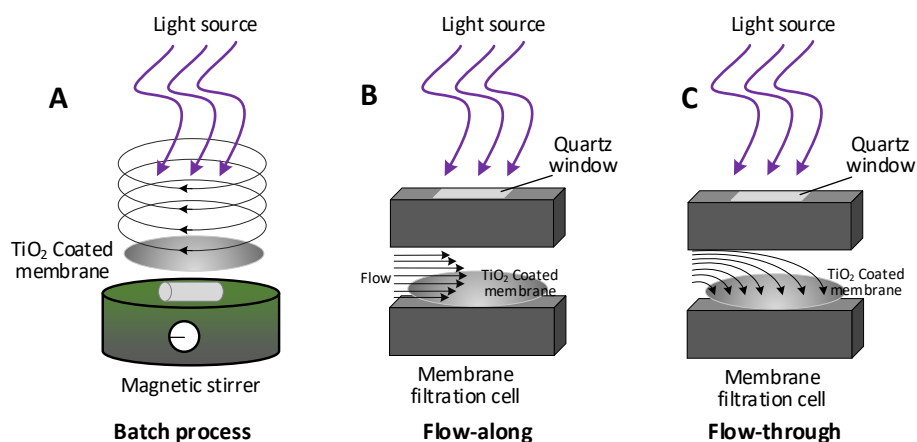
Figure 5-1 Flow pattern in different modes of PMR: (A) photocatalytic membrane in batch, (B) flow along the surface of photocatalytic membrane and (C) flow through the pores of photocatalytic membrane (adapted from (**Regmi *et al.* 2020**))

In the flow-along configuration (**Figure 5-1B**), the feed solution with laminar flow (Reynolds number 4 (**Regmi *et al.* 2020**)) is in the X-direction (along the surface). Therefore, mass transport in the Y-direction (perpendicular to the membrane surface) is limited to axial dispersion and diffusion across parallel layers of feed solution. The velocity profile in this mode in the fully developed region is parabolic. In the flow-along mode, the contact between the pollutants and the photocatalyst is happening only in the closest layer to the surface, and most of the flow passes the reactor intact. Part of the solution would also diffuse to the pores; however, the diffusion is considerably slower than the convection in the channel. Hence the

contribution of pores in the degradation of pollutants during the short residence time of solution in the flow reactor with the flow along the surface mode is negligible.

In the flow-through process (**Figure 5-1C**), the solution is forced to pass through the membrane pores, therefore, it is in contact with the photocatalyst deposited in both surface and the pores and it enhances the degradation significantly. Even though the residence time in the membrane pores in this mode is short (a few seconds), the throughput of the whole process and the degradation efficiency are sufficiently high considering the continuous flow of the PMR **(Lyubimenko *et al.* 2021, Lotfi *et al.* 2022)**.

5.2   Residence time in different configurations

Each of the PMR configurations with its own flow pattern leads to a different residence time. Residence time is considered the total amount of time that pollutants spend inside the reactor and are exposed to ROS and degradation. This plays a critical point in the final removal of the pollutants and the efficiency of the PMR. As the residence time in the reactor extends, the molecules have more time to be degraded (higher removal). In the batch reactor, the residence time is the total time from the moment the light source is turned on until it is turned off. For the batch reactor in this study **Figure 5-1A**, the residence time was **2400 s** and **3000 s** for two experiments with the UV lamp and UV LED lamp respectively **(Regmi *et al.* 2020)**. In the case of flow reactors, flow along and flow-through, the residence time is the time spent by the pollutant molecules in the reaction zone of the reactor and is depending on the flow of the feed following the equations **3-15**, **3-16**, and **3-17**.

For the flow-along configuration, as it was shown in **Figure 5-1B**, the solution does not pass through the membrane, and since there is no convective flow through the membrane in this case and the diffusion through the pores is significantly slower than the flow inside the channel, the reaction inside the pore can be neglected. Therefore, the volume of the reaction zone is equal to the volume of the channel 0.14 cm^3 (details in **Table 3-10**). For flow-through configuration, the feed solution passes through the membrane after spending time inside the channel (**Figure 5-1C**). Therefore, the volume of the reaction zone, in this case, is equal to the sum of channel and membrane volume which is 0.16 cm^3 (0.14 cm^3 channel and 0.02 cm^3 membrane volume). Considering the flow rate of 1 mL/min (300 L/m^{2}h), then the residence time in the flow-along and flow-through reactor is **8.4 s** and **9.6 s** respectively (8.4 s in the channel and 1.2 s in the membrane calculated using equations **3-15**, **3-16**, and **3-17**).

5.3   MB degradation in PMRs

To get information on the performance of the reactor and be able to compare them, photocatalytic degradation of MB was performed. First, the experiment was done in the dark phase to get the adsorption

of MB, then direct photolysis to get the data of degradation by direct light to account for any possible phenomena that could simultaneously decrease the concentration of the MB molecules. In the batch process, the photolysis experiment was performed without the presence of a membrane in two MB concentrations of 1 and 13 mg/L, **Figure 5-2A**. The adsorption on membrane and photolysis were also examined in the flow-through reactor and was compared with photocatalytic degradation of 1 mg/L MB at 300 L/m^{2}h and 10 mW/cm^2, **Figure 5-2B**.
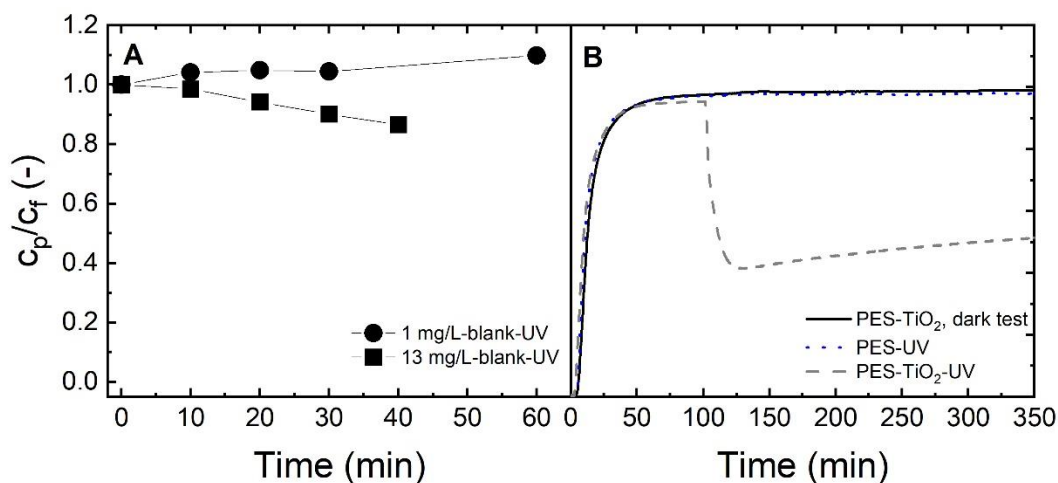
Figure 5-2 (A) Direct photolysis experiment in the batch reactor using UV light in different MB concentrations and in the absence of a membrane (1 and 13 mg/L MB, 200 rpm radial shaking, 10 mW/cm^2) (B) Adsorption with PES-TiO$_2$ membrane in the dark phase, degradation of MB with pristine PES and PES-TiO$_2$ membrane in the flow-through reactor, (1 mg/L MB, 300 L/m^{2}h, 10 mW/cm^2)[8]. Figure reprinted from (**Regmi** *et al.* **2020**).

In the absence of a membrane **Figure 5-2A**, direct UV light could not degrade 1 mg/L of MB. A small rise in the concentration was noticed which could be related to evaporation during the experiment and loss of water. When the MB concentration was increased to 13 mg/L, about 12% decline was observed in the absence of the membrane only by photolysis. This amount was subtracted from the photocatalytic removal calculation later in the batch experiment. **Figure 5-2B** shows that complete adsorption was achieved before 100 min (equal to 100 mL filtration volume) and no further adsorption happened in the rest of the filtration. The amount adsorbed on the surface was calculated to be 0.005 mg/cm^2 (section **3.12** Equation **3-31**) which is less than 3% of the total mass of filtered MB (0.35 mg was filtered in total). Similar to the dark phase, with a PES (pristine) membrane and UV light (356 nm), no MB was degraded from the 1 mg/L MB solution. However, using the PES-TiO$_2$ membrane, MB concentration declined by 50% in presence of light and reached an almost steady state condition. Hence, it can be concluded that the presence of light was necessary for MB degradation.

---

[8] Experiments with batch reactor was performed by IOM (**Figure 5-2A**) and the flow-through reactor data was obtained by Shabnam Lotfi (**Figure 5-2B**).

Further, photocatalytic degradation of MB was performed at different light intensities, **Figure 5-3** and **Figure 5-4**, and different fluxes, **Figure 5-5** and **Figure 5-6** using all 3 PMR configurations. In these experiments, all parameters other than the examined one (light intensity or flux) were kept constant to have similar conditions. The concentration ratio of the MB (c/c_0) at different light intensities in different flow processes is displayed in **Figure 5-3**. In batch mode (**Figure 5-3A**), the dark phase was for 20 min and in this phase, the solution was replaced with fresh MB solution until no decline in MB concentration was noticed. Then the light was turned on. **Figure 5-3B** shows that the first 100 mL was filtered in the dark condition to reach the adsorption-desorption condition and then the light was turned on to filter 250 mL of MB solution. The protocol for each mode was explained in detail in chapter **3** section **3.6.1**.
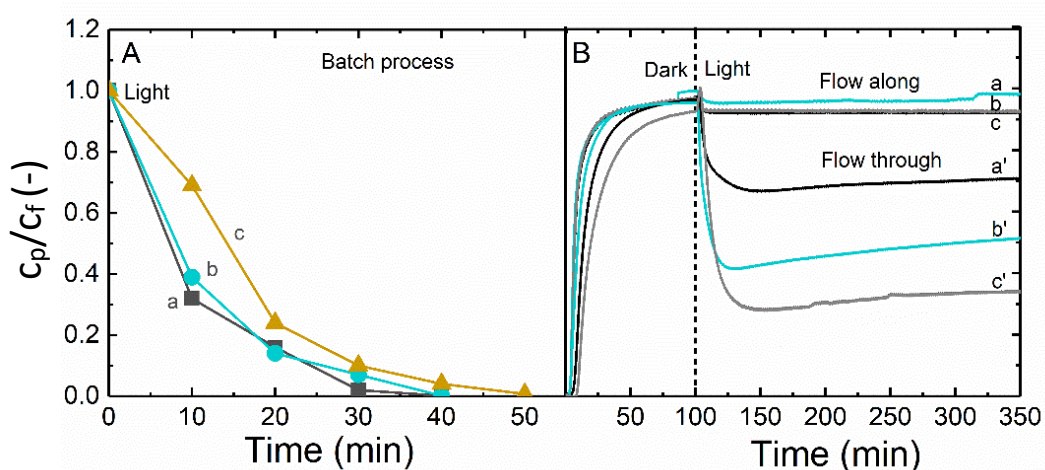
Figure 5-3 A) Concentration ratio of MB over the time of experiment at different light sources in the batch reactor, (a) 13 mg/L-UV lamp, (b) 1 mg/L-UV lamp, and (c) 1 mg/L-UV LED; B) Concentration ratio of MB over the time of experiments (equal to permeate volume for flow reactors at 1 mL/min) at different light intensities and at different continuous flow mode, (a and a′) 2 mW/cm^2, (b and b′) 10 mW/cm^2, and (c and c′) 17 mW/cm^2 flow along and flow-through respectively, 300 L/m^{2}h flux, 1 mg/L MB concentration in background solution 10 mM NaCl and 1 mM NaHCO$_3$, Reprinted from (**Regmi** *et al.* **2020**). Data of experiments in the batch reactor was provided by IOM.

Varying the light intensity which was illuminated to the membrane surface altered the number of received photons by the surface and therefore, the number generated ROS was changed. Increasing the light intensity meant a higher number of photons and therefore higher ROS was presented at the surface and consequently higher photocatalytic degradation. This rise in removal and rate of disappearance was noticed in the flow-through mode (**Figure 5-4**). However, in flow-along mode, the degradation was significantly lower than in flow-through mode and increasing the light intensity did not improve the efficiency of this PMR configuration. This could mean that although a higher number of ROS was generated at a higher light intensity, the access of pollutants to the generated ROSs was limited and this low mass transfer was limiting the degradation efficiency. MB removal in the batch reactor was done at 11.3±1.3 mW/cm^2 with 2 mL solution of 1 mg/L MB. The batch reactor succeeded in degrading almost

all the MB in the solution (>99%), however in the course of 3000 s compared to 8 and 10 s residence times in flow-along and flow-through membranes respectively **(Regmi *et al.* 2020)**.
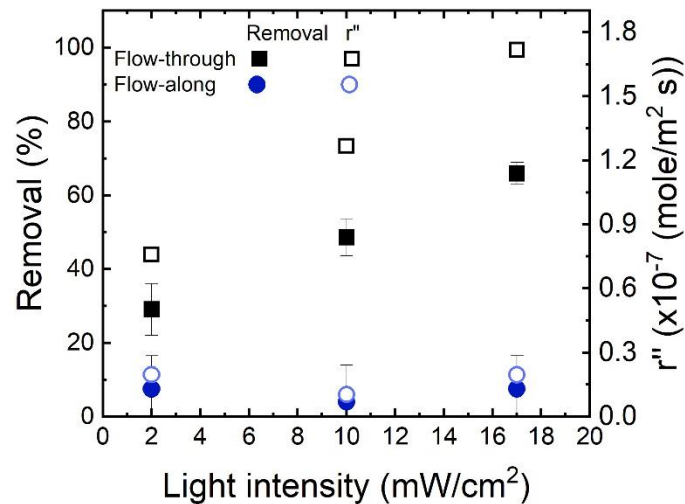
Figure 5-4 MB removal and rate of disappearance (r'') at different light intensities operated in flow-along and flow-through processes, MB concentration 1 mg/L, temperature 22 °C, in flow-along and flow-through, flux 300 L/m²h, pH 8.6±0.4, 1 mM NaHCO₃, 10 mM NaCl. Reprinted from **(Regmi *et al.* 2020)**.

Next, PMRs were assessed at different fluxes. The concentration ratio of MB during the experiment at different fluxes in flow-through and flow-along can be seen in **Figure 5-5**.
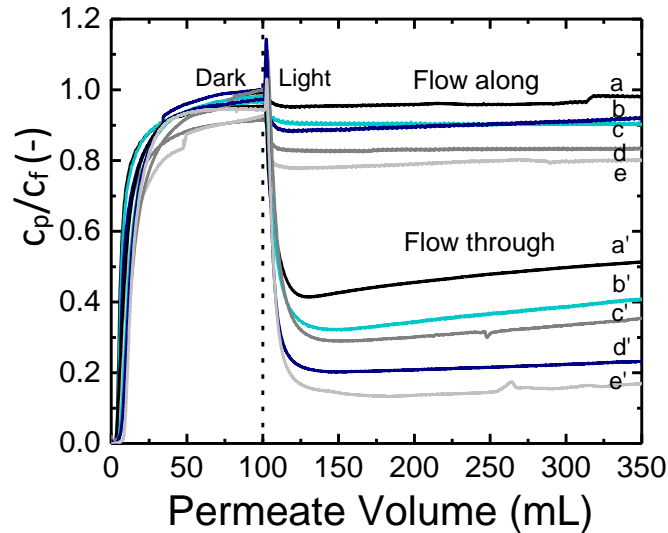
Figure 5-5 Concentration ratio of MB over the permeate volume at different flow rates and different flow mode flow-along and flow-through, (a and a′) 300 L/m²h, (b and b′) 225 L/m²h, (c and c′) 150 L/m²h, (d and d′) 90 L/m²h, (e and e′) 60 L/m²h respectively, 10 mW/cm² light intensity, 1 mg/L MB concentration in background solution 10 mM NaCl and 1 mM NaHCO₃, Reprinted from **(Regmi *et al.* 2020)**.

Figure 5-6 presents the removal and rate of disappearance of MB in flow PMRs at different feed flux operations. The variation in flux was meaningful for flow-through and flow-along reactors, as the tests

in batch reactor were static. Therefore, different flow in flow-along and flow-through was compared with the batch PMR which has no flow (flux zero).
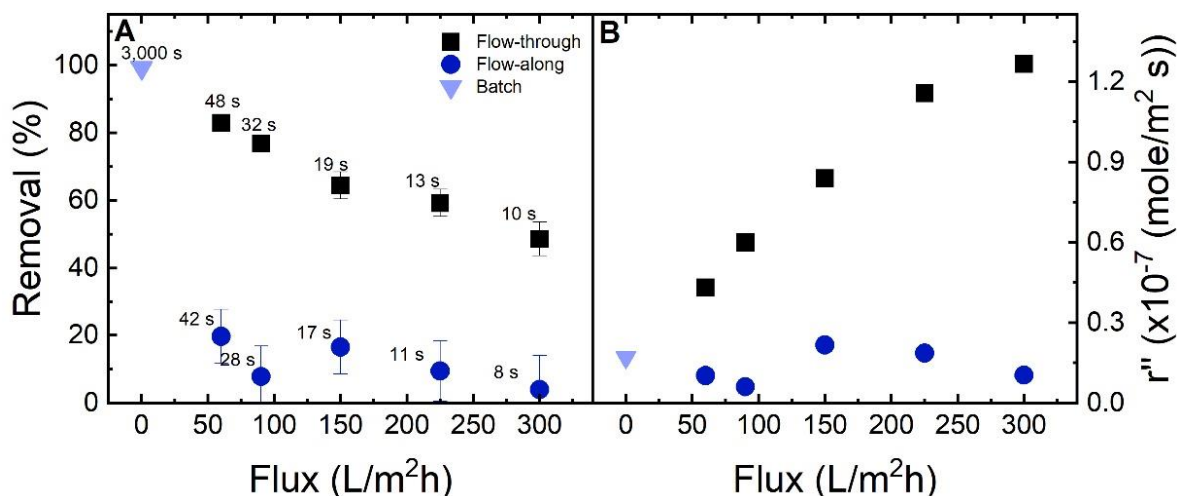
Figure 5-6 (A) MB removal, and (B) rate of disappearance for batch (11.3±1.3 mW/cm², 0 flux), flow-along and flow-through reactor at different fluxes; 10 mW/cm² light intensity, 1 mg/L MB concentration, temperature 22 ⁰C, in flow-along and flow-through pH 8.6±0.4, 1 mM NaHCO₃, 10 mM NaCl. Residence time related to each configuration and flux is shown in the graph at each point. Reprinted (adapted) from (**Regmi *et al.* 2020**).

It can be noticed that the batch reactor could achieve almost complete removal in 3000 s, which is significantly higher than the two other PMRs. In flow PMRs, decreasing the flux and subsequently increasing the residence time resulted in improving the removal of MB. This improvement was remarkable in the flow-through reactor (50% to 83%) compared to a small change in the flow-along reactor (4% to 20%). However, when considering the rate of disappearance, by increasing the flux (lower residence time), the number of degraded molecules per membrane surface area and time increased significantly due to more MB molecules coming in contact with the active catalytic surface per unit of time.

At a constant flux, the flow-through reactor has 12 times higher removal efficiency than flow-along PMR (flux 300 L/m²h and light intensity 10 mW/cm²). This was attributed to the contribution of pores and effective convective mass transfer in the membrane pores with negligible diffusion limitation. The radial diffusion time of the MB and hydroxyl radicals from the membrane pore volume to the surface of the pores was calculated using equation **3-3** (Diffusion time in the radial direction ($t_{D,rad}$)), assuming that hydroxyl radical is the dominant ROS generated by TiO₂ when exposed to UV light. In calculating the diffusion time using equation **3-3**, the diffusion coefficient (D_m) is 7.7×10^{-10} m²/s in case of MB (**Hori *et al.* 1987**) and 27×10^{-10} m²/s for hydroxyl radical (**Kallikragas *et al.* 2014**) at 25 °C.

The calculated diffusion times for MB and hydroxyl radical were 1.58×10^{-05} s and 0.45×10^{-05} s, respectively which was shorter than the residence time at the flux of 300 L/m²h (1.2 s). Therefore, it was

concluded that the diffusion limitation is negligible in such a narrow-confined space (220 nm pores of membranes). Moreover, the tortuosity in the structure of a porous membrane can improve the collision between pollutants and the generated ROSs.

It should be noted that in this work, a decrease in the concentration of MB was realized by changes in the absorbance of this dye at 664 nm. However, this does not always mean complete degradation. Breakage of the chromophore group of the molecule, rearrangement of the conjugate bonds or the complete degradation of the MB molecules to CO_2 and H_2O, all could contribute to the reduction in the absorbance of MB. TOC reduces only in complete degradation since the carbon content is removed from the solution. Therefore, TOC could not be a useful tool for comparison between PMRs if complete degradation is not achieved.

5.4 PMR performance comparison

PMRs were evaluated and compared based on the parameters namely adapted STY and PSTY, SEC and degradation rate constants, as was explained in the methodology section **3.12**. A comparison summary can be seen in **Table 5-1**.

Table 5-1 Comparison of PMR configurations, batch, flow-along, and flow-through reactors, reprinted from (**Regmi *et al.* 2020**).[9]

Reactor	Unit	Batch		Flow-along	Flow-through
Illumination system	--	5 UV lamps	6 LEDs	1 LED	1 LED
Pressure	bar	-	-	0.2	0.2
MB initial concentration, c_0	mg/L	1	1	1	1
Residence time, $\bar{t}$	s	2400	3000	8.4	9.6
MB concentration at time $\bar{t}$, $c_{\bar{t}}$	mg/L	0.004	0.007	0.96	0.5
Reactor volume, V_r	cm^3	4	4	0.14	0.16
Flow rate, Q	mL/min	-	-	1	1
Normalized light power, NLP	W/cm^3	31.3	1.3	23.6	20.1
Power light intensity, PI	mW/cm^2	13	10	10	10
TiO_2 mass	mg	4.0	4.0	2.0	2.0
Active membrane area	cm^2	4.1	4.1	2.0	2.0
SEC $\times 10^{-2}$ [a, b]	$(kWh)/m^3$	156	10.4	0.6	0.6
Degradation rate $- r'_{MB} \times 10^{12}$ [a, c]	mol/s	6.9	4.1	2.1	26.1
$STY_1 \times 10^{12}$ [a, c]	$mol/(cm^3 \ s)$	1.6	1.0	14.9	159
$STY_2 \times 10^{12}$ [a, c]	$mol/(cm^2 \ s)$	1.6	1.0	1.0	13.0
$STY_3 \times 10^{9}$ [a, c]	$mol/(g \ s)$	1.6	1.0	1.0	13.3
$PSTY_1 \times 10^{13}$ [a, b, c]	$mol/(W \ s)$	0.5	8.2	6.3	79.0
$PSTY_2 \times 10^{10}$ [a, b, c]	$mol/(W \ s)$	1.2	1.0	1.0	13.0

---

[9] STY: space-time yield, PSTY: photocatalytic space-time yield, refer to section 3.12 Kinetics for details of calculations.

To account for both water production and energy consumption, SEC values could be considered. The SEC value for flow-along and flow-through was similar as these two PMR were operating using the same light source and the same flux. In the case of the batch reactor, it is noted that PMR with LED lamps has a significantly higher performance by 15 times lower SEC than PMR with UV lamps. The reason for this could be that LEDs are more efficient in the conversion of electric power to light, while conventional lamps are highly energy-consuming **(Wang *et al.* 2011)**. Also, the use of LEDs improves the photon transfer to the reaction environment and minimizes the light energy requirement. However, SEC is not a suitable parameter for evaluating the performance of PMRs, as it does not consider the degree of pollutant degradation.

On the other hand, the degradation rate considers the removal efficiency of pollutants per time but lacks the energy input. This value is higher when the reaction happens faster. Comparing this parameter, flow-through PMR had the highest performance with batch and flow-along being notably lower. However, a comparison based on the degradation rate could also be misleading by not considering the catalyst amount or energy requirement.

For a better comparison, STY and PSTY parameters were introduced which considered the degraded amount and the received number of photons. STY 1, 2 and 3 consider the amount of degraded pollutants per volume of the reactor, membrane area and mass of photocatalyst respectively. Flow-through PMR had the highest value of STY1,2 and 3 while flow-along showed similar results to batch PMR in most cases. This was attributed to the higher reaction constant and the specific mode of the reactor which represents a plug flow reactor with nanometer-sized channels. This reactor benefits from a high surface-to-volume ratio which enhances its efficiency. When considering the energy inputs in the system, PSTY values were obtained, which is the ratio of STY to either the standardized electricity consumption of the lamp/LED (PSTY1) or the power intensity received by the reactor (PSTY2). Therefore, PSTY gives a more comprehensible comparison by considering the three main factors photocatalytic activity, energy efficiency and throughput. When comparing the flow/along PMR with batch reactor with LED light source, it was noticed that these two PMRs had similar performance shown by close PSTY values. It can be understood that both systems suffered from a lack of proper mass transfer. Although flow-along was a microreactor with micrometer-sized channels, the transfer of pollutants molecules to the surface was limited and slow and the photodegradation reaction only took place at the closest vicinity of the surface in a few nanometers distance. The batch reactor had a similar problem which led to its low performance.

All in all, flow-through PMR had the highest performance based on the throughput, energy efficiency and photocatalytic degradation efficiency thanks to its enhanced mass transfer obtained by the forced convective flow inside the membrane pores, providing efficient contact between the solute and catalyst active sites. In flow-through PMR the values of PSTY1 and PSTY2 were about 10 times higher than both the batch and flow-along process.

5.5 References

Fischer, K., P. Schulz, I. Atanasov, A. Abdul Latif, I. Thomas, M. Kühnert, A. Prager, J. Griebel and A. Schulze (2018). "Synthesis of High Crystalline TiO$_2$ Nanoparticles on a Polymer Membrane to Degrade Pollutants from Water." Catalysts **8**: 376.

Hori, T., N. Kamon, H. Kojima, R. M. Rohner and H. Zollinger (1987). "Structure correlation between diffusion coefficients of simple organic compounds and of anionic and cationic dyes in water." Journal of the Society of Dyers and Colourists 103: 265-270.

Horovitz, I., D. Avisar, M. A. Baker, R. Grilli, L. Lozzi, D. Di Camillo and H. Mamane (2016). "Carbamazepine degradation using a N-doped TiO$_2$ coated photocatalytic membrane reactor: Influence of physical parameters." Journal of Hazardous Materials 310: 98-107.

Janssens, R., M. K. Mandal, K. K. Dubey and P. Luis (2017). "Slurry photocatalytic membrane reactor technology for removal of pharmaceutical compounds from wastewater: Towards cytostatic drug elimination." Sci Total Environ 599-600: 61 2-626.

Kallikragas, D. T., A. Y. Plugatyr and I. M. Svishchev (2014). "High Temperature Diffusion Coefficients for O$_2$, H$_2$, and OH in Water, and for Pure Water." Journal of Chemical & Engineering Data 59: 1964-1969.

Leblebici, M. E., G. D. Stefanidis and T. Van Gerven (2015). "Comparison of photocatalytic space-time yields of 12 reactor designs for wastewater treatment." Chemical Engineering and Processing: Process Intensification **97**: 106-111.

Ling, C. M., A. R. Mohamed and S. Bhatia (2004). "Performance of photocatalytic reactors using immobilized TiO$_2$ film for the degradation of phenol and methylene blue dye present in water stream." Chemosphere **57**: 547-554.

Liz, M. V. d., R. M. d. Lima, B. d. Amaral, B. Marinho, J. Schneider, N. Nagata and P. Peralta-Zamora (2017). "Suspended and Immobilized TiO$_2$ Photocatalytic Degradation of Estrogens: Potential for Application in Wastewater Treatment Processes." Journal of the Brazilian Chemical Society 29: 380-389.

Lotfi, S., K. Fischer, A. Schulze and A. I. Schäfer (2022). "Photocatalytic degradation of steroid hormone micropollutants by TiO$_2$ coated polyethersulfone membranes in a continuous flow-through process." Nature Nanotechnology **17**: 417–423.

Lyubimenko, R., O. I. Gutierrez Cardenas, A. Turshatov, B. S. Richards and A. I. Schäfer (2021). "Photodegradation of steroid-hormone micropollutants in a flow-through membrane reactor coated with Pd(II)-porphyrin." Applied Catalysis B: Environmental **291**: 120097.

McCullagh, C., P. K. J. Robertson, M. Adams, P. M. Pollard and A. Mohammed (2010). "Development of a slurry continuous flow reactor for photocatalytic treatment of industrial waste water." Journal of Photochemistry and Photobiology A: Chemistry **211**: 42-46.

Regmi, C., S. Lotfi, J. C. Espíndola, K. Fischer, A. Schulze and A. I. Schäfer (2020). "Comparison of Photocatalytic Membrane Reactor Types for the Degradation of an Organic Molecule by TiO$_2$-Coated PES Membrane." Catalysts **10**: 725.

Teixeira, S., P. M. Martins, S. Lanceros-Méndez, K. Kühn and G. Cuniberti (2016). "Reusability of photocatalytic TiO$_2$ and ZnO nanoparticles immobilized in poly(vinylidene difluoride)-co-trifluoroethylene." Applied Surface Science **384**: 497-504.

Visan, A., J. R. van Ommen, M. T. Kreutzer and R. G. H. Lammertink (2019). "Photocatalytic Reactor Design: Guidelines for Kinetic Investigation." Industrial & Engineering Chemistry Research **58**: 5349-5357.

Wang, Z., J. Liu, Y. Dai, W. Dong, S. Zhang and J. Chen (2011). "Dimethyl Sulfide Photocatalytic Degradation in a Light-Emitting-Diode Continuous Reactor: Kinetic and Mechanistic Study." Industrial & Engineering Chemistry Research **50**: 7977-7984.

Zheng, X., Z.-P. Shen, L. Shi, R. Cheng and D.-H. Yuan (2017). "Photocatalytic Membrane Reactors (PMRs) in Water Treatment: Configurations and Influencing Factors." Catalysts **7**: 224.

Chapter Six

6   Limiting factors of operation in a PMR

After determining the effectiveness of PMs in degrading MB and the most productive PMR configuration, PMs were subjected to steroid hormones degradation using flow-through PMR configuration. These hormones are classified as micropollutants due to their high activity and disruption of the endocrine system of humans and aquatic life. The goal was to get close to the recommended value of 1 ng/L for E2 by WHO. To remove these compounds from water, PMRs are reported to be highly efficient. Therefore, this chapter was specified to identify the challenges of operating in a flow-through PMR and understanding the limiting factors while degrading steroid hormones, including the variation of light intensity, feed flux (residence time), reaction temperature, steroid hormone concentration, pH and surface charge, and type of steroid hormone (molecule structure). Both membrane materials, PES-TiO$_2$ and PVDF-TiO$_2$ were compared in their efficiency for steroid hormone elimination in a flow-through PMR.

6.1   PMR operation in the dark phase, direct photolysis, and photocatalysis

The first step in the evaluation of PMs was to perform an experiment in the dark phase and obtain the mass of E2 adsorbed on the membranes. In this way, the volume required to reach the adsorption-desorption equilibrium was measured. In **Figure 6-1**, it can be noticed that the equilibrium was reached before 100 mL filtration. Therefore, the volume to be filtrated before the UV-LED turns on was set to 100 mL volume.
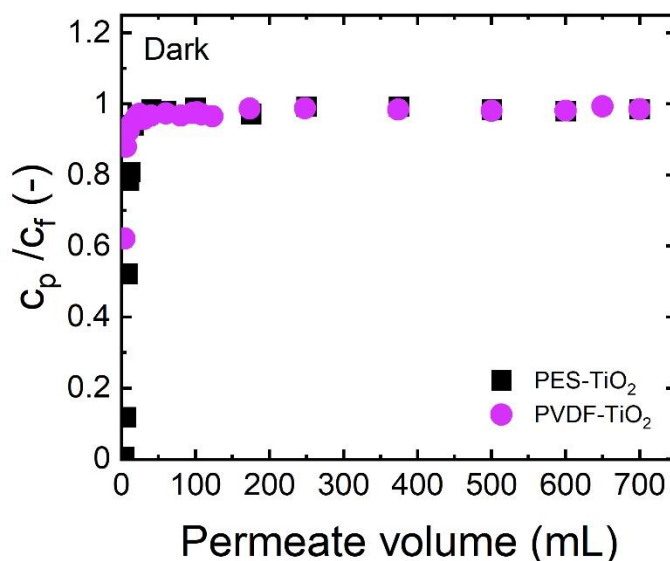
Figure 6-1[10] E2 Concentration ratio of E2 (permeate over feed concentration c_p/c_f (-)) *vs.* cumulative permeate volume in dark phase with no light source, Conditions: 600 L/m^{2}h, 23±0.2 °C, pH 8.6±0.4, 100 ng/L E2, 1 mM NaHCO$_3$, 10 mM NaCl, 79.2 mg/L MeOH, EtOH was 27.2 mg/L for PES-TiO$_2$ and 26.9 mg/L for PVDF-TiO$_2$ experiments. c_p and c_f refer to the concentration of E2 in the permeate and feed, respectively. PES-TiO$_2$ data was reprinted from (**Lotfi** *et al.* **2022**) and PVDF-TiO$_2$ data was reprinted from (**Liu** *et al.* **2023**).

It can also be noticed that the mass adsorbed by both PES-TiO$_2$ and PVDF-TiO$_2$ was low. The mass of E2 adsorbed on the membrane was calculated using equation **3-31** to be in the range of 0.9 ng/cm^2 for PES-TiO$_2$ and 0.45 for PVDF-TiO$_2$. **Figure 6-1** demonstrates that the changes in concentration during the dark phase experiment was negligible and no reduction in concentration was observed after initial adsorption was completed below 100 mL. No variation in permeate concentration in the dark phase was observed and this indicates that the E2 was stable throughout the experiment without light irradiation. Therefore, any decrease in concentration was caused by photocatalytic degradation (or photolysis) while exposure to the UV light source.

It was explained in the Materials and Methods chapter that for preparing the hormone solutions, using methanol or ethanol was unavoidable due to the low solubility of hormones in water. Since methanol was needed in higher amounts when preparing higher concentration of hormones, methanol was added to all experiments to keep the concentration of methanol in the solution constant. More details can be found in section **3.2** in Materials and Methods section. To check the effect of methanol on the photocatalytic degradation, experiments with 100 ng/L E2 was performed without the addition of methanol and compared with the result of the experiment with the addition of methanol, **Figure 6-2**.

---

[10] Experiments using PVDF-TiO$_2$ were carried out by Eleonore Veron under the supervision of Shabnam Lotfi.
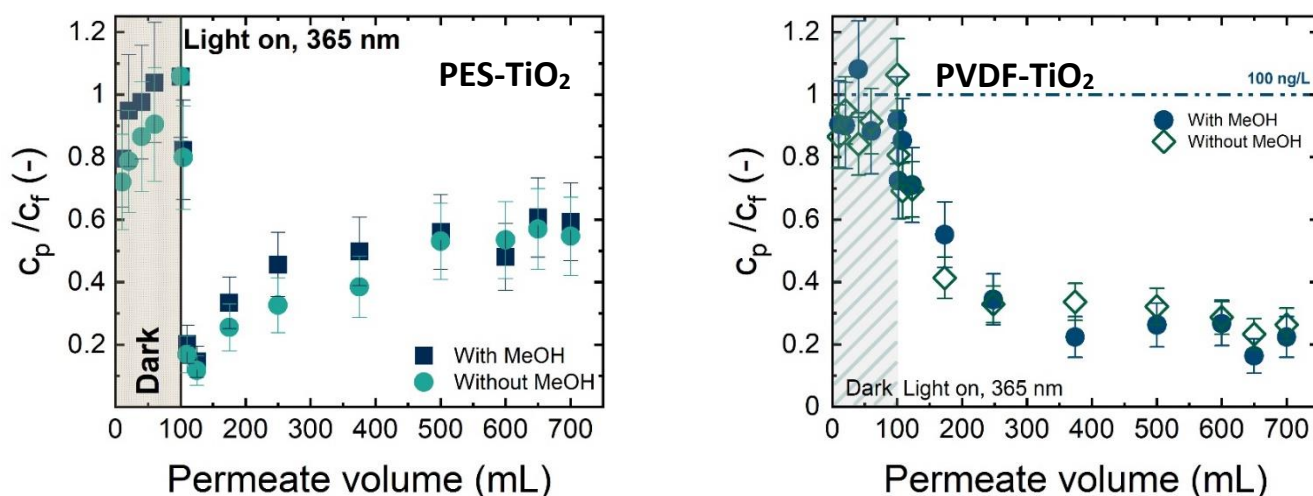
Figure 6-2 E2 removal using PES-TiO$_2$ and PVDF-TiO$_2$ in presence of methanol compared with without addition of methanol, 10 mW/cm^2, 600 L/m^{2}h, 23±0.2 °C, 8.6±0.4, 100 ng/L E2, 1 mM NaHCO$_3$, 10 mM NaCl, EtOH was 27.2 mg/L for PES-TiO$_2$ and 26.9 mg/L for PVDF-TiO$_2$ experiments, in case of addition of methanol the concentration was 79.2 mg/L MeOH. PES-TiO$_2$ data was reprinted from (**Lotfi *et al.* 2022**) and PVDF-TiO$_2$ data was reprinted from (**Liu *et al.* 2023**).

It was noticed that the addition of methanol did not interfere with the degradation of E2 in the conditions of the experiment. One possible answer could be that the amount of available ˙OH was not limiting the degradation process and hence, presence of a radical scavenger did not hinder the degradation process of E2.

In the next step, E2 degradation with direct photolysis was compared with the photocatalysis under a 365 nm UV light source, presented in **Figure 6-3** for both PES-TiO$_2$ and PVDF-TiO$_2$.
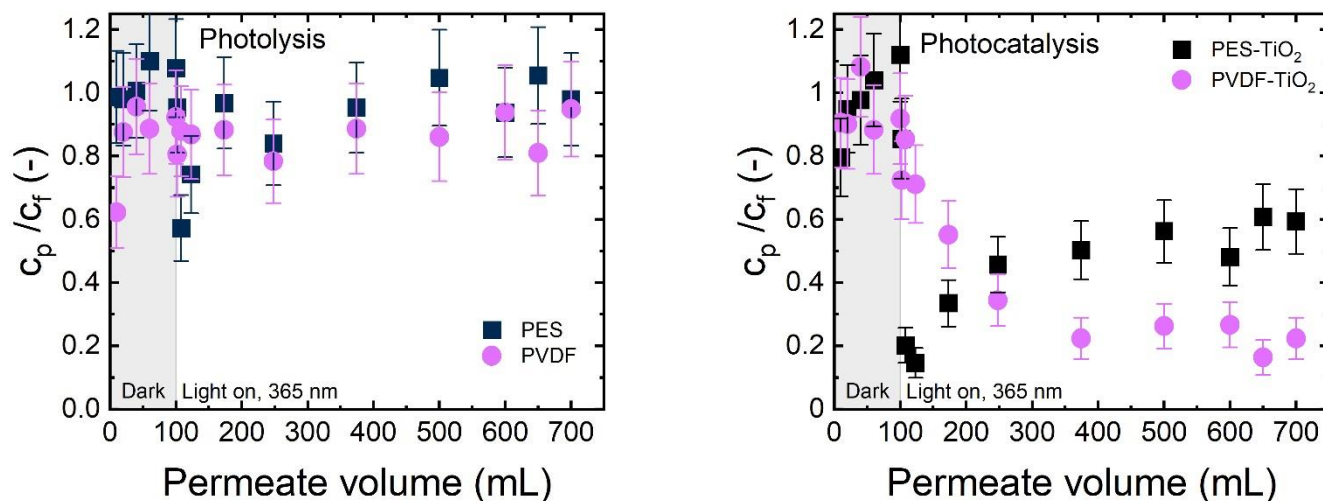
Figure 6-3 Concentration ratio of E2 *vs.* cumulative permeate volume with PES and PVDF for photolysis, PES-TiO$_2$ and PVDF-TiO$_2$ membranes for photocatalysis. Dark phase (100 mL) for adsorption of E2 on the membrane, followed by light irradiation (600 mL) at 365 nm in both cases. Conditions: 10 mW/cm^2, 600 L/m^{2}h, 23±0.2 °C, pH 8.6±0.4, 100 ng/L E2, 1 mM NaHCO$_3$, 10 mM NaCl, 79.2 mg/L MeOH, EtOH was 27.2 mg/L for PES-TiO$_2$ and 26.9 mg/L for PVDF-TiO$_2$ experiments. PES/PES-TiO$_2$ data was reprinted (adapted) from (**Lotfi *et al.* 2022**) and PVDF/PVDF-TiO$_2$ data was reprinted (adapted) from (**Liu *et al.* 2023**).

In both photolysis with pristine membrane and photocatalysis with TiO_2-coated membrane, membrane saturation (permeate concentration equal to feed) was achieved within 100 mL of filtration (50 min at 600 L/m^{2}h). A higher concentration of E2 (compared to feed) was observed in the dark phase for PES and PES-TiO_2 and PVDF-TiO_2, resulting in a concentration ratio >1. The changes are within the error of analysis, 100±15 ng/L for feed concentration, meaning a concentration ratio between 0.85 and 1.15 (-) is expected in adsorption-desorption equilibrium. When turning the UV LED light on, the concentration ratio immediately dropped in the case of PES and PES-TiO_2, to a concentration ratio of 0.57±0.13 and 0.14±0.05 (-) (43±13% and 86±5% removal) for photolysis and photocatalysis, respectively. Concentration in permeate then increased rapidly (meaning lower removal) and after 700 mL filtration, no further photolysis and a steady-state photocatalysis (40±10% removal) were established (c_p/c_f of 1 and 0.6, respectively) for this membrane material. On the other hand, when testing the PVDF membrane, the concentration ratio did not change considerably and stayed in an almost steady state condition with 87±6 ng/L. In the case of PVDF-TiO_2, a milder decline of permeate concentration was noticed after the exposure to UV light and it reached a steady state removal of E2 after 300 mL filtration in the light phase (150 min using 600 L/m^{2}h). PVDF-TiO_2 membrane not only achieved a higher removal of E2 but also showed a more stable removal performance. This could be attributed to the higher stability of this membrane under light. The stability of membranes under light exposure is examined in detail in Chapter 7. **Figure 6-4** presents the reproducibility of E2 degradation at this standard condition by PES-TiO_2 and PVDF-TiO_2.
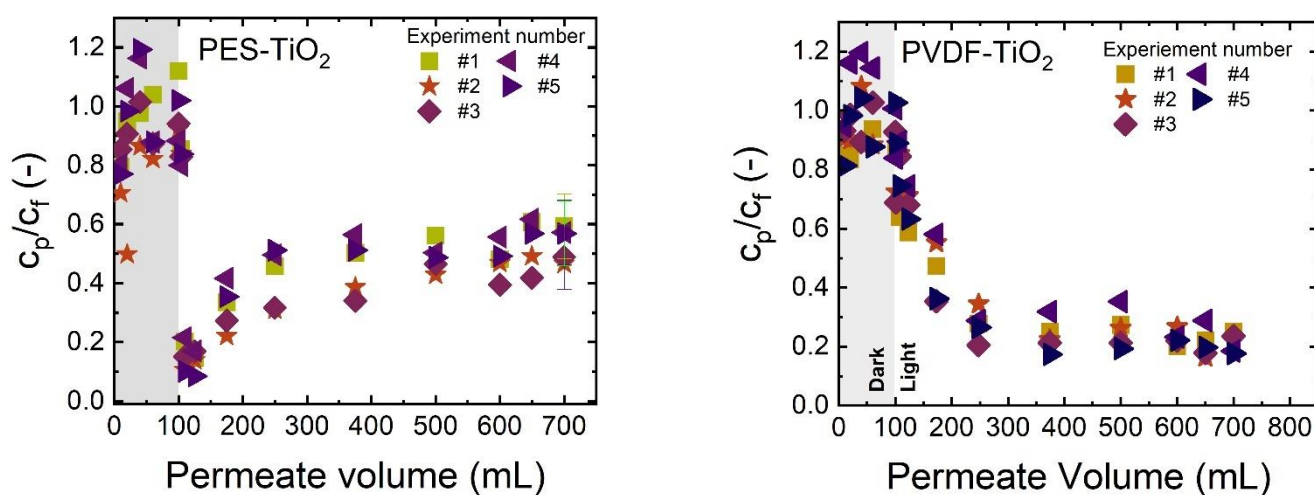
Figure 6-4 Photocatalytic degradation of E2 using PES-TiO_2 and PVDF-TiO_2 in 5 repeats to evaluate the reproducibility of photocatalytic activity, Conditions: 600 L/m^{2}h, 23±0.2 $^\circ$C, pH 8.6±0.4, 100 ng/L E2, 1 mM NaHCO$_3$, 10 mM NaCl, 79.2 mg/L MeOH, EtOH was 27.2 mg/L for PES-TiO_2 and 26.9 mg/L for PVDF-TiO_2 experiments. PES-TiO_2 data was reprinted (adapted) from (**Lotfi et al. 2022**) and PVDF-TiO_2 data was reprinted (adapted) from (**Liu et al. 2023**).

It was important to understand the reason behind the sudden high removal of E2 followed by a decline in photocatalytic membrane activity. Various scientific discussions with Prof. Dr. Schäfer and Dr. Jonathan Espindola were conducted. The hypothesis was that the exposure of the photocatalytic membrane to the UV-light and to the pollutant could affect the properties of the surface of the photocatalytic membrane and cause the initial high activity of the membrane.

6.2   Limiting factors of photocatalytic degradation in a PMR

6.2.1   Overview of all measurements

The studied parameters for evaluation of limiting factors for operation in a PMR for both PES-TiO$_2$ and PVDF-TiO$_2$ were light intensity, water flux and hydraulic resistance time, reaction temperature, hormone concentrations, solution pH and surface charge and type of steroid hormones. While each parameter is discussed in detail in the following sections, an overview of concentration ratio *vs.* permeate volume for PES-TiO$_2$ and PVDF-TiO$_2$ is presented in **Figure 6-5** and **Figure 6-6**.

Figure 6-5 Concentration ratio of E2 *vs.* cumulative permeate volume at different varying parameters, (A) light intensity, (B) temperature, (C) flux, (D) feed concentration, (E) pH, (F) hormone type individually, (G) hormone type in the mixture. Conditions (unless indicated otherwise in the figure): PES-TiO₂, 10 mW/cm², 600 L/m²h, 23±0.2 °C, 8.6±0.4, 100 ng/L E2, 1 mM NaHCO₃, 10 mM NaCl, 27.2 mg/L EtOH and 79.2 mg/L MeOH. In

different hormone-type experiments, the steroid hormone concentration was 200 ng/L, and in the mixture, the total concentration was 200 ng/L which means 50 ng/L per hormone in the mixture. Reprinted from (**Lotfi** *et al.* **2022**).
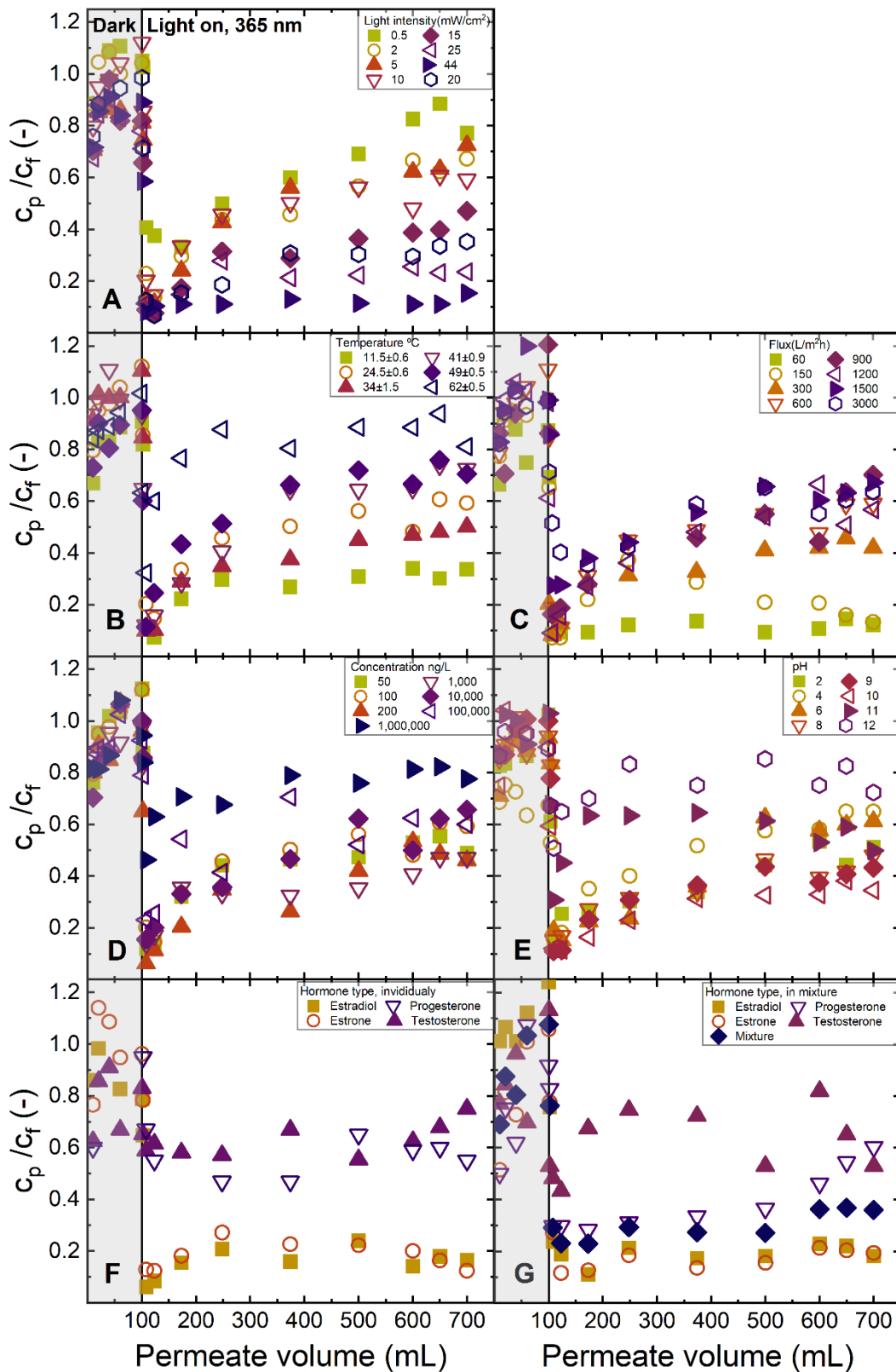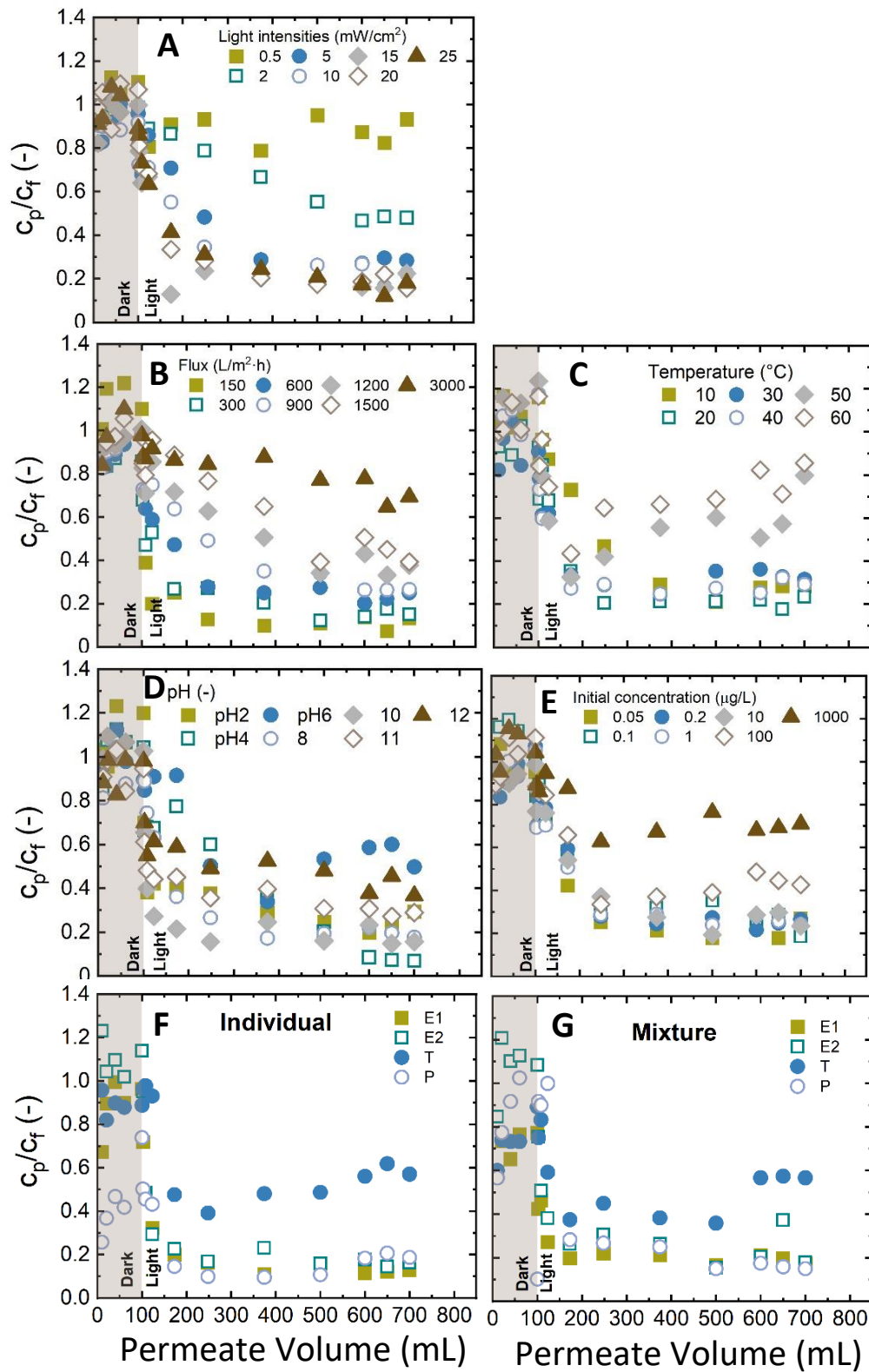
Figure 6-6[11] Concentration ratio of E2 vs cumulative permeate volume at different varying parameters, (A) light intensity, (B) flux, (C) temperature, (D) pH, (E) feed initial concentration, (F) hormone type individually, (G) hormone type in the mixture. Conditions (unless indicated otherwise in the figure): PVDF-TiO$_2$, 10 mW/cm^2, 600 L/m^{2}h, 23±0.2 °C, 8.6±0.4, 100 ng/L E2, 1 mM NaHCO$_3$, 10 mM NaCl, 27.2 mg/L EtOH and 79.2 mg/L MeOH. In the different hormone-type experiments, the steroid hormone concentration was 200 ng/L, and in the mixture, the total concentration was 200 ng/L which means 50 ng/L per hormone in the mixture. Reprinted (adapted) from (**Liu *et al.* 2023**).

6.2.2 Light intensity

Light intensity is one of the main parameters to evaluate. It defines the number of electron-hole pairs and ROS being produced in the reactor. While not enough of it results in a not sufficient degradation, the excess amount of that also is being wasted and not improving the reaction kinetics. Therefore, the optimum value should be determined. The dependency of E2 photocatalytic degradation on light intensity for PES-TiO$_2$ and PVDF-TiO$_2$ is presented in **Figure 6-7**.
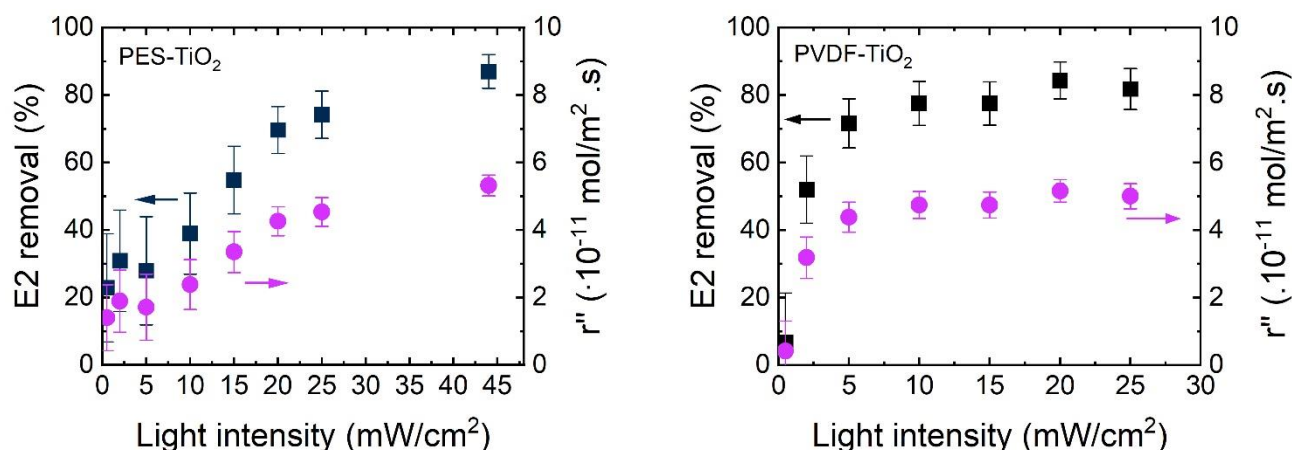
Figure 6-7 The removal and rate of disappearance (r″) of E2 in varying light intensity using PES-TiO$_2$ and PVDF-TiO$_2$, conditions: 100 mL dark phase, 600 mL filtration under light 365 nm, 600 L/m^{2}h, 23±0.2 °C, pH 8.6±0.4, 100 ng/L E2, 1 mM NaHCO$_3$, 10 mM NaCl, 79.2 mg/L MeOH, EtOH was 27.2 mg/L for PES-TiO$_2$ and 26.9 mg/L for PVDF-TiO$_2$ experiments. The removal and r″ are calculated at permeate volume of 700 mL in all figures. PES-TiO$_2$ data was reprinted from (**Lotfi *et al.* 2022**) and PVDF-TiO$_2$ data was reprinted from (**Liu *et al.* 2023**).

Although the amount of TiO$_2$ coated on the PES-TiO$_2$ membrane was higher (the same methods resulted in higher TiO$_2$ uptake), the performance of the PVDF-TiO$_2$ membrane at low light intensities below 10 mW/cm^2 was noticeably better. At 5 mW/cm^2, the removal rate of E2 using the PES-TiO$_2$ membrane was close to 30%, whereas, the PVDF-TiO$_2$ membrane achieved almost 75% removal. The removal and rate of disappearance continued to rise almost linearly with the PES-TiO$_2$ membrane until 20 mW/cm^2 and then started to level off. This trend was different for PVDF-TiO$_2$ which reached the plateau at 10 mW/cm^2 and became independent of light intensity (zero order). At this point when the reaction did not improve with a higher number of emitted photons, either photogenerated holes and electrons

---

[11] Experiments were carried out by Eleonore Veron under the supervision of Shabnam Lotfi.

recombined faster due to the excess of these species, and hence this led to a decline in efficiency **(Ollis et al. 1991)**, or an instantaneously higher temperature at the photocatalyst surface caused by the exothermic recombination reaction of electrons and holes resulted in the lower efficiency **(Herrmann 2010)**. Measuring the temperature at the surface of the membrane in the studied PMR was not possible because not enough space was available for a temperature measuring device. However, the effect of variation of reaction environment temperature was investigated. The concentration ratio versus permeate volume for all parameters and both membranes can be found in **Figure 6-5** and **Figure 6-6**. To continue the examination of the PMR operation, the light intensity of 10 mW/cm^2 was chosen as the standard condition.

6.2.3   Water flux and hydraulic residence time

Water flux through the PMR determines the hydraulic resistance time which is equal to the resistance time of the pollutant inside the PMR unless the pollutants are adsorbed on the membrane surface. **Figure 6-8** shows the removal and rate of disappearance of E2 with varying water flux. The molar flux and residence time of pollutants (top axis) to the correspondence water flux are expressed. Since it was shown in the previous chapter that the majority of the reaction is happening inside the membrane pores, the expressed residence time in the **Figure 6-8** was calculated using equation **3-16** depending only on the geometry of the membrane. The hydraulic residence time inside the membrane pores for a flux decreasing from 3000 to 60 L/m^2h varied from 0.12 to 6.2 s for PES-TiO$_2$ and from 0.09 to 4.5 s for PVDF-TiO$_2$ (differs due to different membrane thickness). In the same range (increasing flux), molar flux increased from 0.6×10^{-11} to 31×10^{-11} mol/m^2s for both membranes as a higher number of moles were brought to the membrane pores with higher flux.
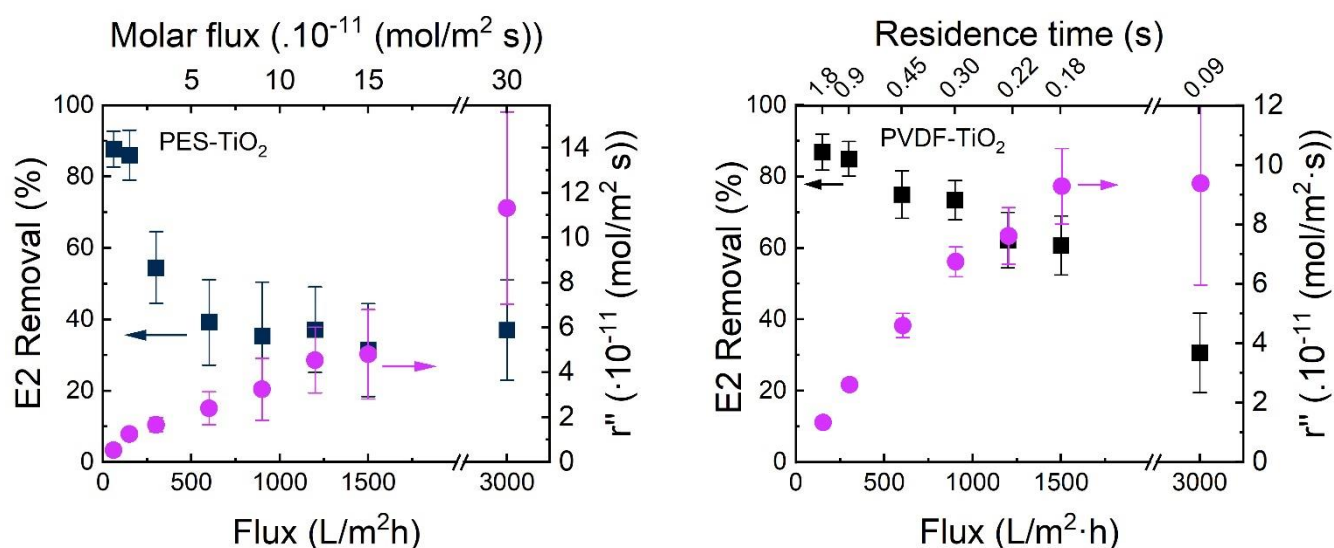
Figure 6-8 The removal and r" of E2 in varying water flux (residence time) using PES-TiO$_2$ and PVDF-TiO$_2$. To show both residence time and molar flux correspondence to the examined flux, the top axis on the left figure shows the molar flux and the top axis on the right figure shows the residence time corresponding to the flux on the bottom axis. Conditions: 100 mL dark phase, 600 mL filtration under light 365 nm, 10 mW/cm^2, 23±0.2 $^{\circ}$C, pH 8.6±0.4, 100 ng/L E2, 1 mM NaHCO$_3$, 10 mM NaCl, 79.2 mg/L MeOH, EtOH was 27.2 mg/L for PES-TiO$_2$ and 26.9 mg/L for PVDF-TiO$_2$ experiments. PES-TiO$_2$ data was reprinted (adapted) from (**Lotfi et al. 2022**) and PVDF-TiO$_2$ data was reprinted (adapted) from (**Liu et al. 2023**).

When flux increased (decline in the residence time), E2 removal using PES-TiO$_2$ declined with a sharp slope until 600 L/m^{2}h and then levelled off, an overall decrease from 88%±5% to 37±14% at 60 to 3000 L/m^{2}h, whereas using PVDF-TiO$_2$ a milder decline was noticed until 3000 L/m^{2}h from 87±5% to 31±11%. In case of the PES-TiO$_2$ membrane, with the increase in molar flux, the rate of disappearance enhanced, which means that in this flux range, the mass transfer of molecules to the surface was limiting the reaction and not the reaction rate. However, experiments with PVDF-TiO$_2$ membrane showed that the rate of disappearance rose until 1500 L/m^{2}h which indicates the mass transfer-controlled regime and then levelled out. This could mean that with this membrane, after 1500 L/m^{2}h, mass transfer was not liming the reaction anymore and the main issue was the low residence time of the molecules inside the membrane pores. This range which is equal to residence time less than 0.18 s is called the surface-reaction-controlled regime. This observation was in accordance with previous literature on flow-through PMRs (**Wang et al. 2011**). However, it is also proved that the photocatalytic reaction is very fast in the range of pico to nanoseconds (**Friedmann et al. 2010**). The results from flow-through PMR using a microfiltration range membrane (flux of 150 L/m^{2}h and pressure of almost 0.03±0.002 bar) were promising compared with nanofiltration membranes with a pressure range of 3-20 bar (**Van der Bruggen et al. 2003**). The study of Imbrogno et al. (**Imbrogno et al. 2019**) on the removal of E2 using nanofiltration membranes reported nearly 75% removal of 100 ng/L E2 using NF90 at 77 L/m^{2}h and 9.6 bar and NF270 at 135 L/m^{2}h and 9.6 bar. Successful photocatalytic degradation using a

microfiltration membrane resulted in the saving of energy and no concentrated side stream to be dealt with.

6.2.4   Reaction temperature

Next, the dependency of the reaction on the temperature of the reaction environment was investigated. The setup was modified somehow to make sure the temperature of the cell is varied and not the feed bottle (**Figure 3-8**). The temperature of the reaction environment can affect the adsorption of the hormones to the surface, the diffusivity of the molecules, the viscosity of the solution, dissolved oxygen (DO), and the reaction kinetic. The E2 removal and rate of disappearance at different reaction temperatures for both PES-TiO$_2$ and PVDF-TiO$_2$ membranes are shown in **Figure 6-9**.
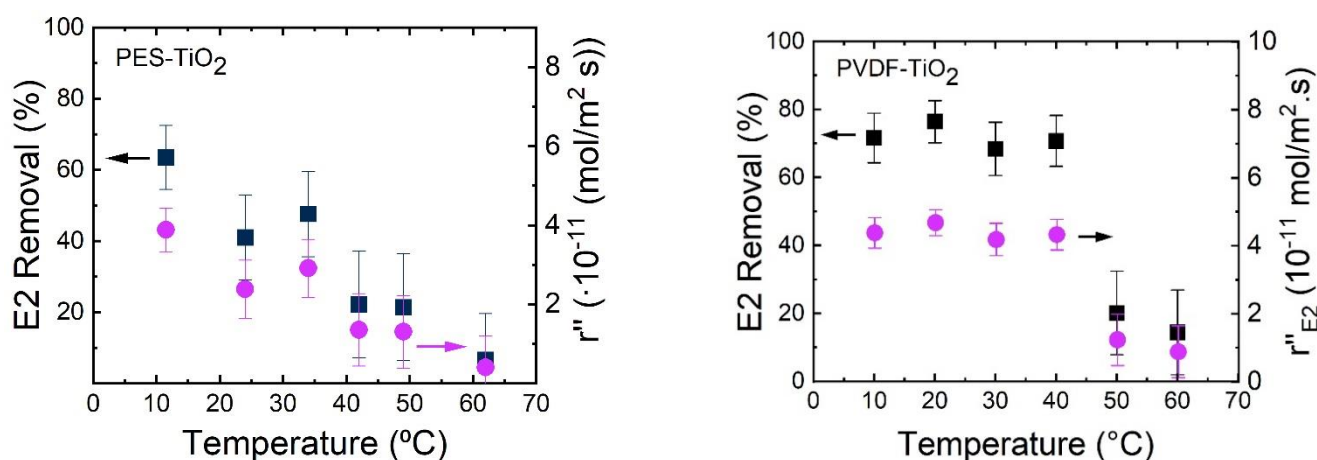
Figure 6-9 The removal and r" of E2 in varying water temperatures using PES-TiO$_2$ and PVDF-TiO$_2$. Conditions: 100 mL dark phase, 600 mL filtration under light 365 nm, 10 mW/cm^2, 600 L/m^{2}h, pH 8.6±0.4, 100 ng/L E2, 1 mM NaHCO$_3$, 10 mM NaCl, 79.2 mg/L MeOH, EtOH was 27.2 mg/L for PES-TiO$_2$ and 26.9 mg/L for PVDF-TiO$_2$ experiments. PES-TiO$_2$ data was reprinted (adapted) from (**Lotfi *et al.* 2022**) and PVDF-TiO$_2$ data was reprinted (adapted) from (**Liu *et al.* 2023**).

Both E2 removal and rate of disappearance declined with increasing the temperature, with a more obvious decline for PES-TiO$_2$, while PVDF-TiO$_2$ was almost resistant to the temperature change until 40 ^{o}C. Although the reaction between $^\bullet$OH and E2 molecules can happen in both adsorbed phase and in the close vicinity of the surface where still $^\bullet$OH exists (**Turchi and Ollis 1990**), the adsorption of the molecules to the surface enhances the probability of the degradation. Since the adsorption of molecules to the surface is an exothermic reaction, decreasing the temperature could improve the reaction and result in enhanced degradation. Moreover, the DO concentration is improved at a lower temperature. It was not possible to measure the DO concentration at the surface of the membrane *in situ*, enhanced removal was noticed for at least the PES-TiO$_2$ membrane. On the other hand, the diffusivity increases with temperature and could result in enhanced removal. But it could be possible that DO concentration and adsorption to the surface had a more obvious impact on the overall degradation and reaction happening inside nano-

meter-sized pores with tortuosity was not affected by the change in diffusivity. It should be also noted that the PMR system noticed a small rise in the pressure from at 60 °C which could be due to the effect of temperature on the system.

6.2.5   Hormone concentration

In the next step, the photocatalytic degradation of E2 in the PMR system was evaluated in a variation of the solution chemistry. The feed concentration of 50 ng/L to 1 mg/L was tested and shown in **Figure 6-10** using both PES-TiO$_2$ and PVDF-TiO$_2$ membranes. The lowest concentration of E2 was chosen based on environmental conditions which were explained in detail in the literature section (**Chapter 2**) and the higher limit was close to the solubility limit of E2.
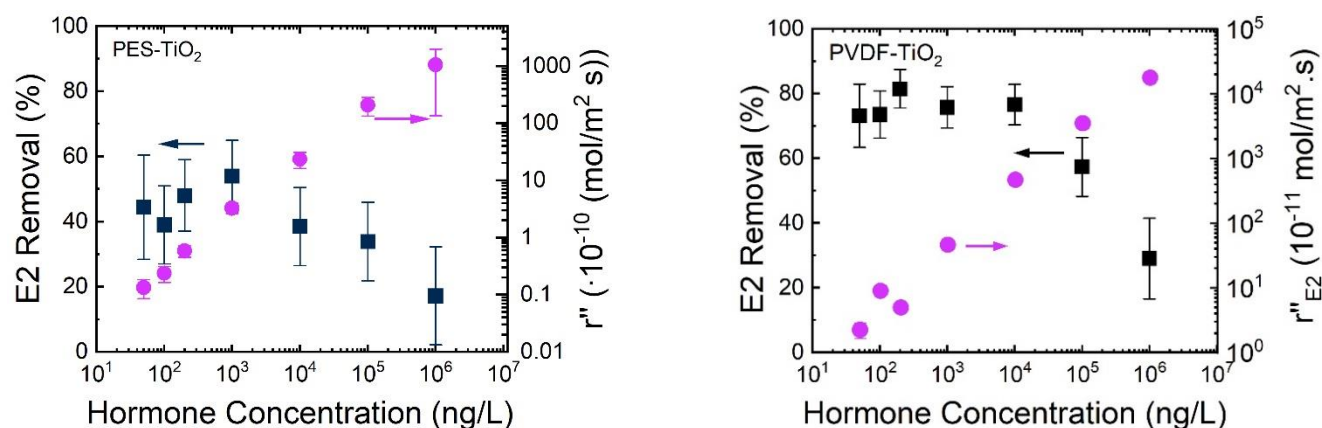
Figure 6-10 The removal and r" of E2 in varying E2 feed concentrations using PES-TiO$_2$ and PVDF-TiO$_2$. Conditions: 100 mL dark phase, 600 mL filtration under light 365 nm, 10 mW/cm^2, 600 L/m^{2}h, 23±0.2 °C, pH 8.6±0.4, 1 mM NaHCO$_3$, 10 mM NaCl, 79.2 mg/L MeOH, EtOH was 27.2 mg/L for PES-TiO$_2$ and 26.9 mg/L for PVDF-TiO$_2$ experiments. PES-TiO$_2$ data was reprinted from (**Lotfi** *et al.* **2022**) and PVDF-TiO$_2$ data was reprinted from (**Liu** *et al.* **2023**).

It was noticed that the rate of disappearance increased almost linearly with the rise in feed concentration. This means that with the higher number of molecules available at the surface, the degradation of E2 happened faster. Although the overall removal was decreased, the removal value shows a proportion of molecules which are removed. The same trend was noticed with PES-TiO$_2$ and PVDF-TiO$_2$ with the difference that overall removal and rate of disappearance for PVDF-TiO$_2$ was higher. For each membrane, it can be assumed that the amount of catalyst mass was similar and therefore, under the same light exposure, the number of generated ROS was the same and the faster degradation of E2 can only be attributed to the higher quantity of molecules present at the surface (first-order reaction rate). This is consistent with other studies for E2 removal with photocatalytic degradation in a slurry TiO$_2$ reactor (**Alvarez-Corena** *et al.* **2016, Perondi** *et al.* **2020**). When increasing concentration, photocatalyst surfaces become saturated with the reactant molecules (E2) at some point, with the reaction rate reaching

a steady-state phase (zero-order) **(Malato *et al.* 2009)**. At the highest tested concentration for PES-TiO$_2$, a higher error in the rate of disappearance, makes the interpretation of linear trend challenging.

6.2.6 Solution pH and surface charge

The next parameter in the solution chemistry to be investigated is solution pH. By variation in pH, the ionic composition of water changes and it affects the surface charge of the membrane as well as the generation of ROS. The surface charge of PMs can be determined by zeta potential through streaming potential measurement. The Zeta potential of the PES-TiO$_2$ and PVDF-TiO$_2$ membrane was presented before in **Figure 4-7**. In both cases, the pristine membrane was mostly negative over the range of tested pH and the isoelectric point (IEP) was below pH 2 and could not be obtained. After the membrane was coated with TiO$_2$, the IEP was changed to 4.8 for PES-TiO$_2$ and 3.3 for PVDF-TiO$_2$ with the membrane being negatively charged above these values. It should be noted that the streaming potential measurement of microfiltration polymeric membranes is quite challenging, as leakage in such a porous structure is a common issue. Therefore, the absolute charge values should be treated carefully. The surface of a TiO$_2$ layer is covered with hydroxyl groups of either OH$^-$ or H$_2$O which is dependent on solution pH according to equations **2-1** and **2-2**. The surface coverage of TiO$_2$ was reported by **(Turchi and Ollis 1990)** to be 5-10 OH$^-$/nm^2. Below IEP which is in this case acidic condition, the surface is changed to TiOH$_2^+$ and above IEP, it is TiO$^-$.

Another effect of pH of the solution is in the speciation of steroid hormones. The speciation of the target MP can affect the degradation process as it can cause repulsion or adsorption. The steroid hormone speciation was obtained by Marvin software (version 20.20.0, ChemAxon) as shown in **Figure 6-11**. To calculate the pKa of steroid hormone, the molecular properties of the hormones were downloaded from PubChem on Nov.2020 and exported to the software.
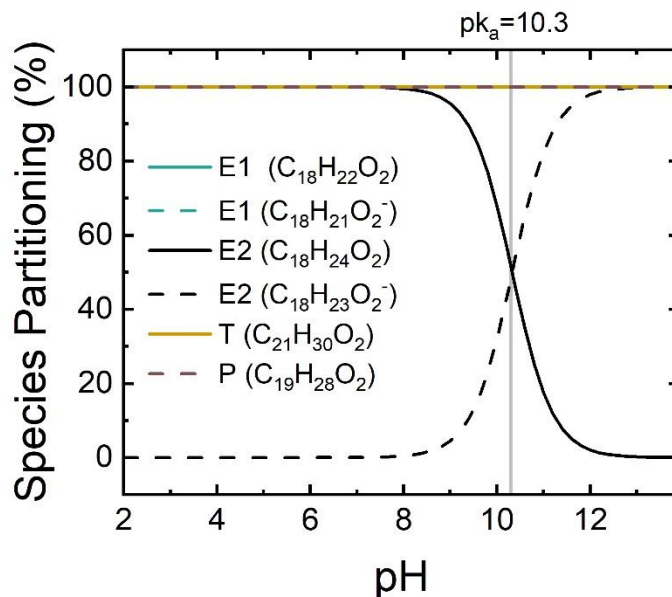
Figure 6-11 The speciation of steroid hormones obtained by Marvin software (version 20.20.0, ChemAxon), reprinted (adapted) from (**Lotfi *et al.* 2022**).

The pKa of E1 and E2 were similarly 10.3 as these two hormones have a very similar molecular structure. Similar results were reported previously in literature (**Hurwitz and Liu 1977, Lewis and Archer 1979**). This means that above pH 10.3, E1 and E2 are deprotonated and negatively charged. Progesterone and testosterone did not dissociate above pH 2. Therefore, the solution pH above 10.3 affected more the degradation of E1 and E2 as both pollutant and the membrane surface are negatively charged (**Figure 4-7**) and there is a repulsion between them. On the other hand, the alkaline solution can favour the production of OH radical through the reaction between OH^- and the photogenerated hole (h+) (**Mozia *et al.* 2010**). The photocatalytic degradation of E2 over a pH range of 2-12 was investigated and presented in **Figure 6-12** for both PES-TiO$_2$ and PVDF-TiO$_2$.
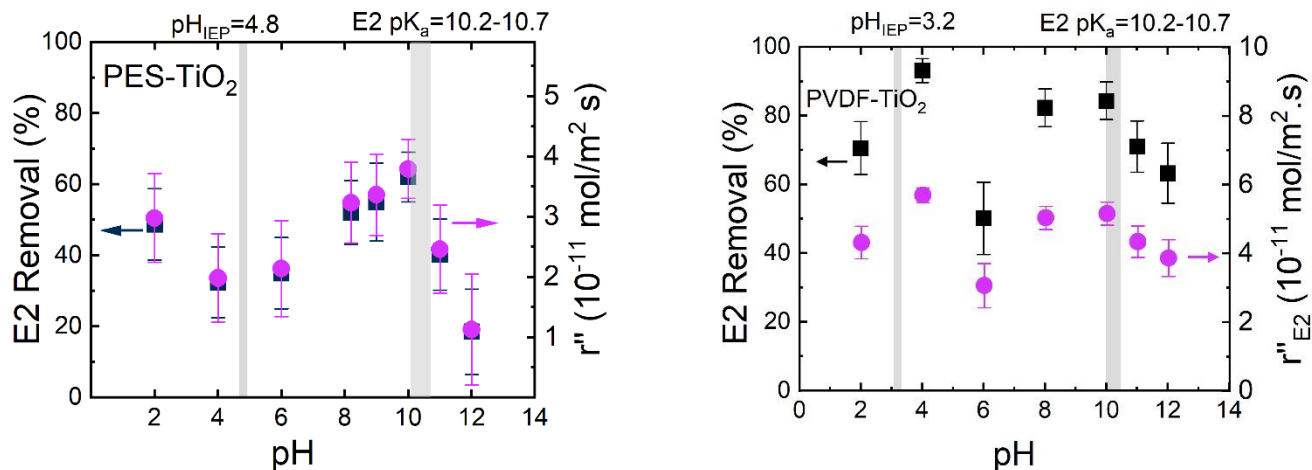
Figure 6-12 The removal and r" of E2 in varying E2 solution pH using PES-TiO$_2$ and PVDF-TiO$_2$. The pH of IEP shown in the figures is an average of some repeats. Conditions: 100 mL dark phase, 600 mL filtration under light 365 nm, 10 mW/cm^2, 600 L/m^{2}h, 23±0.2 ^{o}C, 100 ng/L E2, 1 mM NaHCO$_3$, 10 mM NaCl, 79.2 mg/L MeOH, EtOH

was 27.2 mg/L for PES-TiO$_2$ and 26.9 mg/L for PVDF-TiO$_2$ experiments. PES-TiO$_2$ data was reprinted from (**Lotfi *et al.* 2022**) and PVDF-TiO$_2$ data was reprinted from (**Liu *et al.* 2023**).

In **Figure 6-12**, to get a better idea of the membrane surface charges, the pH of IEP is indicated which is an average of the values obtained from repeats in **Figure 4-7**. For both membranes, the variation of the results is less noticeable compared to other studied parameters. For PES-TiO$_2$, it seems that having more alkaline pH is favorable for photocatalytic degradation until pH of IEP (10.3). Above pH 10, degradation of E2 was declined using both membranes which can be due to the repulsion between the molecules and the membrane surface. For PES-TiO$_2$, the decline was more obvious from pH 10 to 12 (from 62±8% to 18±15%) compared with PVDF-TiO$_2$ (from 82±5% to 60±9%). However, as can be noticed, the errors are higher at lower pH due to getting closer to the limit of detection of analytical device and this makes the comparison more difficult. This should be noted that other studies such as (**Schäfer *et al.* 2003, Hu *et al.* 2007, Banasiak and Schäfer 2010**) also proved the impact of pH on the adsorption of hormones on the membrane surface. The adsorption of E2 showed to decrease above IEP (10.3) for the same reason stated above.

6.2.7   Steroid hormone type

To understand the differences between the photocatalytic degradation of different molecular structures and the combination of hormones in a solution, experiments with four different steroid hormones individually and in the mixture were designed. To have the same concentration, experiments with one single hormone, E1, E2, T and P, with 200 ng/L concentration and one experiment with the mixture of four hormones each 50 ng/L (total 200 ng/L) were performed. The molecular structure and other properties of four hormones are presented in **Table 2-1**. E1 and E2 are mostly similar with a phenolic ring which does not exist in T and P. The comparison of degradation of individual and the mixture of hormones with PES-TiO$_2$ and PVDF-TiO$_2$ is expressed in **Figure 6-13**.
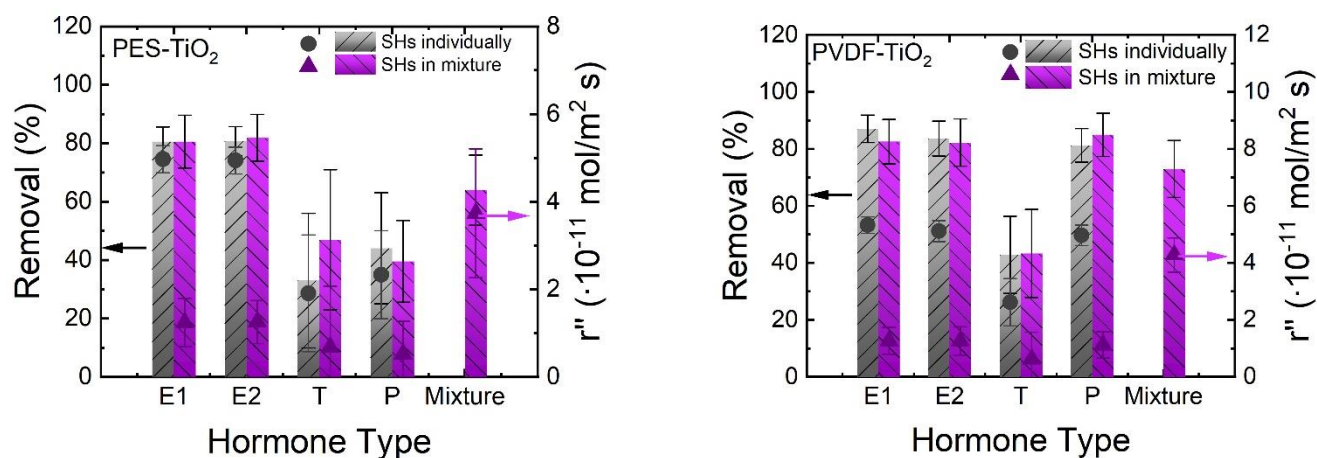
Figure 6-13 The removal and r" of 4 different steroid hormone individually and in a mixture using PES-TiO$_2$ and PVDF-TiO$_2$. Conditions: 100 mL dark phase, 600 mL filtration under light 365 nm, 25 mW/cm^2, 300 L/m^{2}h, 23±0.2 ^{o}C, pH 8.6±0.4, 1 mM NaHCO$_3$, 10 mM NaCl, 79.2 mg/L MeOH, EtOH was 27.2 mg/L for PES-TiO$_2$ and 26.9 mg/L for PVDF-TiO$_2$ experiments, concentration of steroid hormone in individual experiment was 200 ng/L, in the mixture experiment, each hormone was 50 ng/L which made the total mixture concentration 200 ng/L hormone. PES-TiO$_2$ data was reprinted from (**Lotfi *et al.* 2022**) and PVDF-TiO$_2$ data was reprinted from (**Liu *et al.* 2023**).

Using both membranes, E1 and E2 were removed with a high rate of above 80%. The interesting point was that both membranes failed to remove T between 30-40% while PVDF-TiO$_2$ could successfully remove progesterone with almost 80% removal in both individual hormone experiment and mixture of hormones. The removal of mixture of hormones as also almost similar with both membranes, with 64±12% using PES-TiO$_2$ and 73±10% using PVDF-TiO$_2$. Based on Frontier Electron Theory (FET), sites most susceptible to electron extraction and radical attack in E2 are the carbon atoms located in the phenolic group (**Rokhina and Suri 2012**). Also, phenol moiety in E1 and E2 is typically attacked first by ˙OH and have electrons extracted by photo-generated holes (**Ohko *et al.* 2002, Mai *et al.* 2008, Mboula *et al.* 2015**).

A similar degradation ratio for E1 and E2 has been attributed to the similar degradation mechanism of estrogens (**Li Puma *et al.* 2010, Liz *et al.* 2018**). On the contrary, Wang *et al.* (**Wang *et al.* 2016**) reported a faster degradation rate of E1 (1.3 times faster) compared to E2 in a TiO$_2$-PVDF membrane PMR system. This was explained by E1 being a less stable molecule under photocatalytic degradation due to an additional carbonyl group and strong UV light absorption of its double bond (**Wang *et al.* 2016**). In the case of progesterone (P) and testosterone (T), resistance in the degradation of P compared to other MPs and steroid hormones was observed by other researchers as well (**Benotti *et al.* 2009, Klamerth *et al.* 2009**). Benotti *et al.* (**Benotti *et al.* 2009**) found that steroid hormones required different light irradiation energy in the order of P>T>E2=E1 when photocatalytic degradation occurred in a mixture of steroid hormones.

Since the structure of molecules could affect the adsorption of them to the surface, which is an important parameter for photocatalytic degradation, adsorption of steroid hormones to PES-TiO$_2$ and PVDF-TiO$_2$ was also compared, **Figure 6-14** (PES-TiO$_2$ data). Mass adsorbed can be estimated using data of c_p/c_f and formula explained in section 3.12 formula 3.31. Required data for PVDF-TiO$_2$ was obtained from figure **Figure 6-6F**.
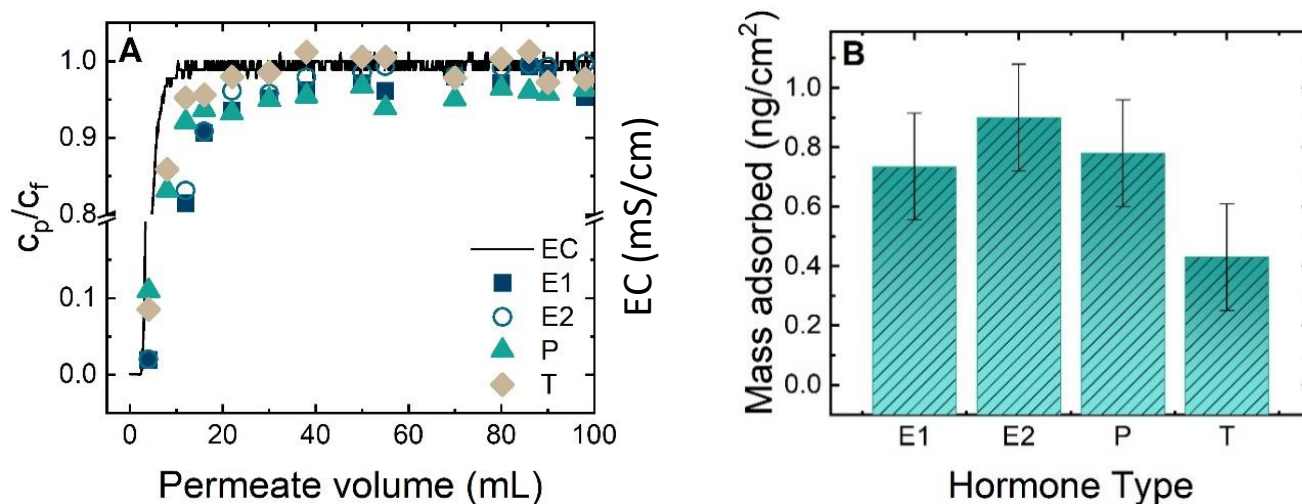

Figure 6-14 (A) Concentration and conductivity ratio of permeate over feed over cumulative permeate volume in the dark phase (first 100 mL), (B) mass adsorbed per membrane area for PES-TiO$_2$, each hormone 200 ng/L, 300 L/m^{2}h, 23±0.2 $^\circ$C, pH 8.6±0.4, 1 mM NaHCO$_3$, 10 mM NaCl, 27.2 mg/L EtOH and 79.2 mg/L MeOH. Reprinted from (**Lotfi** *et al.* **2022**).

In case of PES-TiO$_2$, T had the lowest adsorption while E1, E2 and P showed almost similar mass adsorbed in 100 mL filtration. Whereas, using PVDF-TiO$_2$ membrane, P had the highest mass adsorbed to the surface (**Liu** *et al.* **2023**). This could possibly explain the higher removal of P by PVDF-TiO$_2$ compared to PES-TiO$_2$ as the presence of molecules at the surface enhances the photocatalytic degradation considerably.

6.3   References

Alvarez-Corena, J. R., J. A. Bergendahl and F. L. Hart (2016). "Advanced oxidation of five contaminants in water by UV/TiO$_2$: Reaction kinetics and byproducts identification." Journal of Environmental Management **181**: 544-551.

Banasiak, L. J. and A. I. Schäfer (2010). "Sorption of steroidal hormones by electrodialysis membranes." Journal of Membrane Science 365: 198-205.

Benotti, M. J., B. D. Stanford, E. C. Wert and S. A. Snyder (2009). "Evaluation of a photocatalytic reactor membrane pilot system for the removal of pharmaceuticals and endocrine disrupting compounds from water." Water Research **43**: 1513-1522.

Friedmann, D., C. Mendive and D. Bahnemann (2010). "TiO$_2$ for water treatment: Parameters affecting the kinetics and mechanisms of photocatalysis." Applied Catalysis B: Environmental **99**: 398-406.

Herrmann, J.-M. (2010). "Photocatalysis fundamentals revisited to avoid several misconceptions." Applied Catalysis B: Environmental **99**: 461-468.

Hu, J., X. Jin and S. Ong (2007). "Rejection of estrone by nanofiltration: Influence of solution chemistry." Journal of Membrane Science 302: 188-196.

Hurwitz, A. R. and S. T. Liu (1977). "Determination of Aqueous Solubility and pKa Values of Estrogen." Journal of Pharmaceutical Sciences 66: 624-627.

Imbrogno, A., P. Samanta and A. I. Schäfer (2019). "Fate of steroid hormone micropollutant estradiol in a hybrid magnetic ion exchange resin-nanofiltration process." Environmental Chemistry **16**: 630.

Klamerth, N., N. Miranda, S. Malato, A. Agüera, A. R. Fernández-Alba, M. I. Maldonado and J. M. Coronado (2009). "Degradation of emerging contaminants at low concentrations in MWTPs effluents with mild solar photo-Fenton and TiO$_2$." Catalysis Today **144**: 124-130.

Lewis, K. M. and R. D. Archer (1979). "pKa values of estrone, 17β-estradiol and 2-methoxyestrone." Steroids 34: 485-499.

Li Puma, G., V. Puddu, H. K. Tsang, A. Gora and B. Toepfer (2010). "Photocatalytic oxidation of multicomponent mixtures of estrogens (estrone (E1), 17β-estradiol (E2), 17α-ethynylestradiol (EE2) and estriol (E3)) under UVA and UVC radiation: Photon absorption, quantum yields and rate constants independent of photon absorption." Applied Catalysis B: Environmental **99**: 388-397.

Liu, S., E. Véron, S. Lotfi, K. Fischer, A. Schulze and A. I. Schäfer (2023). "Poly(vinylidene fluoride) membrane with immobilized TiO$_2$ for degradation of steroid hormone micropollutants in a photocatalytic membrane reactor." Journal of Hazardous Materials 447: 130832.

Liz, M. V. d., R. M. d. Lima, B. d. Amaral, B. A. Marinho, J. T. Schneider, N. Nagata and P. Peralta-Zamora (2018). "Suspended and Immobilized TiO$_2$ Photocatalytic Degradation of Estrogens: Potential for Application in Wastewater Treatment Processes." Journal of the Brazilian Chemical Society **29**: 380-389.

Lotfi, S., K. Fischer, A. Schulze and A. I. Schäfer (2022). "Photocatalytic degradation of steroid hormone micropollutants by TiO$_2$ coated polyethersulfone membranes in a continuous flow-through process." Nature Nanotechnology **17**: 417–423.

Mai, J., W. Sun, L. Xiong, Y. Liu and J. Ni (2008). "Titanium dioxide mediated photocatalytic degradation of 17beta-estradiol in aqueous solution." Chemosphere **73**: 600-606.

Malato, S., P. Fernández-Ibáñez, M. I. Maldonado, J. Blanco and W. Gernjak (2009). "Decontamination and disinfection of water by solar photocatalysis: Recent overview and trends." Catalysis Today **147**: 1-59.

Mboula, V. M., V. Héquet, Y. Andrès, Y. Gru, R. Colin, J. M. Doña-Rodríguez, L. M. Pastrana-Martínez, A. M. T. Silva, M. Leleu, A. J. Tindall, S. Mateos and P. Falaras (2015). "Photocatalytic degradation of estradiol under simulated solar light and assessment of estrogenic activity." Applied Catalysis B: Environmental **162**: 437-444.

Mozia, S. (2010). "Photocatalytic membrane reactors (PMRs) in water and wastewater treatment. A review." Separation and Purification Technology 73: 71-91.

Ohko, Y., K.-I. Iuchi, C. Niwa, T. Tatsuma, T. Nakashima, T. Iguchi, Y. Kubota and A. Fujishima (2002). "17β-Estradiol Degradation by TiO$_2$ Photocatalysis as a Means of Reducing Estrogenic Activity." Environmental Science & Technology **36**: 4175-4181.

Ollis, D. F., E. Pelizzetti and N. Serpone (1991). "Photocatalyzed destruction of water contaminants." Environmental Science & Technology **25**: 1522-1529.

Perondi, T., W. Michelon, P. R. Junior, P. M. Knoblauch, M. Chiareloto, R. de Fatima Peralta Muniz Moreira, R. A. Peralta, E. Dusman and T. S. Pokrywiecki (2020). "Advanced oxidative processes in the degradation of 17beta-estradiol present on surface waters: kinetics, byproducts and ecotoxicity." Environmental Science and Pollution Research **27**: 21032-21039.

Rokhina, E. V. and R. P. S. Suri (2012). "Application of density functional theory (DFT) to study the properties and degradation of natural estrogen hormones with chemical oxidizers." Science of The Total Environment **417-418**: 280-290.

Schäfer, A., L. Nghiem and T. Waite (2003). "Removal of the natural hormone estrone from aqueous solutions using nanofiltration and reverse osmosis." Environmental Science & Technology 37: 182-188.

Turchi, C. S. and D. F. Ollis (1990). "Photocatalytic degradation of organic water contaminants: mechanisms involving hydroxyl radical attack." Journal of Catalysis **122**: 178-192.

Van der Bruggen, B., C. Vandecasteele, T. Van Gestel, W. Doyen and R. Leysen (2003). "A review of pressure-driven membrane processes in wastewater treatment and drinking water production." Environmental Progress **22**: 46-56.

Wang, M., F. Qu, R. Jia, S. Sun, G. Li and H. Liang (2016). "Preliminary Study on the Removal of Steroidal Estrogens Using TiO_2-Doped PVDF Ultrafiltration Membranes." Water **8**: 134.

Wang, Z., J. Liu, Y. Dai, W. Dong, S. Zhang and J. Chen (2011). "Dimethyl Sulfide Photocatalytic Degradation in a Light-Emitting-Diode Continuous Reactor: Kinetic and Mechanistic Study." Industrial & Engineering Chemistry Research **50**: 7977-7984.

Chapter Seven

7 Evaluation of photocatalytic membranes' photostability

In the previous chapters, polymeric membranes were shown to be effective in combination of high throughput (low pressure) and high photocatalytic degradation of MP. However, the disadvantage of these types of membranes is their low photostability under UV light exposure and ROS attack. For this reason, to understand the stability of tested polymeric membranes, PES, PVDF, PES-TiO$_2$ and PVDF-TiO$_2$ were subjected to a series of accelerated aging tests. The accelerated ageing procedure was developed to provide information in a shorter time in the laboratory. For the accelerated aging experiments, the simplest assumption could be that the degradation only depends on the total absorbed photons and is independent of the duration and the intensity of light **(Martin *et al.* 2003)**. This is called reciprocity law and can be shown as the following equation (**7-1**):

$$light\ intensity \times time = constant \qquad \textbf{7-1}$$

Assuming that reciprocity law applies, then by increasing the light intensity, the duration of photostability test can be reduced. This method has been utilized in different sectors such as polymeric material evaluation, medical sectors, and biological industries. A modification on reciprocity law is Schwarzschild's law (defined for the first time by an astronomer K. Schwarzschild as a modification on reciprocity law to fit his data **(Schwarzschild 1900)**) which is given in equation **7-2**:

$$(light\ intensity)^p \times time = constant \qquad \textbf{7-2}$$

where p is the Schwarzschild coefficient and if p is equal to one, the Schwarzschild's law becomes the reciprocity law. Some researchers such as Chin *et al.* **(Chin *et al.* 2005)** and Diepens *et al.* **(Diepens *et al.* 2009)** reported p to be 1 in their experiments. While others reported values between 0.5 and 1 depending on the materials and irradiation conditions **(Fairbrother *et al.* 2019** and **Mehmandoust *et al.* 2014)**. Chin *et al.* **(Chin *et al.* 2005)** validate the reciprocity law for UV photodegradation of acrylic melamine by performing tests at different irradiation intensities and in different modes. They verified the method and concluded that by increasing the intensity the damage to the polymer rises correspondingly. Other researchers also reported failure of reciprocity law **(Therias *et al.* 2021)**.

Assuming that the reciprocity law applies in this study (p equal to 1), membranes were aged for almost ten days under high light intensity which equals to above seven months under 10 mW/cm^2 of UV light which was used in previous chapters for photocatalytic degradation of MB and hormones. The chosen light wavelengths were 365 nm and 405 nm, with a total intensity of 222 mW/cm^2. The wavelengths are

sufficient for electron-hole generation using the synthesized TiO_2 nanoparticles. The details of the testing procedure can be found in Material and method Chapter 3. Membranes were placed in the UV-violet-LED chamber for a maximum of 250 h. During this time, 8 samples were collected at different times, 5, 25, 50, 75, 100, 125, 175, and 250 h. Pristine and TiO_2 coated membranes showed loss of their performance or changes in their characteristic by time at different paces. Following, the results of each test are presented.

7.1   Ageing the membranes

The procedure of ageing the membranes were explained in detail in Materials and Methods chapter section **3.8**. When ageing membranes, the first try was to put all membranes in Al holders to achieve the highest heat exchange and keep the membranes cool. However, later through SEM images, it was noticed that only on PVDF-TiO_2 membranes some octahedral structures were formed (**Figure 7-1**). Also, through SEM and EDX analysis (**Figure 7-1** right figure), it was shown that the formed octahedral has the Aluminum element in their composition. The ICP-OES analysis (**Table 7-1**) was also performed on the water sample collected after the aging of membrane using Aluminum holder and glass petri dish. In the samples aged in a glass petri dish, no Aluminum was found (<0.1 below the limit of detection). Therefore, it was understood that the additional element on the surface are Al and O and the octahedral could be attributed to Al_2O_3. Therefore, PES-TiO_2 and PVDF-TiO_2 membranes were both aged again in glass Petri dishes. Observing the temperature of the water inside the petri dish showed that the variation is negligible, and the temperature is almost 20 °C over the ageing time.

Table 7-1 Elemental analysis of water samples from two holders of Al and glass, data reprinted from (**Raota** *et al.* **2023**).

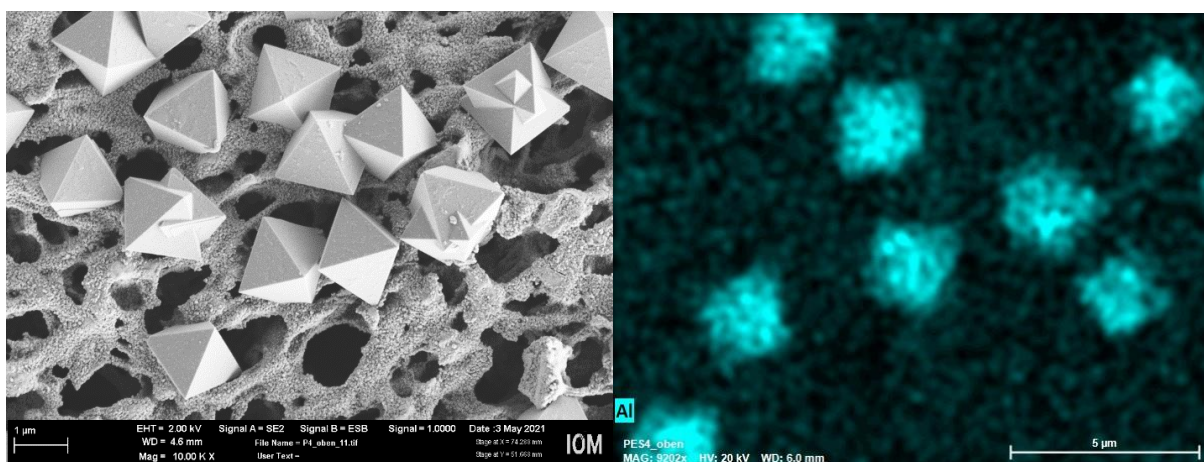| Element Sample	Ti (mg kg⁻¹)	S (mg kg⁻¹)	Si (mg kg⁻¹)	Al (mg kg⁻¹)
Method limit-of-detection	0.003	0.1	0.130	0.1
PES-TiO₂ in Al holder	< 0.003	21.1 ± 2.1	0.391 ± 0.098	13.4 ± 0.3
PES-TiO₂ in Al holder	0.005 ± 0.001	36.5 ± 3.7	0.756 ± 0.189	28.2 ± 0.7
PES-TiO₂ in glass Petri dish	0.587 ± 0.029	115 ± 12	< 0.130	< 0.1

Figure 7-1 SEM (left) and EDX (right) images of PVDF-TiO$_2$ after ageing in Al holders showing new octahedra formed which comprise Al.

7.2 Visual changes of aged photocatalytic membrane

Polymers normally show a change in their color (normally from a white/colorless to yellow), after ageing **(Rabek 1995)**. Hence, membranes were first observed visually for any change in color or obvious cracks and breakage. **Figure 7-2** expresses the changes in TiO$_2$ coated membrane over time and the fresh pristine membrane and 250h aged pristine membrane.
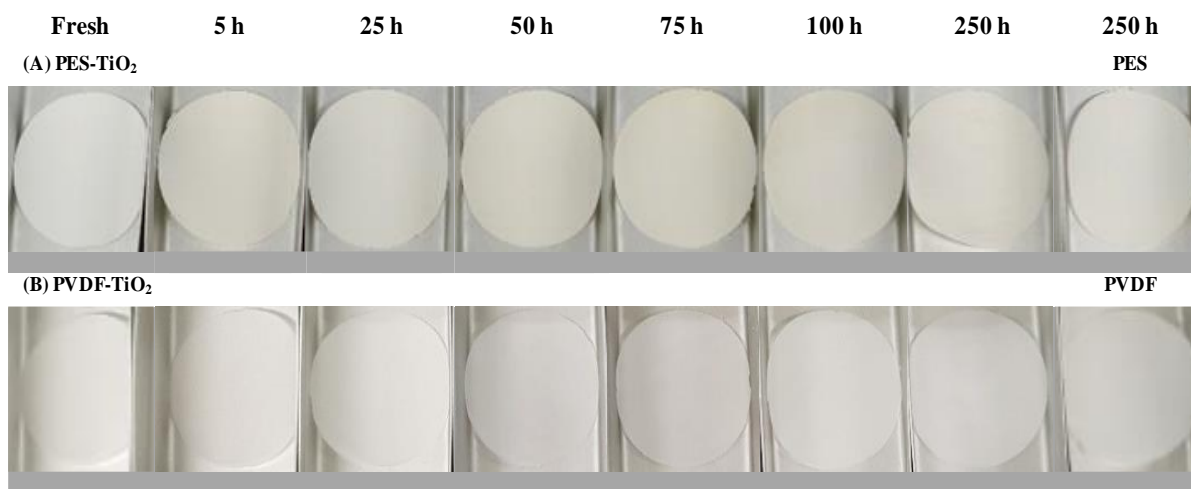
Figure 7-2 Photographs of the (A) PES-TiO$_2$, (B) PVDF-TiO$_2$ and after different light exposure durations (combined 365 nm and 405 nm). The pristine membranes were only aged for 250 h which are shown on the right side of the figure, reprinted (adapted) from **(Raota et al. 2023)**.

The yellowish color was only noticed in PES and PES-TiO$_2$ membranes. This shows that this polymer was altered more by the light exposure. The PES membrane was the only membrane type which showed cracks after drying in air. This could mean that, although TiO$_2$ coating could make damage to the membrane by generating ROS under light exposure, but it can also absorb the UV light and prevent the direct chain scission of the polymer by the photon energy. PVDF and PVDF-TiO$_2$ membranes did not

show any obvious visual changes. However, after testing the membrane inside the glass Petri dishes instead of Al holders, PVDF-TiO$_2$ membranes showed a bit of brownish color which could possibly be due to the total reflection of light from the copper plate surface.

After observing the membranes with a bare eye, microscopic images of fresh and aged membranes were investigated by scanning electron microscopy.

7.3   SEM images for surface morphology evaluation

SEM images can present the morphology of the surface and hence the TiO$_2$ coating on the membrane. The disadvantage of SEM is that only a small spot on the membrane can be checked, which is challenging to say if it is representative of the whole membrane coupon. However, the assumption here is that the noticeable changes of the surface happened to the full membrane due to the homogenous ageing condition. SEM images of aged pristine and coated membranes are presented in **Figure 7-3**.
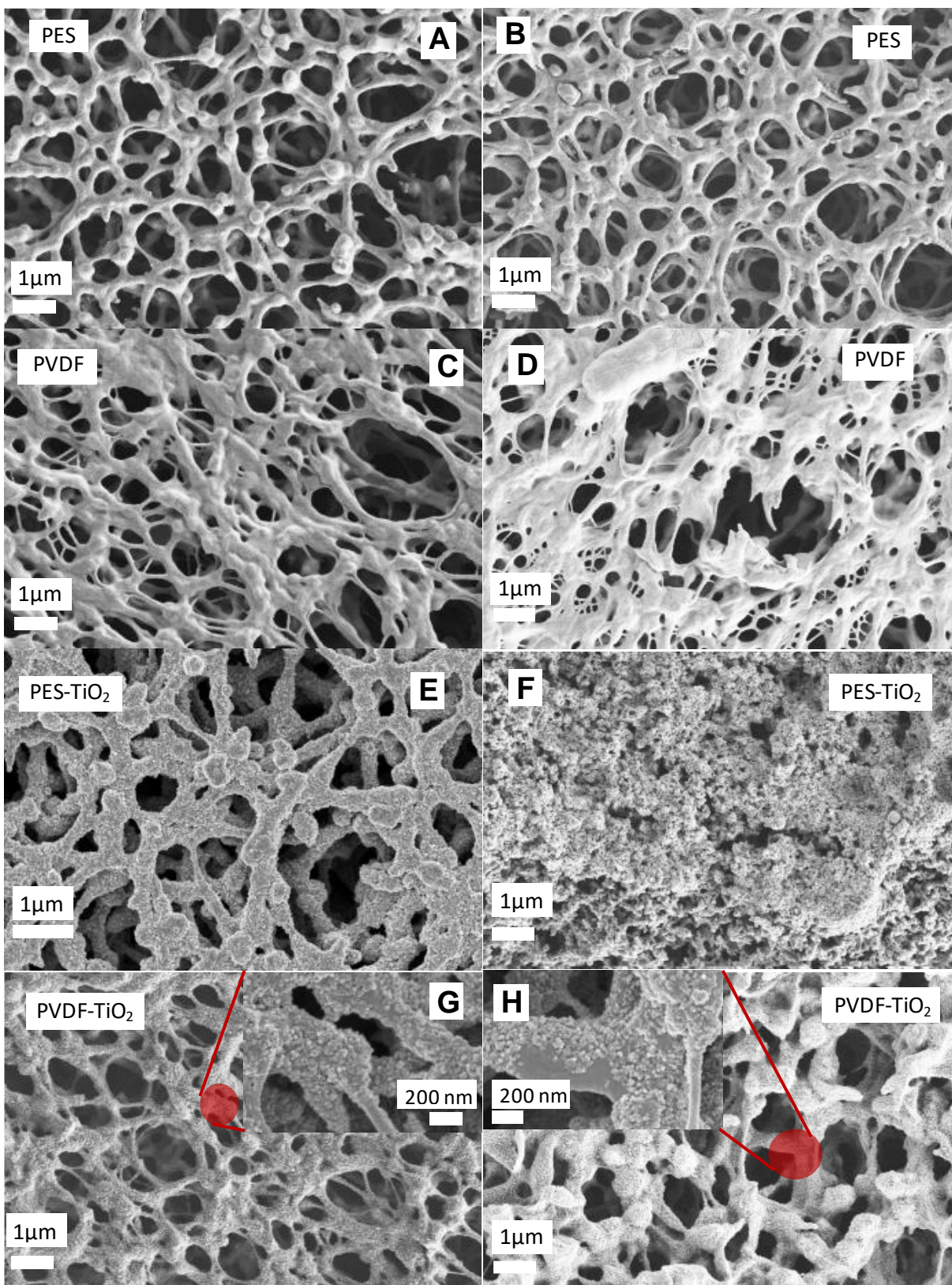
Figure 7-3 Surface SEM images revealing the morphology of fresh (left column) and 250 h aged membranes (right column): (A, B) PES, (C, D) PVDF (E, F) PES-TiO$_2$, (G, H) PVDF-TiO$_2$, (I, J) PVDF. Note: All membranes except PES-TiO$_2$ and PVDF-TiO$_2$ are aged in Al holders, those two were aged in glass Petri dishes to avoid the formation of Al$_2$O$_3$ structures. Reprinted (adapted) from (**Raota** *et al.* **2023**).

While the PES membrane did not show any drastic morphological changes on the surface (**Figure 7-3A&B**), PES-TiO$_2$ membranes had severe damages resembling a melting on the surface (**Figure 7-3E&F**). Similarly, the PVDF membrane depicted an intact membrane surface after ageing while PVDF-TiO$_2$ had some small spots without TiO$_2$ which could be due to the loss of TiO$_2$ nanoparticles (**Figure 7-3C&D**). This observed surface destruction disagreed with other research that mentioned TiO$_2$ coating on PES membranes protected the membranes from photodegradation (**Labuto** *et al.* **2021**). This observation could be an indication of ROS attack which were formed in-situ during light exposure that shows the higher resistance of PVDF in comparison with PES.

When membranes were left to dry for the SEM, the PES membrane bend upward (to the exposed side to the light) as presented in **Figure 7-4**. More careful observation with bare eyes showed obvious cracks after drying which could be due to membrane bends. This was most obvious in the PES membrane and then in PES-TiO$_2$.
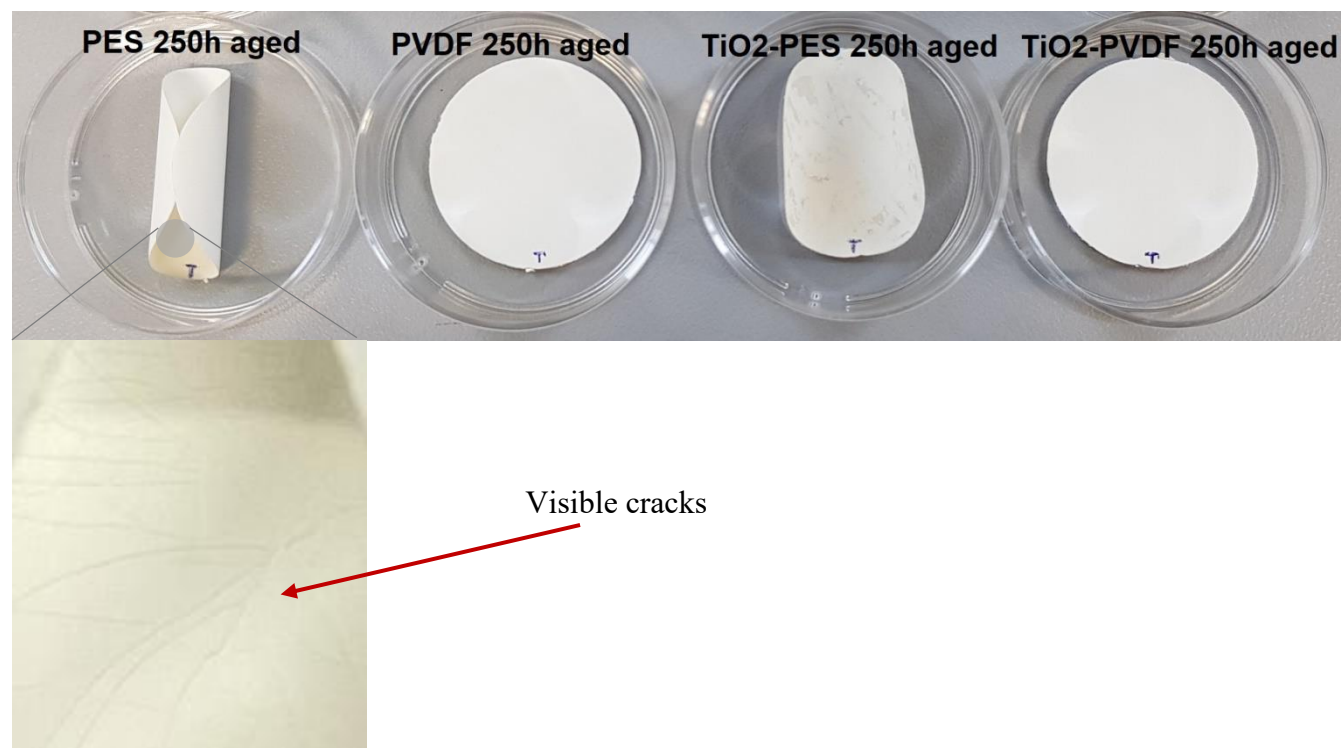
Figure 7-4 Photographs of aged membranes before taking SEM images and visible cracks of PES-250 h aged membrane due to bending upward.

These cracks occurred due to mechanical damage and were also visible in the cross-section images of the membrane (**Figure 7-5**), which should not be confused with cracks from direct light exposure.
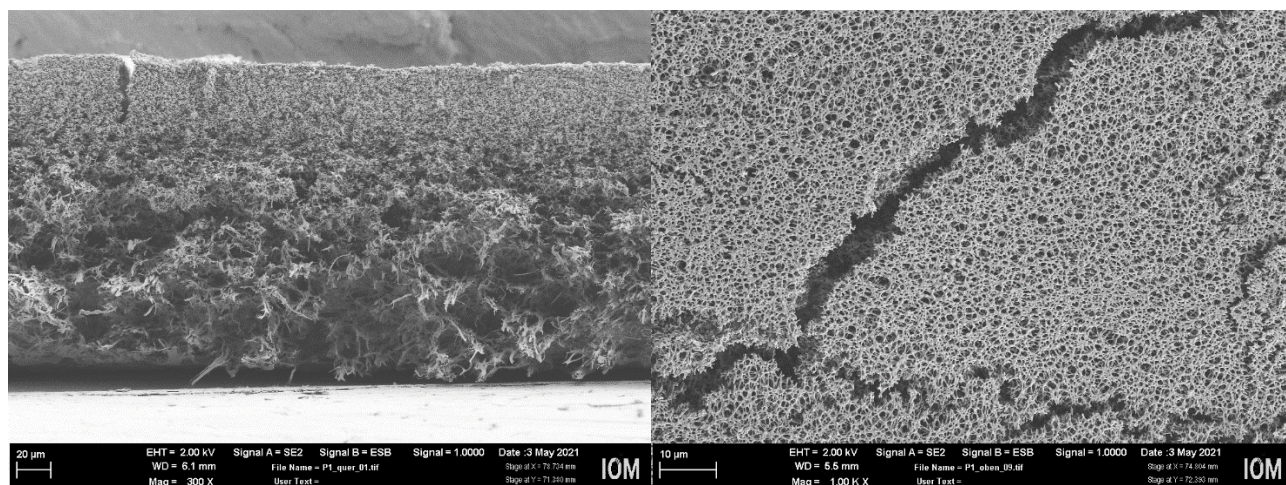
Figure 7-5 SEM Images of cross-section and surface of PES-250h aged.

Next, UV-Vis absorption spectroscopy was performed to understand the changes in the optical properties of the aged PMs.

7.4   UV-Vis absorbance spectra

The damage to the structure of membranes including changes in the polymer material or the bond between the photocatalyst and the membrane surface can cause photocatalyst loss. These structural changes can alter the light absorption by the membrane as the light is absorbed by the chemical bonds. TiO_2 nanoparticles mainly absorb in the UV light region (<410 nm) due to their large band gap. The variation in light absorption of membranes is presented in **Figure 7-6**.

Figure 7-6 The UV-Vis absorbance spectra of fresh and aged (A) PES and PES-TiO$_2$ (B) PVDF and PVDF-TiO$_2$ membranes at the different irradiation intervals in the photodegradation chamber (ageing conditions 365 nm + 405 nm, 222 mW/cm^2, aluminum holders). Reprinted (adapted) from (**Raota *et al.* 2023**).

Comparing the PES and PES-TiO$_2$ membranes, the PES membrane had a noticeable increase in light absorption while for the PES-TiO$_2$ membrane this change is less. Again, here it can be understood that coating with 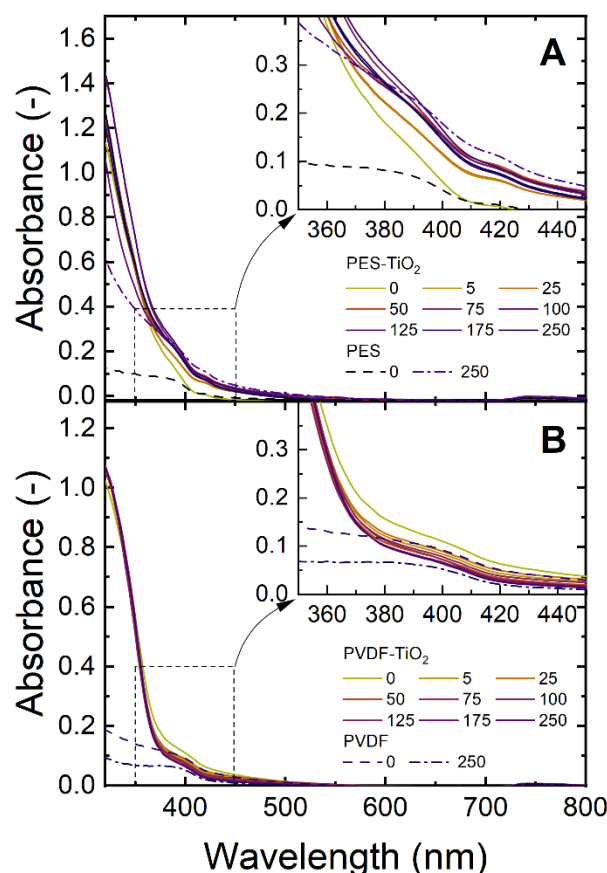TiO$_2$ could have a protective function for the membrane. The rise in PES membrane light absorption could be due to polymer chain scission resulting in (unsaturated) polyene structures (for example, quinone groups) (**Rabek 1995**). The molecular structure of membranes as well as the energy required for the bond scission are discussed in **Table 2-5**. It can be noticed in this table that the Cph –O– Cph bond of the PES membrane has low dissociation energy which makes it more prone to degradation. In contrast to PES, the PVDF membrane has experienced a small decrease in the membranes' light absorption which can be a result of the leaching of polyene-like additives. While PVDF-TiO$_2$ has remained mainly unchanged. However, PVDF and PVDF-TiO$_2$ had higher stability which was noticeable by light absorption spectroscopy.

7.5   ATR-FTIR analysis

Alteration in the chemical structure of membranes can be understood by ATR-FTIR (**Figure 7-7**). The chain scission in the structure of polymeric membranes PVDF (C–F, C–H bands) and PES (S=O, C–O–

C, C=C aromatic bands) can occur by the energy of UV-light photon according to **Table 2-5** through homolytic fission or by ROS attack and following hydrogen abstraction and/or chain scission **(Loginova *et al.* 1983, Giannetti 2005)**.
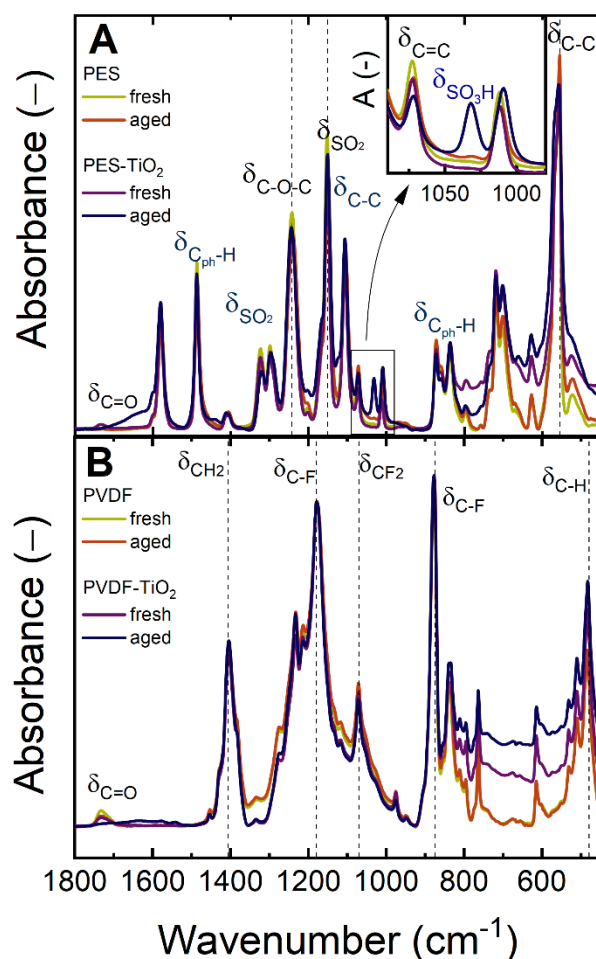
Figure 7-7 ATR-FTIR spectra of fresh and 250 h aged (A) PES-TiO$_2$, (B) PVDF-TiO$_2$ membranes in the region of 1800-450 cm^{-1}. For the PES-TiO$_2$ membrane (A), the magnification of the 980-1090 cm^{-1} shows the appearance of the SO$_3$H vibration band after 250h ageing. Reprinted (adapted) from **(Raota *et al.* 2023)**.

It can be noticed that in pristine PES and PVDF membranes, a band at 1734 cm^{-1} disappeared after 250 h ageing. It is worth mentioning that both PES and PVDF membranes are supplied as hydrophilic membranes, even though they are by nature hydrophobic. Therefore, the loss of the carbonyl group band (R-CO-O-R, 1734 cm^{-1}) under ageing conditions (light exposure and ROS attack) could be related to the instability of hydrophilic additives.

In the PES-TiO$_2$ membrane, a new weak band at 1031 cm^{-1} is formed related to the sulphonic group which can be due to chain scission in C$_{ph}$–SO$_2$ bond by $^{\bullet}$OH attack (**Table 2-5**). Elimination of the chains of hydrophilic additives could also result in loss of TiO$_2$ since the TiO$_2$ is coated on the surface and is

also attached to these chemical groups. To understand the changes to the surface and TiO_2 coating, next SEM imaging was done, and membranes were compared before and after ageing.

7.6   Changes of surface potential revealed *via* zeta potential studies

Zeta potential studies provide valuable information about the surface charge of materials (including PM). For that, changes in the zeta potential of pristine and photocatalyst-coated membranes before and after ageing were presented as a function of pH (**Figure 7-8**).

Figure 7-8 Zeta potential as a function of pH of fresh and 250 h aged membranes (A) PES, (B) PES-TiO_2, (C) PVDF, (D) PVDF-TiO_2, electrolyte solution KCl **10 mM**. The arrow shows the trend of the experiment when changing the pH from acidic to alkaline (number 1) and then continuation to acidic pH (number 2). Reprinted from (**Raota** *et al.* **2023**).

In general, the zeta potentials of membranes were slightly less negative after ageing which shows lower surface charge in other words. Since in FTIR spectra a weak sulfonic group appeared in the PES membrane, it was expected that this membrane shows higher negative values because the sulfonic group can contribute to the negative charge of the surface (**Tsehaye** *et al.* **2018**). However, the porous nature of membranes caused the electrokinetic leakage which could be due to the contribution of pores to the surface charge. This issue caused irreproducible results which were more significant when using 1 mM KCl as an electrolyte (**Figure 7-9**) and therefore made it difficult to make a conclusion on the effect of ageing on the surface charge.
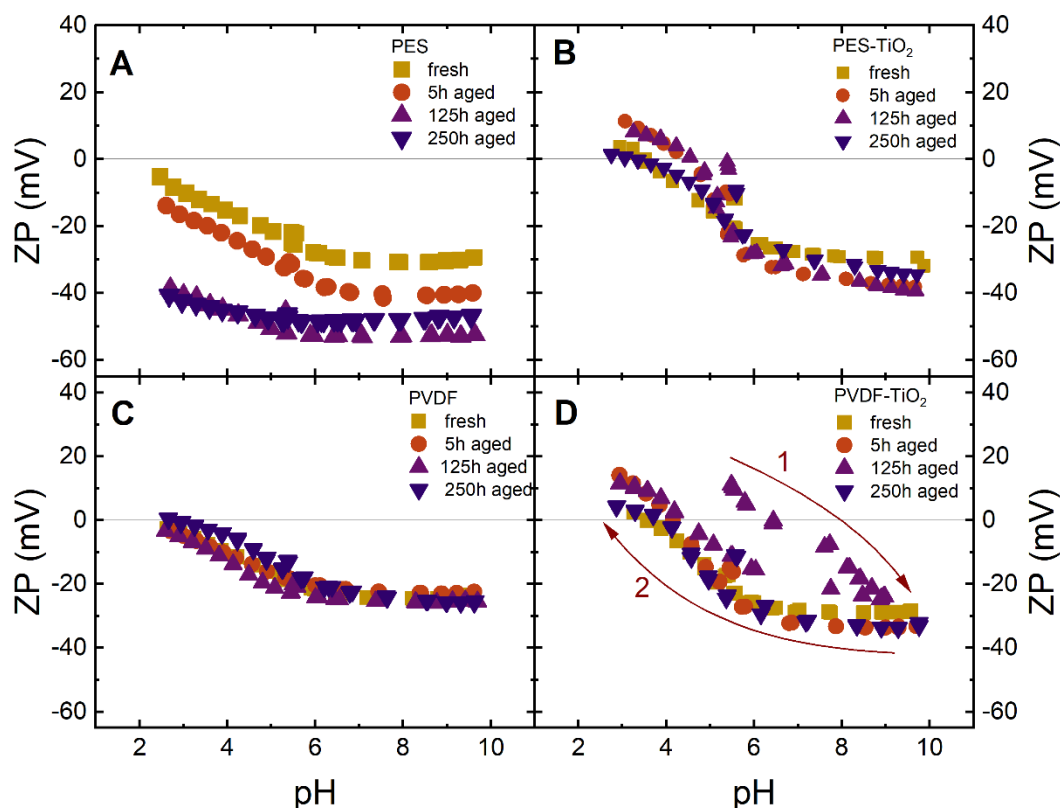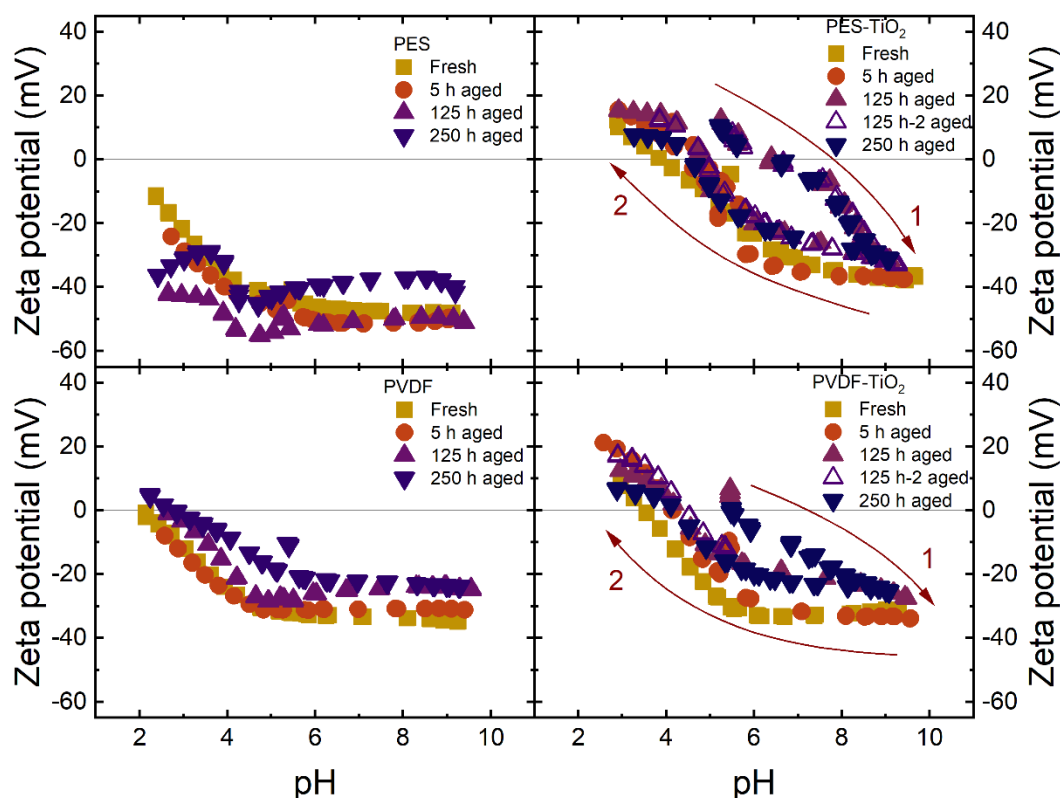
Figure 7-9 Zeta potential as a function of pH of fresh and 250 h aged membranes PES, PES-TiO₂, PVDF, PVDF-TiO₂, electrolyte solution KCl **1 mM**. The arrow shows the trend of the experiment when changing the pH from acidic to alkaline (number 1) and then continuation to acidic pH (number 2), reprinted from **(Raota *et al.* 2023)**.

The release of organic carbon released during the accelerated ageing of PMs was investigated using TOC analysis and presented in the next section.

7.7   Total organic carbon release in water by aged membrane

Surface deterioration of aged membranes was noticed in the previous sections. Since the membrane material is polymeric, the membrane degradation could release carbon-containing compounds into the water in the sample holder. These compounds can be detected by a total organic carbon analyser as shown in **Figure 7-10**.

Figure 7-10 Release of carbon from aged pristine and coated membranes shown by TOC measurement, blank samples are sample holders without membranes exposed to light in the UV-LED-light chamber, reprinted from (**Raota** *et al.* **2023**).

PVDF membrane was the only membrane showing good stability compared to others by releasing minimal carbon-containing compounds into the water. PES and PVDF-TiO$_2$ membranes had significant destruction of material by ageing time. Since all the mem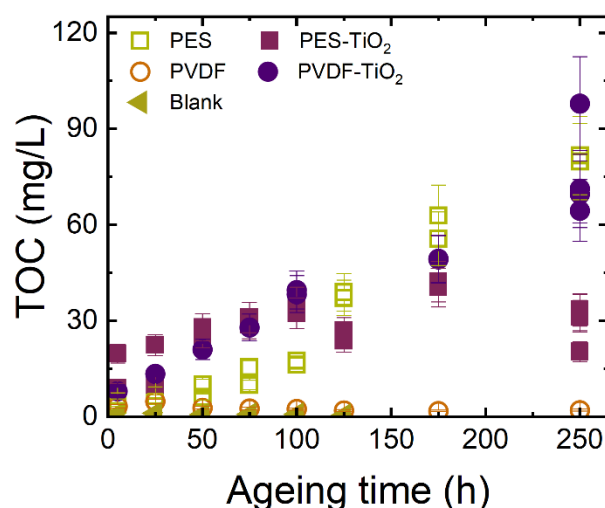branes had hydrophilic additives, the release of carbon could be related to those which in the case of PES were due to degradation by direct UV light exposure and no ROS involved. TOC level from PES-TiO$_2$ aged membrane levelled out after 175 h ageing. One idea could be that the coating of TiO$_2$ resulted in the absorption of light by TiO$_2$ instead of the polymeric material (protecting the PES membrane) and therefore the degradation of PES was higher compared to PES-TiO$_2$. In the case of PVDF-TiO$_2$, the release of TOC could be attributed to the ROS presence as it was noticed that the pristine PVDF membrane was not damaged. The significant release of TOC from TiO$_2$-coated membranes was in accordance with the hypothesis of degradation of hydrophilic additives (FTIR spectra **Figure 7-7**) and the observed damaged surface of membrane's by SEM images (**Figure 7-3**). In literature also, Labuto *et al.* (2022) have noticed the protective effect of a TiO2 coating on PES membranes comparing with the non-coated membrane after irradiation with a mercury lamp (**Labuto** *et al.* **2022**).

7.7.1 Catalyst loss detection by ICP-OES

Previous observations offered the possibility of photocatalyst loss during the ageing process. This release of Ti (from TiO$_2$) to the water during the ageing of the PMs can be quantified by ICP-OES analysis as presented in **Figure 7-11**.
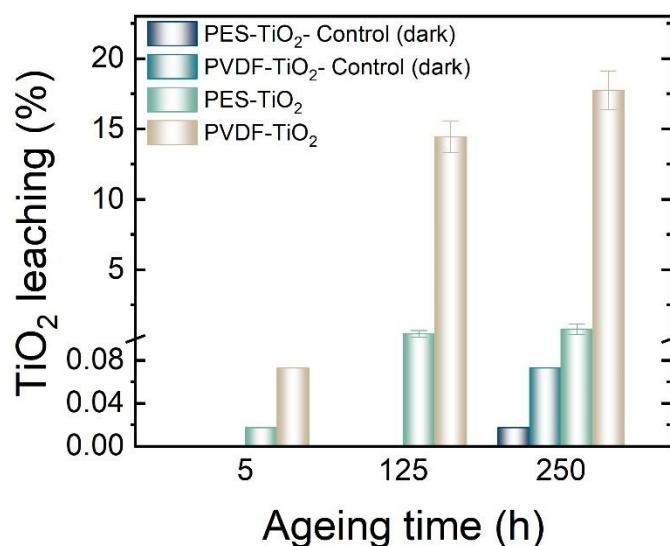
Figure 7-11 TiO$_2$ leaching of aged PES-TiO$_2$ and PVDF-TiO$_2$ membranes plus the dark (control) (TiO$_2$ coated membranes remained in the absence of light irradiation) analyzed by ICP-OES, the leaching is a percentage of the total mass of the TiO$_2$ loaded on the membrane. Reprinted from (**Raota *et al.* 2023**).

TiO$_2$ loading on the membrane was quantified using TGA analysis as explained in Chapter **4** to be 0.39±0.04 mg/cm^2 and 0.09±0.05 mg/cm^2 for PES-TiO$_2$ and PVDF-TiO$_2$ respectively. Then using the Ti content in the water and the initial TiO$_2$ concentration, the loss of TiO$_2$ from the initial value was measured (**Figure 7-11**). The dark samples only presented a very low amount of TiO$_2$ after 250 h of membranes staying in water under dark condition. Both membranes released TiO$_2$ into the water after irradiation, with PVDF-TiO$_2$ releasing a significantly higher amount. The rise in the loss of TiO$_2$ by ageing time was also obvious which could be due to the release of hydrophilic compounds to which the TiO$_2$ nanoparticles were attached. This observation confirmed the lack of TiO$_2$ which was also noticed in SEM images of aged PVDF-TiO$_2$. In another test, the surface of the membranes was analyzed before and after ageing by XPS analysis to investigate the changes in the Ti content on the surface mainly (**Table 7-2**). However, these measurements were not successful in showing a clear difference as all elements were altered by ageing and the test was not sensitive to give a clear answer.

Table 7-2 Surface composition of the TiO$_2$-coated membranes obtained by XPS analysis; data reprinted from (**Raota *et al.* 2023**).

	Atomic percentage (%)					
	F	S	Si	C	O	Ti
PES-TiO$_2$ fresh	---	3.0	0.8	57	32	6.4
PES-TiO$_2$-250 h aged	---	6.4	1.0	53	34	5.3
PVDF-TiO$_2$ fresh	15	---	0.9	52	25	7.1

PVDF-TiO$_2$ 250 h aged	17	---	1.1	44	28	9.2

Next, the capability of the PMs to degrade the pollutants after ageing was evaluated.

7.8   Photocatalytic performance of aged PMs

Assessment of the photocatalytic activity of the membrane could be one of the best ways to identify if the membrane is still functional. Therefore, MB degradation was evaluated at different ageing time intervals to see at which point photocatalytic membrane lost the ability to degrade the pollutants which can be seen in **Figure 7-12**.
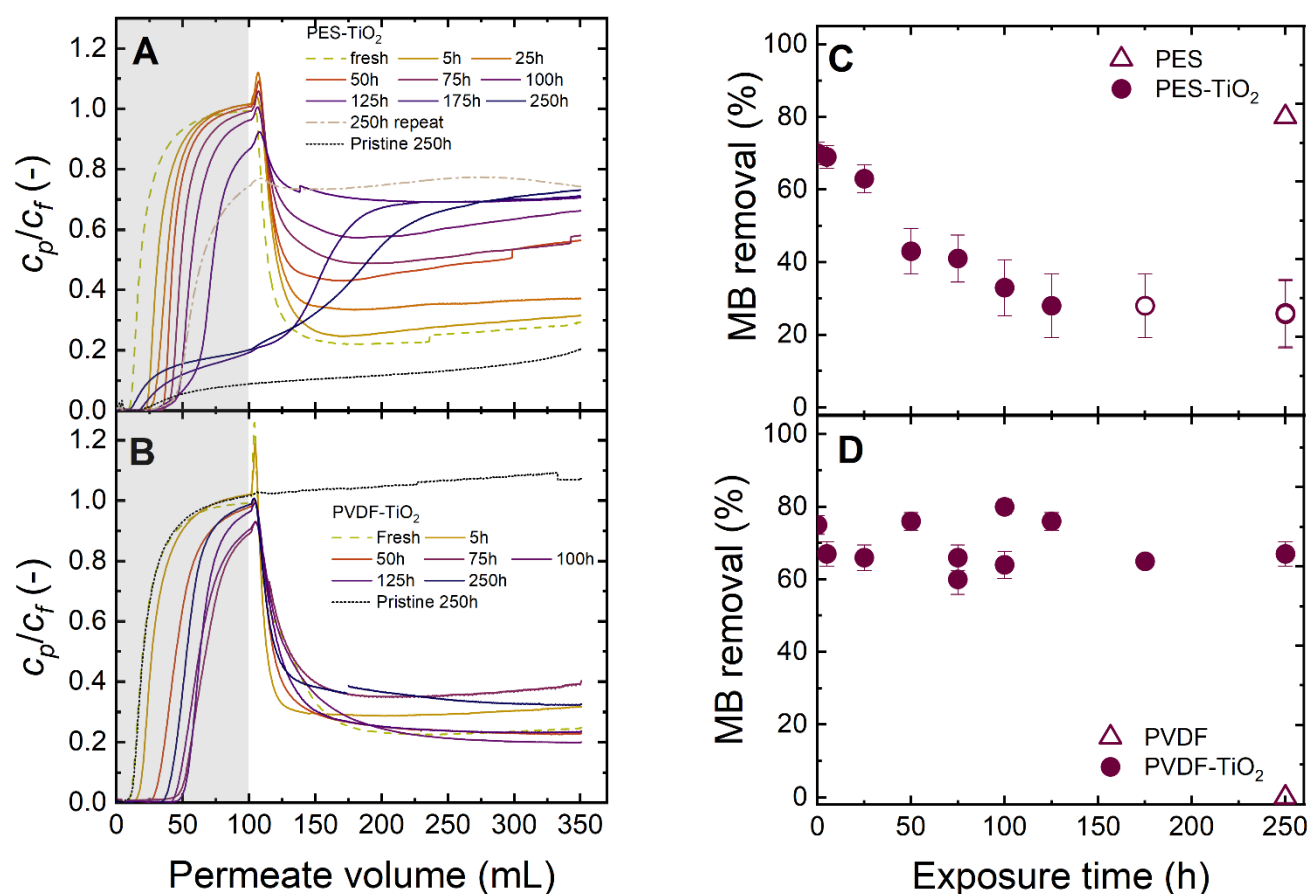
Figure 7-12 MB concentration ratio (c_p/c_f) at different ageing time intervals: (A) PES-TiO$_2$ and (B) PVDF-TiO$_2$ membranes, 300 L/m^{2}h, wavelength of photocatalytic degradation 365 nm and the intensity 11.8 mW/cm^2, c_{MB} 1 mg/L, background solution 1 mM NaHCO$_3$, 10 mM NaCl. The first 100 mL filtration shown in the grey area was performed in the dark phase without light exposure to reach adsorption-desorption equilibrium. The variation in MB removal and membrane absorbance at 365 nm as a function of ageing time is presented for (C) PES-TiO$_2$, and (D) PVDF-TiO$_2$. In the case of PES-TiO$_2$, the adsorption-desorption equilibrium was not reached for the last two points of ageing (175 h and 250h) and therefore are shown in hollow symbols (○). Reprinted (adapted) from (**Raota et al. 2023**).

While PES-TiO$_2$ had drastic changes over the ageing time, the alteration in MB degradation and adsorption with PVDF-TiO$_2$ was considerably less severe. With an increase in ageing time, the

concentration ratio (c_p/c_f) in the dark phase lowered in both membranes (more significant in PES and PES-TiO$_2$) which means that the adsorption of MB to the membrane surface enhanced significantly. This boost in adsorption increased with ageing, to the point that in PES-TiO$_2$ after 175 h, the concentration ratio only reached around 0.25. A repeat in photocatalytic degradation by 250 h aged membrane achieved a concentration ratio of almost 0.75. However, the final removal of two repeats of 250 h aged PES-TiO$_2$ membranes achieved the same result. It is worth mentioning that in these cases the adsorption/desorption equilibrium did not reach and therefore, a combination of adsorption and photocatalytic degradation is happening which cannot be distinguished. In contrast to the PVDF membrane which did not have any change compared to its fresh membrane, the PES membrane had the highest MB elimination by adsorption/degradation. **Figure 7-13** shows the membranes after MB experiments and the darker blue color of the membrane by ageing time is clearly noticeable.
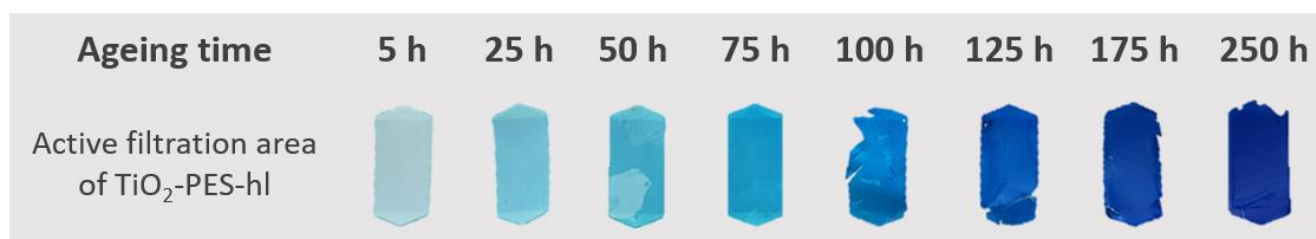
Figure 7-13 PES-TiO$_2$ membrane getting darker by ageing after MB degradation test showing higher adsorption of MB by aged membranes. Reprinted (adapted) from **(Raota *et al.* 2023)**.

These changes can be attributed to the alteration in surface roughness and hydrophilicity plus membrane morphology and pore structure. It is interesting to note that even though a loss of TiO$_2$ in PVDF-TiO$_2$ was observed in ICP-OES, it did not affect the MB removal. In the last step, the filtration capability of the PMs was tested by investigating the permeability of fresh and aged membranes.

7.9   Variation in water permeability of photocatalytic membranes after ageing

Destruction in the morphology and structure of membranes after ageing can alter the water permeability of the membranes. This effect is shown in **Figure 7-14**.

Figure 7-14 water permeability of aged pristine and coated membranes. The time of zero indicates the fresh membranes. Reprinted from **(Raota *et al.* 2023)**.

It was noticed that the aged membrane had quite similar behavior to fresh membranes considering the error bar of experiments. However, a slight increase in the permeability PMs, mainly in PES-TiO$_2$, was observed after 175 h ageing. This can be due to structural damage to the membrane which can cause tiny cracks and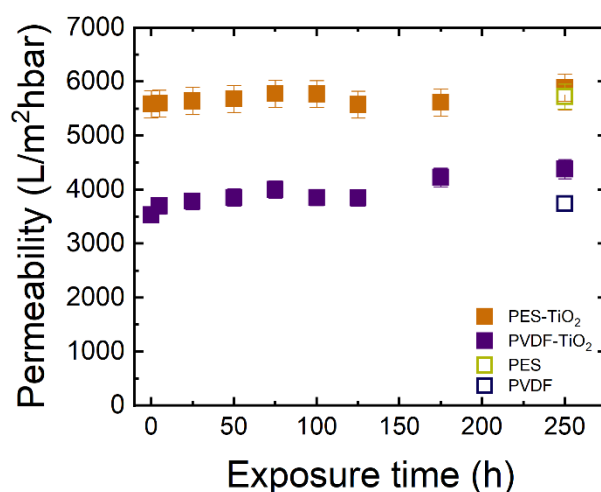 fractures. This observation contradicted the SEM images of aged PES-TiO$_2$ which showed a melted surface. Hence, it can be understood that the collapse in structure was only on the surface and did not affect the pore structure noticeably. In the previous sections, it was concluded that PVDF-TiO$_2$ has lost some of its hydrophilic additives, while it was not affecting the permeability of the membranes. It can be understood that the permeability test in microfiltration membranes is considerably high and is not easily affected by ageing.

7.10 References

Chin, J., T. Nguyen, E. Byrd and J. Martin (2005). "Validation of the reciprocity law for coating photodegradation." JCT research **2**: 499-508.

Diepens, M. and P. Gijsman (2009). "Influence of light intensity on the photodegradation of bisphenol A polycarbonate." Polymer Degradation and Stability 94: 34-38.

Fairbrother, A., H.-C. Hsueh, J. H. Kim, D. Jacobs, L. Perry, D. Goodwin, C. White, S. Watson and L.-P. Sung (2019). "Temperature and light intensity effects on photodegradation of high-density polyethylene." Polymer Degradation and Stability **165**: 153-160.

Ghaebi Mehmandoust, S., R. Alizadeh and A. A. Babaluo (2014). "Kinetic study of the poly (vinyl chloride)/titanium dioxide nanocomposites photodegradation under accelerated ultraviolet and visible light exposure." Polymers for advanced technologies 25: 799-808.

Giannetti, E. (2005). "Thermal stability and bond dissociation energy of fluorinated polymers: A critical evaluation." Journal of Fluorine Chemistry **126**: 623-630.

Labuto, G., S. Sanches, J. G. Crespo, V. J. Pereira and R. M. Huertas (2021). "Stability of polymeric membranes to UV exposure before and after coating with TiO$_2$ nanoparticles." Polymers 14:124.

Loginova, N. N., L. Y. Madorskaya and N. K. Podlesskaya (1983). "Relations between the thermal stability of partially fluorinated polymers and their structure." Polymer Science U.S.S.R. **25**: 2995-3000.

Martin, J. W., J. W. Chin and T. Nguyen (2003). "Reciprocity law experiments in polymeric photodegradation: a critical review." Progress in Organic Coatings **47**: 292-311.

Rabek, J. F. (1995). Polymer Photodegradation Mechanisms and experimental methods, Springer Science+Business Media Dordrecht.

Raota, C. S., S. Lotfi, R. Lyubimenko, B. S. Richards and A. I. Schäfer (2023). "Accelerated ageing method for the determination of photostability of polymer-based photocatalytic membranes." Journal of Membrane Science: 121944.

Schwarzschild, K. (1900). "On the deviations from the law of reciprocity for bromide of silver gelatine." Astrophysical Journal 11: 89.

Therias, S., G. Rapp, C. Masson and J.-L. Gardette (2021). "Limits of UV-light acceleration on the photooxidation of low-density polyethylene." Polymer Degradation and Stability 183: 109443.

Tsehaye, M. T., S. Velizarov and B. Van der Bruggen (2018). "Stability of polyethersulfone membranes to oxidative agents: A review." Polymer Degradation and Stability **157**: 15-33.

Chapter Eight

8   Optimization of photocatalytic membranes for higher removal

In previous chapters, PMs were evaluated from different aspects. The lowest concentration of E2 on the permeate side was above 10 ng/L using both PES-TiO$_2$ and PVDF-TiO$_2$ (Chapter **6**). However, following the requirements of WHO, the concentration of E2 needed to be reduced to below 1 ng/L **(European Union 2020)**. Therefore, it was necessary to understand what the possible ways are to optimize and maximize the degradation of E2 in the water. For this purpose, first, the TiO$_2$ coating on the PVDF-TiO$_2$ membrane was varied to see if the amount of photocatalyst is limiting the reaction, and then the effort was made to improve the uptake of TiO$_2$ by the membrane. However, the limit of detection and limit of quantification of the analytical device (UHPLC), 1.5-2.4 ng/L and 3.4-4.3 ng/L respectively **(Lyubimenko *et al.* 2020)**, should be taken into consideration which makes the maximum potential of PMs for photocatalytic degradation of MPs unclear.

8.1   TiO$_2$ loading on PMs

To vary the TiO$_2$ content loaded on the membrane, after the synthesis of TiO$_2$ Nanoparticle (NP), the precursor solution was diluted multiple times to give a different concentration of NP and then the membrane was dipped into the solution with different concentrations. The procedure of TiO$_2$ coating on the membranes was previously described in Chapter **3**, section **3.4**. The membrane with 100% TiO$_2$ is prepared by dipping the PVDF membrane in the NP solution synthesized from a precursor solution containing 4 mL TTIP, and 80 mL 0.1 M HCl. As an example, the 25% TiO$_2$ on the membrane means diluting 50 mL of the 100% suspension into 150 mL MilliQ and then dip-coating the membrane into the solution. Then the prepared membrane with different concentrations was analyzed using XPS and the correlation can be seen in **Figure 8-1A**. These membranes then were subjected to photocatalytic degradation of E2 to understand the effect of TiO$_2$ content on the rate of degradation **Figure 8-1B**.
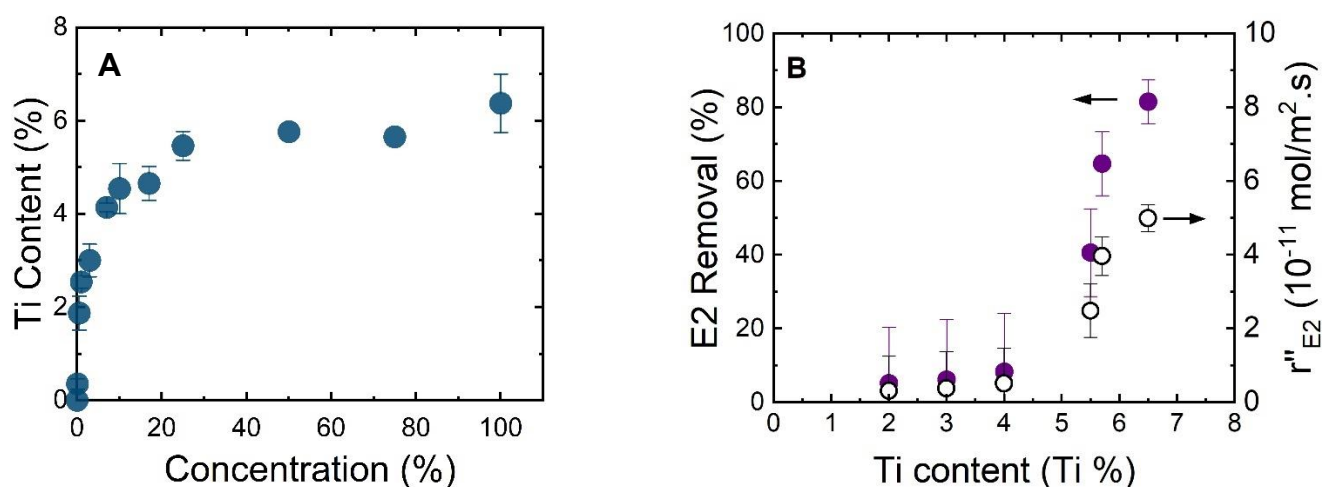
Figure 8-1[12] (A) Ti percentage obtained by XPS vs the TiO$_2$ NPs dilution in the synthesis solution. 100% TiO$_2$ NP solution prepared from precursor solution containing 4 mL TTIP, 80 mL 0.1 M HCl. (B) Photocatalytic degradation and r" of E2 using PVDF-TiO$_2$ membrane at different loading of TiO$_2$ (Ti content obtained by XPS), conditions: 100 mL dark phase, 600 mL filtration under light 365 nm, 10 mW/cm^2, 600 L/m^{2}h, 23$\pm$0.2 $^\circ$C, 100 ng/L E2, 1 mM NaHCO$_3$, 10 mM NaCl, 27.2 mg/L EtOH and 79.2 mg/L MeOH. Reprinted from (**Liu** *et al.* **2023**).

The amount of Ti on the membrane levelled out after almost 25% NP concentration, which means it was the maximum that the membrane could uptake on the surface. However, there was a noticeable increase in the E2 removal from 5.5% Ti content and 6.4% from almost 40$\pm$12% to 81$\pm$6%. With increasing the TiO$_2$ loading on the membrane, the ROS generation would increase correspondingly (**Herrmann 2010**). It is expected that by increasing the TiO$_2$ enough, the removal levels out at one point when the surface is saturated with TiO$_2$, and the ROS generation is not the limiting parameter. The higher TiO$_2$ deposition can also cause agglomeration and reduce the efficiency of the coated TiO$_2$ (**Kumari** *et al.* **2020**). However, using XPS analysis, the surface of the membranes had nearly maximum loading after 25% concentration considering the error of analysis by changing slowly from 5.5$\pm$0.3% to 6.4$\pm$0.6%.

One explanation for the inconsistency between the two figures, **Figure 8-1A&B**, is that the XPS is only a surface analysis and can investigate a few nanometers depth from the surface (**Mudalige** *et al.* **2019**). While increasing the concentration of TiO$_2$, it can be assumed that the surface of the membrane was saturated with TiO$_2$ at 5.5$\pm$0.3% (25%) and increasing it further to 100% helped the TiO$_2$ to penetrate into the pores of the membrane. The complete surface coverage was also noticed *via* SEM images above 5% Ti content (25% dilution) (**Figure 8-2**).

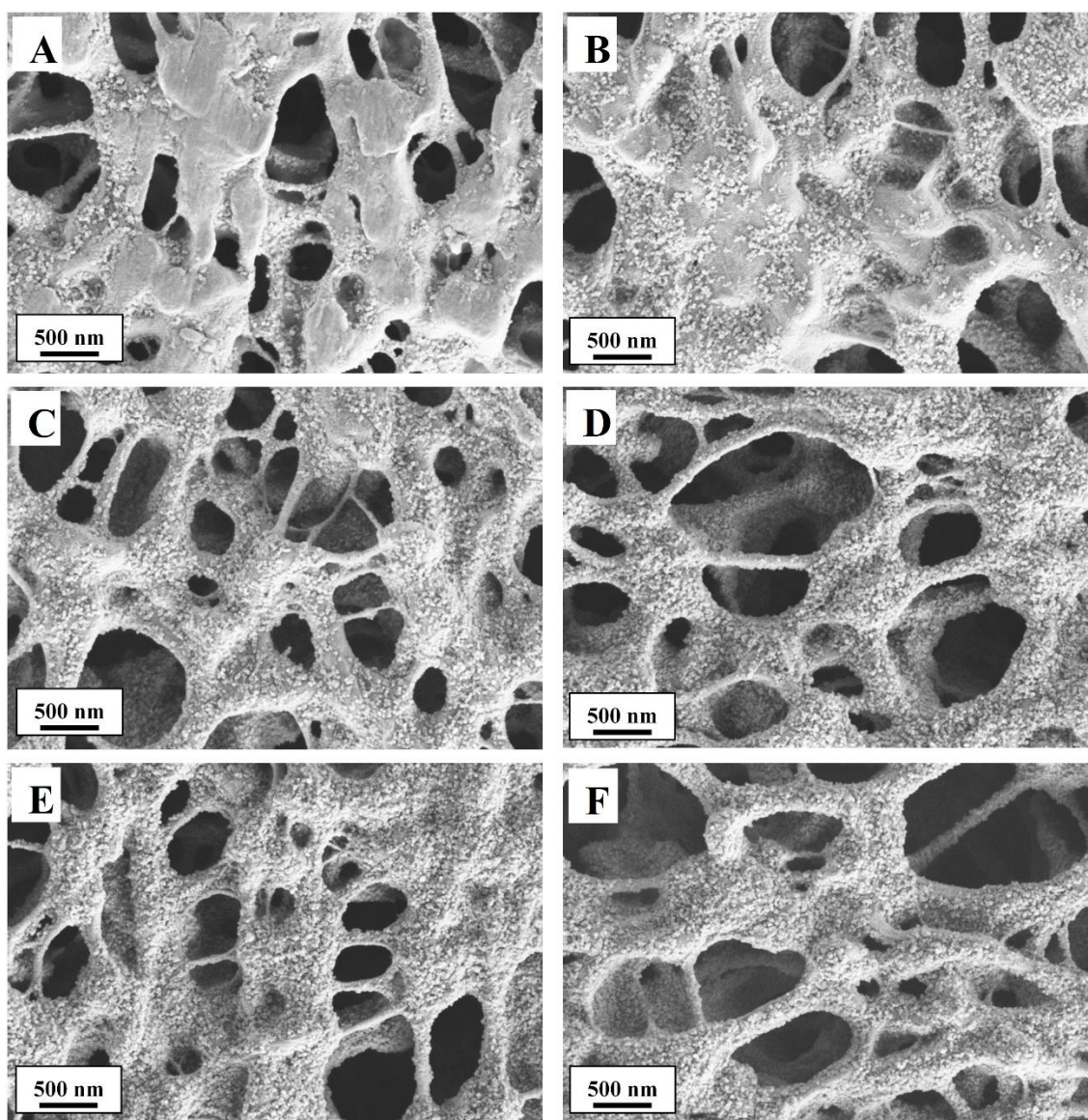[12] Data was provided by IOM institute.

Figure 8-2 SEM images of top view of the PVDF-TiO$_2$ at different loading percentage showing the nanoparticle coverage, (A) 0.5% (1.9% Ti), (B) 3% (3% Ti), (C)7% (4.1% Ti), (D) 25% (5.5% Ti), (E) 75% (5.7% Ti) and (F) 100% (6.5% Ti). Reprinted from (**Liu** *et al.* **2023**).

All in all, it was understood that the uptake of TiO$_2$ using the preparation method was limited, and an effort was made to modify the surface of the membrane to increase the TiO$_2$ uptake.

8.2   Improve in TiO$_2$ coating by variation in membrane substrate

The loading of TiO$_2$ can be increased by adding carboxylic groups to the surface by modification prior to coating (**Schulze** *et al.* **2013**). While the standard PVDF-TiO$_2$ membrane was only sonicated during coating to disperse the TiO$_2$ NP homogeneously, two methods were taken to modify the PVDF membranes. First by dipping into either water or 0.01% PAA solution, then being irradiated by E-beam and finally the same coating method as the standard photocatalytic membrane were modified. The

procedure was described in more detail in Chapter **3** section **3.3**. These two membranes were named PVDF-H$_2$O-TiO$_2$ and PVDF-PAA-TiO$_2$. Various membranes used for optimization are presented in **Table 8-1**.

Another approach to improve the TiO$_2$ loading was to change the membrane pore size. A membrane substrate from another supplier (GVS) was chosen with a bigger pore size (0.45 μm) **(GVS Filter Technology 2021)**. It was expected that TiO$_2$ NP could penetrate deeper into membrane pore size during the deposition process. Two other membranes with smaller pore sizes, 0.1 μm, from different suppliers, Merck Millipore and Novamem, were also chosen to be coated by TiO$_2$. Both were hydrophobic when received from the supplier and were modified with PAA solution and electron beam to help the hydrophilicity and uptake of TiO$_2$. The idea here was that by using a smaller membrane pore size, the probability of collision between the MP and ROS would increase and this can boost the removal. It is worth mentioning that the 0.1 μm membrane from Novamem (PVDF-VVHP-PAA-TiO$_2$-0.1μm) had a thinner thickness (50 μm) compared to others (thicker than 125 μm) as mentioned in **Table 3-2**. This difference in thickness altered the residence time of the pollutant in the membrane as a higher residence time results in higher degradation (**Section 6.2.3**).

Table 8-1 Various membranes used to optimize the photocatalytic degradation capability of the photocatalytic membrane s, errors are derived from measurements on different pieces of membranes at least three times. XPS data reprinted from (**Liu *et al.* 2023**).

Name	Supplier	Pore size, μm	Hydrophilicity	Surface Ti content (XPS), %	Ti content (TGA), mg/cm^2
PVDF-TiO$_2$ (standard)				5.2±0.2	0.09±0.05
PVDF-H$_2$O-TiO$_2$	Merck Millipore	0.22		6.0±1.2	0.35±0.05
PVDF-PAA-TiO$_2$			Hydrophilic	5.8±0.5	0.37±0.18
PVDF(GVS)-TiO$_2$-0.45 μm	GVS	0.45		8.5±0.6	0.25±0.02
PVDF-PAA-TiO$_2$-0.1μm	Merck Millipore	0.1		4.9	---
PVDF-VVHP-PAA-TiO$_2$-0.1μm	Novamem	0.1	Hydrophobic	7.15	---
PES-TiO$_2$	Millipore	0.22	Hydrophilic	6.6±1.2	0.39±0.04

It is interesting to compare the data obtained from TGA and XPS analysis. Comparing membranes *via* XPS, the highest TiO$_2$ coating is on PVDF(GVS)-TiO$_2$-0.45 which basically showed the coating on the surface and very few nanometers depth from the surface. However, when comparing the TGA results, the highest coating was on PVDF-H$_2$O-TiO$_2$ and PVDF-PAA-TiO$_2$ which means that in these two

membranes, TiO_2 penetrated better into the pores of the membranes. The FTIR spectra of the modified membranes and different loading on the membranes are demonstrated in **Figure 8-3**. FTIR analysis reveals information on the bonds formation and helps comparing different synthesis approaches.
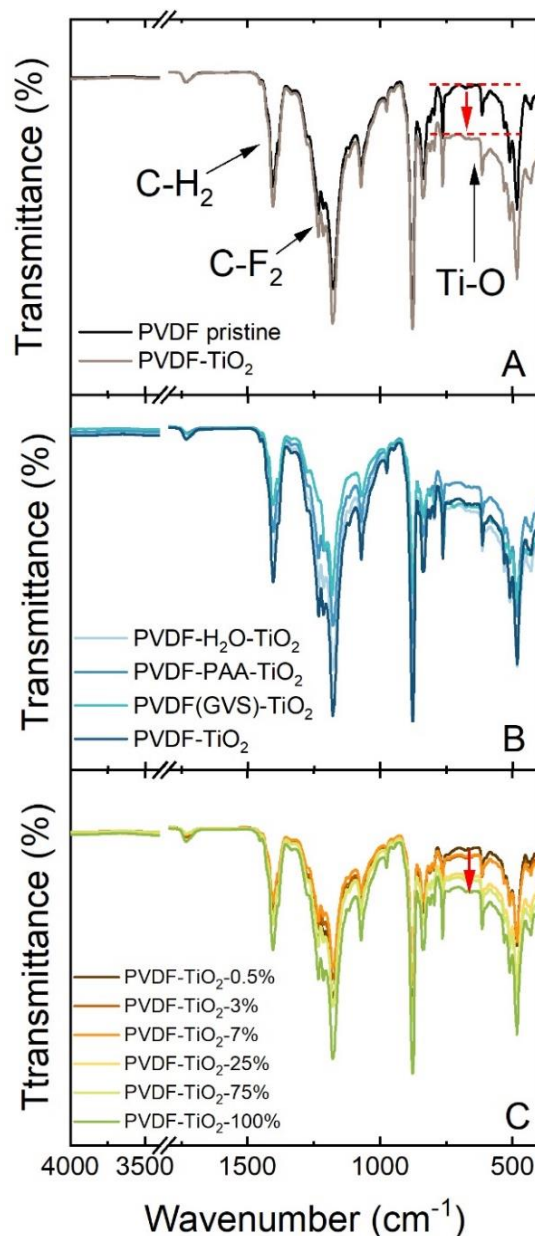
Figure 8-3[13] FTIR spectrum of (A) PVDF pristine and PVDF-TiO_2, (B) PVDF-PAA-TiO_2, PVDF-H_2O-TiO_2, PVDF(GVS)-TiO_2, and (C) PVDF-TiO_2 membrane with different loading of TiO_2, reprinted from (**Liu *et al.* 2023**). The FTIR comparison of PVDF membrane with the coated membrane (PVDF-TiO_2) was assessed in detail in Chapter **4**, section **4.1.1**, **Figure 4-2**. Similarly, **Figure 8-3B&C** also demonstrated the Ti-O transmittance and confirmed the addition of TiO_2 nanoparticles on different membranes and different

---

[13] Measurements were carried out by Siqi Liu.

loading of TiO_2 nanoparticles. The weakest data was related to 0.5% TiO_2 nanoparticles which was consistent with the SEM images.

The light absorption by different membranes is displayed in **Figure 8-4**, including the PVDF membrane, PVDF-TiO_2 with different substrates, and different coating strategies, and range of 0.5-100% loading of TiO_2 on the membranes. In this figure, the wavelength of 365 nm is emphasized as the chosen wavelength for photocatalyst activation, since its energy (3.4 eV) is greater than the bandgap energy of TiO_2 (3.1 eV), allowing for the excitation of electrons from the valence band to the conduction band. This results in the creation of more photoactive carriers, which can lead to a higher efficiency in photocatalytic degradation as higher absorbance generates more of these carriers.
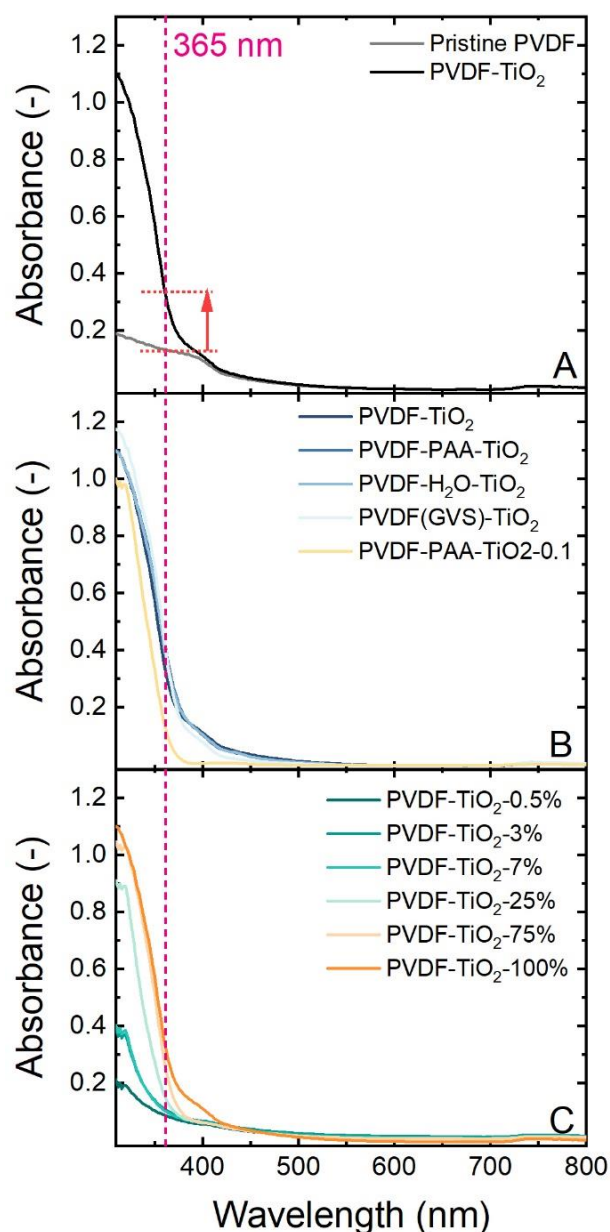
Figure 8-4[14] Light absorption of (A) PVDF and PVDF-TiO₂, (B) PVDF-PAA-TiO₂, PVDF-H₂O-TiO₂, PVDF(GVS)-TiO₂, PVDF-PAA-TiO₂-0.1µm, and (C) PVDF-TiO₂ membrane with different loading of TiO₂, reprinted from (**Liu** *et al.* **2023**).

A higher light absorption was noticed in all coating methodologies at wavelength of 365 nm compared with the pristine membrane. Increasing the loading of TiO_2 from 0.5 to 100% TiO_2 suspension also improved the light absorption. Therefore, the increase of light absorption could be related to the TiO_2 active sites on the membranes.

---

[14] Measurements were carried out by Siqi Liu.

In order to examine the surface charge of both PVDF and PVDF-TiO$_2$ at different pH levels, measurements of zeta-potential were conducted using a 0.001 M KCl electrolyte solution with a pH range of 2 to 10 **Figure 8-5**.
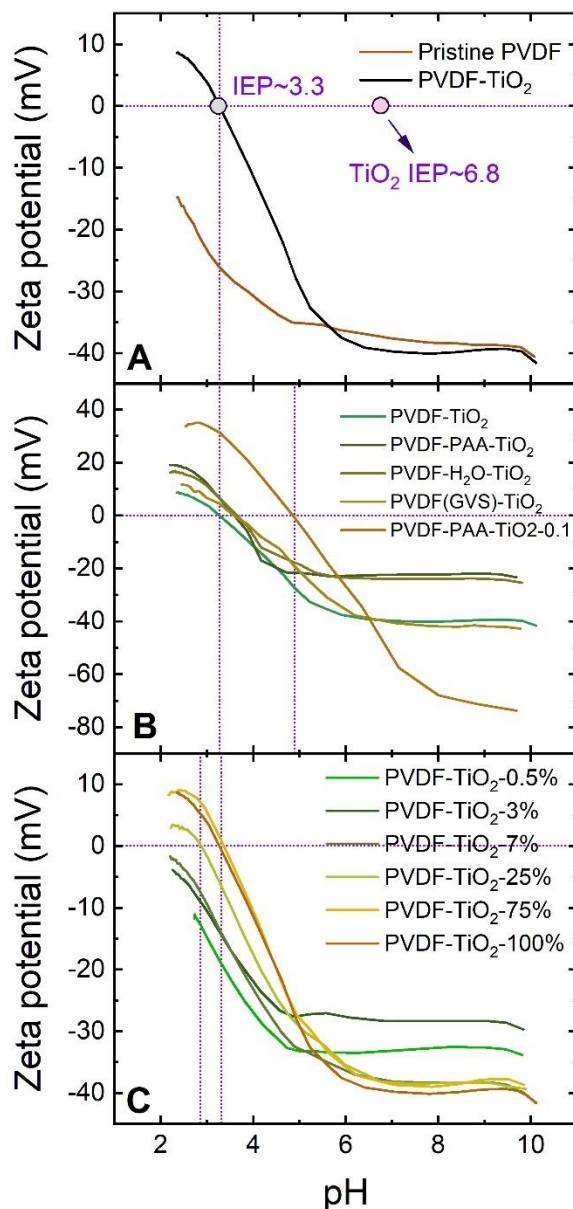
Figure 8-5[15] Zeta potential measurement of modified membranes and different loading as function of pH. 1 mM KCl electrolyte solution, pH adjustment was done using 50 mM HCl and 50 mM NaOH, reprinted from (**Liu _et al._ 2023**).

The surface charge of the PVDF membrane was negative across the pH range of 2 to 10. The TiO$_2$ coated membranes (PVDF-TiO$_2$, PVDF-PAA-TiO$_2$, PVDF-H2O-TiO$_2$, and PVDF(GVS)-TiO$_2$) had an isoelectric point (IEP) within the range of pH 3.3 to 3.6. PVDF-PAA-TiO$_2$-0.1μm membrane displayed an IEP at pH 4.8. The higher surface charge in coated membranes could be due to the TiO$_2$ nanoparticles

---

[15] Measurements were carried out by Siqi Liu.

coverage which was positively charged at pH levels below 6.8. While membranes with lower TiO_2 coverage (below 7% TiO_2 suspension) showed negative charge throughout the tested pH range, PVDF-TiO_2-25% and PVDF-TiO_2-75% exhibited an IEP at pH 2.8 and 3.3, respectively, possibly because of the complete surface coverage with TiO_2 nanoparticles.

The SEM images of lower pore size membranes (0.1 µm) before and after coating with TiO_2 are presented in **Figure 8-6** which shows the full coverage of membranes with TiO_2.
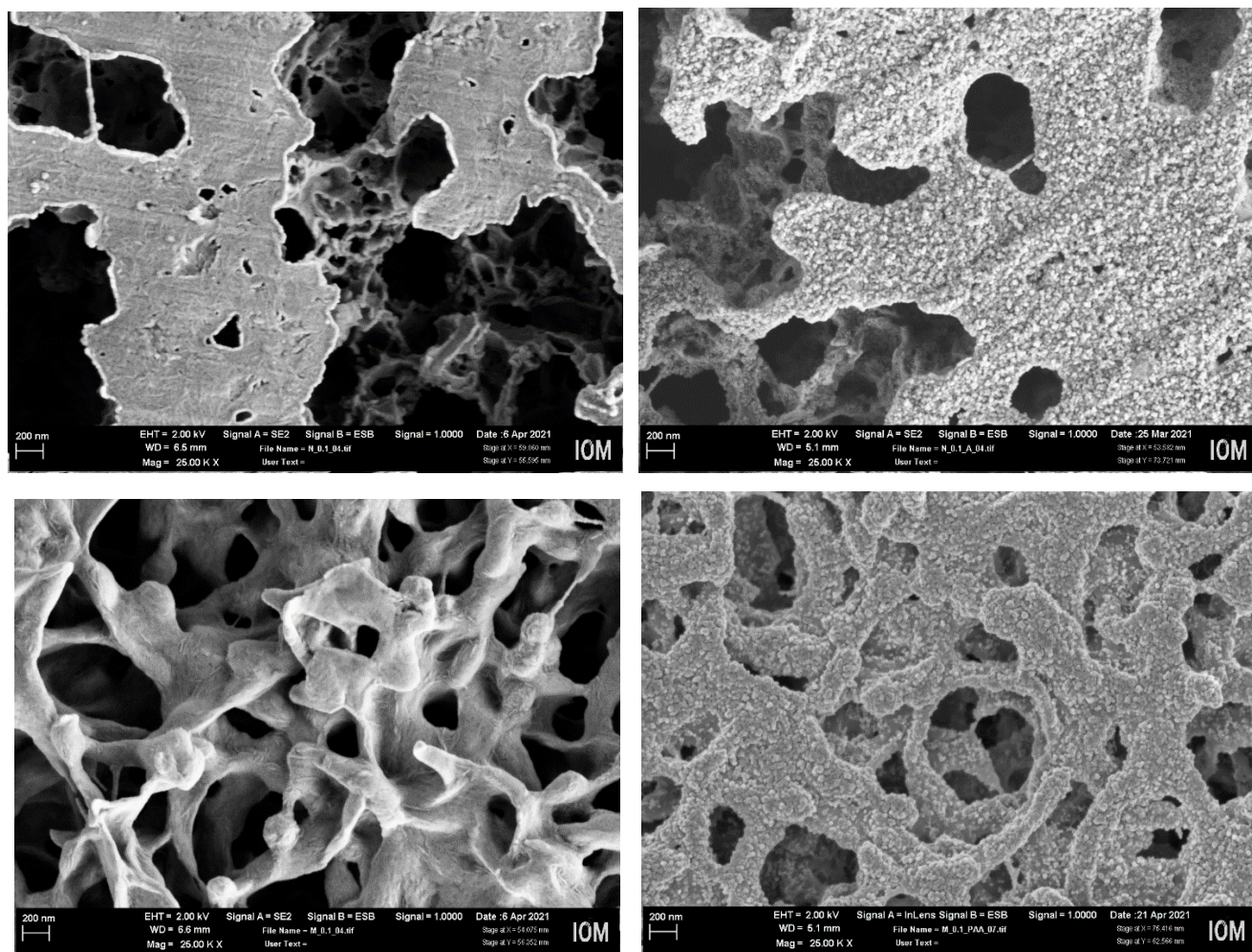
Figure 8-6 SEM images of pristine and coated 100 nm pore size membranes PVDF-VVHP-PAA-TiO_2-0.1µm and PVDF-PAA-TiO_2-0.1µm. Reprinted from (**Liu *et al.* 2023**).

To compare these three PVDF membranes with the highest TiO_2 content better *via* TGA measurement and with the standard PVDF-TiO_2 membrane, they were compared by SEM-EDX measurement to be able to the distribution of TiO_2 over the thickness of the membranes (**Figure 8-7**).
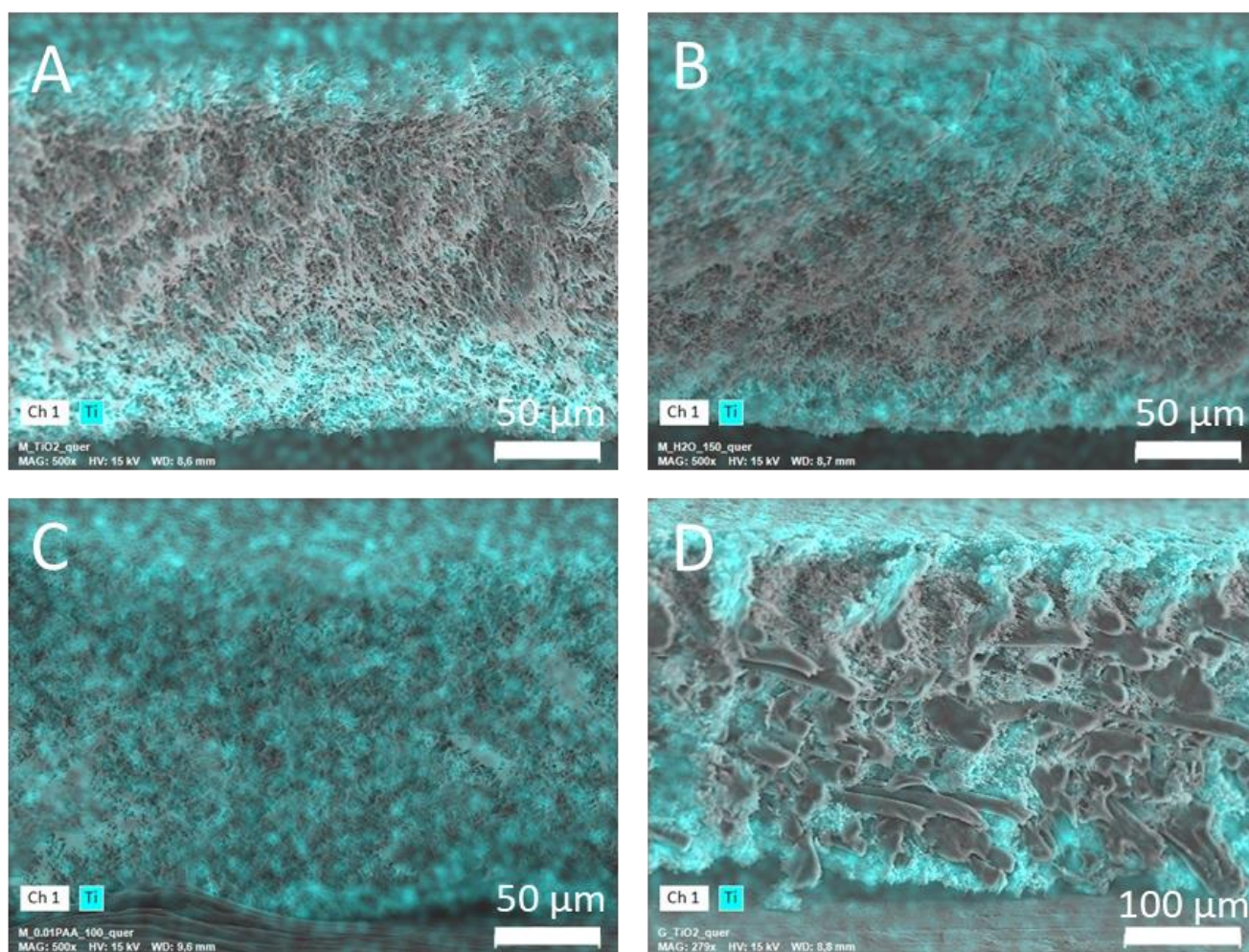
Figure 8-7 SEM-EDX of the cross-section of (A) PVDF-TiO$_2$, (B) PVDF-H$_2$O-TiO$_2$, (C) PVDF-PAA-TiO$_2$, and (D) PVDF(GVS)-TiO$_2$. Reprinted from **(Liu *et al.* 2023)**.

It can be noticed in **Figure 8-7** that the best TiO$_2$ distribution was in PVDF-PAA-TiO$_2$. Since this membrane was modified using PAA solution and E-bean irradiation, it can be assumed that the great number of carboxylic groups added to the membrane enhanced the attachment of the TiO$_2$. The addition of carboxylic groups to the membrane enhances the hydrophilicity of the membrane **(Temmel *et al.* 2006)**. These new functional groups improve the attachment of TiO$_2$ NPs to the surface through the connection between Ti^{+4} and the oxygen atoms of carboxylate groups or by hydrogen bonds between the carbonyl group and the hydroxyl group on the surface of TiO$_2$ **(You *et al.* 2012, Leong *et al.* 2014)**. This modification was explained in detail in section 2.6.3.

8.3   Photocatalysis comparison

To understand the impact of these modifications on the capability of the membranes to degrade the E2, all membranes were subjected to photocatalytic degradation experiments at the same condition as demonstrated in **Figure 8-8**. Here, all experiments were performed at the same flux (L/m^{2}h), however,

this means that the hydraulic residence time of E2 molecules inside the membrane was not the same because of different membrane thickness.
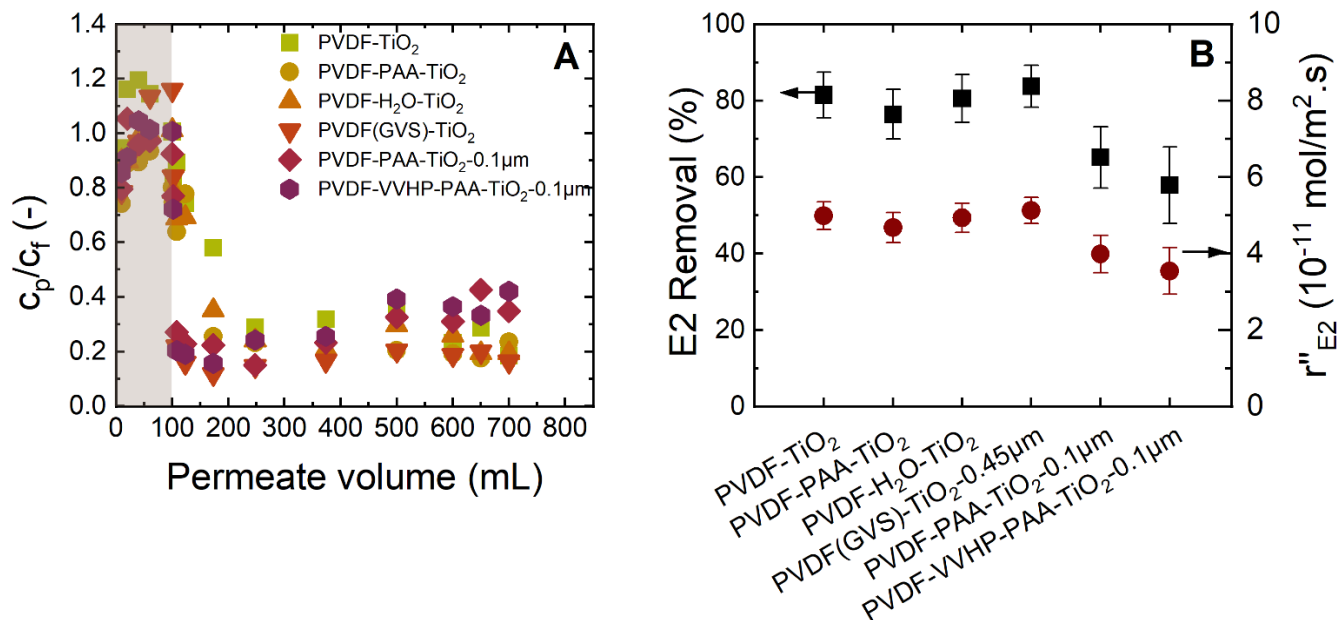

Figure 8-8[16] (A) Concentration ratio over the permeate volume and (B) the removal and r" of E2 using different modified membranes and membrane pore size. Conditions: 100 mL dark phase, 600 mL filtration under light 365 nm, 10 mW/cm^2, 600 L/m^{2}h, pH 8.2±0.2, 100 ng/L E2, 1 mM NaHCO$_3$, 10 mM NaCl, 27.2 mg/L EtOH and 79.2 mg/L MeOH. Part of the data is reprinted from (**Liu et al. 2023**).

It was surprising to find out that modified membranes with higher TiO$_2$ loading as well as GVS membranes with a bigger pore size degrade the E2 almost similarly. PVDF(GVS)-TiO$_2$-0.45μm membrane immediately removed E2 by 80% when the light was turned on (**Figure 8-8A**) and remained almost stable. While the other membranes had a slower removal of E2 at the beginning of the light phase. Although both TiO$_2$ loading and distribution of E2 were improved, one reason for the similar photocatalytic degradation with standard PVDF-TiO$_2$ was limited light penetration through the membrane pores were limited. Light attenuation through the membrane thickness (after a few micrometers from the surface) caused the reduced ROS generation within the pores of the membrane and prevented the rise in E2 degradation.

Reducing the membrane pore size to 0.1 μm resulted in lower E2 removal. Reducing the pore size would improve the mass transfer by shortening the diffusion length of the E2 molecule. Therefore, since ROSs in general have a very short lifetime and diffusion length (**Carretero-Genevrier et al. 2012, Yamada and Kanemitsu 2012**), the collision between ROS and E2 could be enhanced. In the case of PVDF-VVHP-PAA-TiO$_2$-0.1μm the membrane thickness was 50 μm which was less than half of others like

---

[16] Experiments were carried out by Eleonore Veron under the supervision of Shabnam Lotfi.

standard PVDF-TiO$_2$ and this lower hydraulic residence time could have a more dominant impact on the E2 removal. However, both PVDF-TiO$_2$ (pore size 0.22 μm) and PVDF-PAA-TiO$_2$-0.1μm (pore size 0.1 μm) had a similar thickness of 125 μm. Hence, it can be assumed that the mass transfer withing the pores was sufficient and not limiting the photocatalytic degradation.

8.4   Optimized experimental condition

In the last step, the condition of the experiment was optimized to achieve the highest possible degradation. In the previous section, higher TiO$_2$ loading or better distribution did not result in getting close to the goal of 1 ng/L recommended by WHO. **Figure 8-9** presents the result of an experiment with high light intensity and low flux (highest hydraulic residence time in the membrane).
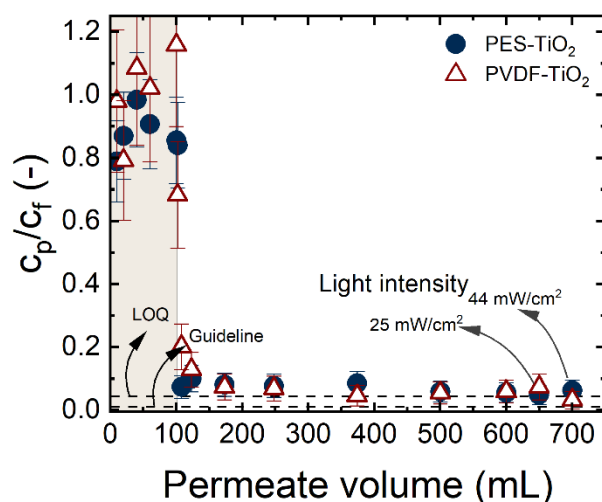

Figure 8-9[17] Concentration ratio of E2 over the permeate volume using PVDF-TiO$_2$ and PES-TiO$_2$. Conditions: 100 mL dark phase, 600 mL filtration under light 365 nm, 25 and 44 mW/cm^2 for PVDF-TiO$_2$ and PES-TiO$_2$ respectively, 60 L/m^{2}h, pH 8.2±0.2, 100 ng/L E2, 1 mM NaHCO$_3$, 10 mM NaCl, 79.2 mg/L MeOH, EtOH was 27.2 mg/L for PES-TiO$_2$ and 26.9 mg/L for PVDF-TiO$_2$ experiments. PES-TiO$_2$ data reprinted from (**Lotfi *et al.* 2022**) and PVDF-TiO$_2$ data reprinted from (**Liu *et al.* 2023**).

As can be seen in **Table 8-1**, the TiO$_2$ loading on PES-TiO$_2$ was higher than PVDF-TiO$_2$. However, considering the results obtained in Chapter 6 which showed lower E2 removal with PES-TiO$_2$, it was decided to use higher light intensity for this membrane to ensure maximum E2 removal. Using both membranes at the specified condition, the E2 in permeate side reduced close to the limit of quantification of the analytical device, 3.5±2.8 ng/L E2 using PVDF-TiO$_2$ and 6.3±3.3 using PES-TiO$_2$. This shows the great potential of these membranes in reducing the concentration of MP in water.

---

[17] Experiment using PVDF-TiO$_2$ were carried out by Eleonore Veron under the supervision of Shabnam Lotfi.

8.5   References

Carretero-Genevrier, A., C. Boissiere, L. Nicole and D. Grosso (2012). "Distance dependence of the photocatalytic efficiency of TiO$_2$ revealed by in situ ellipsometry." Journal of the American Chemical Society **134**: 10761-10764.

GVS Filter Technology. (2021). "Polyvinylidene Fluoride (PVDF) Hydrophilic - PVDF-Plus™." from https://www.gvs.com/en/catalog/pvdf-hydrophilic-filtration-membrane?q=PVDF%20membrane.

Herrmann, J.-M. (2010). "Photocatalysis fundamentals revisited to avoid several misconceptions." Applied Catalysis B: Environmental **99**: 461-468.

Kumari, P., N. Bahadur and L. F. Dumée (2020). "Photo-catalytic membrane reactors for the remediation of persistent organic pollutants – A review." Separation and Purification Technology 230: 115878.

Leong, S., A. Razmjou, K. Wang, K. Hapgood, X. Zhang and H. Wang (2014). "TiO$_2$ based photocatalytic membranes: A review." Journal of Membrane Science **472**: 167-184.

Liu, S., E. Véron, S. Lotfi, K. Fischer, A. Schulze and A. I. Schäfer (2023). "Poly(vinylidene fluoride) membrane with immobilized TiO$_2$ for degradation of steroid hormone micropollutants in a photocatalytic membrane reactor." Journal of Hazardous Materials 447: 130832.

Lotfi, S., K. Fischer, A. Schulze and A. I. Schäfer (2022). "Photocatalytic degradation of steroid hormone micropollutants by TiO$_2$ coated polyethersulfone membranes in a continuous flow-through process." Nature Nanotechnology **17**: 417–423.

Lyubimenko, R., B. S. Richards, A. Turshatov and A. I. Schäfer (2020). "Separation and degradation detection of nanogram-per-litre concentrations of radiolabelled steroid hormones using combined liquid chromatography and flow scintillation analysis." Scientific Reports **10**: 7095.

Mudalige, T., H. Qu, D. Van Haute, S. M. Ansar, A. Paredes and T. Ingle (2019). Chapter 11 - Characterization of Nanomaterials: Tools and Challenges. Nanomaterials for Food Applications. A. López Rubio, M. J. Fabra Rovira, M. martínez Sanz and L. G. Gómez-Mascaraque, Elsevier**:** 313-353.

Schulze, A., M. F. Maitz, R. Zimmermann, B. Marquardt, M. Fischer, C. Werner, M. Went and I. Thomas (2013). "Permanent surface modification by electron-beam-induced grafting of hydrophilic polymers to PVDF membranes." RSC Advances **3**: 22518.

Temmel, S., W. Kern and T. Luxbacher (2006). "Zeta Potential of Photochemically Modified Polymer Surfaces." Characterization of Polymer Surfaces and Thin Films **132**: 54-61.

Yamada, Y. and Y. Kanemitsu (2012). "Determination of electron and hole lifetimes of rutile and anatase TiO$_2$ single crystals." Applied Physics Letters **101**.

You, S. J., G. U. Semblante, S. C. Lu, R. A. Damodar and T. C. Wei (2012). "Evaluation of the antifouling and photocatalytic properties of poly(vinylidene fluoride) plasma-grafted poly(acrylic acid) membrane with self-assembled TiO$_2$." Journal of Hazardous Materials **237-238**: 10-19.

Chapter Nine

9   Conclusion and Summary

PES and PVDF membranes, together with the TiO_2 nanoparticles coated membranes were characterized in this work. First, membranes needed to be characterized before being used to answer the questions raised in the introduction, Chapter **1**, (characterization of membranes in Chapter **4**). Both membranes had good TiO_2 coverage shown by SEM imaging, with PES-TiO_2 having a better distribution of membrane over the thickness of the membrane based on SEM-EDX images, and higher TiO_2 content on the surface of the membrane obtained by XPS measurements. The surface charge of membranes was determined by streaming potential measurements, and both membranes had a negative surface charge at pH 8 which is the standard pH in photocatalytic degradation experiments with both MB and hormones. The band gap of TiO_2 nanoparticles coated on the membranes was determined to be 3.02 eV equal to a wavelength of 412 nm, which shows the UV-LED 365 nm used in the experiment is sufficient for the photocatalytic degradation experiments. All in all, both PES-TiO_2 and PVDF-TiO_2 membranes showed remarkable properties and are promising candidates to be further investigated for micropollutants elimination using a PMR.

Following, the conclusion and summary of the answers found within this thesis is presented one by one:

I. *What is the performance of the proposed flow-through PMR in comparison with the flow-along and batch reactor with the submerged photocatalytic membrane in the solution (Chapter 5)?*

To investigate the potential of the proposed PMR system, two configurations of flow-along and flow-through in this work were compared with a batch system from another research institute. Their performance was compared regarding MB degradation under different light intensities and water flux (relative to hydraulic resistance inside the membrane). These data were used to calculate different figures of merit namely adapted space-time yield (STY) and photocatalytic space-time yield (PSTY), specific energy consumption (SEC) and rate of disappearance. The modified version of PSTY showed to be the most reliable index for a fair comparison of reactors by including reactor throughput together with energy efficiency and photocatalytic activity. The flow-through PMR had better PSTY than both the flow-along and flow-through reactor. This PMR (flow-through) had the benefit of forcing the flow through the membrane pores with a higher mass transfer rate inside the nanometer-sized pores and a high probability of pollutant and reactive oxygen species collision due to the tortuosity of the porous membrane structure. All in all, batch reactors could be beneficial for small volumes to be treated completely, while flow reactors can treat significantly higher throughput over time.

ii.   What are the limiting factors of operation in a PMR while degrading the steroid hormones in a concentration as low as the environment (Chapter 6)?

In the next phase, the photocatalytic activity of two PMs, PES-TiO$_2$ and PVDF-TiO$_2$, was compared by steroid hormones degradation. The limiting factors of operation in a flow-through PMR were evaluated and compared with both membranes, including the operational condition and water solution chemistry. The concentration of steroid hormones was in the range of 100 ng/L based on the concentration available in the environment, mostly in the effluent of water and wastewater treatment plants (**Table 2-2**).

When increasing the light intensity, the removal and rate of disappearance of E2 (r″) rose significantly, with a sharp rise almost linear at lower light intensities and a slower one (nonlinear) above 20 mW/cm^2 for PES-TiO$_2$ and above 10 mW/cm^2 for PVDF-TiO$_2$. This change of patterns showed that until a certain limit, the photocatalytic degradation was dependent on the generated reactive oxygen species which was limited by the exposed photons. Above these values, the photons were in abundance and the reaction was limited by another factor. This finding led to the hypothesis that the reason could be the lack of TiO$_2$ sites. By increasing the water flux (shorter hydraulic residence time), the E2 removal decreased, as a higher number of molecules presented inside the pores in a shorter time and therefore a lower portion of them were degraded. However, by increasing the flux and accordingly the molar flux, r″ rose almost linearly in the full range of flux for PES-TiO$_2$ and until 900 L/m^{2}h for PVDF-TiO$_2$, which shows that the molar flux was controlling the apparent degradation kinetic regime. Above this value, r″ started to level out and was independent of molar flux. Similarly, by increasing the concentration of E2 from 50 ng/L to 1 mg/L, r″ went up which shows that the reaction sites provided by TiO$_2$ were not limiting the reaction which contradicted the above-mentioned hypothesis.

By increasing the temperature of the reaction environment, the efficiency of the system lowered significantly which could be due to different parameters. Lower adsorption of molecules to the surface or the lower concentration of oxygen at a higher temperature could have been among the reasons. Increasing the pH to above 10 lowered the degradation of the E2 as this molecule dissociates to a negatively charged ion at pKa almost 10.3 and this causes repulsion between the negatively charged membrane surface and the anions. When comparing E2 removal with other steroid hormones at pH 8-9, room temperature, 300 L/m^{2}h and 25 mW/cm^2, E1 with an almost similar molecule structure had the same removal, whereas testosterone was removed less using both membranes (30-40%). While PES-TiO$_2$ was unable to degrade progesterone sufficiently (almost 44%), this hormone was removed at almost 80% same as E2 and E1 using PVDF-TiO$_2$. In overall, both membranes proved to be capable of degrading steroid hormones effectively from a low-concentration solution which is necessary to avoid their

presence in the environment even as low as a few ng/L. In all situations, PVDF-TiO$_2$ had higher efficiency under the same condition which makes it a good candidate for future research.

iii.   What is the degree of the photostability of the photocatalytic membranes tested under accelerated ageing and analyzed with different techniques (Chapter 7)?

In the next phase, the photostability of the membranes was evaluated as a potential parameter in limiting the photocatalytic reaction. An accelerated ageing test in the UV-violet-LED chamber was conducted to present a harsh condition of degradation of polymer-based membranes (no pollutants, no water flow, high light intensity). The duration (250 h) and irradiation intensity (222 mW/cm^2) were chosen such that exposure of polymer-based membranes to UV-Vis light was sufficient to gain insights into the changes in material properties, photocatalytic, and filtration performance.

The significant decline in MB removal of the PES-TiO$_2$ after 250 h of the accelerated ageing test was assumed to be due to the instability of the membrane and loss of photocatalyst. In contrast to the PES-TiO$_2$ membrane, the PVDF-TiO$_2$ membranes preserved their photocatalytic activity after 250h of UV-light/ROS exposure without signs of degradation. Both the PVDF-TiO$_2$ and PES-TiO$_2$ membranes exhibited a release of organic carbon (> 30 mgC/L) to the water under light irradiation which could be from the detachment of the hydrophilic additives of the membranes. Although this issue did not affect the permeability of the membranes which could be due to the microfiltration range of the membranes and high permeability in this range. Overall, PVDF materials are considered stable support for photocatalysts, however, the modification of membranes (hydrophilic or hydrophobic) should be further considered in terms of the potential degradation of membrane additives.

iv.   How improving the membrane structure and TiO$_2$ coating can enhance steroid hormone degradation (Chapter 8)?

In the last section, the aim was to optimize the degradation efficiency of the membranes. First, the loading of TiO$_2$ on PVDF-TiO$_2$ was investigated. Increasing the surface Ti content from zero up to 6.5% (XPS elemental characterization) resulted in a significant increase in the E2 removal. Then TiO$_2$ loading on the membrane was increased successfully by modifying the membrane surface and also using a different PVDF substrate with a bigger pore size. While PVDF-PAA-TiO$_2$ had the highest TiO$_2$ content and a very homogenous loading over the thickness of the membrane, all of the modifications showed similar removal of 80% E2 from a 100 ng/L solution. Two other membranes with smaller pore sizes, 100 nm, were also coated with TiO$_2$ and tested for photocatalytic degradation of E2. However, these two membranes had lower removal and it can be assumed that varying the pore size in the range of 0.45 μm

to 0.1 μm did not affect the mass transfer inside the pore majorly and had a minimum impact on the E2 removal. Lastly, the conditions of the experiments were modified such that the maximum removal can be achieved using the basic PES-TiO$_2$ and PVDF-TiO$_2$. E2 degradation below 5 ng/L recommended by WHO could be obtained by both membranes while using higher light intensity for PES-TiO$_2$ compared to PVDF-TiO$_2$. However, the limit of detection of the analytical device made it difficult to see the actual potential of the photocatalytic membranes in the range of 1 ng/L.

Outlook

Photocatalytic membranes proved to be a promising solution in the degradation of recalcitrant MP. They have advantages over common slurry photocatalyst reactors such as preventing the loss of the photocatalyst as nanoparticles to the effluent which can be a major health issue on its own. Further studies on this topic with a focus on the estrogenic activity of permeate samples are recommended to evaluate the removal of their toxicity after photocatalytic degradation (more specifically vital to aquatic life as they are more sensitive compared to humans). This requires extensive testing procedure methodologies and was not possible in the course of this thesis due to challenges related to the small sample volume. Another important point to assess is the interaction of parameters on each other as many of the studied parameters are not independent from one another. Moreover, the transition from synthetically prepared wastewater (steroid hormone solution) to real wastewater should be evaluated. This is challenging regarding the analysis of low concentrations of hormones and low volume of samples in the studied photocatalytic membrane reactor. However, to be able to utilize the system in real applications, this transmission is critical and necessary.